TECHNICAL DIGEST
1995

PHOTONICS IN SWITCHING

MARCH 15–17, 1995

SALT LAKE CITY, UTAH

1995 TECHNICAL DIGEST SERIES
VOLUME 12

SPONSORED BY
OPTICAL SOCIETY OF AMERICA

DISCLAIMER NOTICE

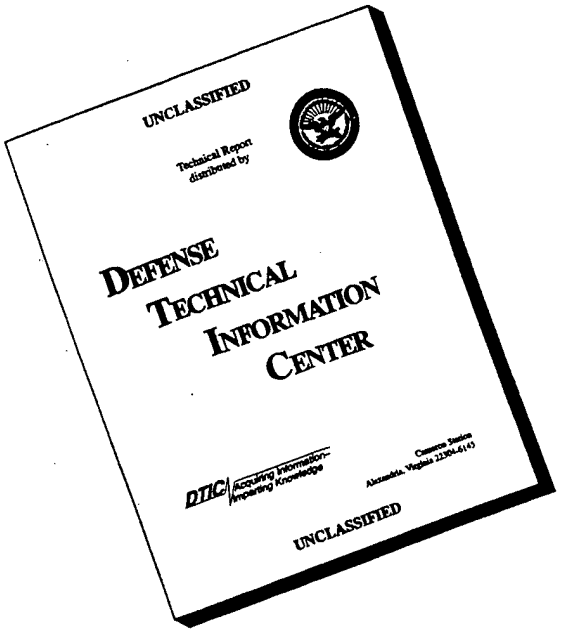

THIS DOCUMENT IS BEST QUALITY AVAILABLE. THE COPY FURNISHED TO DTIC CONTAINED A SIGNIFICANT NUMBER OF PAGES WHICH DO NOT REPRODUCE LEGIBLY.

CONFERENCE EDITION

Summaries of the papers presented at the topical meeting

PHOTONICS IN SWITCHING

March 15–17, 1995
Salt Lake City, Utah

1995 Technical Digest Series
Volume 12

Sponsored by
Optical Society of America

Articles in this publication may be cited in other publications. To facilitate access to the original publication source, the following form for the citation is suggested:

Name of Author(s), "Title of Paper," in *Photonics in Switching*, Vol. 12, 1995 OSA Technical Digest Series (Optical Society of America, Washington DC, 1995), pp. xx-xx.

Optical Society of America

ISBN

Conference Edition	1-55752-393-2
Postconference Edition	1-55752-394-0
(Note: Postconference Edition includes postdeadline papers.)	
1995 Technical Digest Series	1-55752-368-1

Library of Congress Catalog Card Number

Conference Edition	95-67804
Postconference Edition	95-67800

Printed in the U.S.A.

Contents

PHOTONICS IN SWITCHING
TECHNICAL PROGRAM COMMITTEE

Rod C. Alferness, *General Chair*
AT&T Bell Laboratories

Lars Thylen, *Program Chair*
Royal Institute of Technology, Sweden

Godfrey Hill, *European Chair*
British Telecom Laboratories

Kunio Tada, *Japanese Chair*
University of Tokyo, Japan

Paul Prucnal
Princeton University

Thomas J. Cloonan
AT&T Bell Laboratories

Daniel J. Blumenthal
Georgia Institute of Technology

Robert Leheny
ARPA

Jack Tomlinson
Bellcore

Rodney S. Tucker
University of Melbourne, Australia

Masahiko Fujiwara
NEC Corporation, Japan

Ken-ichi Yukimatsu
NTT Communications Switching Laboratory, Japan

Takeshi Ozeki
Sophia University, Japan

Marko Erman
Alcatel Alsthom Recherche, France

Sonny Johansson
Ellemtel Telecommunications Systems Laboratory, Sweden

H. Venghaus
Heinrich Hertz Institute, Germany

RED LION EAST

8:30am
Opening Remarks
Rod Alferness, *AT&T Bell Laboratories, Chair*

RED LION EAST

8:45am–10:15am
PWA • Plenary: 1
Rod Alferness, *AT&T Bell Laboratories, Presider*

8:45am (Plenary)
PWA1 • Photonics beyond information transport? Herwig Kogelnik, *AT&T Bell Laboratories.* Photonics has rapidly become the dominant technology for the transmission of information in the national and global infrastructure, including undersea, terrestrial long-haul, CATV and local telephone access applications. Expanding this success deeper into the network, we are challenged by new requirements such as conforming to the new ATM (asynchronous transfer-mode) standards and by new opportunities such as wavelength routing and transparent high-capacity networking.

Herwig Kogelnik is Director of Photonics Research at AT&T Bell Laboratories. He received the Dipl.-Ing and Dr. techn. degrees from the Technical University of Vienna, and the D.phil. from Oxford University. He was elected to the National Academy of Science and the National Academy of Engineering. He served as President of the Optical Society of America and is an Honorary Fellow of St. Peter's College at the University of Oxford. **(p. 2)**

9:30am (Plenary)
PWA2 • Who will be the winner, photonics, electronics or photoelectronics? Tetsuhiko Ikegami, *NTT, Japan.* Once 'photonic switching' has been demonstrated, the performance has been taken over by electronics in a past decade, like the competition between GaAs and Si in the micro-electronics technologies. Recently, bit-greedy telecommunication services like Multimedia are coming up and multi-wavelength networking, in which multi-wavelength will be used for new functions, not for a simple idea of increasing channel capacity, is revealing a new horizon to 'photonic switching'. We will discuss how to share each role of photonics and electronics in the emerging field.

Dr. Ikegami, Senior V.P. of NTT, and a Senior Executive Manager of Science and Core Technology Labs and NTT Basic Research Labs, has performed pioneering works on semiconductor lasers including finding of resonance-like phenomenon which was an essential property in directly modulated semiconductor lasers, reliability study on the devices which led the device into undersea application, and development of single mode operation under the direct modulation enabling the large capacity and long distance fiber transmission at Giga bit per second range. He has been heading the development of optical devices passive components like the Photonic Lightwave Circuit as well as active devices in order to realize emerging photonic systems for Photonic-Through-The-Network. **(p. 3)**

GRAND BALLROOM C

10:15am–10:30am
Coffee Break/Exhibits

RED LION EAST

10:30am–11:15am
PWB • Plenary: 2
Lars Thylen, *Royal Institute of Technology, Sweden, Presider*

10:30am (Plenary)
PWB1 • The role of photonic switching in future high-capacity telecommunication networks, Olle Nillsson, *Ellemtel, Sweden.* The role of photonic switching in future telecommunications has been the subject of intense research and discussions ever since the realization in the early eighties that fiber optics could furnish virtually limitless broadband transmission. The basic idea is that, eventually, one will face an electronic bottle neck when it comes to switching the predicted enormous bitstreams and that photonic switching may then offer a solution. Questions of a fundamental nature based on presently known physical limitations and some possible telecommunication network demand scenarios will be raised. **(p. 6)**

RED LION EAST

11:15am–12:00m
PWC • Optical Interconnect
Tom Cloonan, *AT&T Bell Laboratories, Presider*

11:15am (Invited)
PWC1 • Optical interconnection technology for large computing and switching systems, Niloy K. Dutta, *AT&T Bell Laboratories.* This talk will focus on current applictions and future directions of optical interconnection technology. This technology will be initially driven by applications in large computing and switching systems. Advances in system architectures, subsystem modules and optoelectronic integrated circuits aimed at lower cost implementation of the entire system are necessary to create a wide application base for optical interconnection technology. **(p. 12)**

11:45am
PWC2 • 8 × 8 array of optoelectronic switching nodes comprised of flip-chip solder-bonded MQW modulators on silicon CMOS circuitry, A. L. Lentine, K. W. Goossen, J. A. Walker, L. M. F. Chirovsky, L. A. D'Asaro, S. P. Hui, B. T. Tseng, R. E. Leibenguth, D. P. Kossives, D. W. Dahringer, D. A. B. Miller, *AT&T Bell Laboratories.* We describe an array of smart pixels with multiple quantum well (MQW) modulators and detectors flip-chip solder-bonded to a silicon CMOS circuit, individually operating at 250 Mb/s. **(p. 13)**

RED LION EAST

1:30pm–3:00pm
PWD • Transport Network Switching and Routing:1
Dan Blumenthal, *Georgia Institute of Technology, Presider*

1:30pm (Invited)
PWD1 • The RACE multiwavelength transport network project: results and conclusions, Godfrey Hill, *British Telecom, U.K.* The RACE MWTN project has developed technology for wavelength routing networks and has demonstrated their feasibility both theoretically and in a field environment. **(p. 18)**

2:00pm
PWD2 • Telecom networks going photonic: reconciling transparency with scalability, Philip Dumortier, Thierry Van Landegem, *Alcatel Corporate Research Center, Belgium;* Francesco Masetti, Michel Sotom, *Alcatel Corporate Research Center, France.* A simple yet flexible high-capacity network architecture is proposed, featuring a reasonable degree of signal transparency, while still ensuring network scalability. **(p. 21)**

2:15pm
PWD3 • OFDM cross-connect with an embedded free-space switch, B. Kuhlow, G. Teich, G. Walf, *Heinrich-Hertz-Institut für Nachrichtentechnik GmbH, Germany.* The implementation of a dense OFDM cross-connect consisting of a frequency conversion stage with tunable frequency selective receivers and a 3D free-space switching fabric is described. **(p. 24)**

2:30pm
PWD4 • Free-space optical sliding Banyan network, Michael W. Haney, *George Mason Univ.;* Marc P. Christensen, James J. Levy, *BDM Federal, Inc.* The smart-pixel-based 3D sliding Banyan architecture offers significant throughput advantages over electronic approaches. Design and experimental aspects of the network are presented. **(p. 27)**

2:45pm
PWD5 • Development of a 16 × 16 reconfigurable holographic interconnection system, P. Gravey, L. Bonnel, *France Télécom CNET LAB/RIO/PCO, France.* We present the design and the realization of a 16 × 16 two-stage holographic interconnection system between single-mode fibers based on photothermoplastic holograms, including its optical addressing system. The diffraction efficiency of the holograms can be higher than 20% at 1.3 μm. We demonstrate an accurate collimation of the beams issued from linear fiber arrays over the distance necessary to the system implementation. **(p. 30)**

GRAND BALLROOM EAST

3:00pm–3:30pm
Coffee Break/Exhibits

RED LION EAST

3:30pm–5:30pm
PWE • Wavelength and Time Switching
Godfrey Hill, *British Telecom Laboratories, U.K., Presider*

3:30pm (Invited)
PWE1 • Wavelength conversion devices and applications, B. Mikkelson, *Electromagnetics Inst., Technical Univ. of Denmark, Denmark.* Applications and desired features of wavelength converters are discussed. Different methods for wavelength conversion are surveyed with emphasis on all-optical wavelength conversion by SOAs. **(p. 36)**

4:00pm
PWE2 • A photonic WDM packet switch with reduced complexity due to wavelength converters, S. L. Danielsen, B. Mikkelsen, C. Joergensen, T. Durhuus, K. E. Stubkaer, *Technical Univ. Denmark, Denmark.* The influence of wavelength converters on the complexity of an optical WDM packet switch is analyzed. Based on measured data, power penalties for a 16 × 16 switch using 4 or 8 wavelengths are calculated. **(p. 39)**

4:15pm
PWE3 • Multichannel optical filters using birefringent planar optical platforms, Katsuhiko Hirabayashi, Masayasu Yamaguchi, *NTT Network Service Systems Laboratories, Japan.* We propose a novel multichannel filter possible to select arbitrary several wavelengths with arbitrary transmittance simultaneously. We show a seven-channel filter module with 1-nm channel spacing. **(p. 42)**

4:30pm
PWE4 • Optical TDM systems, Kristin Rauschenbach, Katie Hall, John Moores, Steve Finn, Rick Barry, *MIT Lincoln Laboratory;* William Wong, Hermann Haus, Eric Ippen, *MIT;* Mark Haner, *AT&T Bell Laboratories.* We present recent developments in technologies for ultra-high-bit-rate time-division-multiplexed systems, including network architecture, high-speed sources, optical switches, clock recovery, and memory. **(p. 45)**

5:00pm (Invited)
PWE5 • All-optical self-routing switch using a nonlinear InGaAs/InAlAs MQW waveguide, Tatsuo Kanetake, S. Tanaka, H. Inoue, *Hitachi Ltd., Japan.* All-optical switching is demonstrated in the Mach–Zenhder interferometer with a nonlinear InGaAs/InAlAs MQW waveguide designed for 1.55 μm toward self-routing operation. **(p. 47)**

GRAND BALLROOM C

6:30pm–8:00pm
Conference Reception

RED LION EAST

8:30am–10:00am
PThA • Packet-Switched Photonic Networks: 1
T. Yasui, *Mitsubishi Electric Corp., Japan, Presider*

8:30am (Invited)
PThA1 • Photonic ATM switching for broadband network services, Tohru Matsunaga, Koji Sasayama, Yoshiaki Yamada, Keishi Habara, Ken-ichi Yukimatsu, *NTT, Japan.* After briefly reviewing recent photonic ATM switching research, NTT's frequency division multiplexing-based ATM switches will be described with some experimental results. **(p. 52)**

9:00am
PThA2 • Experiment on photonic ATM switches with WDM output buffers, Akira Misawa, Masato Tsukada, *NTT Network Service Systems Laboratories, Japan.* We propose photonic ATM switches with WDM output buffers made of fiber-delay lines and experimentally demonstrated two-wavelength-division-multiplexed cell switching at 10 Gbit/s. **(p. 55)**

9:15am
PThA3 • Ultrafast photonic packet switching with optically processed control, I. Glesk, P. R. Prucnal, *Princeton Univ.;* Baolin Wang, *Siemens Corporate Research.* We report the first demonstration, to our knowledge, of all-optical address recognition and self-routing of photonic packets for a case of two-bit addressing. The packet bit period is only 4 picoseconds. The packet-switching bit error rate was measured to be less than 10^{-9}. **(p. 58)**

9:30am
PThA4 • Gigahertz clock synchronization using a nonlinear optical loop mirror as an all-optical phase comparator, K. L. Hall, K. A. Rauschenbach, E. A. Swanson, S. R. Chinn, *MIT Lincoln Laboratory;* G. Raybon, *AT&T Bell Laboratories.* A 10 GHz and a 40 GHz optical pulse stream are synchronized using a nonlinear optical loop mirror as the phase comparator in a phase-lock loop. **(p. 61)**

9:45am
PThA5 • Optical cell synchronizer for packet-switched nodes, M. Burzio, P. Cinato, R. Finotti, P. Gambini, M. Puleo, E. Vezzoni, L. Zucchelli, *Centro Studi E. Laboratori Telecomunicazioni, Italy.* Optical synchronization of cells in high-speed packet-switched nodes is discussed and an experimental system based on switchable delay lines and fiber-chromatic dispersion is demonstrated. **(p. 64)**

GRAND BALLROOM C

10:00am–10:30am
Coffee Break/Exhibits

RED LION EAST

10:30am–12:00m
PThB • Operation of Photonic Networks
Charles Brackett, *Bellcore, Presider*

10:30am (Invited)
PThB1 • Management of optical networks, Sonny Johansson, *Ellemtel AB, Sweden.* Before introducing a new optical network layer, the management aspects should be solved. Experience is gained by implementing such a demonstration system in RACE-MWTN. **(p. 68)**

11:00am
PThB2 • Proposal and implementation scheme of an optical network management system, Tatsuya Shiragaki, Naoya Henmi, Masahiko Fujiwara, *NEC Corp., Japan.* An optical network management system, with newly defined optical paths and optical sections, and its implementation scheme utilizing wavelength-division-multiplexing are proposed. The optical-loss-budget consideration confirms the application feasibility. **(p. 70)**

11:15am
PThB3 • Optical cross-connect architecture incorporating failure recovery using reserved wavelengths, S. Kuroyanagi, K. Hironishi, T. Maeda, *Fujitsu Laboratories, Ltd., Japan.* This paper proposes an optical cross-connect architecture that provides failure recovery based on reserved wavelengths and consists of a routing block and a bypass block. **(p. 73)**

11:30am (Invited)
PThB4 • Wavelength stabilization as a practical standard light source for WDM systems at 1.55 micrometer, Yoshihiko Tachikawa, Yasuyuki Suzuki, Mamoru Arihara, Takeshi Inoue, Shinichi Nakajima, Takaaki Hirata, *Yokogawa Electric Corp., Japan;* Jun Ishikawa, *National Research Laboratory of Metrology, Japan.* We developed a compact wavelength stabilized light source in 1.55 μm with the wavelength controlled to the bottom of the HCN gas absorption line. We discuss the wavelength stabilization method and the precision wavelength calibration method. **(p. 76)**

12:00m–1:30pm
Lunch on Own

RED LION EAST

1:30pm–3:00pm
PThC • Packet-Switched Photonic Networks: 2
Robert Leheny, *ARPA, Presider*

1:30pm (Invited)
PThC1 • Photonics and ATM switching, Jacques Dupraz, *Alcatel, France.* ATM in switching and optics in transmission are the key technologies of future broadband networks. This paper discusses the problems associated with the introduction of photonics in ATM switching from a technical viewpoint. **(p. 80)**

2:00pm
PThC2 • Photonic switching of optical interconnects in large telecom nodes, Magnus Buhrgard, *Ellemtel Telecommunication Systems Laboratories, Sweden.* Photonic switching of optical interconnects can make future broadband telecom nodes more efficient and flexible. Switch designs using photonic switching are presented. **(p. 81)**

2:15pm
PThC3 • Novel photonic architecture for high-capacity ATM switching applications, D. Chiaroni, *Alcatel CIT, France;* C. Chauzat D. De Bouard, S. Gurib, M. Sotom, J.-M. Gabriagues, *Alcatel Alsthom Recherche, France.* A novel photonic ATM switching architecture based on broadcast-and-select principle is presented. First results of experimental feasibility assessment at 2.5 Gbit/s are reported. **(p. 84)**

2:30pm
PThC4 • Fanout, replication, and buffer sizing for a class of self-routing packet-switched multistage photonic switch fabrics, Ashok V. Krishnamoorthy, *AT&T Bell Laboratories;* Fouad E. Kiamilev, *Univ. North Carolina–Charlotte.* We investigate performance-cost tradeoffs for a new class of self-routing, packet-switched multistage interconnection networks. We discuss the implications for a smart-pixel photonic switch implementation. **(p. 87)**

2:45pm
PThC5 • Efficient signal distinction scheme for large-scale free-space optical networks using genetic algorithms, Ahmed Louri, Hongki Sung, Yoonkeon Moon, Bernard P. Zeigler, *Univ. Arizona.* We present a novel incoming signal distinction scheme for large-scale free-space optical interconnection networks. The scheme significantly reduces the number of detectors per node. **(p. 90)**

GRAND BALLROOM C

3:00pm–3:30pm
Coffee Break/Exhibits

RED LION EAST

3:30pm–5:00pm
PThD • Optoelectronic Devices for Photonic Switching
H. Venghaus, *Heinrich Hertz Institute, Germany, Presider*

3:30pm (Invited)
PThD1 • Semiconductor guided-wave switching, J. E. Zucker, *AT&T Bell Laboratories.* Recently a systems pull from new fiber-optic networks has spurred development of custom semiconductor switches using novel materials, fabrication methods, and sophisticated optical design tools. **(p. 94)**

4:00pm
PThD2 • Transmission experiments on fully packaged 4 × 4 semiconductor optical amplifier gate-switch matrix, Claus Popp Larsen, Wim van Berlo, Jan-Erik Falk, Lars Gillner, Mats Gustavsson, *Ericsson Components AB, Sweden;* Erland Almström, *Ellemtel AB, Sweden;* Fransesco Testa, *Ericsson Telecommunicazione S.p.A., Italy.* Promising results regarding cascaded paths and WDM transmission for fully packaged 4 × 4 switches are reported. Dynamic ranges and polarization dependence are determined for a BER optimized device. **(p. 95)**

4:15pm
PThD3 • Low-voltage electroabsorption in InGaAsP/InP MQW electron transfer structures, Ulf Olin, *Institute of Optical Research, Sweden;* Dana Varga, Krister Fröjdh, Johan Wallin, Gunnar Landgren, *Royal Institute of Technology, Sweden.* We demonstrate experimentally an enhancement of the electroabsorption in InGaAsP/InP barrier reservor and quantum well electron transfer structures with multiple quantum wells (MQWs) per period. **(p. 98)**

4:30pm
PThD4 • Vertical-cavity x-modulators, J. A. Trezza, J. S. Powell, M. Morf, J. S. Harris, Jr., *Stanford Univ.* Experimentally and theoretically, a vertical-cavity photon-conserving reversible optoelectronic intensity modulator that simultaneously and bidirectionally switches reflectivity and transmission is displayed and analyzed. **(p. 101)**

4:45pm
PThD5 • BER studies of diode-clamped FET-SEED receivers, T. K. Woodward, A. L. Lentine, L. M. F. Chirovsky, *AT&T Bell Laboratories.* The bit error rate (BER) performance of diode-clamped FET-SEED optical receivers with electrical output is reported. The digital nature of the receiver is confirmed and operation to 1 Gbit/s is obtained. **(p. 104)**

RED LION EAST

7:30pm–9:00pm
Postdeadline Session
Lars Thylen, *Royal Institute of Technology, Sweden, Presider*

RED LION EAST

8:30am–10:00am
PFA • Transport Network Switching and Routing: 2
S. Johansson, *Ellemtel, Sweden, Presider*

8:30am
PFA1 • Review of ARPA-sponsored WDM networking projects, Charles A. Brackett, *Bellcore.* The concepts and progress of current ARPA-sponsored WDM networking projects will be reviewed, with emphasis on what has been learned and where new challenges lie. **(p. 108)**

9:00am
PFA2 • Comparison of coherent cross-talk-induced BER floors in four types of N × N space photonic switches, D. J. Blumenthal, *Georgia Institute of Technology;* P. Granestrand, *Ericsson Components, AB, Sweden;* L. Thylen, *Royal Institute of Technology, Sweden.* The coherent cross talk properties of four photonic-switch structures, active-passive, passive-active, active-split/active-combine, and gated-amplifier, are analyzed and the size-dependent cross talk bounds for low bit error rate (BER) operation is derived. It is shown that this type of cross talk causes BER floors once critical size-dependent cross talk levels have been exceeded. **(p. 109)**

9:15am
PFA3 • Duality between space, time, and wavelength in all-optical networks, Hisashi Kobayashi, *Princeton Univ.;* Ivan P. Kaminow, *AT&T Bell Laboratories.* We exploit duality between space, time, and wavelength in multiplexed optical signals, and derive new optical routers and switches with nonblocking or rearrangeably nonblocking properties. **(p. 112)**

9:30am
PFA4 • Mechanical optical fiber cross connect, Sven Sjölinder, *Ericsson Cables AB, Sweden.* A mechanical fiber-optic switch with N × M matrix and loss <1.7 dB has been developed. 2700 switch operations are demonstrated without cleaning of ferrules. **(p. 115)**

9:45am
PFA5 • Thermal considerations in the design of optoelectronic device mounts, D. B. Buchholz, A. L. Lentine, R. A. Novotny, *AT&T Bell Laboratories.* The temperature variation across a FET-SEED is modeled and compared with experimental measurements. The effect of chip-mount design is also discussed. **(p. 118)**

FOYER

10:00am–10:30am
Coffee Break

RED LION EAST

10:30am–12:30pm
PFB • Photonic Network Components
T. Ozeki, *Sophia University, Japan, Presider*

10:30am (Invited)
PFB1 • Recent advances in planar lightwave functional devices, Kaname Jinguji, K. Takiguchi, M. Kawachi, *NTT, Japan.* Abstract not available at time of printing. **(p. 122)**

11:00am
PFB2 • Evolution of fiber arrays for free-space interconnect applications, Nagesh Basavanhally, Richard Borutta, Randall Crisci, Casimir Nijander, Laurence Watkins, *AT&T Bell Laboratories.* Fiber arrays are used in free-space interconnect systems for bringing in and taking out optical signals from the computing or switching environment. We discuss the optomechanical challenges in fabrication of 2D fiber-input array, and alignment and attachment of microlens arrays to fiber bundle. **(p. 124)**

11:15am
PFB3 • Optical beam routing through time-domain spatial-spectral filtering, W. R. Babbitt, *Univ. Washington;* T. W. Mossberg, *Univ. Oregon.* It is proposed to use spatial-spectral gratings to route high-bandwidth data according to addresses encoded in the temporal waveform of each routed bit. **(p. 129)**

11:30am
PFB4 • Multifunctional surface-emitting laser-based integrated photonic/optoelectronic switch for parallel high-speed optical interconnects, J. C. Lu, Julian Cheng, *Univ. New Mexico;* Y. C. Zolper, J. Klem, *Sandia National Laboratories.* We describe a multifunctional optical/optoelectronic switch that can convert data between various combinations of electrical and optical input/output formats at 350–500 Mbit/s. **(p. 132)**

11:45am
PFB5 • High-speed 2D CMOS designs of bypass-and-exchange switch arrays for free-space optoelectronic MINs, Osman Kibar, Philippe J. Marchand, Sadik C. Esener, *UC–San Diego.* We present two CMOS designs of bidirectional switches suitable for free-space optoelectronic MINs. The second design is a novel self-routing concept that uses three-level logic. **(p. 135)**

12:00m
PFB6 • Gigabit per second switching of smart-pixel receiver-transmitter pairs, G. Livescu, L. M. F. Chirovsky, T. Mullally, *AT&T Bell Laboratories;* Arza Ron, *Technion, Israel.* We use trains of 1.5 picosecond mode-locked laser pulses spaced 1 nanosecond apart to transmit Gbit/s data patterns through GaAs/AlGaAs smart-pixel receiver-transmitter pairs. **(p. 138)**

12:15pm
PFB7 • Distributed forward- and backward-coupling laser—novel laser diode for wide-wavelength tuning, Kenji Sato, Yoshiaki Nakano, Kunio Tada, *Univ. Tokyo, Japan.* Another type of laser diode for wide-wavelength tuning is proposed and analyzed. Over 40-nm tuning around 1.55-μm is obtainable by changing only one control current. **(p. 141)**

Wednesday, March 15, 1995

Plenary: 1

PWA 8:45 am-10:15 am
Red Lion East

Rod Alferness, *Presider*
AT&T Bell Laboratories

Photonics Beyond Information Transport?

Herwig Kogelnik
AT&T Bell Laboratories
Holmdel, NJ 07733

Photonics has rapidly become the dominant technology for the transmission of information in the national and global infrastructure, including undersea, terrestrial long-haul, CATV and local telephone access applications. Expanding this success deeper into the network, we are challenged by new requirements such as conforming to the new ATM (asynchronous transfer-mode) standards and by new opportunities such as wavelength routing and transparent high-capacity networking.

Who will be the winner, photonics, electronics or photo-electronics?

Tetsuhiko Ikegami
Nippon Telephone and Telegraph Co.
NTT Science and Core Technology Laboratory Group
Morinosato, Atsugi-shi, Kanagawa, 243-01, Japan

Once 'photonic switching' has been demonstrated, the performance has been taken over by electronics in a past decade, like the competition between GaAs and Si in the micro-electronics technologies. Recently, bit greedy telecommunication services like Multimedia are coming up and multi-wavelength networking, in which multi-wavelength will be used for new functions, not for a simple idea of increasing channel capacity, is revealing a new horizon to 'photonic switching'. We will discuss how to share each role of photonics and electronics in the emerging field.

Wednesday, March 15, 1995

Plenary: 2

PWB 10:30 am-11:15 am
Red Lion East

Lars Thylen, *Presider*
Royal Institute of Technology, Sweden

The role of photonic switching in future high capacity telecommunication networks

Olle Nilsson
Ellemtel AB, S-12525 Älvsjö, Sweden

1. The purpose of the talk

The role of photonic switching in future telecommunications has been the subject of intense research and discussions ever since the realisation in the early eighties that fiber optics could furnish virtually limitless broadband transmission. The basic idea is that, eventually, one will face an electronic bottle neck when it comes to switching the predicted enormous bitstreams and that photonic switching may then offer a solution.

Rather than trying to come up with definite answers in these matters I will raise some questions of a fundamental nature based on presently known physical limitations and some possible telecommunication network demand scenarios, say, ten years from now.

2. Scenario

The discussion will be based on a scenario where every subscriber has access to a basic bi-directional channel capacity of order 100 Mbit/s. This will probably be enough for video transmission with the resolution of the human eye i. e. some 4000 times 3000 pixels depending on the viewing angle. It is furthermore assumed that the number of subscribers is about the same as the present number of ordinary telephone subscribers. Two "networks" are considered; one with ten million subscribers corresponding to a small country and one global with one billion subscribers.

3. Estimate of trunk transmission costs

Say that all subscribers should be able to simultaneously occupy one 100 Mbit/s channel of length 500 km each. This means that of order $5 \cdot 10^5$ times $10^7 = 5 \cdot 10^{12}$ meters of 100 Mbit/s channels have to be installed. It is to be understood here and in the following that we are only making rough estimates. Since 100 Gbit/s can be transmitted in one fiber, a cable containing 100 fibers can be used to transmit 10^5 channels of 100 Mbit/s each. Thus $5 \cdot 10^7$ cable meters are needed. The present cost per meter of such cable is about $ 15 in installation and $ 15 in manufacturing, i.e. $ 30/m totally. Therefore the total cost per subscriber would be of order $ 150 only. There are good reasons to believe that the costs for repeaters could be kept in the same order of magnitude: Assuming conservatively a repeater every 50 km and that each repeater handles one 10 Gbit/s channel, i.e. 100 subscriber channels, one would need 10^6 such repeaters or one per every ten subscriber. In mass production using integrated technology a cost of $ 1500 should be possible even if the costs today is some ten times higher. The conclusion is therefore that the trunk transmission costs will be very low, of order $ 300 per subscriber, and that they will be insignificant compared to the costs of the local network and the subscriber terminals. The costs of the local network will be relatively high independent of bitrates simply because each subscriber needs a physical connection. Thus there seems to be limited economic room for measures to increase the utilisation efficiency of a given transport network rather than to simply add basic hardware capacity. This is a new situation in the history of telecommunications and might limit the future market for sophisticated rerouting and maintenance equipment except in the local networks and perhaps also in the transcontinental and intercontinental networks.
Even in the somewhat unrealistic global scenario with one billion subscribers making calls over average distances of 5000 km the cost per subscriber for the trunk network would only increase by a factor of order ten and would still be moderate.

4. Switching

When it comes to switching capacity requirements it is more difficult to make even order of magnitude estimates since there are uncertainties in both switching architecture and hardware possibilities. However, to get some idea of the problem one may, as a thought experiment, consider the total network as one large switch and apply classical switching theory to calculate the necessary number of switch elements, i.e. gates, in different known configurations.

Thus with $N = 10^7$ one finds that a non blocking switch of crossbar type requires about 10^7 gates per subscriber. This may not seem prohibitive but one must remember that the power consumption per gate at 100 Mbit/s is about 0.1 mW with present day technology leading to a power consumption of 1 kW per subscriber. Even if future technology may well reduce the power consumption by a factor of hundred such a switching architecture does not seem realistic.

Employing well known architectures for very low blocking probability, on the other hand, the number of gates per subscriber required is proportional to $^2\log N$ rather than N and both the number of gates and the power consumption per subscriber become insignificant even if the proportionality constant is taken as large as 1000 and if the global scenario with one billion subscribers is considered. (Feasibility studies of full ATM interleaved Banyan type electronic switching systems of more than 1 Tbit/s throughput have already been made with positive results. Here optical interconnects between subunits are assumed to be used).

There are other problems, however. Even if a large switch may be strictly non blocking or have a very low blocking probability the amount of computation to find a free path may become excessive, especially if the load approaches the theoretical capacity. It is therefore probably essential that the huge switches considered here can be subdivided into a fairly large number of independent switching nodes at different geographical locations each of which loaded well below capacity even at peak traffic. To my knowledge it is not known with certainty if such an architecture can be realised keeping the $N\ ^2\log N$ proportionality of the total gate count but it seems likely. If so an attractive solution might be to build a simple but very high capacity network of a self routing type relying on the subscriber terminals to define the paths on the "road map" of the network and having very limited central intelligence and control. Some possible features of such a network are discussed in section 6 below.

5. Photonic versus electronic switching

There is no indication that the networks considered above cannot be realised by use of electronic switching in combination with optical transmission and interconnects. A cost effective approach is probably to use standardised switching modules in form of chips or wafers with only a few high speed external connections each handling of order one hundred 100 Mbit/s channels. This would require 10 Gbit/s integrated electronics that is already within present state of art. The external connections could possibly be electric if they are within one board. Otherwise they should probably be optical and may be partly of free space type to avoid excessive intra- and interboard cabling.

Thus photonic switching does not seem to be necessary in these scenarios.

It will be advantageous, however, if it can be used to reduce the costs. An obvious application is when there is a need to switch a large bitstream, 10 Gbit/s say, for rerouting or protection switching purposes. A less obvious but in many ways more interesting application is packet switching on a granular level like e. g. ATM. If a low cost electrically (or optically) controlled variable delay optical memory could be developed this could be very attractive.

Another option is a space switch based on free space optical propagation that takes advantage of the fact that optical beams can cross without disturbing each other. Such a switch consisting of an array of optical transmitters facing an array of receivers with individual beam steering and focusing for each transmitter could, at least in principle,

be made very compact. Assuming diffraction limited focusing and limiting the deflection angle to about 0.25 radians the side of the square arrays has to exceed about ten times the product of the wavelength, λ, and the number of pixels, N. Thus using diffractive liquid crystal microoptics for deflection a 1000x1000 switch (N = 1000) using $\lambda = 1$ μm could be built in form of a 4 cm long bar with 1 cm square end facets incorporating the arrays. Each pixel would have a diameter of about 320 μm and could readily be connected to a fiber as well as to an LED or a detector. Since the response time of liquid crystals will probably be limited to the order of 100 nanoseconds such a switch can probably only be used for circuit switching or fairly slow package switching, however.

If used for granular switching with 100 Mbit/s in each subscriber channel such a switch could handle a throughput of 100 Gbit/s and it might well be competitive with an electronic switch even if electronics would still be needed for the demultiplexing/multiplexing from and back to the connecting high bitrate, of order 10 Gbit/s, optical TDM signal format that is needed in order to use the fiber efficiently. With a moderate power consumption of 10 mW per transmitter pixel the total switching power consumption would be only 10 W. It is interesting to compare this with an electronic three stage Clos switch of the same size. The gate count would in this case be about $2 \cdot 10^5$ and the switching power consumption 20 W assuming 10^{-4} W/gate as above. Additional power would in both cases be required for multiplexing, demultiplexing, control functions etc. but probably more so for the electronic switch due to the power consumption associated with the many internal interconnections. Note, however, that a working electrically steerable deflection system based on liquid crystal diffractive optics remains to be demonstrated.

6. A vision of future high capacity broadband networks.

With my own scientific background in basic electron physics, microwave engineering and quantum optics I am inclined to be optimistic about the future development of electronic and optical devices. We are still very far from the fundamental limits, indeed. The present switching energy of about 1 pJ per gate is thus many orders of magnitude larger than the fundamental limit of about 20 kT $\approx 10^{-19}$ J at room temperature. Also, requiring say 20 photons per bit in a photonic device, the energy per bit at $\lambda = 1$ μm would be $40 \cdot 10^{-19}$ J, i. e. 40 times higher than the electronic limit but still very low.

In view of this and the cost estimates above I believe it may become cost effective to build a broadband network with a very high capacity such that the average load at peak traffic is well below capacity at all points in the network. Under such conditions the switching nodes could have a very simple standardised structure with essentially no internal intelligence and with buffering only for synchronisation. Since bandwidth would be cheap simple circuit switching may be advantageous. If so, the free space optical switch mentioned in section 5 may be competitive. Most of the control and routing functions would be taken over by the subscriber intelligent terminals as described in the end of section 4.

For example, if a link in the network is broken each terminal using that link will detect the interruption and set up a new connection using an altogether different path. In that way all traffic will be removed from the faulty link and re-established along new paths within a time not much larger than the signalling round trip time between the subscribers.

The "road map" of the network could be stored in each terminal and could be updated from a central data base perhaps broadcasting information to all terminals continuously.

Subscribers needing sophisticated control and security functions could either use specially equipped terminals or rely on specialised independent service providers connected to the network.

Such a network would, in many ways, be analogous to a road network where the control and routing are left to the individual car driver while a traditional network with centralised intelligence and control is more like a railroad system.
Much more could of course be said in this context but since the real truth is hardly available I will conclude this paper by formulating some questions of possible strategic importance for the research aimed at photonic switching.

Can electronics provide the switching capacity desired within the foreseeable future?
If the answer is yes;

Can photonic switching still have a cost advantage?
Personally I doubt it, possibly making exceptions for free space switches and switches using yet unexplored phenomena.

Can such phenomena be identified today?
Devices using coherent mesoscopic quantum interaction between light and matter may be among the candidates.

Are there other applications for photonic switching than in telecommunication networks?
Why not in future computers? Today we don't even know the algorithms to perform the advanced speech understanding and image recognition that is needed to make full use of information technology and it may well be that photonic switching of interconnects within a computer structure will be needed.

Wednesday, March 15, 1995

Optical Interconnect

PWC 11:15 am-12:00 pm
Red Lion East

Tom Cloonan, *Presider*
AT&T Bell Laboratories

Optical Interconnection Technology for Large Computing and Switching Systems

Niloy K. Dutta
AT&T Bell Laboratories
Room 6E-414, 600 Mountain Avenue
Murray Hill, NJ 07974

This talk will focus on current applications and future directions of optical interconnection technology. This technology will be initially driven by applications in large computing and switching systems. Advances in system architectures, subsystem modules and optoelectronic integrated circuits aimed at lower cost implementation of the entire system are necessary to create a wide application base for optical interconnection technology.

8 x 8 Array of optoelectronic switching nodes comprised of flip-chip-solder-bonded MQW modulators on silicon CMOS circuitry

A. L. Lentine[1], K. W. Goossen[2], J. A. Walker[2], L. M. F. Chirovsky[3], L. A. D'Asaro[3], S. P. Hui[3], B. T. Tseng[3], R. E. Leibenguth[4], D. P. Kossives[3], D. W. Dahringer[3], and D. A. B. Miller[2]

AT&T Bell Laboratories

[1]Naperville IL 60566, [2]Holmdel NJ 07733, [3]Murray Hill NJ 07974, [4]Breinigsville PA 18031

One approach to improving the performance of large processing or telecommunications switching systems is to interconnect integrated circuits using optics. Smart pixels, with integrated optical detectors, modulators, and electronic logic, could potentially be used in these systems. The FET-SEED, consisting of the monolithic integration of multiple quantum well (MQW) optical modulators and detectors with GaAs field effect transistors, is one design platform for these smart pixels [1,2]. Another potential design platform uses the hybrid integration of MQW modulators and detectors with commercial electronic circuits [3-7]. This latter approach allows one to design circuits with greater complexity and circuit yield, because it uses available established VLSI processes.

We describe an 8 x 8 array of smart pixels, designed and fabricated using MQW modulators and detectors flip-chip-solder-bonded to a silicon CMOS circuit. The modulators were designed for 850 nm operation and the substrate was removed to avoid excess absorption in the substrate [5,7]. The individual circuits implement embedded control switching nodes. Thirty-one of the 64 nodes functioned correctly at low speeds and the center 4 x 5 array of the nodes operated at 250 Mb/s without readjusting individual bias voltages.

The CMOS circuit shown in Fig. 1 is functionally similar to switching nodes previously made using the monolithic FET-SEED technology [8]. The circuits used two different receiver designs, with different designs placed in alternating columns of the array. The first receivers consisted of a pair of series connected MQW diodes, with their center tap connected to the input of an inverter. The second receivers were similar except that the center tap was also connected to a pair of clamps [8]. These clamps were implemented with a pair of transistors (not diodes) with the gate connected to drain [9]. The control memory was designed using a standard static random access memory cell and the 2:1 multiplexer was designed using pass gates [10]. An inverter on the output of the multiplexer drove the output modulators.

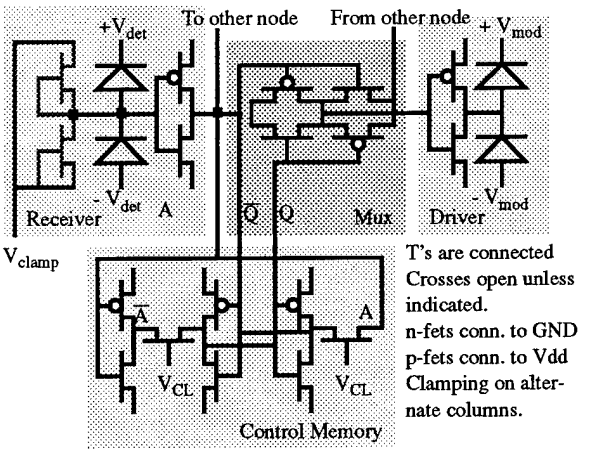

Fig. 1 Schematic diagram of embedded control 2 x 1 nodes

The circuit was designed using MAGIC and fabricated using Hewlett-Packard's 1.2 μm CMOS obtained through the MOSIS service. The center to center spacing of the nodes was 135 μm x 120 μm. The solder bond sizes and optical window sizes were 15 μm x 15 μm with a minimum space between two solder bonds of 15 μm.

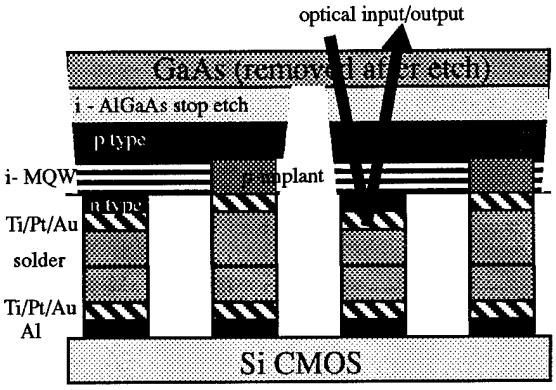

Fig. 2 Structure showing two MQW diodes bonded to Si CMOS before substrate removal

The MQW modulator was made using processes similar to the monolithic FET-SEED [2]. The layer structure consisted of 95 periods of 9 nm GaAs quantum wells with 3.5nm $Al_{0.3}Ga_{0.7}As$ barriers. Additional steps to the process included a deep mesa etch between diodes and the deposition of solder on the pads.

After receiving the CMOS chips from MOSIS, additional metal layers (Ti, Pt, Au) and solder were deposited on the solder bump pads. After the GaAs chip was bonded to it, the substrate was removed, and the device was packaged and antireflection coated [7]. A diagram and photograph of the bonded chip are shown in Figs. 2 and 3. The total height of the front of the modulator from the surface of the CMOS chip is ~ 10 μm

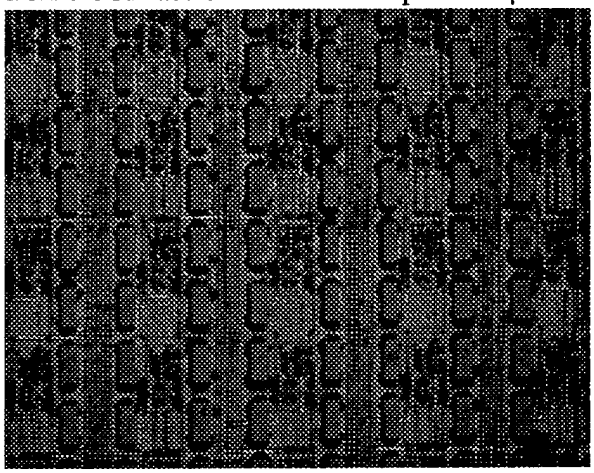

Fig. 3 Photograph of a section of the array. Rectangles are the individual mesas which measure ~ 20 μm x 50 μm.

All testing was done sequentially, one node at a time. Initially, a pair of low power (a few μW) optical signals were focussed onto the input detectors. A low power read beam, split into two by a binary phase grating, was focussed onto the output detectors. The optical signals were generated using diode lasers with wavelengths between 848 and 852 nm. The modulator bias voltages were -5V and 10V, so that the voltage across the modulators varied between 5 and 10V. Providing an offset like this gives less loss in the high reflectivity state. The detectors were biased at 0 and 5V, the clamp voltage was 2V and V_{dd} was 5V. The inputs were switched by alternately blocking each of the two signals. The outputs were checked for visible modulation for each of the two inputs to a particular node. In all of the clamped receivers, the low power optical signals could not set the control memories unless the clamping voltage was adjusted. This is a result of the receiver not being able to supply enough current to change the static RAM cell. Had we designed the input of the static RAM cell with a dual gate FET to ground [8], this would not have been a problem. When the power was increased in the high speed measurements, we could set the state of the control memory without any voltage readjustments.

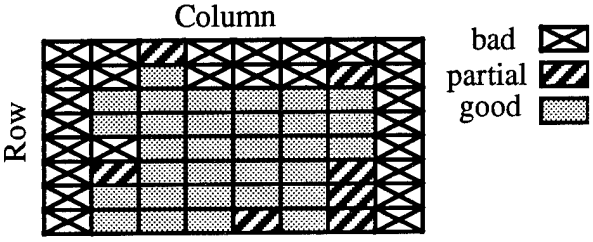

Fig. 4 Diagram of operating nodes as a function of spatial position across the array. Partially working nodes typically had one modulator operating per differential pair

In Fig. 4., we show a plot of which nodes had full functionality at low speed. The first and last columns were missing modulators and detectors due to some of the etchent attacking the modulators from the sides. Other inoperable pixels near the edge of the array also had partially removed modulators.

Next, high speed testing was done on this center 4 x 5 array by current modulating the two input laser diodes with complementary sets of non-return to zero (NRZ) data from a digital word generator. For the unclamped receiver, the detector voltages were set at 0 and 2 volts. For the clamped receiver, the clamping voltage was set at 2V and the detector voltages were set to +/- 10V. One column was tested for full functionality (i. e. both memory states), the others were tested in only one path except for spot testing.

Fig 5 shows the reflected outputs from one of the modulators for the center 4 x 5 array. All devices operated at 250 Mb/s (2 devices barely) with average photocurrents of 60uA (240 fC). However, the power (energy) was ~150 uW ave (600 fJ) for the clamped receiver and 400-500 uW ave (1.6-2.0 pJ) for the unclamped receiver because of the lower responsivity. The current required is about the same for clamped and unclamped cases, (i. e. the swing in each case is

about the same) but the higher responsivity helps in the clamped case. Individual devices would work with about 1/2 of these energies if voltages and powers are carefully tweaked, but it was difficult to do the whole array at lower powers.

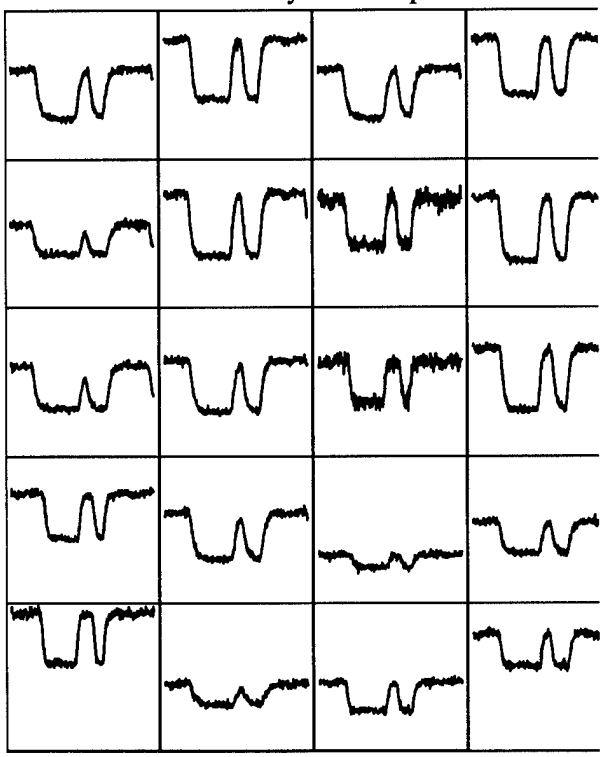

Fig. 5 Detected oscilloscope outputs from one modulator from each 2 x 1 switching node in the center 4 x 5 section of the array at a data rate of 250 Mb/s. The 8 bit repetitive input data pattern was '0 0 0 1 0 1 1 1'

There is some variation of the modulator performance across the array. We think the reason for this that an imperfect antireflection coating allowed a low-finesse Fabry-Perot resonance to exist. The thickness variation across the array caused by the substrate removal caused changes in the wavelength of the Fabry-Perot resonance, which in turn causes the observed changes in the reflectivities. Also, the reflectivity of the metal on the top of the modulators when illuminated from the back side is estimated to be only about 40%.

In conclusion we have designed, built, and tested an 8 x 8 array of embedded control 2 x 1 nodes. The device array was made by flip-chip-solder bonding of MQW optical modulators and detectors onto a silicon CMOS integrated circuit. Approximately one half of the array was operational and the center 4 x 5 section was operated at 250 Mb/s. It is important to note that this is a first demonstration of this technology applied to smart pixels. Therefore, although the performance of this chip is not quite up to that of the monolithic technology [8], simulations with improved receiver and circuit designs show much better capabilities. We expect rapid progress in this area to continue.

This work was partially sponsored by ARPA under Air Force Rome Laboratories contract number F 30602-93-C-0166.

1. D. A. B. Miller, M. D. Feuer, T. Y. Chang, S. C. Shunk, J. E. Henry, D. J. Burrows, D. S. Chemla, "Field-effect transistor self-electrooptic effect device: integrated photodiode, quantum well modulator and transistor", IEEE Photonics Tech. Lett., **1** 61-64 (1989).

2. L. A. D'Asaro, L. M. F. Chirovsky, E. J. Laskowski, S. S. Pei, T. K. Woodward, A. L. Lentine, R. E. Leibenguth, M. W. Focht, J. M. Freund, G. D. Guth, and L. E. Smith, "Batch fabrication and operation of GaAs-AlGaAs field effect transistor self electro-optic effect device (FET-SEEDs) smart pixel arrays," IEEE J. Quantum Electron., **29** 670-677 (1993).

3. J. Wieland, H. Melchoir, M. Q. Kearly, C. Morris, A. J. Mosley, M. G. Goodwin, and R. C. Goodfellow, "Optical receiver array in silicon bipolar technology with self aligned, low parasitic III-V detectors for DC-1Gb/s parallel data links," Electron. Lett., **27** 2211 (1991)

4. C. Camperi-Ginestet, M. Hargis, N. Jokerst, and M. Allen, "Alignable epitaxial lift-off of GaAs materials with selective deposition using polyimide diaphrams," IEEE Photon. Technol. Lett., **3** 1123 (1991)

5. K. W. Goossen, J. E. Cunningham and W. Y. Jan, "GaAs 850nm modulators solder-bonded to silicon," IEEE Photon. Technol. Lett **5** 776 (1993)

6. D. J. Goodwill, F. A. P. Tooley, A. C. Walker, M. R. Taghizadeh, M. McElhinney, F. Pottier, C. R. Stanley, D. G. Vass, I. Underwood, M. W. G. Snook, M. H. Dunn, J. Hong and B. D. Sinclair, "InGaAs S-SEEDs and silicon CMOS smart pixels for 1047-1064 operation," 1993 Topical meeting on Smart Pixels, p 20-21 (1994)

7. K. W. Goossen, J. A. Walker, L. A. D'Asaro, S. P. Hui, B. Tseng, R. Leibenguth, D. Kossives, L. M. F. Chirovsky, A. L. Lentine, and D. A. B. Miller, "GaAs MQW Modulators integrated with silicon CMOS," submitted to IEEE Photon. Technol. Lett and IEEE LEOS Annual Meeting, postdeadline papers (1994).

8.A. L. Lentine, R. A. Novotny, T. J. Cloonan, L. M. F. Chirovsky, L. A. D'Asaro, G. Livescu, S. Hui, M. W. Focht, J. M. Freund, G. D. Guth, R. E. Leibenguth, K. G. Glogovsky, T. K. Woodward, "4 x 4 arrays of FET-SEED embedded control 2 x 1 optoelectronic switching nodes with electrical fan-out," IEEE Photon. Technol. Lett. **6** 1126-1129 (1994)

9. D. A. Jared and K. M. Johnson, "Optically addressed zero-crossing edge detection spatial light modulator," Topical Meeting on Spatial Light Modulators pp. 66-68 (1993)

10. N. H. E. Weste and K. Eshraghian, Principles of CMOS VLSI design Addison-Wesley (1993)

Wednesday, March 15, 1995

Transport Network Switching and Routing: 1

PWD 1:30 pm-3:00 pm
Red Lion East

Dan Blumenthal, *Presider*
Georgia Institute of Technology

The RACE Multi-Wavelength Transport Network Project: Results and Conclusions

Goff Hill

BT Research Laboratories, Martlesham Heath, Suffolk, IP5 7RE, UK

Tel: +44 473 642219
E-mail: hill_g_r@bt-web.bt.co.uk

Introduction

The RACE Multi-Wavelength Transport Network project (MWTN) began in January 1992 with 10 partners including operators, manufacturers and universities (Fig. 1) with completion scheduled for December 1995. The overall goals are to demonstrate the feasibility of an optical network layer that is transparent to signal bit rate and format and to identify evolutionary routes and standards. From an operators viewpoint, these attractive features will provide increased flexibility to carry a wide range of future services. The network approach is based on wavelength routing and uses optical amplifiers, WDM transmission and space switching [1,2]. The project has three key themes: the development of preferred technologies, practical demonstrations of multi-wavelength networking and the application of design and evaluation tools to support the technology development and demonstration activities.

Principle of MWTN

An MWTN node allows WDM signals to be processed either as a multiplex or as individual channels. In particular, it provides wavelength add-drop and cross-connect functions that are controlled by a management system. Many component and node configuration options are possible using the basic elements of optical amplifiers, wavelength multiplexers and space switches. In the configuration chosen for the MWTN demonstrations (Fig 2), four principle sub-systems are implemented: a line sub-system with optical amplifiers, a transmission sub-system with wavelength switchable sources, a switching sub-system and a management sub-system.

Fibres entering an MWTN node carry multiple wavelength signals. The wavelengths are first amplified, then demultiplexed and routed via a space switch array, either to outgoing fibres or dropped to local receivers. Locally generated signals can be introduced via the space switches and can be multiplexed with other "local" or "through" signals. The practical work in MWTN is based on 4 coarse wavebands in the erbium fibre window, each capable of carrying 4 fine grain channels spaced at 10 GHz, but the wavelength plan allows for twice this number.

Project Review

The first year of the project concentrated on developing a comprehensive specification for the experimental demonstrator, initiating component development programmes and developing sub-system test beds, whilst the second year saw the assembly, testing and integration of the line transmission and control and management sub-systems for the "mid-term demonstrator". This first demonstrator became operational at BT Laboratories in September 1993 and a managed network node was then demonstrated in January 1994,. A second node was built into BT's "Innovation '94" exhibition as the "network of the future carrying services of the

future". The possibility of upgrading the network using fine grain WDM was also demonstrated using both coherent and direct detection techniques.

The third year continued the development of technologies [3] and experimental demonstrators. For example, packaged indium phosphide 4 x 4 gate array switches were incorporated into the experimental test bed. The two nodes were shipped to Sweden where they were upgraded with the more recently developed components and have been integrated with a TMN (Telecommunications Management Network) management system with full Q3 interface[4]. The third year "final demonstrations" staged in the Stockholm Gigabit Network showed service configuration and network protection applications. The two nodes were sited at physically separate locations and controlled via an X25 packet network. Further demonstrations are planned in both UK and Sweden during 1995.

The experimental activity is supported by a substantial theoretical and modelling studies programme. Physical models are used in demonstrator design and to predict possible network dimensions. The modelling has shown that the maximum practical network dimensions are strongly influenced by noise build-up and the losses in a node. This in turn depends on the chosen architecture and the component performance. For example a switch loss of 12dB will limit the network size to between 10 and 20 nodes at a bit rate of 2.5Gb/s whereas a loss of 1dB pushes the noise limiting performance up to over 100 nodes. However other factors such as cross talk, dispersion and non-linear transmission may reduce this range.

Some of the project achievements include:
- development of a wide range of WDM and switching components
- a series of successful managed network demonstrations
- development of modelling tools for design and evaluation
- development of standards for layered network architecture and wavelength allocation

Conclusions

Since the start of this project optical amplifiers have been deployed in transmission systems and long distance operators are beginning to make commitments to use WDM. Opto-mechanical space switches are now commercially available and seem likely to be used in applications such as flexibility frames and network protection. MWTN represents the next step. The technology developments, demonstrations and analyses made in this project all suggest that wavelength routing is feasible and should be considered as a medium term technology rather than something for the long term.

References

[1] G R Hill et al, "A transport layer based on optical network elements", IEEE Journal of Lightwave Technology, May, 1993

[2] P J Chidgey, "Multi-wavelength transport networks", IEEE Communications, Vol. 32, No 12, Dec., 1994

[3] P Granestrand et al, "Integrated photonics for optical networks", Ericsson Review, No 3, 1994

[4] S Johansson et al, "An optical transport network layer - concept and demonstrator", Ericsson Review, No 3, 1994

[5] J Zhou et al, "Power management system design modelling of optical multi-wavelength transport networks", Globecom '94, San Francisco

BT Laboratories	**Ericsson Telecom AB**	**Telia AB/Ellemtel**
Ericsson Telecommunicazione	**Pirelli Cavi SPA**	**Italtel**
CSELT	**CNET**	
University of Essex	**University of Paderborn**	

Fig. 1 The MWTN project partners

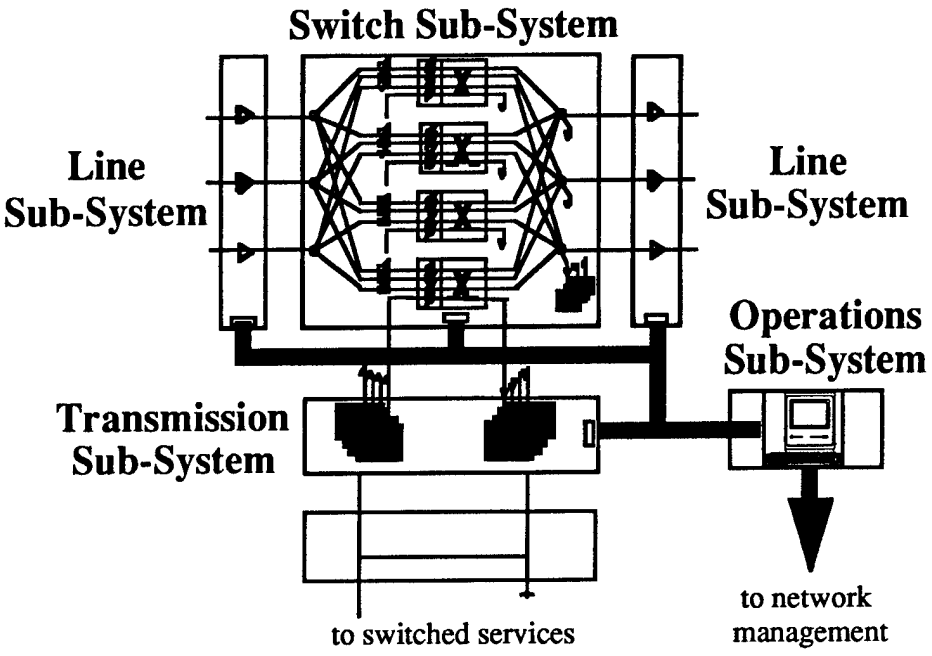

Fig 2 The MWTN Node Architecture

Telecom Networks Going Photonic: Reconciling Transparency with Scalability

Philip DUMORTIER, Thierry VAN LANDEGEM
Alcatel Corporate Research Center, Antwerp
F. Wellesplein 1, B-2018 Antwerpen, Belgium

Francesco MASETTI, Michel SOTOM
Alcatel Corporate Research Center, Marcoussis
route de Nozay, F-91460 Marcoussis, France

Introduction

The introduction of Wavelength Division Multiplexing (WDM) techniques into fiber networks opens perspectives for a global transparent optical telecommunication backbone. One of the most promising features of optical telecommunications is to provide a common infrastructure which could become an integration factor in a heterogenous but interconnected network environment. Furthermore optics can provide a degree of network transparency to bitrate, transfer mode and signal format of the transported signals. By using transparent optical crossconnect nodes, based on space and wavelength routing, a rearrangeble network topology can be achieved. Local exchanges could, in principle, be connected directly to each other through end-to-end transparent optical paths.

The future network needs to be centered around the idea of a trade-off between bandwidth and simplicity favouring easier management and operations. In particular simpler software structures are only possible if the basic hardware infrastructure becomes simultaneously simpler and articulated in a reduced number of hierarchical and administrative planes. Nevertheless, to attain a full-meshed interconnection, a relatively large number of wavelength channels is required between two nodes, growing rapidly to unrealistic numbers. Therefore, in order to achieve a more scalable network architecture, it is necessary to improve the routing granularity, without compromising too much the optical transparency and network simplicity.

The architecture proposed introduces the required granularity by dividing the network in overlapping partitions [1]. The time-domain is only accessed at the border of two partitions or of the network, through time-slotted optical crossconnect nodes : transparent optical paths are terminated here and new ones created. These nodes break the continuity of the signal transparent optical paths, and are therefore called 'hopping nodes', referring to the possibility for a time-slot to migrate from one transparent optical path to another (multihop routing, fig.1.b., as opposed to single hop routing, fig.1.a.). By equipping a hopping node with both transparent and time-slotted optical crossconnects, end-to-end optical paths can still be provided.

Network nodes

Three main node types eventually persist in the core network [2]: transparent optical crossconnects, time-slotted optical crossconnects and time-slotted optical switches (fig.1). Each of them operate in a distinct transport network sublayer [3,4,5]: the Transparent Path, the Virtual Path and the Virtual Circuit Sublayer respectively (fig.2).

Transparent optical crossconnect [6,7,8]

This transport node operates in the path layer and configures according to demand the core network by routing transparent optical paths through semi-permanent connections. It provides connections between any input/output ports, as well as bridging and multicasting capabilities, all in strictly non-blocking mode. This means that there is always a unique and straightforward way to establish any connection independently of the configuration status of the crossconnection fabric, in contrast with a rearrangeble non-blocking fabric which would need wavelength reallocation of the already set channels. Disruptions are thus avoided when

reconfigurations are needed to meet traffic changes. No specific configuration algorithm is needed to establish any set of connections at the node level and congestion matters which have to be addressed at the network level can be solved by considering only the availability of link transmission resources. Optical paths are created by exploiting both wavelength and space domain; to get higher flexibility, wavelength is assigned and reused on per link basis; therefore wavelength is seen as a transport resource and has no end to end significance. A practical consequence is that wavelength conversion is needed at the optical crossconnect. The exploitation of all-optical wavelength-conversion and space-division-switching grants this node a high level of transparency to accommodate a wide range of digital signals with different frame formats, coding schemes or bitrates.

Time-slotted optical crossconnect [9,10]
This routing system also operates in the path layer and provides the same functionalities of transparent optical crossconnects. Differences arise from the fact that it deals with time-slotted rather than transparent optical paths to provide the path layer with finer granularity. Time-slots are fixed-length packets, statistically but synchronously multiplexed. Consequently, the crossconnection fabric is operated synchronously and reconfigured on a time-slot basis. As a result of statistical multiplexing, collision may occur between packets with the same destination. Contention can be resolved either by optical buffering through fiber delay lines, or by expansion in the wavelength domain. Because dealing with transparent or virtual paths translates into different functional requirements, a distinction has to be made between the two kinds of crossconnects but it should be understood that some nodes of the core network could be equipped with both. Optical crossconnects capable of handling both transfer modes simultaneously in an arbitrary mix might be envisaged as well.

Time-slotted (optical) switch [10,11]
This type of node is necessary to handle end-to-end connections. It is located in the core network at the boundary with the access network, which provides customer traffic concentration and multiplexing. This node handles the ATM traffic generated by customers. It will eventually be completely implemented in optics, but a substantial amount of electronics will remain in the short term, to perform complex functionalities usually required, such as traffic concentration, multiplexing and bitrate increase, header processing.

Evolution scenario: gradual introduction of optics
The transport network building blocks will gradually be upgraded following state-of-the-art technology, but a basically non-hierarchical network architecture will remain throughout this evolution.
In the short term, a core optical network is constructed using transparent optical crossconnects only. While the number of network nodes grows, the interconnection matrix will become more complex, and soon a full-meshed node interconnection will not be achievable anymore with the number of wavelength channels available with state-of-the-art technology. Partitioning of the core network then becomes mandatory, and thus also hopping between network partitions, thereby accessing the time domain. It should be observed that still a limited number of end-to-end transparent optical channels can be maintained, which cross partition boundaries without interference.
Despite the fact that *optical* time-slotted crossconnects may not be available by that time, hopping can already be achieved *electrically* at the border of the core network, by utilising larger switching fabrics with additional capacity and functionality in the local exchanges (LEX, fig.1.c., 2.c.). This scenario preserves the optical integrity of the inner-core. In a later stage, *optical* time-slotted crossconnects can replace the *electrical* ones, enabling all-optical hopping. These *optical* time-slotted crossconnects could either remain located at the core network border, or can be embedded inside the core network. Considering the current trend towards photonisation of the access network (PONs, optical distribution networks,...), the ultimate customer-to-customer optical transport will eventually be achieved when also the switching function in local exchanges (LEX) becomes completely optical, including processing at the interfaces.

Conclusion
A simple yet flexible high-capacity network architecture is proposed, featuring a reasonable degree of signal transparency through the availability of transparent end-to-end channels, while still ensuring scalability through a fine routing granularity between network partitions. Early partitioning is possible with electro-optical rather than photonic technology, ensuring scalability throughout the process of network photonisation.

References

[1] Hac A., "Improving Reliability Through Architecture Partitioning in Telecommunication Networks", IEEE Journal on Selected Areas in Communications, vol. 12, no. 1, Jan. 1994, pp. 193-204.

[2] Fioretti A., Masetti M., Sotom M, "Transparent Routing: The Enabling Factor Towards All-Optical Networking", Proc.ECOC'94, Florence, Italy, Sep.1994.

[3] CCITT, "Architectures of Transport Network Based on the Synchronous Digital Hierarchy (SDH)", Draft Recommendation G.803, CCITT Meeting Report R-106 (WP XVIII), June 1992.

[4] Sato K.I., Okamoto S., Hadama H., "Network Performance and Integrity Enhancement with Optical Path Layer Technologies", IEEE Journal on Selected Areas in Communications, vol. 12, no. 1, Jan. 1994, pp. 159-170.

[5] Buckley J.F., "Switching and Service Delivery in Futuristic Networks", BT Technology Journal, vol. 11, no. 4, Oct. 1993, pp. 64-72.

[6] Pontallier C., "TMN and New Network Architectures", IEEE Communications Magazine, Apr. 1993, pp. 84-88.

[7] Sotom M., Jourdan A., Perrier P.A., Berthelon L., "Photonic Network and Node Architectures for a Flexible Multigigabit Transport Network", Proc. ICC '93 Workshop on Challenges of All-Optical Networks, Geneva, Switzerland, May 1993, pap. 2.

[8] Jourdan A., Soulage G., Clesca B., Sotom M., Da Laura G., Beylat J.L., Doussiere P., Gurib S., Vinchant J.F., "All Optical Crossconnect for Transparent Multiwavelength Transport Networks", Proc. ECOC '94, Florence, Italy, Sep. 1994.

[9] Boettle D., Eilenberger G., Loesch K., Rehm W., Schilling M., Wunstel K., "System Approach for a Photonic Multidimensional Switching Technique", Proc. ICC '93, Geneva, Switzerland, May 1993, pp. 1220-1224.

[10] Gabriagues J.M., Jacob J.B., "Photonic ATM Switching Matrix Based on Wavelength Routing", Proc. Topical Meeting on Photonic Switching, Minsk, Belarus, July 1992, pap. 2H2.

[11] Chiaroni D., Gavignet-Marin, Perrier P.A., Ruggeri S., Gauchard S., De Bouard D., Jacquinot J.C., Chauzat J., Jacquet J., Doussiere P., Monnot M., Grard E., Leclerc D., Sotom M., Gabriagues J.M., Benoit J., Jacob J.B., "Rack-Mounted 2.5 Gbit/s ATM Photonic Switch Demonstrator", Proc. ECOC '93, Montreux, Switzerland, Sep. 1993, postdead. pap. ThP12.7.

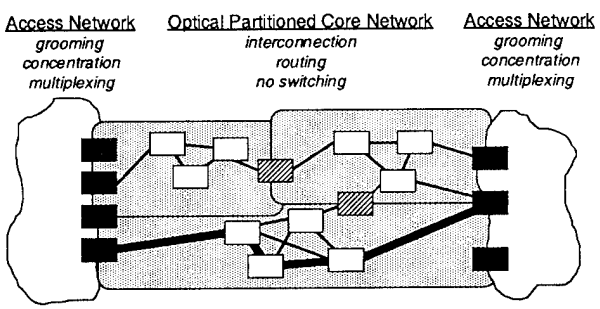

1.a. Single hop routing

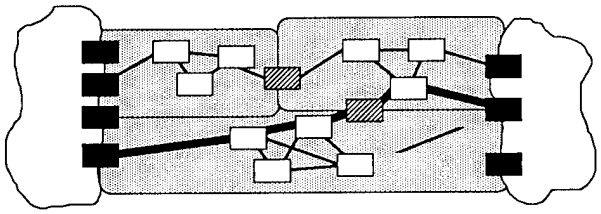

1.b. Multi hop routing (over optical time-slotted crossconnect)

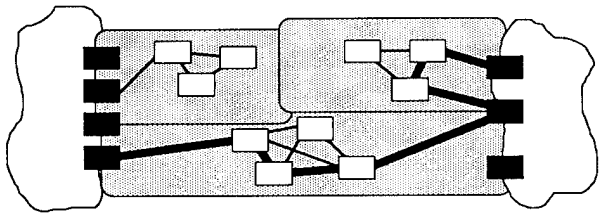

1.c. Multihop routing (over electrical time-slotted crossconnect in LEX)

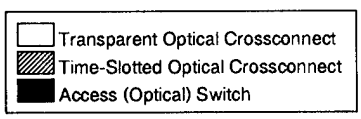

Fig.1 Optical transport network architecture

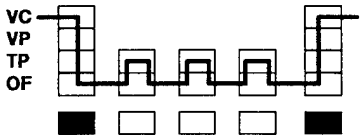

2.a. Single hop routing

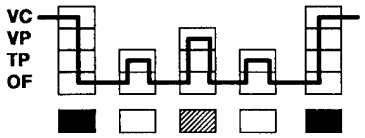

2.b. Multihop routing (over optical time-slotted crossconnect)

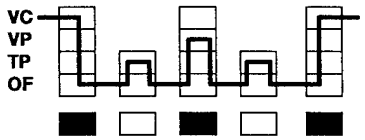

2.c. Multihop routing (over electrical time-slotted crossconnect in LEX)

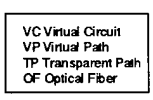

Fig.2 Layered structure of the transport network

OFDM cross-connect with an embedded free-space switch

B.Kuhlow; G.Teich; G.Walf

Heinrich-Hertz-Institut für Nachrichtentechnik GmbH

D-10587 Berlin, Einsteinufer 37

Fax: +049 30 31002 250, Tel: +049 30 31002 215, E-mail: Ferstl@hhi.de

Introduction

The underlying node model of the cross-connect is sketched in Fig. 1. Eight incoming fibers each supporting 16 densely multiplexed frequencies can be routed arbitrarily to 16 frequencies carried on each of eight outgoing fibers. After power splitting of an incoming OFDM signal, tunable frequency selective receivers select a prescribed OFDM channel using the circuit switched mode. Due to their high selectivity the tunable heterodyne receivers provide the required signal demultiplexing function and in turn a reordering function. Conceptually, switching is performed in the space domain by electrical space switching stages with free-space interconnects between them. The choice of 1.5 µm for the wavelength is suitable for an optical transparent network, where the electronic switches will be replaced by optical switches in a further step of development.

Free-space switch

In order to investigate free-space operation capabilities [1] an experimental demonstrator has been realized, Fig. 2. The complete space switching fabric (data array size 16x16) is designed as a compact 3D microsystem containing several space switching stages interconnected with arbitrary but fixed interstage patterns. Thus, multistage operation is required for strict non-blocking operation. Driven by practical aspects, the space switching stages are designed as a cube consisting of 16 stacked switching planes. Each of these carries signal regeneration circuitries as well as lasers [2] and photo diodes for 16 links. The performance of the free-space system has been explored using a limited number of representative signal paths. Packaging tolerances may cause beam spot displacements on the photo diodes with a reduction in beam power. In order to overcome this difficulty, a low capacitance (< 0.8 pF) MSM-photo detector has been used with a large sensitive area of 350 µm in diameter [3]. Despite the application of these photo diodes as well as non-optimized electronics a maximum bit rate of > 622 Mb/s per link could be achieved. As a result, the total aggregated throughput of the 16x16 fabric amounts to >150 Gb/s.

Holographical optical elements (HOE) were used for the free-space interconnects. They met best the demands of flexible interconnection schemes in a compact system at high efficiency. Computer generated holograms in the form of Fresnel zone lenses (FZL) for collimating and focusing of light were combined with volume gratings optically recorded in dichromated gelatin (DCG) utilized as deflection elements. The individual holograms are each 2 mm in diameter, which corresponds to the lateral spacing of the IO-ports in the space switching stages, [4]. 16x16 arrays of FZL have been fabricated as "binary optical elements" in quartz glass, [5,6]. The surface profiles in each zone of the lenses have been approximated by a stepped profile up to 32 levels. Volume phase holograms in DCG proved to be very suitable to achieve large deflection angles in combination with high efficiency [7]. A two layer anti-reflection coating was deposited on all holographic elements. The used FZL as well as deflection elements showed efficiencies of >80 %. The measured transmission loss in the complete HOE interconnection stage was lower than 6 dB and a crosstalk of less than -23 dB could be estimated.

Frequency stage

The frequency stage consists of two blocks. At the input side there is a passive 1 to N optical coupler distributing the incoming signal to N frequency selective receivers. At the output side

the block consists of N transmitters and a network recombining their signals for onward transmission on one fiber. For demonstration purposes the frequency stage was realized for one incoming fiber and for 4 optical channels. The signals are frequency modulated with a bit rate of 140 Mbit/s (CMI line coded). A frequency shift of 2.4 GHz was chosen to avoid a high sensitivity penalty due to the relatively large linewidth of the available lasers (10 to 40 MHz). The spacing in optical frequency amounts to 9 GHz. To test the performance for a larger number of incoming signals a 10 channel OFDM signal is fed to the frequency stage. Tunable fully engineered, balanced, heterodyne polarization diversity receivers are key elements of the frequency stage. During the last years DFB and tunable lasers have become available, which have linewidth less than 10 MHz. This enables different detection schemes. Now a delay-line frequency discriminator can be used for data detection. Additionally the sensitivity can be improved by using the orthogonal Manchester code. With the implementation of the above laser and coders the sensitivity was improved essentially, Fig. 3. Thus, the system can be operated with a system loss > 50 dB without any optical amplification or any repeater.

The block diagram of the realized receivers is depicted in Fig. 4. The incoming signals are superimposed with the light of the tunable local laser in a 3 dB coupler of an optical all fiber polarization diversity front-end. To avoid a polarization fading the superimposed signals are separated in two orthogonal states of polarization and fed to two balanced receivers, one for each state of polarization. The LO is a tunable TTG-Laser [8] with a typical tuning range of 500 GHz. Microwave circuits for the IF processing are realized by employing surface mounted components on standard glass epoxy printed circuit boards. The sensitivity of the receivers is better than -48 dBm (BER=10^{-9}, PRBS=2^{23}-1). Each receiver is equipped with a microprocessor to perform the supervision of the status of the LO-laser and to perform the switching operation. The switching time between two optical channels amounts to less than 5 ms. Besides coherent receivers, direct detection receivers with tunable filters and optical amplifiers were investigated. Their sensitivity was comparable but their tuning speed was with 800 ms much slower than in the case of coherent receivers.

At the output side of the frequency stage 4 transmitter lasers are FSK modulated and their signal is fed via a 8 to 1 coupler to the output fiber. To avoid interference between different channels and to guarantee fast channel selection at the receiver side, frequency monitoring and controlling of each transmitted signal is inevitable. Therefore one channel is stabilized absolutely and all other channels are stabilized relative to this channel, [9].

Conclusion

Key components of a dense OFDM cross-connect have been developed as a first step to exploit the inherent parallelism of optics for telecommunication purposes. In order to prove 1.5 µm system operation from the practical point of view, an experimental demonstrator has been built. It can be concluded that free-space interconnects designed for the long wavelength range are a viable alternative to meet the bulk of connectivity demands in conventional and future switching networks. In addition, a frequency stage with tunable coherent polarization diversity receivers was developed and stable operation of the frequency stage was demonstrated.

References

[1] E. Dietrich et al.: ECOC 1994, pp. 293-296
[2] W. Pittroff: Annual report Ferdinand-Braun-Institut, 1992/93, Chapter 5.2
[3] F. Hieronymi et al.: IEEE Photonics Technology Letters,`93, Vol. 5, No. 8, pp. 910-913
[4] B. Kuhlow et al.: SPIE Proc., 1992, Vol. 1751, pp. 66-75
[5] M. Ferstl. et al.: SPIE Proc., 1993, Vol. 1992, pp. 90-101
[6] E.Pawlowski et al.: Optical Engineering 33, 1994, pp. 647-652
[7] H. Kobolla: Journ. Mod. Optics, Vol. 41, No.1, 1994, pp. 19-29
[8] M. Amann: ECOC 1990, paper Tu F1.1
[9] U. Hilbk et al.: EFOC/LAN 1992, Paris, p 32

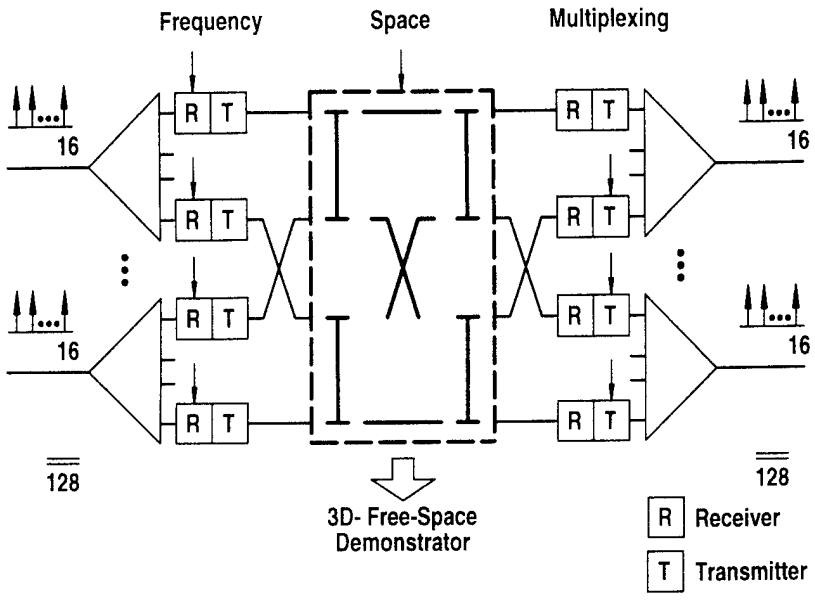

Fig. 1: Experimental switch

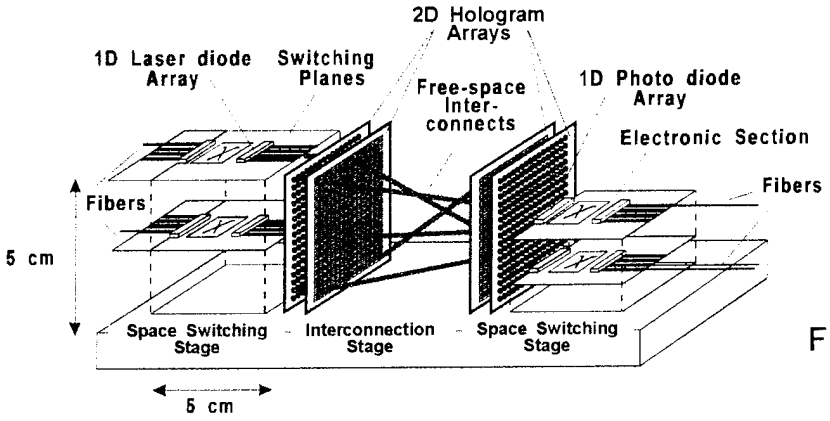

Fig. 2: 3D free-space fabric

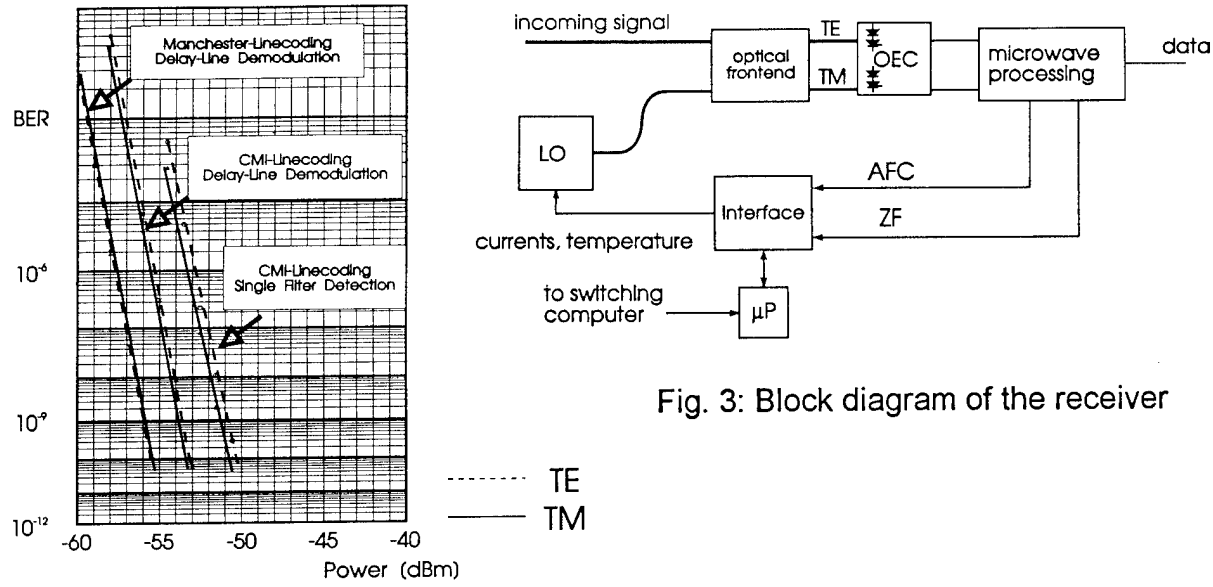

Fig. 3: Block diagram of the receiver

Fig. 4: BER for different detection schemes and line codings

Free-Space Optical Sliding Banyan Network

Michael W. Haney
ECE Department
George Mason University
Fairfax, VA 22030-4444

Marc P. Christensen
James J. Levy
BDM Federal, Inc.
McLean, VA 22102-3204

Background/Motivation

There is an ever increasing demand for high throughput, cost effective, broadband data switching networks, as demonstrated by the explosive growth in the Asynchronous Transfer Mode (ATM) equipment industry. Future networks must handle thousands of high bandwidth channels, implying an aggregate capacity in the terabit/second regime [1]. These requirements will exceed the ability of VLSI based switching technology.

Self-routing banyan based networks, which utilize a deflection algorithm to efficiently route packets to their destinations while minimizing resources for a given blocking rate, have been proposed [2]. To minimize latency and switching resources, the deflection routing approach requires an available output driver at each node at each stage. Smart pixel based free-space optical interconnections have been shown to provide the necessary interstage connections for this architecture, thereby eliminating the need for thousands of bulky, power hungry electrical interconnections [3].

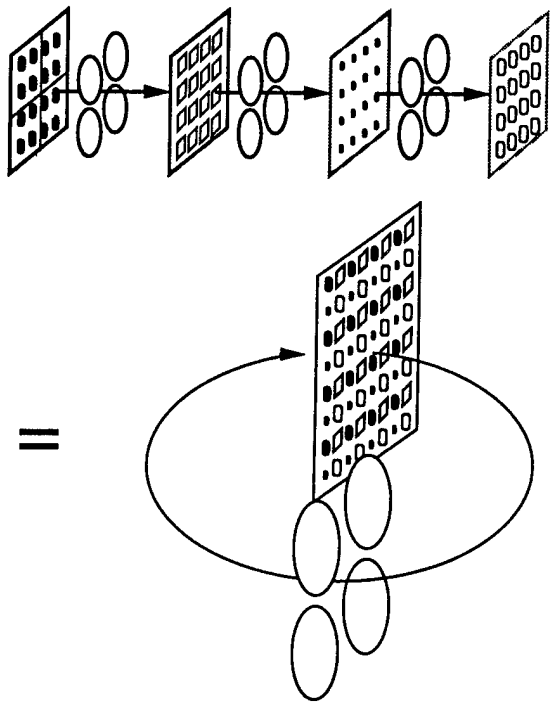

Figure 1. Sliding Banyan partitioning scheme.

In this paper the Sliding Banyan (SB) [4], a 3-D optical Multi-stage Interconnection Network (MIN) architecture, is evaluated. The SB is a pipelined MIN based on identical perfect shuffle [5] interconnections between stages. Since it is a banyan, simple destination tag routing can be employed by setting the switches at each stage according to the destination address located in the header. If a conflict occurs between two packets, a prioritization scheme resets to destination address decoder to the first bit for the lower priority packet. The SB utilizes a unique three dimensional partitioning of resources, which provides for efficient packet routing in a deflection routing scheme, while minimizing the number of line drivers. Figure 1 depicts the SB partitioning scheme. Rather than the traditional physically separated stages, in which the switching and I/O resources are distributed longitudinally, the SB's resources are distributed laterally, in the same physical plane. In this configuration the multiple stages of the switching fabric are physically interleaved, such that all stages for a given node reside in close proximity (i.e., on the same chip). This partitioning utilizes a single macro-optical shuffle interconnection module, which is simultaneously used by all stages. Simulations of unity permutation traffic were shown to achieve 10^{-12} blocking probability in 30 stages for a 1024 node network. This is a 50% improvement over a Tandem Banyan [6].

Approach

Figure 2 is a schematic depiction of an unfolded SB, showing an output link at each stage for the immediate removal of packets which have reached their destination. This immediate removal provides a significant reduction in the number of stages required for a given blocking rate. Figure 2 shows the number of output drivers

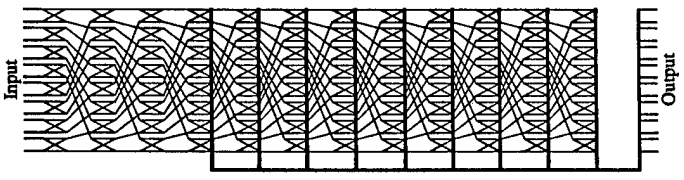

Figure 2. Unfolded Sliding Banyan architecture.

required for an unfolded deflection routing scheme to be $N(M-\log_k N)$, where M is the number of stages (e.g., 30 for 10^{-12} blocking probability), k is the shuffle order, and N is the number of nodes. By implementing the SB resource partitioning shown in Figure 1, the number output drivers is reduced to N. For a 1024 node network, with k = 4, and M = 30 stages, the reduction in interchip drivers (optical or electronic) is 1024×25=25,600 -- a significant reduction (1/25). Figure 3 depicts the folded SB switch. Packets enter the SB switching fabric on a fiber optic or coax bundle, as depicted on the left. Electronic boards or MCMs are used at the interface if needed (e.g., for line card functionality). The smart pixels are distributed across an array of Optoelectronic Integrated Circuits (OEICs), which comprise an "optoelectronic backplane." This backplane is envisioned to be tens of centimeters across. Each OEIC consists of Vertical Cavity Surface Emitting Lasers (VCSELs) and detectors for data transfer, and integrated or hybrid electronics (several hundred gates) for data switching. For a 1024 node switch, consisting of 30 stages, there will be over 30,000 VCSEL/detector pairs distributed across the backplane. We estimate power consumption of 10mW/optical link, and assume that it dominates the smart pixel power budget. This power estimate is consistent with conservatively projected VCSEL technology. Estimating power dissipation on a chip at a maximum of $2W/cm^2$, results in a maximum smart pixel density of $200/cm^2$. The SB architecture consisting of 30,000 optical links would then require ~$150cm^2$ of OEIC chip area. A backplane of 20cm×20cm would have a OEIC fill factor of ~40%, which is consistent with practical MCM packaging.

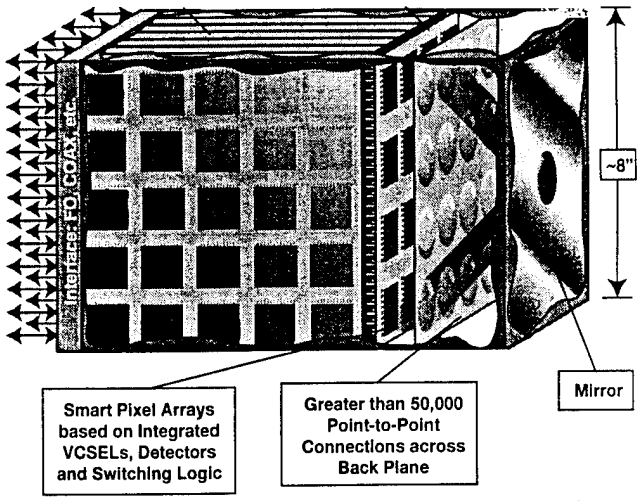

Figure 3. Sliding Banyan switching network depiction.

The optical shuffle interconnect depicted in Figure 3 consists of a macrolenslet array, with an identical lenslet for each OEIC. These lenslets perform the wide angle off-axis interleaved imaging necessary for the shuffle link pattern. The lenslets may be refractive or diffractive lenses. A mirror is used to fold the SB onto itself, so that each lens performs as both a transmitting and receiving element. The length of the system is determined by the size of the optical back plane and the speed of the lenslets. Preliminary estimates show that a system length approximately equal to the dimension of the backplane is achievable with reasonably simple lens designs. This optical interconnection, in conjunction with local smart pixel routing, provides the necessary perfect shuffle pattern (e.g., a 2- shuffle or a 4-shuffle) to implement of the simple self routing SB.

Experimental Evaluation

In the SB, the basic imaging system consists of a lenslet, a mirror, and another lenslet that is laterally offset from the first lens. The amont of lateral dispalcement is determined by the relative positions of the OEICs on the back plane. This imaging system is required to perform wide angle imaging defined by the dimensions of the OEICs in the object and image planes. For each lens, this requirement is similar to existing miniature video camera lens specifications, since video cameras perform wide angle imaging across a field defined by a CCD array. The SB has several optical design issues to be resolved. These include: alignment, interleaved registration, distortion, focal length variation tolerances, VCSEL image resolution, and folding of the optical system. These issues combine to determine the ability of the optical system to image the interleaved VCSEL array onto the interleaved detector array with good efficiency and low crosstalk. The alignment tolerances are determined by the size and spacing of the detectors and VCSELs. Our experiments used 10μm VCSELs separated by 630μm and we analyzed the results assuming 40μm detectors spaced the same. Current chip placement technology provides the ability to align chips to approximately 10μm accuracy. If we assume that the smart pixel OEICs will have sub-micron optoelectronic registration (comparable to modern photolithographic IC technology capabilities), then the dominant source of optical misalignment and loss of efficiency will come from the lenslet array itself. Consequently, we are focusing on evaluating the SB wide field optics. Our initial approach is to use conventional off-the-shelf refractive optical elements, leading to an eventual custom design.

Figure 4 depicts a typical experimental setup for validating the SB optical system. A VCSEL array (supplied by Honeywell) was used as the input source, and off-the-shelf video camera lenses were used to image the VCSELs onto a CCD detector array. The evaluation VCSEL array consisted of 4×4 individually addressable 10μm wide emitters, operating at 0.84 μm. These particular devices operated at about 10-20 mW of power consumption. Figure 5 shows the results of a registration experiment in which 3 collinear VCSEL elements, spaced by 630 μm, were imaged onto a CCD array for evaluation. The white outline squares indicate the locations and size of evenly spaced 40um detectors that would be part of the smart pixel. As shown in the figure, the off-the-shelf video lens performs fairly well in this off-axis imaging system. The inherent distortion of the imaging system (primarily due to vignetting of the narrow VCSEL beam by the barrel of the lens mount) begins to become apparent for total fields of view greater than about 20 degrees. In addition to the broadening of the focused VCSEL imaged spots, at the widest angles the array's images are beginning to misalign with the target detector array patterns. The widest angle data for the imaged VCSEL array correspond to a back-plane of size of about 4 inches and a total system length of about 12 inches due to the video lenses filed of view limitations. To achieve the desired length-to-width ratio of ~1 in the SB optical system requires flat field imaging optics with a total field of view of approximately 56 degrees. Although this is not a trivial design, our preliminary studies indicate that a detailed optical design, which meets the distortion and off-axis imaging criteria is not overly difficult. Such a design is currently being pursued.

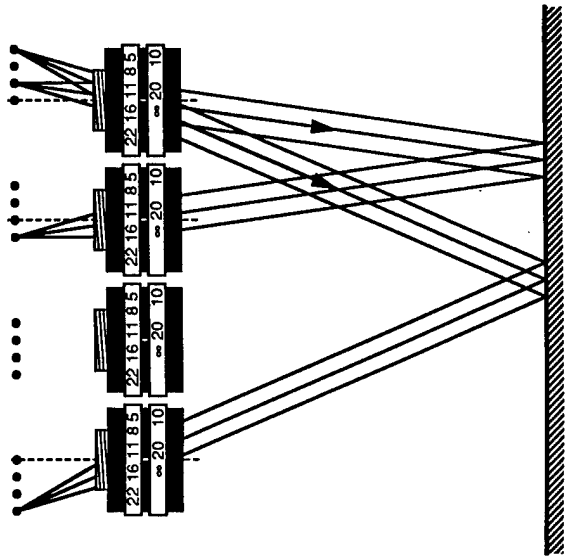

Figure 4. Experimental shuffle interconnection setup.

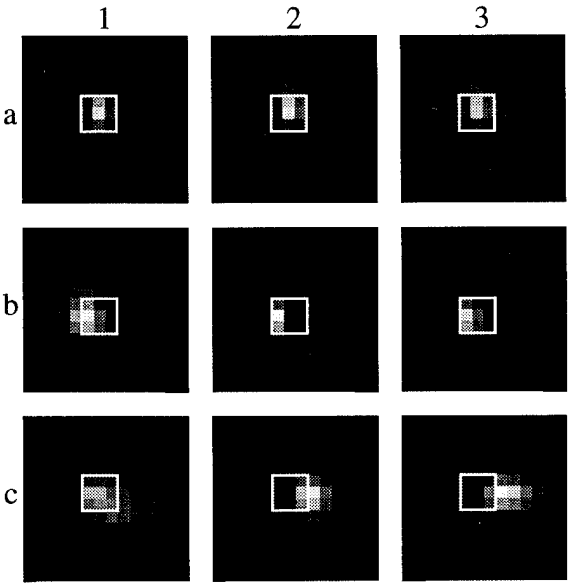

Figure 5. Data for 3 co-linear VCSELs separated by 630μm. a: on-axis, b: 10° FOV, c: 20° FOV.

Conclusion

The optical SB network evaluated in this paper is an example of utilizing a fundamental advantage of 3-D optical interconnects over 2-D VLSI technology. The co-location of the multiple stages' switching resources makes possible a significant reduction in the resources required to achieve very low blocking probability, as well as a large reduction in the number of output drivers required.

This research is sponsored by the Advanced Research Projects Agency through a contract with the Air Force Office of Scientific Research.

References

1. J. Hui, *Proc. of IEEE*, Vol. 79, No. 2, Feb., 1991.
2. M. Decina *et al*, ISS Vol. 2, IEICE, Oct., 1992.
3. T. Cloonan, *Opt. Eng.*, Vol. 33, No. 5, May, 1994.
4. M. Haney & M. Christensen, OC' 94, Aug., 1994.
5. H. S. Stone, *IEEE Trans Comput*, **C-20**, 153, 1971.
6. F. A. Tobagi *et al*, *IEEE JSAC*, Vol 9, No 8, Oct 91.

Development of a 16 x 16 reconfigurable holographic interconnection system

P. Gravey, L. Bonnel
France Télécom CNET LAB/RIO/PCO
Route de Trégastel BP 40 22301 LANNION France

Introduction

The use of arrays of reversible holograms is an attractive method to perform reconfigurable free-space interconnections of N inputs x N outputs high bit rate communication channels. Indeed, when the number of channels N increases, holographic switching systems have in principle less optical losses than those based on shuttered geometries such as vector-matrix or matrix-matrix architectures [1]. All the holographic switching system reported until now are made with a single deflection stage and they are therefore not suited to single mode fibre interconnections [2-4]. However, using single mode output fibres is very important because it enables the insertion of single mode optical amplifiers (either semi-conductor amplifiers or doped-fibre amplifiers) in order to compensate the switching losses and to realize quasi-transparent sytems for cross-connects applications.

This paper deals with the realization of a two-stage holographic reconfigurable interconnection system, which has been designed to connect two linear arrays of 16 single mode fibres. We report here on the main issues relative to the system design and give first results concerning two key aspects of the system performance, namely the possibility of an accurate collimation of the beams to be deflected and the fibre to fibre loss after diffraction by two successive holograms. Complete system characterizations will be presented during the conference.

System design

System capacity

The capacity of a N x N holographic switching system based on two arrays of holograms, (where each zone within the arrays is associated to a particular collimated beam issued from a single mode fibre) is essentially governed by the available spatial frequency range of the holograms and the propagation of a gaussian beam. These two constraints yields a relationship between the size of the hologram array and N which takes the form $N = (1/\lambda)\, k^2\, F_s\, h$, when the hologram array is a square one with a side h and $N = (1/\lambda)\, k\, F_l\, h^{1/2}$, when this array is a linear one of length h. In these expressions λ is the operating wavelength of the switch, k is a "filling factor" of the hologram array (ratio of the 1/e beam diameter over the pitch of the holograms), F_s and F_l are geometrical factors which depend on the beam angle of incidence θ and on the minimum and maximum grating periods (P_{min}, P_{max}). Table 1 shows the size of a 128 x 128 switching system with square matrices for different values of (P_{min}, P_{max}), for a normal incidence and k = 0.5. These grating period values correspond either to standard holographic recording materials like photothermoplastics (in particular P_{min} = 4 µm and P_{max} = 6 µm correspond to the devices which we are using) or to lower resolution devices such as optically addressed liquid-crystal spatial light modulators. We consider that $P_{max} = 2\, P_{min}$ to avoid overlapping with second-order diffracted beams.

(P_{min}, P_{max}) (µm)	matrix side (mm)	intermatrix distance (mm)	dispersion-limited capacity
(2,4)	5.3	22.1	260
(4,6)	17.2	296	230
(5,10)	26.3	403	506
(10,20)	31.2	1000	538
(20,40)	62.4	4056	549

Table 1
128 x128 holographic switching system dimension and maximum capacity for different grating period ranges

When h increases, the maximum capacity is limited by the hologram dispersion. In a two-deflection-stage system the dispersions of the two successive holograms compensate each other. However, the finite

size of the second hologram limits the acceptable wavelength dispersion. Table 1 gives also the highest N value compatible with the dispersion limit under the following hypothesis: the wavelength dispersion is lower than ± 1 nm and the deflected beam position variation is kept within 10% of the hologram pitch. The results of table 1 show that it is important to use high resolution (< 10 µm) hologramms in order to keep the size of the systems within reasonnable limits.

The implementation of a complete interconnection system requires the realization of an array of collimated beams by assembling an array of single mode fibres with a microlens array. The realization of 2D single mode fibre arrays is a very difficult issue, even though promising results have been recently reported [5]. We have therefore decided, for a first demonstration, to simply consider a 1D system, which yields a reduced capacity when compared to a 2D system. There are different possible configurations for the linear hologram arrays in a 1D system. We have selected a "vertical" one, where the direction of the two arrays is perpendicular to the mean grating vector direction, instead of an "horizontal" one, where the two arrays and the grating vectors are parallel. This configuration provides the highest capacity when taking into account the limited spatial bandwidth of the holograms. This is illustrated in figure 1 where both configurations are compared. The dispersion limit is defined as in table 1.

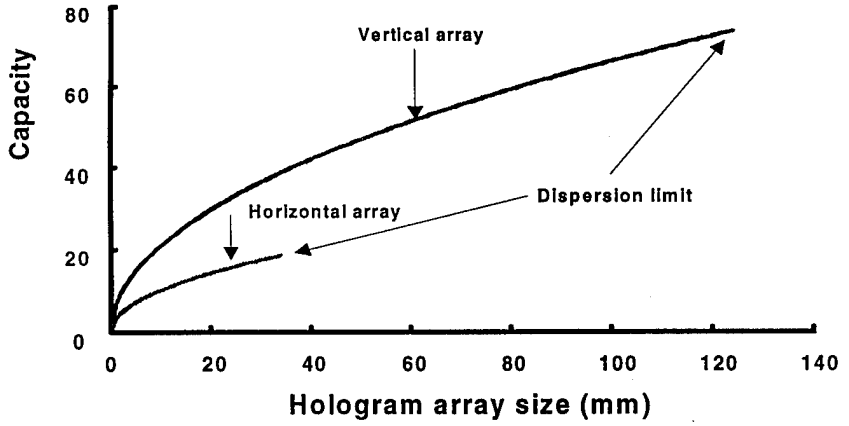

Figure1

Capacity of an holographic switching system based on linear hologram arrays with P_{min}= 4 µm and P_{max}= 6 µm.

We have choosen photothermoplastic devices for the hologram arrays. These devices are difficult to operate because they require an accurate control of their recording parameters (Corona voltage and heating current) and have a limited cycling capability [6]. However, their performances in terms of diffraction efficiency at telecommunication wavelength and resolution are still much better than those of any other spatial light modulator: we have obtained a diffraction efficiency higher than 20% (at 1.3 µm) for an optimum 5 µm grating period [7].

For the system design we assume a grating period range of 4 to 6 µm. This yields, according to figure 1, a maximum capacity of 22 for an array size of 12 mm. In this case the inter-array distance is about 50 mm. We have decided to realize a 16 x 16 interconnection system, with an hologram pitch of 750 µm (the size of each hologram being 650 x 650 μm^2). The two arrays are situated on a common glass/ITO substrate. The distance between these arrays is 4.5 mm. An intermediate mirror allows to direct the diffracted beams emerging from the first array towards the second one. The substrate to mirror distance is 25 mm.

Optical addressing system

The interconnection holograms are programmed through an optical addressing system which has been derived from an original proposition by Mikaelian and Salakhutdinov [4]. This system, which is entirely made with commercial devices, is represented on figure 2; it involves a 100 mW diode-pumped doubled YAG laser and two bi-dimensionnal deflection systems. The first one is based on acousto-optic deflectors (whith a 250 x 250 resolution) and performs the control of the grating period by mean of a beam duplication optics. The second allows to select what hologram is to be exposed. Such system based on a localized exposition of the holograms is much more efficient in terms of optical power than those where the holographic plane is completely illuminated [2,3]. Moving mirrors are used for this deflection system because of the relatively large pupil (20 x 20 mm^2). The stability and response time of both deflection systems have been characterized by injection measurements of the deflected beams into 532 nm single mode fibres. The response time of the

moving mirror system is lower than 2 ms. The reconfiguration time for one interconnection (corresponding to two hologtams) is shorter than 10 ms [7]. We expect the global reconfiguration time (for the 32 holograms) to be shorter than 100 ms. This is less than 32 times a single hologram recording because the larger part of the elementary photothermoplastic recording cycle (5 ms Corona charge) can be performed in parallel. The dimension of the set-up is 120 cm x 75 cm.

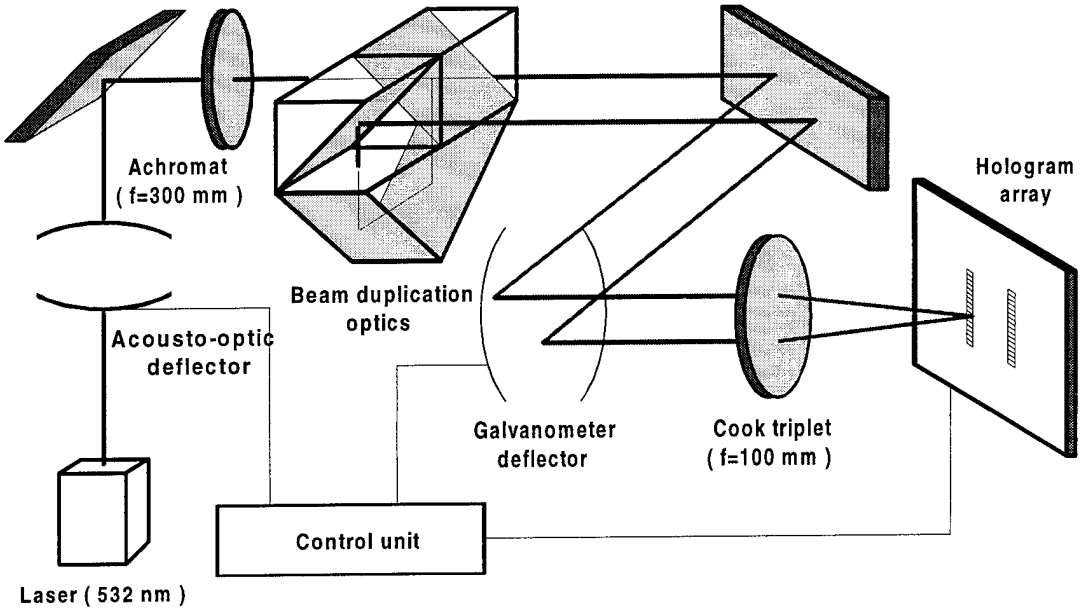

Figure 2
Optical addressing system for the recording of the interconnection holograms.

Connection losses

As already noted, one of the most critical issues which limits the theoretical and practical performances of such an interconnection system is the possibility of an accurate collimation of the beams to be deflected. We have realized this function by using linear arrays of fibres placed in silicon V grooves and SMILE™ microlens arrays from Corning. These lenses have a 700 µm diameter and a f = 2.9 mm focal length. The maximum propagation distance of a nearly 1.32 µm collimated beam issued from a single mode fibre with beam radius 4.5 µm is expected to be [8] about $f^2/z_R \approx 18$ cm (z_R is the Rayleigh distance). We have performed coupling maesurements between two arrays of 16 single mode fibres with these microlenses for different interconnection distances d. We have inserted a -1m focal length diverging lens between the two arrays to compensate what seems to be a residual curvature defect arising from the lens array fabrication process. The results are shown in figure 3 for d = 8 and 11 cm. The mean coupling losses are respectively 5.3 and 5.8 dB.

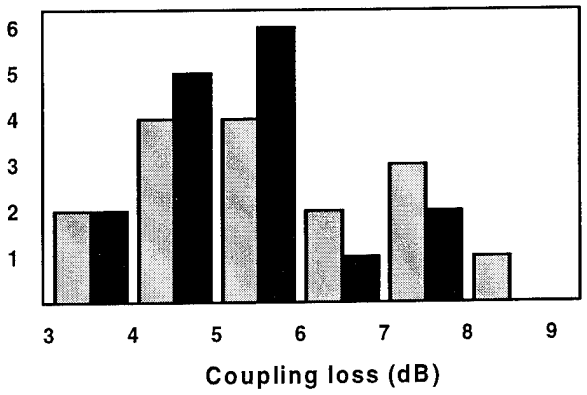

Figure3
Histogram of coupling loss for each of the 16 free-space links
(distance between microlenses = 8 cm (in black) and 11 cm (in grey))

These results can be improved because the highest losses are due to the some mispositionning (about 2 µm) of the extreme fibres in the arrays while more recent arrays show a submicron accuracy. On the other hand, the choice of larger aperture lenses would reduce the klipping phenomena that occurs in our set-up and yield lower losses and a propagation distance closier to the theoretical limit. Whatever, the distance that we have achieved meets the requirements of the interconnection system design and is, to our knowledge, significantly longer than previously published datas (1 cm and 2.5 dB losses) [9]. With optimized devices we believe that all the connection losses can be smaller than 6 dB.

Before the assembly of the complete system, we have measured the fibre-to-fibre loss through two interconnection grating. In this case, the beam collimation was performed using microscope objectives. We obtained an overall loss of 18 dB (4.4 dB for coupling losses and 13.6 dB for diffraction losses). The grating diffraction efficiencies for this connection were more than 20%. If we assume in the final system a minimum diffraction efficiency of 12% and 6 dB coupling losses, the total losses should be approximately 25 dB.

Discussion

The resolution of this system is significantly higher than the number of different holograms that are necessary to perform all the interconnections (31). This additionnal degree of freedom may be used to compensate residual misalignements of the set-up; it may also serve to match the grating spacing to the different input wavelengths (of couse the wavelength dispersion for each channel should still be limited to a few nanometers). Moreover, we can note that, if the linear hologram and fibre arrays would be replaced by square ones (with higher theoretical capacity), the size of the addressing system would be practically unchanged.

Presently the reconfiguration speed of the interconnections is mainly limited by the speed of the galvanometer deflectors. These deflectors could be replaced in the future by electrically addressed spatial light modulators using ferroelectric-liquid crystals. This would yield an architecture comparable to the one of [1] where a low-resolution electrically addressed spatial light modulator is used to control an high-resolution optically-addressed one using spatial multiplexing. In our case the difference of resolution is compensated by the time-multiplexed reconfiguration procedure. With such a faster addressing system, the overall reconfiguration time should be limited by the recording time of one hologram (about 10 ms).

Whatever, the optical addressing system represents most of the overall system volume, even with 2D hologram arrays. A more sophisticated engineering of the optical system could reduce this volume. The use of electrically addressed spatial light modulators is the only solution to completely avoid this drawback. These devices could be competitive in the future if their resolution becomes higher than 100 mm^{-1} for a diffraction efficiency at telecommunication wavelength at least in the 10 to 20% range.

Conclusion

We have presented the first realization of a 16 x 16 two-stage holographic interconnection system based on photothermoplastic holograms and its optical addressing system. The diffraction efficiency of the holograms can be higher than 20% at 1.3 µm. We have shown that the beams issued from linear arrays of single mode fibres can be accurately collimated over the distance necessary to the system implementation.

References

1 - D. C. O'Brien, W. A. Crossland, and R. J. Mears, Opt. Comp. and Proc., 1, 233 (1991)

2 - P. Gravey, L. Bonnel, and J-Y. Moisan, 2nd Int. Conf. on Holographic Systems, Components, and Applications, IEE Conference #311, Bath, UK, 195 (1989)

3 - H. Yamazaki, and M. Yamaguchi, Int. Topical Meeting on Photonic Switching, Minsk, Belarus, 3D4 (1992)

4 - A. L. Mikaelian, and V.K. Salakhutdinov, Int. Topical Meeting on Photonic Switching, Minsk, Belarus, 2C2 (1992)

5 - J. M. Sasian, R. A. Novotny, M. G. Beckman, S. L. Walker, M. J. Wojcik, and S. J. Hinterlong, Opt. Eng., 33, 2979 (1994)

6 - J-Y. Moisan, P. Gravey, R. Lever, and L. Bonnel, Opt. Eng., 25, 151 (1986)

7 - L. Bonnel, and P. Gravey, 4th Int. Conf. on Holographic Systems, Components, and Applications, IEE Conference #379, Neuchatel, Switzerland, 112 (1993)

8 - F. B. Mc Cormick, F. A. P. Tooley, T. J. Cloonan, J. M. Sasian, H. S. Hinton, K. O. Merserau, and A. Y. Feldblum, Opt. and Quant. Elect., 24, S465 (1992)

9 - T. Y. Yamamoto, M. Yamaguchi, and K. Hirabayashi, Proc. IEICE, March 1994, B-1107 (in japanese)

Wednesday, March 15, 1995

Wavelength and Time Switching

PWE 3:30 pm-5:30 pm
Red Lion East

Godfrey Hill, *Presider*
British Telecom Laboratories, U.K.

Wavelength conversion devices and applications

B. Mikkelsen, T. Durhuus, C. Joergensen, S.L. Danielsen,
R.J.S. Pedersen and K.E. Stubkjaer.

Center for Broadband Telecommunications, Technical University of Denmark
DK-2800 Lyngby, Denmark, Tel.: +45 42 88 14 44, Fax: +45 45 93 16 34

Introduction: Implementation of simple wavelength converters can be considered an enabling technology for taking the full advantage of the wavelength dimension in wavelength division multiplexed (WDM) networks [1-2]. Therefore, much attention has been devoted to the realisation of all-optical wavelength converters relying on mechanisms such as cross-gain modulation (XGM) and cross-phase modulation (XPM) in semiconductor optical amplifiers (SOAs) [3-6], optical modulation of lasers [7-9] and four-wave-mixing in fibers and SOAs [10-11]. In this paper, applications as well as desired features of wavelength converters are discussed. Additionally, different methods for wavelength conversion will be surveyed with emphasis on all-optical wavelength conversion by XGM and XPM in SOAs.

Applications of wavelength converters: Future optical networks are expected to exploit the wavelength dimension in two conceptionally different ways: (*i*) to perform routing functions either internal in switches or in wavelength routed networks, or (*ii*) simply as a transport resource without any end-to-end significance of the actual wavelength (strictly wavelength multiplexing). In such networks, wavelength converters can efficiently be used to accomplish the following functions:

- Re-use of wavelengths in wavelength routed networks [2]
- Avoid wavelength blocking in WDM cross-connects [2]
- Dynamic routing in switches (together with optical filters) [2,12]
- Address free-space in optical buffers [12-13]
- Decentralise network management (no global wavelength assignment) [1]

An example of a WDM cross-connect utilising wavelength converters is shown schematically in Fig. 1. Here, the wavelength converters have two different functions: the input converters perform space routing (together with the tunable filters at the outputs), whereas the output converters are used to avoid wavelength blocking when channels are multiplexed.

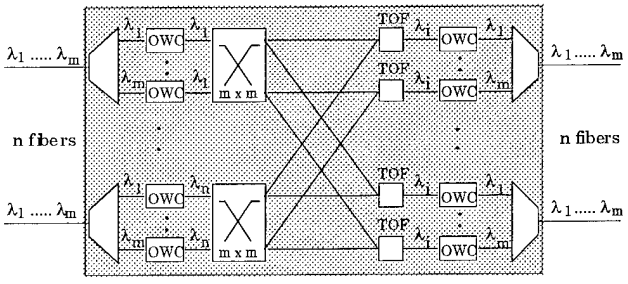

Fig. 1 WDM cross-connect utilising optical wavelength converters (OWCs) for routing (input-converter) and to avoid blocking (output-converters) when channels are multiplexed. TOF: tunable optical filter.

The requirements to the performance of the wavelength converters are application dependent. For example, all the converters used in the WDM cross-connect (Fig .1) have fixed output wavelengths, while tunability is required for other applications [2,12]. Furthermore, the input converters in the WDM cross-connect have known input wavelengths, whereas the output converters must be able to handle a given range of input wavelengths. Moreover, the input converters must be insensitive to the polarisation of the input signal. In general, the following features of wavelength converters are desired:

- Bit-rate transparent (up to 10 Gbit/s)
- No extinction ratio degradation
- High signal-to-noise ratio at the output (to ensure cascadability)
- Moderate input power levels (~0 dBm)
- Large wavelength span for both input and output signals
- Low chirp
- Fast set-up time of output wavelength
- Polarisation insensitive to input signal
- Simple implementation
- Possibility for same input and output wavelengths (no conversion)

Wavelength conversion by XGM in SOAs: Cross-gain modulation in SOAs is a simple scheme for wavelength conversion as shown schematically in Fig. 2. The optical input signal to be wavelength converted modulates the SOA-gain by saturation and, consequently, modulates the gain experienced by a CW signal at the desired new wavelength. Very importantly, the conversion is independent of the polarisation of the incoming signal since the SOA gain is polarisation insensitive. The maximum bit rate that can be converted is determined by the gain dynamics of the SOAs. Operating at high optical power levels (~1 mW) and at high bias current, conversion of 20 Gbit/s data is possible [4-5]. Examples of 10 Gbit/s converted pulse patterns and the corresponding BER performance are shown in Fig. 3 for conversion from 1560 to 1553 nm.

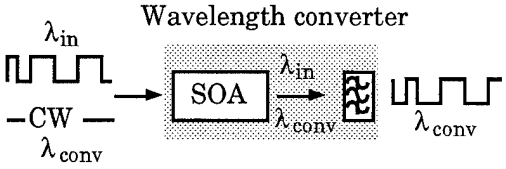

Fig. 2 Schematic of wavelength conversion by XGM in SOAs

The conversion can be performed over the entire gain bandwidth of the SOA (i.e., 40-50 nm), but the best results are obtained going from longer to shorter wavelengths because the differential gain is largest at the short wavelength side of the gain peak [4]. Furthermore, XGM results in converted data that are inverted compared to the input data (see Fig. 2). Since conversion based on XGM implies a large carrier density modulation to achieve an acceptable extinction ratio for the converted signals, and because the refractive index in the SOA depends on the carrier density, XGM results in significant chirp (phase modulation) of the converted signal (typically 30-40 GHz at 10 Gbit/s). This chirp will prevent converted high bit-rate signals to be transmitted over non-dispersion shifted fiber and might, moreover, introduce excess cross-talk to neighbour channels when passing optical filters/demultiplexers.

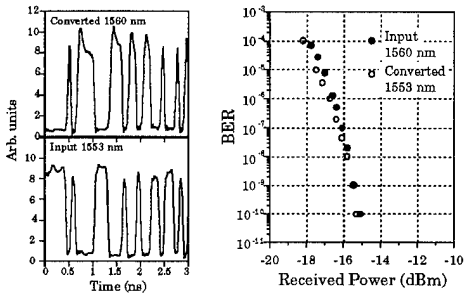

Fig. 3 Pulse patterns for a 10 Gbit/s converted signal and input signal as well as corresponding BER.

Wavelength conversion by XPM in SOAs: The dependency of the refractive index on the carrier density and hence an optical input signal can be used to perform wavelength conversion based on cross-phase modulation (XPM). To make use of the XPM, the SOAs have to be placed in an interferometric configuration as, e.g., a Mach-Zehnder interferometer (MZI) [3] or a Michelson interferometer (MI) [6] (see Fig. 3).

The advantage of XPM compared to XGM is that conversion to longer and shorter wavelengths give equal performance, because the differential refractive index is almost wavelength independent. Furthermore, with XPM the converted signal is not inverted and the chirp is very small as reported in [6]. Monolithically integrated SOA-MI and SOA-MZI are described in [6,3], therefore only representative results are given here. As examples of the excellent performance of the interferometric converters, Fig. 5

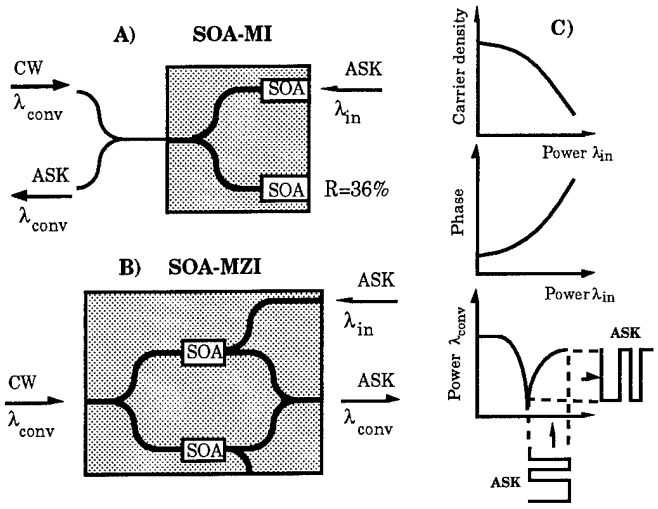

Fig. 4 Schematic of interferometric converters: (A) SOA-MI and (B) SOA-MZI, and (C) operation principle.

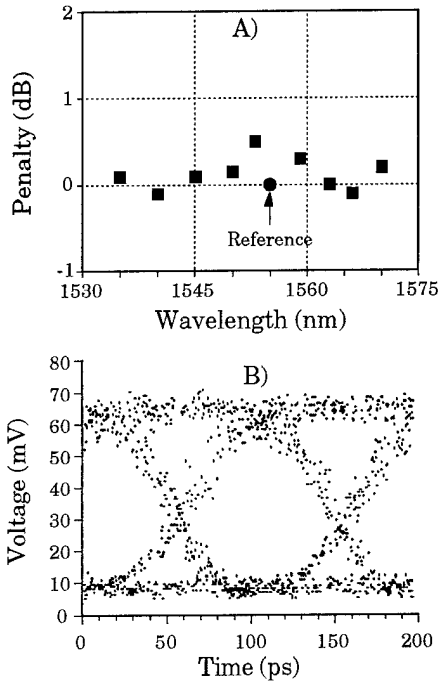

Fig. 5 A) Penalty for up- and down-conversion of 10 Gbit/s data . B) Eye diagram for converted data (1550 to 1560 nm).

shows the measured penalty for the case of up- and down-conversion of 10 Gbit/s data with an integrated SOA-MI. Note that virtually penalty-free conversion is achieved over 35 nm. The figure also shows a measured eye-diagram for conversion from 1550 to 1560 nm. Finally, it should be emphasised, that converters based on XPM can easily be cascaded because of both the high extinction ratio and a high signal-to-noise ratio for the converted signals [6].

Summary: The emergence of practical optical wavelength converters will have a large impact on future networks, since they will allow the full exploitation of the wavelength dimension. Both XGM and XPM in SOAs are very promising techniques for realisation of such practical wavelength converters.

Acknowledgement: Alcatel Alsthom Recherche, Thomson CFS, France, Ericsson Components, Sweden are acknowledged for supplying the devices used in the experiments.

References:

[1] K. Sato et al., J. Selected Areas in Com., Vol. 12, No. 1, pp. 159-170, Jan. 1994.
[2] J.M. Gabriageues and JB. Jacob, Techn. Dig. of ECOC'92, pp. 59-66, Paris, Sept., 1992.
[3] T. Durhuus et al., Techn. Dig. of OFC'95, paper TuO6, San Diego, Feb. 1993.
[4] B. Mikkelsen et al., Techn. Dig. of ECOC'93, pp. 73-76, Montreux, Sept., 1993.
[5] J.M. Wisenfield et al., Electron. Lett., Vol. 30, pp. 720-721, 1994.
[6] B. Mikkelsen et al., Techn. Dig. of ECOC'94, PD-paper, pp. 67-70, Firenze, Sept. 1994.
[7] R.J. Pedersen et al., Techn. Dig. of OFC'94, paper ThQ3, San Jose, Feb. 1994.
[8] E. Lach et al., Techn. Dig. of ECOC'93, paper TuC5.4, Montreux, Sept., 1993.
[9] H. Yasaka et al., Electron Lett., Vol. 30, pp. 133-134, Jan. 1994.
[10] D.M. Patric and R.J. Manning, Electron Lett, Vol. 30, pp. 252-253, Feb. 1994.
[11] H.G. Weber et al., Techn. Dig. of OAA'94, paper FC1, Breckenridge, July 1994.
[12] S.L. Danielsen et al., to be presented at PT'95, Salt Lake City, Marts 1995.
[13] M. Calzavara et al., Techn. Dig. of ECOC'94, pp. 567-570, Florence, Sept. 1994.

A photonic WDM packet switch with reduced complexity due to wavelength converters

S. L. Danielsen, B. Mikkelsen, C. Joergensen, T. Durhuus, K. E. Stubkjaer
Technical University of Denmark, Electromagnetics Institute, Bldg 348,
Center for Broadband Telecommunications, DK-2800 Lyngby,
Tlf.: +45 42 88 14 44, Fax: +45 45 93 16 34

Summary: Future broadband networks are expected to utilise WDM and optical switching to increase the network capacity and flexibility [1]-[3]. Furthermore, ATM is selected as standard for future broadband services, hence, optical packet/ATM switches [4,5] for WDM networks are of considerable interest. Of major concern for such all optical switches is the optical buffering as well as the complexity of the space-switch block addressing the optical buffers. We show, that by implementing tuneable optical wavelength converters (TOWC) the number of delay-lines in the buffer can be reduced and thereby also the size of the space-switch block. Based on measured features for semiconductor optical amplifier (SOA) gates that are used to build the space-switch, we predict that a 16x16 switch with 4 or 8 wavelength channels is feasible.

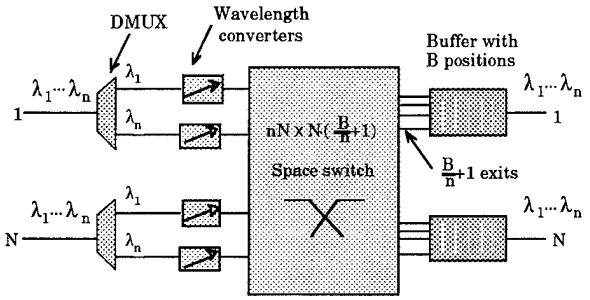

Fig.1: WDM packet switch utilising tuneable optical wavelength converters (TOWC) to reduce the switch complexity.

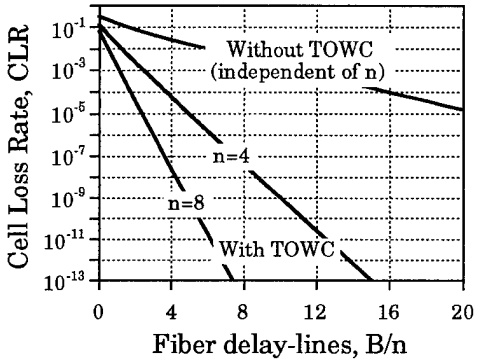

Fig.2: Cell loss probability versus the number of fiber delay-lines, B/n, for a 16x16 switch with a load of 0.8 Erlang and with the number of wavelengths, n, as parameter.

The general WDM packet/ATM switch considered here is shown in Fig. 1. It consists of three main blocks: 1) The cell encoder where a demultiplexer selects the cells arriving at n fixed wavelengths $\lambda_1,\ldots,\lambda_n$ and TOWC's address free space in the fiber delay-line output buffers; 2) A space-switch to access the buffers; 3) Cell buffers, that are realised by fiber delay-lines. As seen from the figure, the size of the space-switch is nN·N(B/n+1) where B is the number of cell positions in the buffer, n the number of wavelengths, N the number of in- and out-lets and B/n the number of fiber delay-lines.

To decrease the complexity of the switch the number of delay-lines should be reduced. This can be obtained by using wavelength converters as clearly illustrated in Fig. 2 that gives the calculated cell loss probability (CLR) versus the number of delay-lines, B/n. Results are shown for a 16x16 switch (N=16) with a load of 0.8 Erlang for each of the n wavelength channels per inlet. Assuming uniform traffic, the required number of delay-lines are 12 and 6 (@ CLR=10^{-10}) for n=4 and n=8 wavelengths, respectively, while without converters 47 delay-lines are required independent of the wavelength number, n. Since the size of the space switch is nN·N(B/n+1), these values demonstrate that the switch capacity can be increased linearly with n without increasing the space-switch complexity when using TOWC's, whereas without TOWC's the space-switch grows linearly with the number of wavelengths.

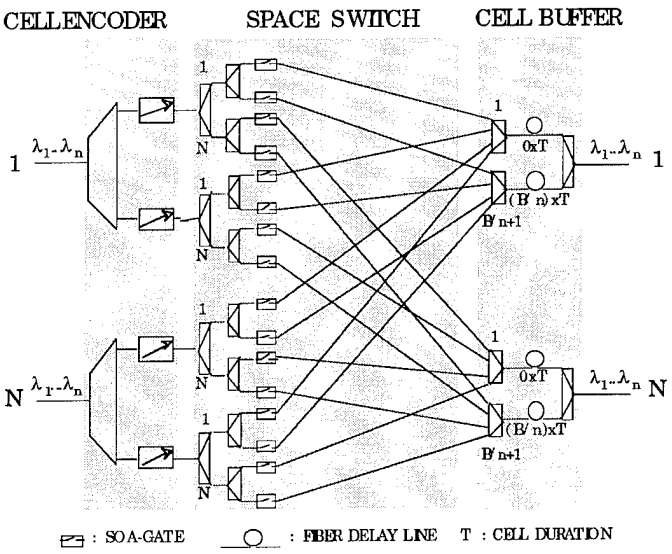

Fig.3: WDM packet/ATM switch where the space switch is build from SOA-gates and the buffer is realised by fiber delay-lines.

Strong candidates for the TOWC's are interferometric converters as well as converters based on cross gain modulation [6]. Obviously, a critical part of the packet/ATM switch in Fig. 1 is the space-switch block which could be build using SOA-gates [7] that offer loss compensation, nsec switching times and polarisation insensitivity. The implementation of the space switch is shown in Fig. 3 where also the fiber delay-line based cell buffers are shown. Note that this switch configuration is capable of multicasting, since if more gates at an input are opened at the same time, a cell can be distributed to more outlets.

Based on measured data for a SOA-gate, Fig. 4 shows that a 16x16 switch with 4 or 8 WDM channels per port and with bit rates of 10 Gb/s are possible for the proposed

configuration. In the figure, the resulting power penalty is shown versus the output power of the TOWC's with the number of wavelengths as the parameter. A minimum penalty with respect to the output power is observed: at low output power levels the penalty is caused by a low signal to noise ratio while the penalty at high power levels is due to the extinction ratio degradation resulting from the gain non-linearities of the SOA-gate. Finally, it is noted that the penalty increases with n since the number of open gates that contribute to spontanous emmision increases. The measured parameters used in the model are detailed in the figure caption of Fig. 4.

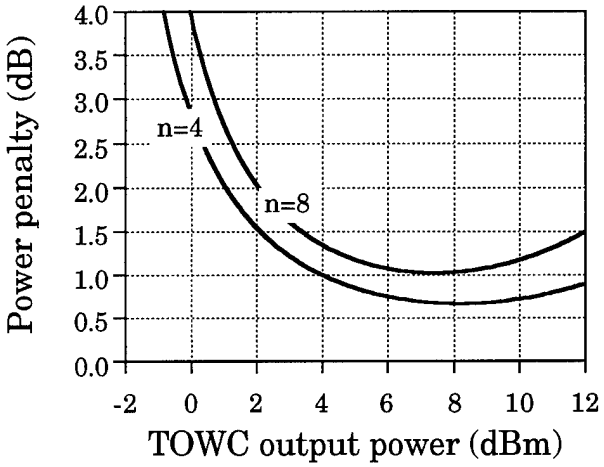

Fig.4: Power penalty (@ CLR=10^{-10}) versus TOWC output power for a 16x16 switch. n is the number of wavelengths (channels) per inlet. The channel bit rate is 10 Gb/s and the signal extinction ratio at the input is 11 dB. The SOA-gates are characterised by noise figures of 7 dB, on-state gain of 24 dB and the gain non-linearities of the gates are included in the model. The on/off ratio of the gates is assumed to be 40 dB which is realistic for guard bands of 1-2 nsec.

In summary, the use of wavelength converters is a tool to reduce the switch complexity resulting in a nearly constant size of the space-switch for the proposed configuration. Calculations based on measured data indicate that a 16x16 switch using 4 or 8 wavelengths channels is realistic with a space-switch block constructed from SOA-gates.

REFERENCES

[1] P. Green et al., Jour. of Light. Tecnol., vol. 11, pp. 754-763, May 1993.
[2] S. Johansson et al., Jour. of Light. Tecnol., vol. 11, pp. 688-694, May 1993.
[3] C. Brackett., IEEE Jour. on Select. Areas in Comm., vol. 8, pp. 948-964, Aug. 1990.
[4] W. De Zhong et al., in Proc of ECOC' 94, vol.2, pp. 541-544, Florence, Italy, Sept 1994.
[5] J. M. Gabriagues et al., in Proc. of ECOC' 91, vol.2, pp. 59-66, Paris, France, Sept. 1991.
[6] B. Mikkelsen et al., in Proc. of ECOC' 93, vol.3, pp. 73-76, Montreux, Schweiz, Sept. 1993.
[7] M. Gustavsson et al., in Proc. of OA' 92, Paper PD9 , pp. 39-42, June 1992.

Multi-channel Optical Filters Using birefringent planar optical Platforms

Katsuhiko Hirabayashi and Masayasu Yamaguchi
NTT Network Service Systems Laboratories
3-9-11, Midori-cho, Musashino-shi, Tokyo 180, Japan
TEL: +81-422-59-4812, FAX: +81-422-59-2473, E-mail: hira@csl.ntt.jp

Introduction

For WDM systems, tunable optical filters have been actively studied.[1] Most tunable filters can select only one wavelength at a time, the tuning speeds are as slow as 1 - 100 ms, and they need wavelength-stabilizing circuits. For communication switching, filters are thus required that can select several wavelengths simultaneously, and can switch quickly without stabilization. To meet these requirements, we have studied a novel multi-channel filter consisting of a birefringent planar optical platform.

Structure and Principle

(a) Birefringent planar optical platform

The basic structure of the birefringent planar optical platform we used is shown in Fig. 1(a). A layer of calcite is sandwiched by $\lambda/4$ plates, and again by highly reflective dielectric mirrors. The optical beam propagates towards the right via multiple reflections. The dependence of the light intensity on the channel number is shown in Fig. 2. The simulation result is also shown. When mirrors with reflectivity of 99.5% are used, the channel where the light intensity decrease was -3 dB is as far as No. 22. Thus, the loss of the birefringent planar optical platform is smaller than that of a glass optical platform. [2]

We next insert a liquid-crystal (LC) cell between the calcite plate and the Au mirror as a polarization controller, as shown in Fig. 1(b). On one side is an indium-tin-oxide (ITO) transparent striped electrode and on the other side is an Au mirror/electrode. Thus at the reflection points, the propagation direction can be switched by changing the polarization of the beam. An optical beam is reflected back in the case of channels having a phase retardation of $\pi/2$.

(b) Multi-channel filter

A thin-film interference filter is inserted between the $\lambda/4$ plate and the LC layer, as shown in Fig. 3(a). This filter is assumed to have a sharp transmission peak and to reflect the non-peak wavelengths. The transmission peak wavelengths are location-dependent (1 nm/mm). When wavelength-division multiplexed light (λ_1-- λ_n) is input into the calcite plate, the light beam propagates straight to point B. At B, the λ_1 light beam passes through the filter while light beams with other wavelengths are reflected up to point C. The λ_1 beam passes through the $\lambda/4$ plate and the LC layer. If the LC layer does not change its polarization, it propagates up to point C. If its polarization is rotated by 90°, it returns to point A. The ratio of light propagating to points A and C can be controlled by changing the voltage applied to the LC layer. By separating the light beams returning to point A with a circulator, a reflection-type multi-channel selector can be obtained.

The structure of Fig. 3(a) is a reflection-type filter, which needs the circulator. A transmission-type multi-channel filter, which does not need the

circulator, can also be made according to a similar principle. Its structure is shown in Fig. 3(b). Two calcite plates sandwiched by λ/4 plates are stacked, with an LC layer sandwiched by thin-film interference filters between them. They are again sandwiched by two dielectric mirrors. The light is input at point A and is output at point X and Y. The output X is complementary to the output Y.

Performance of a multi-channel filter module

The calcite plates were 9.93-mm thick, so the channel pitch was 1 mm. The wavelengths of the thin film interference filters are stable, dependent on their location; their distance dependence is about 1.0 nm/mm. The full-width at half maximum was about 1 nm and their loss was 1 dB. They were cemented by adhesive with good parallelism. The fabrication was easy. The pigtail module of the transmission-type multi-channel filter is shown in Fig. 4. The output spectra at the point Y are shown in Fig. 5; the left figures correspond to one or multi-wavelength selection, and the right figures correspond to multi-wavelength selection with an arbitrary transmission. The transmittance-type filter had smaller crosstalk: less than -18 dB. Its loss from the input fiber to the output fiber was about 10 dB.

The nematic LC, which was used in the experiment, was useful because it can continuously tune the phase retardation, but its tuning speed was as slow as 10 ms. We also used ferroelectric LC (FLC) cells, and the channel switching speed was improved as high as 100 μs.

Summary

We designed and tested multi-channel optical filters. They consist of thin-film interference filters, birefringence plates, λ/4 plates, mirrors, and liquid-crystal layers. They utilized the multi-reflection properties of optical beams in the birefringence optical platforms sandwiched by the λ/4 plates and mirrors. We demonstrated the feasibility of a seven-channel filter. These filters have stable wavelengths, can select wavelengths without stabilizing circuits, can select arbitrary channels with arbitrary transmittance, and have a high switching speed.

References

[1] C. A. Brackett, "Dense wavelength division multiplexing networks: principle and applications," IEEE J selected areas in Communications, vol. **8**, pp.948-964, 1990.
[2] J. Jahns and A. Hung, "Planar integration of free-space optical components," Appl. Opt., vol. 28, pp. 1602-1605, 1989.

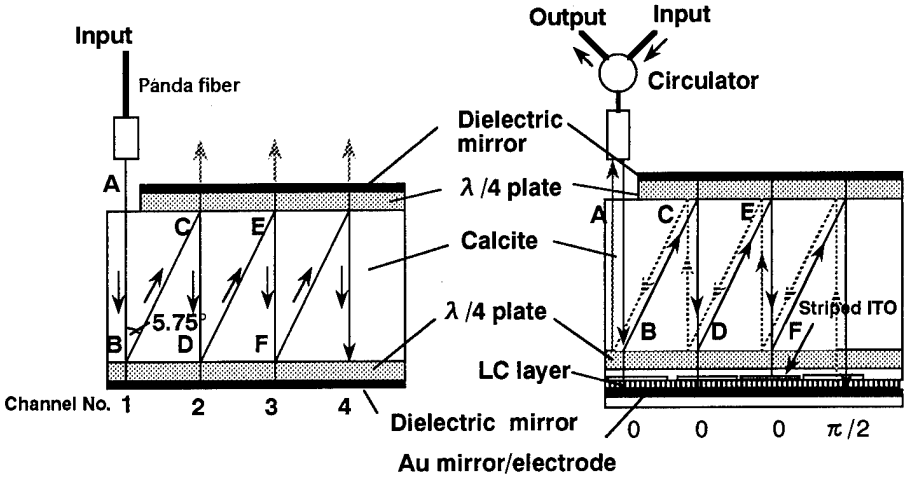

(a) Birefringent optical platform. The optical beam propagates to the right via multiple reflections.

(b) Liquid-crystal layer inserted between the λ/4 plate and the mirror as a polarization controller.

Fig.1 Structure and Principle of the birefringent planar optical Platform

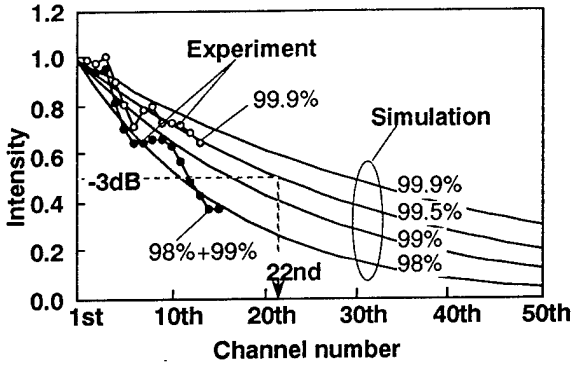

Fig. 2 Dependence of light intensity on the channel number (experiment and simulation).

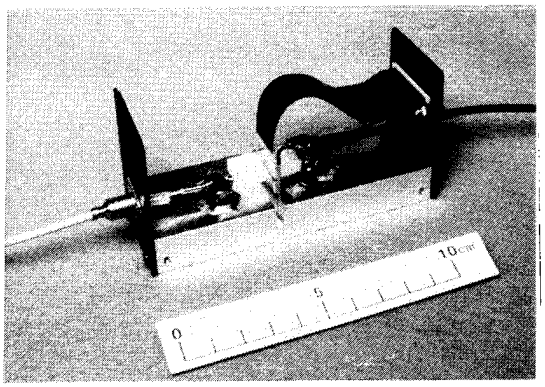

Fig. 4 Multi-channel filter module

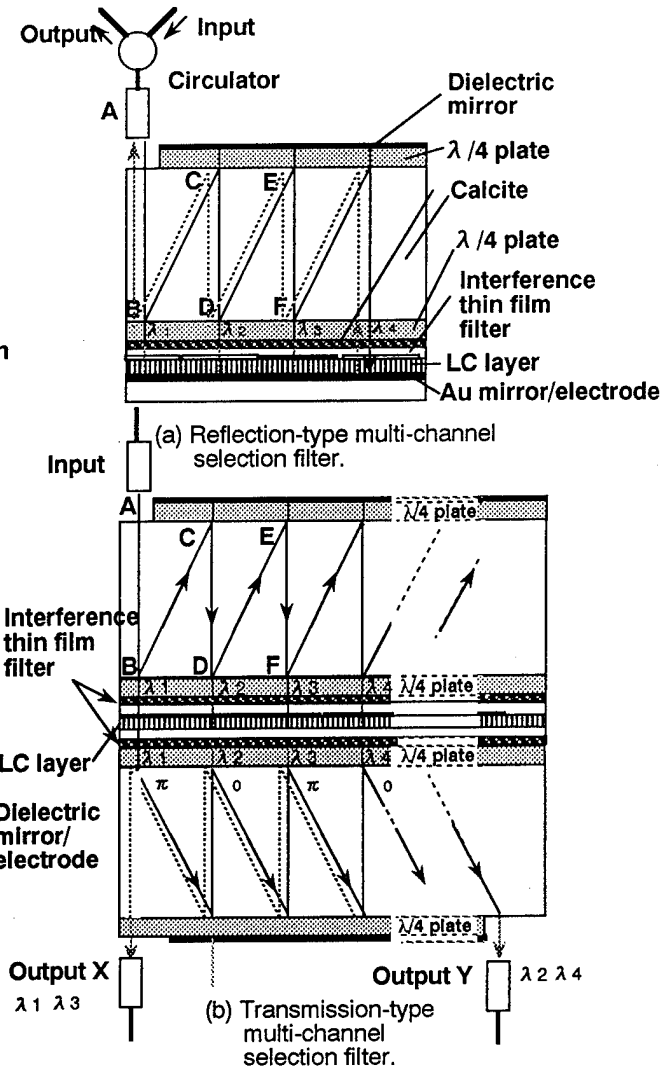

Fig. 3 Structure and principle of multi-channel selection and structures of multi-channel filters.

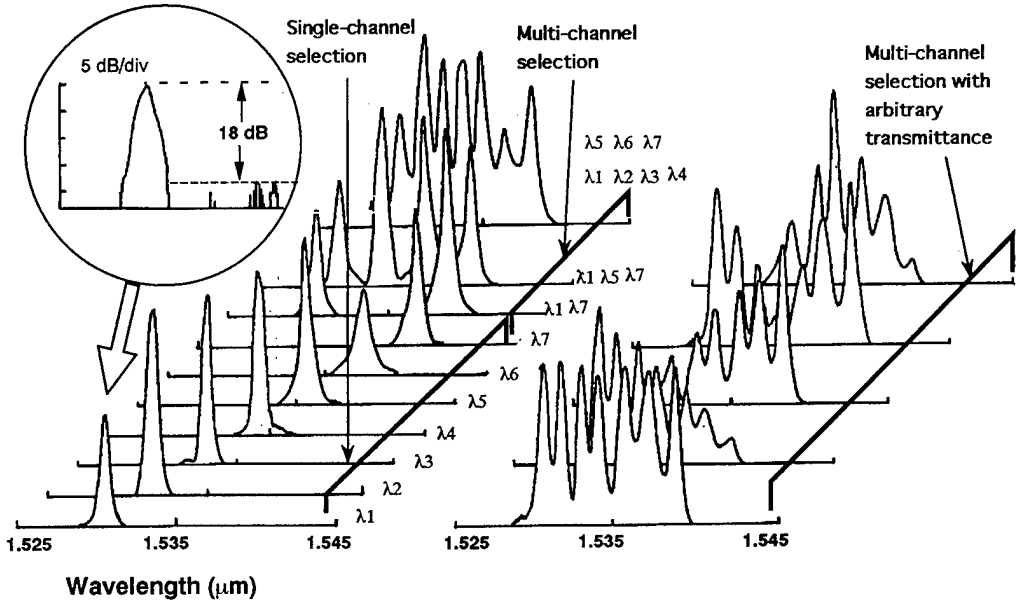

Fig. 5 Output spectra for transmission-type multi-channel filter

Technologies for Ultra-High-Bit-Rate Time-Division-Multiplexed Networks

Kristin Rauschenbach, Katie Hall, John Moores, Steve Finn and Rick Barry
MIT Lincoln Laboratory, Lexington, MA

William Wong, Hermann Haus and Eric Ippen
MIT, Cambridge, MA

Mark Haner
AT&T Bell Laboratories, Murray Hill, NJ

Ultra-high-speed optical time-division multiplexed systems, operating at single stream rate of 100 Gbps, may offer important operating advantages over other multiplexing schemes. These advantages include increased "intelligence" within the network to perform dynamic routing which enables packet service and truly flexible bandwidth on demand. Transmission limitations and the availability of key technologies impact the system architectures and operating performance which can be expected from these systems. In this talk, we present recent developments in the architecture and technology for ultra-high-bit-rate networks.

Figure 1 shows a strawman architecture we use to guide our technology and architecture development. High-end single users, as well as aggregates of lower speed users form a network with a single-stream operating speed of ≈100 Gbps. These systems are targeted to provide packet service. Transmission limitations in optical fiber may practically limit these systems to geographical spans on the order of hundreds of kilometers. Five main subsystem functions are required to enable this type of a system including transmission, synchronization, multiplexing and demultiplexing, packet header processing, and an all-optical gateway to provide access to wider-area transmission. Several key technologies support these functions including short pulse sources, clock recovery, soliton transmission, optical buffers, and pulse-width and wavelength converters.

We will present recent results on high-speed soliton transmission simulations and experiments. We have developed a 100 Gbps soliton compression source which produces picosecond transform-limited pulses with low timing jitter. The source is tunable in repetition rate, and we have demonstrated an optical phase-lock loop to provide picosecond-accuracy synchronization. The clock recovery we have constructed allows simultaneous all-optical modulation or demultiplexing within the access node. Optical buffers are being developed to eventually provide for asynchronous access in these systems. We describe an optical fiber loop memory that stores a 1.7 kilobit pattern at 20 Gbps, for periods of over 1 hour. We also show an all-optical pulse width and wavelength converter that converts signals compatible with local 100 Gbps transmission to signals compatible with long-haul transmission. The technologies we describe represent an important first step towards eventual system demonstrations.

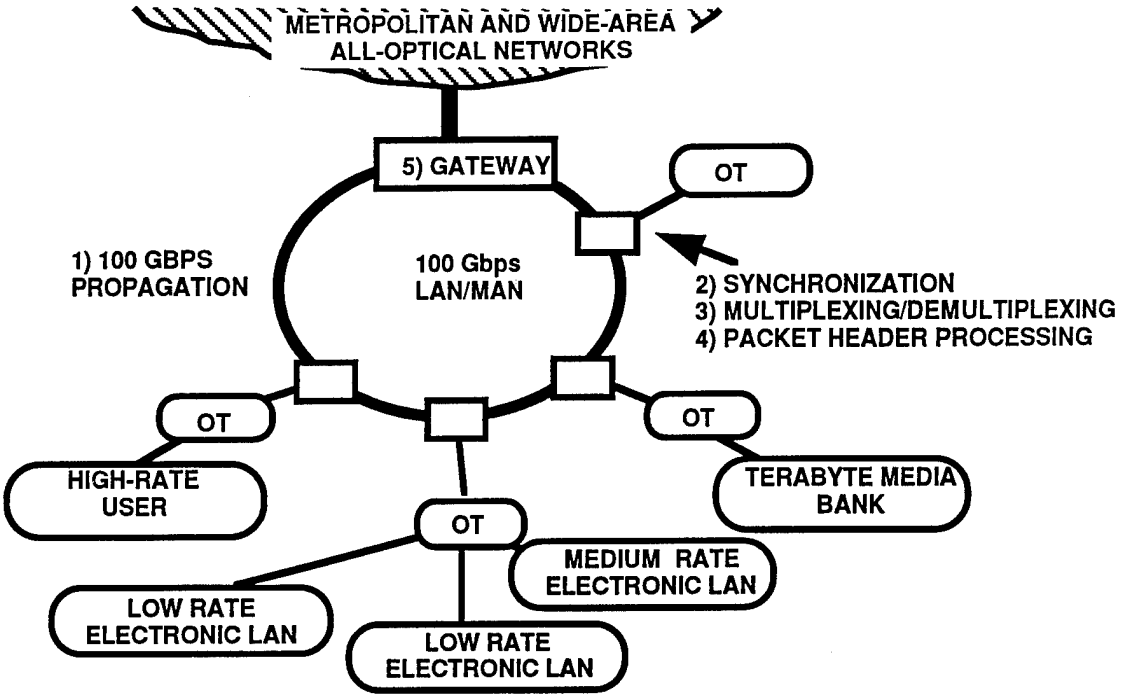

Figure 1. Strawman architecture.

All-Optical Self-Routing Switch Using a Nonlinear InGaAs/InAlAs MQW Waveguide

T. Kanetake
Advanced Research Laboratory, Hitachi Ltd.,
Hatoyama, Saitama 350-03, Japan;

S. Tanaka, and H. Inoue,
Central Research Laboratory, Hitachi Ltd.,
Kokubunji, Tokyo 185, Japan.

1. Introduction

Intelligent society demands diverse communication services such as the telephone, facsimile and the high definition TV. To improve flexibility and efficiency of the transmission system under these diverse demands, Asynchronous Transfer Mode will be installed as a new standard method. In this mode, information is divided into many cells of a constant bit-length with headers. Each cell chooses its own route by itself, depending on address information in its header. To realize ATM network for massive demands in future, optical communication technology will be applied. For this, an all-optical self-routing switch, which changes signal route by address information on optical signal itself, is strongly required. Figure 1 shows our approach to realize this switch. That is a Mach-Zehnder interferometer with nonlinear optical medium inserted into one arm. An address light, whose wavelength is slightly different from that of a signal light, controls the phase status of the interferometer through the refractive nonlinearity. Therefore, it also controls which output-port a signal cell passes through.

The large refractive nonlinearity in semiconductor quantum wells [1] is attractive for this switch. However, much less study has been made on feasibility of the MQW in the 1.5-1.6μm wavelength region. For the first time, we demonstrate all-optical switching operation of Mach-Zenhder interferometer with a nonlinear InGaAs/InAlAs MQW waveguide designed for 1.55μm, which can open the way to all-optical self-routing.

2. Result and discussion

A waveguide with a 30-periods of intrinsic InGaAs/InAlAs (7 nm/7 nm) MQW as a guide layer was grown by Molecular-Beam Epitaxy. Absorption spectra of it exhibit clear e_1-lh_1 and e_1-hh_1 excitonic resonances at 1.435 μm and at 1.490 μm, respectively. It indicates fine confinement of excitons into the MQW. The refractive nonlinearity was evaluated by the change in transmittance of a signal light ($\lambda \sim 1.55\mu m$) through the Fabry-Perot Resonator with cleaved

facets. Figure 2 shows the spectral change of the FPR under various CW control light (1.48μm) power levels. The shift toward the shorter wavelength shows that the control-light decreases the refractive index. The evaluated phase shifts with the CW and the pulsed control-light are plotted as a function of the pump power in the inset. A half π phase shift, which is required for switching operation, occurs at 3.3mW of the pulsed control-light power at the facet.

Using these characterized waveguides, we made up a Mach-Zenhder interferometer of fiber optics to demonstrate all-optical switching operation as the first step for self-routing. Experimental setup is shown in Fig.3 (left). The nonlinear InGaAs/InAlAs MQW waveguide was inserted into one arm of the interferometer. The pulsed control light (1.48μm) modulates the refractive index of the MQW waveguide and changes the optical path of the signal light (λ~1.55μm) from the output-port 1 to the output-port 2. Signal light was intensity-modulated at 200MHz. The pulse width of the control light was about 30nsec, which was limited by the laser diode used in this experiment. Figure 3 (right) shows the waveforms of the signal light, the control light pulse, and the light pass through the output-port 2. This result shows that the signal light passes through output-port 2 only when the control light pulse exists in the nonlinear waveguide, indicating that the address light controls the optical path of signal cell as the header.

Switching power is evaluated to be 3 mW at the facet of the waveguide. This value coincides with the value estimated from the above result with FPR.

3. Conclusion

For the first time, we succeeded in demonstrating all-optical switching operation of Mach-Zenhder interferometer with a nonlinear InGaAs/InAlAs MQW waveguide designed for 1.55μm. Switching occurs at 3 mW of the incident control-light power into the waveguide. We convince that such a low power nonlinearity will open the way to all-optical self-routing and all-optical ATM network.

References

1. D.S. Chemla, D.A.B. Miller, P.W. Smith, A.C. Gossard, and W. Wiegmann, IEEE J. Quantum Electron., vol. QE-20, no. 3, p.265-275, 1984.
2. T. Kanetake, H. Inoue, S. Tanaka, and S. Hanatani; IEEE Photon. Technol. Lett., 6(3), 418, 1994.

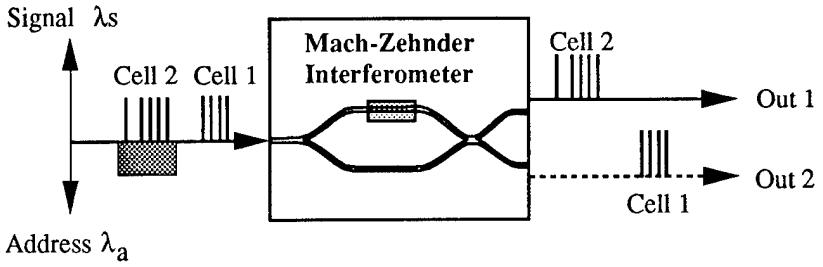

Fig.1. One approach to realize all-optical self-routing switch. Nonlinear optical medium is inserted into one arm of Mach-Zehnder interferometer. The route of signal cell is selected with address light as a header.

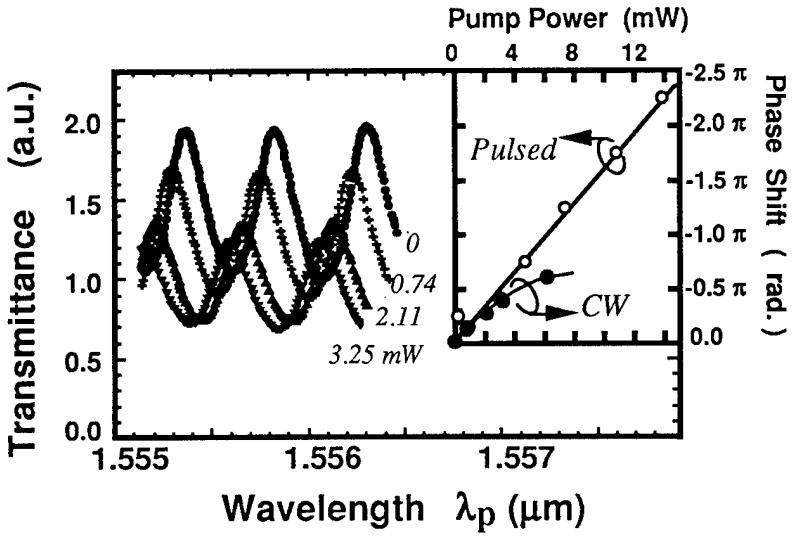

Fig.2. Transmission spectra of the FPR under various optical pumping levels. The inset shows the phase shifts under CW (closed circle) and pulsed (open circle) pumping conditions versus the launched pump power.

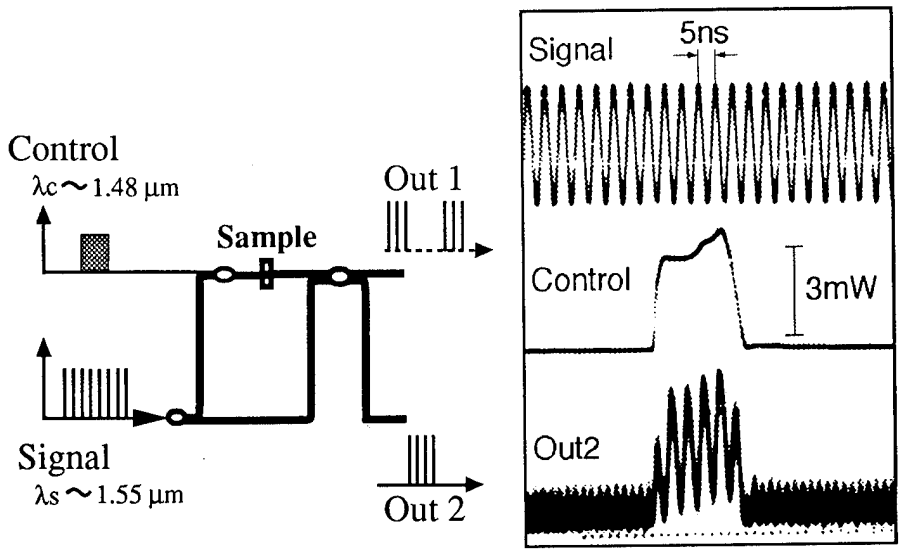

Fig.3. Experimental setup of the nonlinear Mach-Zenhder interferometer and the result. The signal light is intensity-modulated at 200MHz. The cotrol (address) light changes the optical path of the signal light from the Output-port 1 to the Output-port2.

Packet-Switched Photonic Networks: 1

PThA 8:30 am-10:00 am
Red Lion East

T. Yasui, *Presider*
Mitsubishi Electric Corporation, Japan

Photonic ATM switching for broadband network services

Tohru Matsunaga, Koji Sasayama, Yoshiaki Yamada, Keishi Habara and Ken-ichi Yukimatsu
NTT Network Service Systems Laboratories
3-9-11 Midori-cho, Musashino-shi, Tokyo 180, Japan
Tel: +81 422 59 3004; Fax: +81 422 59 2473

1. Introduction

Asynchronous transfer mode (ATM) is a promising switching and transport technology for carrying multimedia traffic in broadband ISDN (B-ISDN). With ATM, end-to-end information is transported as fixed-size packets, called cells; this provides the flexibility needed for multimedia traffic, which ranges from kilobits per second to gigabits per second. ATM is now being introduced in LANs, MANs and WANs to carry data traffic and will soon penetrate widely into public networks carrying voice and pictures as well as data. The throughput of ATM networks will grow rapidly as the provision of fiber-optic subscriber loops stimulates the demands for broadband multimedia services. To meet this increasing demands, higher speed ATM switches will be needed.

A tera-bps ATM switch requires an efficient combination of electronics and photonics. A variety of photonic ATM switches have been investigated [1-8]:

- A free-space interconnection-based system using VSTEPs [1] has demonstrated the operation of buffer memory and self-routing with 1.6-Gbit/s cells.
- An ultrashort pulse-based system with a broadcast-and-select star network [2] has been developed that uses time-division multiplexing of pico-second optical pulses. Video distribution demonstration has been achieved with a 25-Gbit/s throughput system [3].
- A high-speed space-switch-based system using a hypercube structure has been discussed, along with its routing algorithms [4].
- Frequency division multiplexing (FDM)-based systems [5-7] have drawn much attention, since laser diodes with a wide tuning range [9] and a low-loss high-resolution multi/demultiplexer [10] have become available.

This paper describes FDM-based photonic ATM switches and some experimental results.

2. Single-hop FRONTIERNET

Figure 1 shows the FDM-based photonic ATM switch, called "FRONTIERNET", we proposed in Ref. [5]. At the center of the switch, an arrayed waveguide grating filter (AWGF) [10] works as a frequency router; it routes optical signals from an input port to a particular output port determined uniquely by the combination of the signal's optical frequency and the input port number. The frequency of an ATM cell arriving at an incoming line interface (ILI) is converted to an appropriate one according for its destination. The AWGF, then routes the cell to its destination outgoing line interface (OLI). Although only one cell arrives at each input port at one time, multiple cells with different frequencies may be sent to an output port at the same time. Therefore, each OLI must have a multi-input buffer memory. Cell transfer operations are synchronized in the whole system.

This architecture is a simple modular structure with fewer components. Cells need to make only one hop in the system before reaching their destination OLI.

3. Multi-hop FRONTIERNET

The single-hop FRONTIERNET architecture is theoretically possible that many cells might be sent to one output port. This makes it difficult to design a large system because of the gain saturation of the optical amplifiers. We thus propose a multi-hop FRONTIERNET architecture (Fig. 2). It is based on a hypercube network along with detour routing [4]. Although cells need to hop several times before reaching their destination OLI, and so a loop-back function from OLI to ILI is necessary, the number of frequencies handled by each OLI is small and constant (= $\log_2$(total number of input/output-port pairs)). Thanks to the detour routing, this architecture requires less buffer memory than usual input- or output-buffer-type ATM switches even though it needs an input buffer memory. Figure 2 shows one possible routing for a cell arriving at ILI #7 ([111] in binary expression) with a destination of OLI #0 ([000]). The route is

Line Interface #7 ([111]) -- f_5 --> #6 ([110]) -- f_0 --> #2 ([010]) -- f_2 --> #0 ([000]).

Since the available optical bandwidth is limited by the bandwidths of the system components, mainly the optical amplifiers, and the number of ports on a single AWGF chip is limited, expandability is an important issue. Multi-hop FRONTIERNET has good expandability when the AWGFs have additional ports for system expansion.

Figure 3 shows the connection pattern for expanding using four AWGFs, each of which has two expansion ports. The pattern is based on the rule of hypercube interconnection. Cells going to a same AWGF are frequency-multiplexed on the expansion output ports, sent to the adjacent AWGF, and routed again to output ports according to their frequencies. The figure suggests that 2^n AWGFs with $(2^d + n)$ ports form a 2^{d+n}-line system using less than $(2^d + n)$ frequencies. That is, a 1024-line system is obtained by using 16 AWGFs with 68 (= 64 + 4) ports.

4. Experiment

Figure 4 (a) shows the experimental setup we used for testing a single-hop FRONTIERNET [5]; it has a 16-port AWGF with one-cell memory in OLI #12. The tunable frequency convertor in ILI #9 consists of two distributed-Bragg-reflector laser diodes (DBR-LDs), a 2x2 $LiNbO_3$ Mach-Zehnder-type switch, and a $LiNbO_3$ intensity modulator. The 2x2 switch allows alternating operation of the duplex DBR-LDs. The frequency-channel spacing of the AWGF is 100 GHz. The one-cell memory consists of a 2x2 switch based on semiconductor LD gates (SLGs), an optical-fiber loop, a semiconductor LD amplifier (SLA) including an isolator and a filter, an Erbium-doped fiber amplifiers (EDFAs), and a frequency selective 1x2 switch made of a splitter, filters, and a 2x2 $LiNbO_3$ Mach-Zehnder-type switch. OLI #12 receives cells of 1553.2 nm (f4) and 1552.4 nm (f5) from ILIs #9 and #10, respectively. Each cell contains 160 bits of 2.5-Gbit/s data. Figure 4 (b) shows the observed waveforms.

Figure 5 (a) shows the experimental setup we used to investigate the performance of the FDM loop buffer memories [11]. The structure of the buffer loop is the same as that in Fig. 4 (a), although some of the component characteristics are different. A 3-nm bandpass filter is used in the loop to eliminate spontaneous emission noise from the SLA. Two frequencies, 1554.6 and 1553.8 nm, are stored in the buffer loop; they are shown in Fig. 5 (b). A bit error rate of less than 10^{-9} was measured for 2.5-Gbit/s cells after ten circulations.

5. Conclusion

Two types of FDM-based photonic ATM switches; the single- and multi-hop FRONTIER-NETs, were described. Due to the frequency routing characteristics of AWGFs, their structure is simple. Multi-hop FRONTIERNET, furthermore, has the modularity needed to easily expand system size. Experimental results show the feasibility of both architectures.

References

[1] M. Nishio, et al.: "Photonic ATM switch using Vertical to Surface Transmission Electro-Photonic Devices (VSTEPs)", Proc. ISS '92, B10.4, 1992

[2] Y. Shimazu, et al.: "Ultrafast photonic ATM switch with optical output buffers", IEEE J. LT, Vol. 10, No. 2, pp. 265-272, 1992.

[3] H. Nakano, et al.: "Photonic ATM switching systems", Proc. APCC '93, 1C.1, 1993.

[4] T. Matsunaga: "Sorting-based routing algorithms of a photonic ATM cell switch: HiPower", IEEE Tr. Commun., Vol. 41, No. 9, pp. 1356-1363, 1993.

[5] K. Sasayama, et al.: "Demonstration of a photonic ATM switch using a frequency-routing-type time-division interconnection network (FRONTIERNET)", Proc. ECOC '94, pp. 533-536, 1994.

[6] S. Kuroyanagi, et al.: "A photonic ATM switching system using wavelength routing cell selector and optical fiber traveling-type buffer memory", Proc. ECOC '94, pp. 545-548, 1994.

[7] B. Bostica, et al.: "Photonic ATM cross-connect node based on cell aggregation and compression", Tech. Digest PS '93, PMA2, 1993.

[8] T. Matsunaga, et al.: "Photonic ATM switching technologies", IEEE Denshi Tokyo, No. 30, pp.138-142, 1991.

[9] H. Yasaka, et al.: "Broad-range wavelength conversion of 10 Gbit/s signal using a superstructure grating distributed Bragg reflector laser", Electron. Lett. Vol. 30, pp. 133-134, 1994.

[10] H. Takahashi, et al.: "Arrayed-waveguide grating for wavelength division multi/demulti-plexer with nanometer

resolution", Electron. Lett., Vol. 26, pp. 87-88, 1990.
[11] Y. Yamada, et al.: "Demonstration of a frequency-division-multiplexed optical loop buffer and its applications to a photonic ATM switch: Frontier Net", To be published in OFC '95.

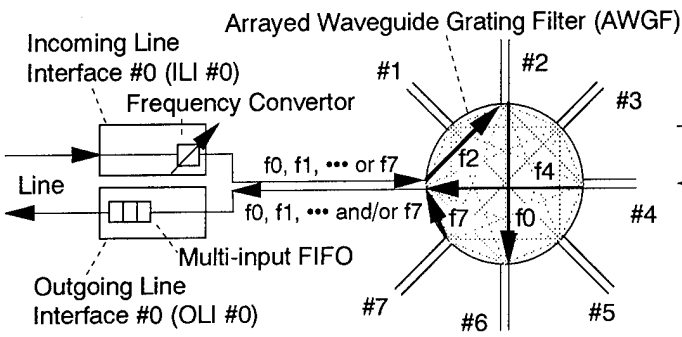

Fig. 1 Single-hop FRONTIERNET

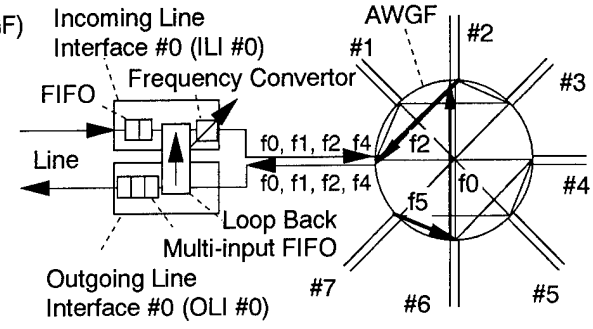

Fig. 2 Multi-hop FRONTIERNET

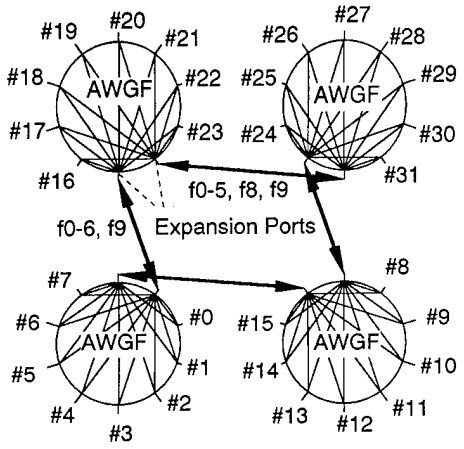

Fig. 3 Expansion of Multi-hop FRONTIERNET

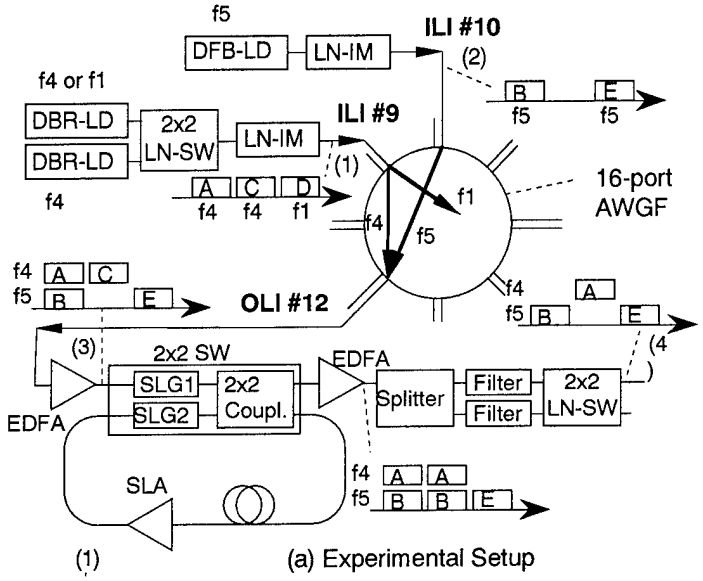

(a) Experimental Setup

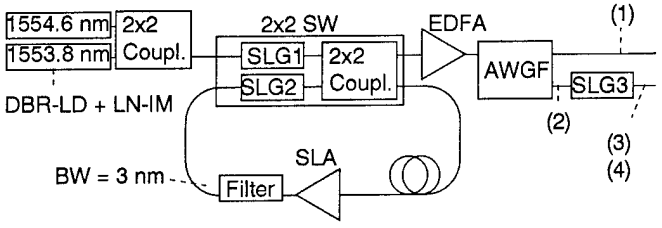

(a) Experimental Setup

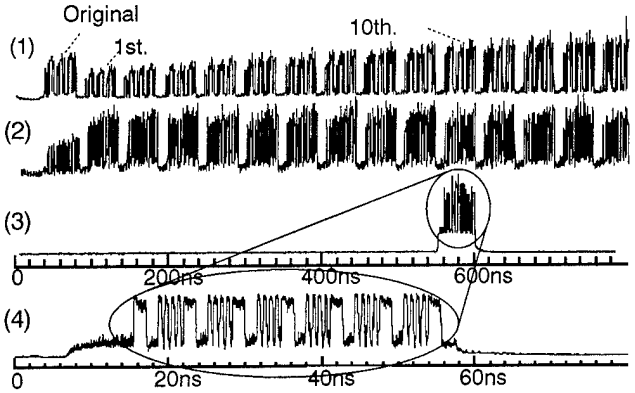

(b) Observed Waveform

Fig. 5 Experiment on Single FDM Loop Buffer

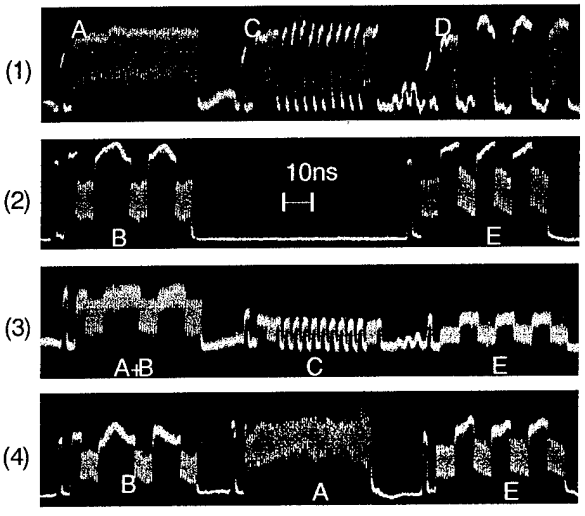

(b) Observed Waveform

Fig. 4 Experiment on Single-hop FRONTIERNET

Experiment on photonic ATM switches with WDM output buffers

Akira Misawa and Masato Tsukada
NTT Network Service Systems Laboratories
9-11, Midori-Cho 3-Chome, Musashino-Shi, Tokyo 180 Japan

Introduction

The asynchronous transfer mode (ATM) is attractive because it supports services having various bit rates. High-bandwidth optical technology using ATM will be the key to overcoming the throughput limitations of electrical systems. Some experiments on ATM switching with optical buffers have recently been presented[1, 2]. To increase the capacity of switching systems, wavelength division multiplexing is a promising technology in photonic switching[3]. We describe photonic ATM switches with wavelength-division multiplexed (WDM) output buffers. We use WDM technology to allow cell collision in a broadcast-and-select network, which leads simple network architecture. We also propose and experimentally demonstrate a WDM output buffer to read collided cells one by one.

Switch architecture

The architecture of the proposed switch is schematically shown in Fig.1. This switch is a broadcast-and-select network type ATM switch. Each input port is assigned a fixed wavelength (from $\lambda 1$ to λn). Optical cells are sent through a starcoupler, so all cells that are wavelength-division multiplexed are received without problems resulting from the cell collision. Every output of the starcoupler is connected to a WDM buffer. At each WDM buffer, only cells whose addresses match are selected. In Fig. 2, shaded cells denote ones with non-matching addresses, which are not selected. WDM buffers convert parallel WDM cells into time-serial cells in order that the O/E/O modules may receive one cell at most in one time slot.

Because this switch has inherent loss caused by division in the starcoupler, the switch size is limited by the receiver sensitivity of the O/E/O modules. However, the switch size can be increased by using a multistage network.

Buffer configuration

The WDM buffers we propose are schematically shown in Fig. 2. We adapted WDM fiber delay lines[4, 5] for optical buffer since they are transparent, so it is easy to treat WDM signals with little additional hardware.

The buffer functions are copy, delay, time-slot selector (T selector), and wavelength selector (W selector). An input stack of multiplexed cells is copied into m+1 stacks. Copy and delay is achieved by coupler and fiber line, respectively. These copied stacks are delayed by from 0 to mT, where T is the cell length and m is the buffer size. The T selector selects the oldest stack of cells in one time slot. Then the W selector selects one cell among the stacks. In Fig. 2, stacks of cells A and B are selected through gates having delay 0 or T and stacks of D and E through a gate of delay 0: Then cells A, B, and D pass out. Selectors are achieved by optical gates or photonic switches, which are controlled by an electric WDM buffer controller.

The buffer can control the cell throughput at the switch module according to back-pressure signals from the next stage[4].

Experimental setup

For our cell switching experiments using an optical WDM output buffer, we used the experimental setup shown in Fig. 3. Though the switch size n was 2, only one output buffer was demonstrated in the setup. The data rate was 10 Gbit/s. Optical cell streams were generated by two

10-Gbit/s pulse pattern generators and E/O modules. Two wavelengths (λ_1=1550.2 nm and λ_2=1553.2 nm) were multiplexed by the coupler. The cell length was 64 bytes (T=51.2 ns), which consisted of a guard band and data field. The guard band was 8 bytes (6.4 ns), which is large enough compared with the switching time of optical gates, which is around 5 ns.

In the WDM buffer, we used semiconductor optical amplifiers (Anritsu SD3A101P2) for optical gates (GT0 and GT1, GW1 and GW2) of the T and the W selector. All four gates of the T and W selector were controlled by a 3-Gbit/s multi pulse pattern generator operating at 19.53 Mbit/s.

Results

Cell sequences of buffer input and output are observed by an oscilloscope as shown in Fig. 4. The cell notation in Fig. 4 is as follow: A and B correspond to output port addresses, the first and second numbers are input port number (i.e. wavelength) and serial number of the input cell, respectively. In this experiment, the output port address in Fig. 3 has address A. The buffer passes only cells that have address A and outputs them sequentially. Cells B11, B21, B22, B23, and B12 are not selected. Cell A11 passes through GT0 and GW1. A12 passes through GT0 and GW1 and then goes out in the same way. A21, which is input simultaneously with cell A12, waits for A12 to be output. Then in the next time slot, A21 goes out through GT1 and GW2. A13 is discarded because the demonstrated buffer can hold only two cells at a time. A22, A23, and A14 go out after delayed T.

Eye patterns of input and output signals are shown in Fig. 5 (a) and (b). For the data field, a 2^7-1 pseudo-random-pattern is used. Though the eye pattern of the output signal has small eyes resulting from the path lengths and loss difference among the received cells, we observed a bit error rate of 2×10^{-11} in the output cell sequences of -12.94 dBm.

Conclusion

We proposed and experimentally demonstrated a fast photonic ATM switching system using WDM output buffers. Two wavelength-division multiplexed 10-Gbit/s optical cells could be switched by semiconductor optical gates. This switch inherently has multicast and broadcast functions, which have recently become important.

Acknowledgments

We would like to thank Ken-ichi Watanabe for his experimental assistance, Dr. Yoshihiro Shimazu and Jun Nishikido for discussion, and Tohru Matsunaga for encouragement.

REFERENCES

[1] M. Eiselt, G. Grosskoph, R. Ludwig, W. Pieper, and H. G. Weber, "Photonic ATM switching with semiconductor laser amplifier gates", Electron. Lett., 28, 15, pp.1438-1439 (July 1992).

[2] J. Spring and R. S. Tucker, "Photonic 2x2 packet switch with input buffers", Electron. Lett., 29, 3, pp.284-285 (Feb. 1993).

[3] K. Sasayama, K. Habara, W. De Zhong, and K. Yukimatsu, "Photonic ATM switch using frequency-routing-type time-division interconnection network", Electron. Lett., 29, 20, pp.1778-1779 (Sep. 1993).

[4] M. Tsukada, A. Misawa, J. Nishikido, Y. Shimazu, and H. Nakano, "Experiments on photonic cell switching with an optical input buffer", Elctron. Lett., 30, 13, pp.1081-1082 (June 1994).

[5] P. Morin and D. Chiaroni, "Photonic time-switching using semiconductor optical amplifier gates and fiber delay line optical buffer", Proc. Photonic Switching '92, 1992, Paper 2k3, pp.476-484.

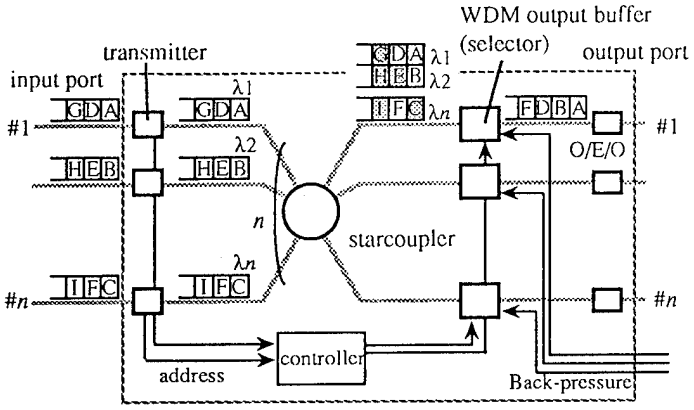

Fig. 1 Schematic of photonic ATM switch with WDM output buffers
(n denotes the network size)

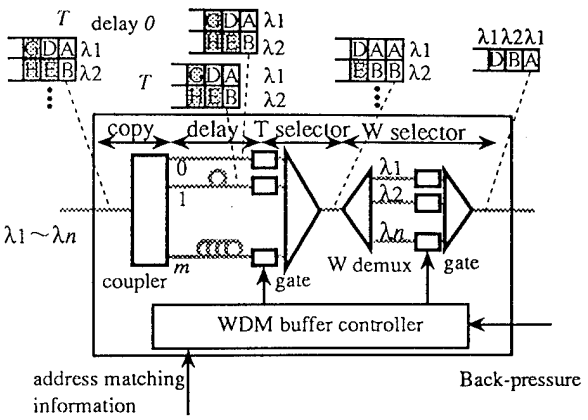

Fig. 2 Schematic of WDM output buffer that has selector function n: switch size, m : buffer size

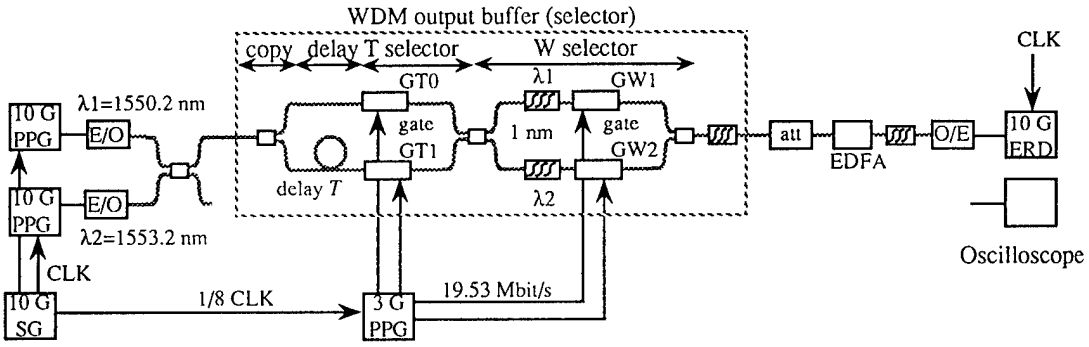

Fig. 3 Experimental setup of WDM output buffer type photonic ATM switches

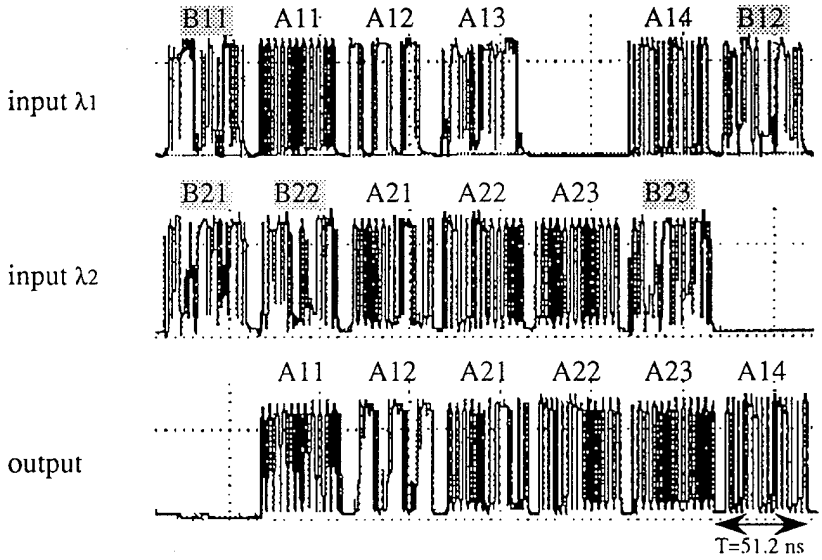

Fig. 4 Cell sequences of input and output of WDM output buffer

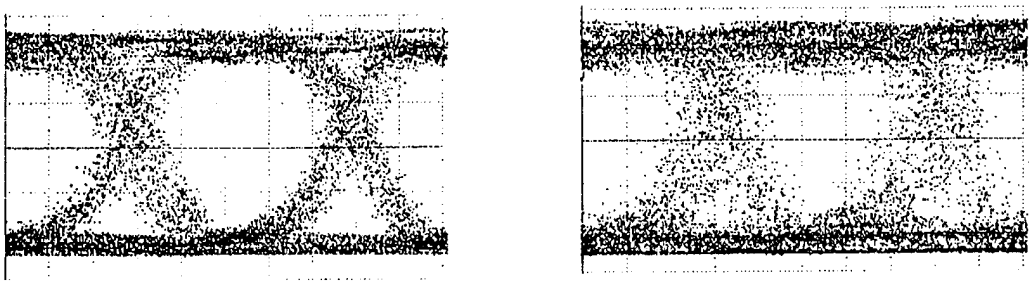

(a) input λ1 (b) output

Fig. 5 Eye pattern of WDM buffer input(after E/O) and output signal

Ultra-fast Photonic Packet Switching with Optically Processed Control

I. Glesk and P.R. Prucnal

Department of Electrical Engineering Princeton University, Princeton, NJ 08544

Tel: (609) 258 - 2041

Baolin Wang

Siemens Corporate Research, Princeton, NJ 08540

Tel: (609) 734 - 6535

In ultra-high speed networks individual address bits are spaced only picoseconds apart, and address recognition can be made by an ultra-fast demultiplexer which allows the packet to be routed without any opto-electronic conversion. One low-power device capable of performing the critical operation of reading address bits in an optically compressed packet header is the Terahertz Optical Asymmetric Demultiplexer (TOAD)[1].

To demonstrate all-optical address recognition and self-routing of photonic packets, one node of a network of 2x2 switches was used (see figure 1b). Packets, with 4 ps bit periods, were composed of a large amplitude leading clock pulse, a three bit header, and an empty payload. The switching node consists of an electro-optic switching element SW (e.g. 2x2 $LiNbO_3$ cross-bar switch) in a switched (cross) or unswitched (bar) state, an ultra-fast all-optical address recognition unit, routing controller which sets the state of the switching element, and an optical buffer that matches the delay of the input packet to the processing delay of the routing controller. Before entering the buffer a portion (10%) of the packet was split off and sent to the address recognition unit (two TOADs) to read two bits packet destination address. Demultiplexed address bits were sent to a routing controller which set the state of the 2x2 switch to a cross or bar state. Packets with destination address "11" were made to exit output port 2, while packets with destination address "10" were made to exit output port 1. Figure 1a shows the input multiplexed high intensity clock

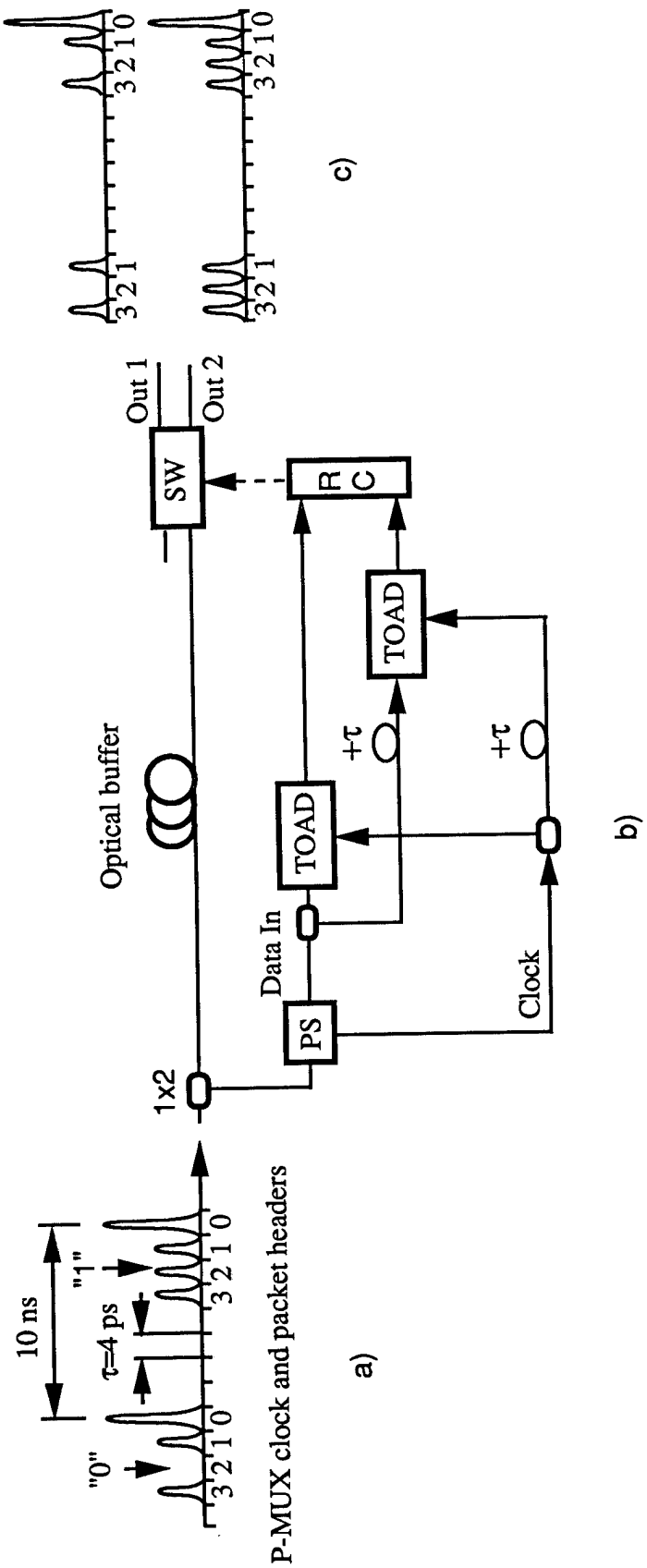

Figure 1. Self-routing of the photonic packet. a) Node input; b) Switching node diagram; c) Node output: routed photonic packets; output 1- packets with destination address "10", output 2 - packets with destination address "11".

and two packets: "1110 . . . 0" and "1010 . . . 0".

Figures 1c show the output of the routing switch SW, when the clock pulse has been synchronized to simultaneously demultiplex address bits 1(always "1") and 2("1" or "0"). When both address bits 1 and 2 are ("1") packets are routed to port 2. However, when bit 1 is "1" and bit 2 is "0" the packet is always routed to port 1.

In conclusion, these data demonstrate the all-optical processing and self-routing of a photonic packet without the need for any opto-electronic conversion for a case of two bit addressing. The address bit rate was 0.25 Tb/s (4 ps spacing between address bits). BER measurements of the set switching state were made by modulating bit 2 with a pseudorandom bit stream and monitoring the bit-error rate at the switching element. BERs of less than 10^{-9} were measured. This optically-transparent self-routing switching node can serve as a modular building block for 2-connected optical mesh networks.

References:

1. I. Glesk, J.P. Sokoloff, and P.R. Prucnal, *Electron. Lett.* **30**, 339 (1994).

Gigahertz Clock Synchronization using a Nonlinear Optical Loop Mirror as an All-Optical Phase Comparator

K.L. Hall, K. A. Rauschenbach, E.A. Swanson, S.R. Chinn

MIT Lincoln Laboratory
244 Wood Street
C-372
Lexington, MA 02173-9108
(617) 981-0229
khall@ll.mit.edu

and

G. Raybon
AT&T Bell Laboratories, Holmdel, NJ 07733

High-speed clock recovery or clock synchronization is an important function in realizing future 100 Gb/s time division multiplexed (TDM) communication systems. Optical clock recovery techniques are attractive because they can accommodate bit rates in excess of those allowed by electronics. To date, a number of optical clock recovery and synchronization schemes have been demonstrated including injection-locking diode [1] and fiber [2] lasers. Also, optical phase lock loops have been demonstrated using nonlinear crosscorrelation of two pulse streams as a bit phase sensor. Such schemes have included four wave mixing [3] and gain modulation [4] in diode amplifiers and second harmonic generation in a $LiIO_3$ crystal [5]. In this paper, we demonstrate all-optical bit phase comparison using a nonlinear optical loop mirror. In addition, we show that a harmonically modelocked external cavity laser can be synchronized to a 40 GHz pulse train generated using soliton compression of a Mach-Zehnder modulator output[6].

A schematic of the experimental set-up is shown in Figure 1. A 10 GHz pulse stream of 8 ps pulses is generated by harmonically modelocking a diode laser in an external cavity. These pulses have a center wavelength of 1541.6 nm and the electrical drive to the diode is a voltage controlled oscillator (VCO). The 40 GHz pulse stream is generated by soliton compression in dispersion tailored fiber. In this scheme, the output from a DFB laser is amplitude modulated using a commercially available Mach-Zehnder modulator. This modulator is biased at a null in transmission and is driven differentially by a 20 GHz r.f. signal. These bias conditions result in an optical output signal modulated at twice the applied frequency. This signal is amplified and compressed in a 4.65 km length of "comb-like" dispersion fiber, yielding a 40 GHz train of 3 ps pulses with a center wavelength of 1552.4 nm. Figure 2 shows the autocorrelation functions for the two pulse streams.

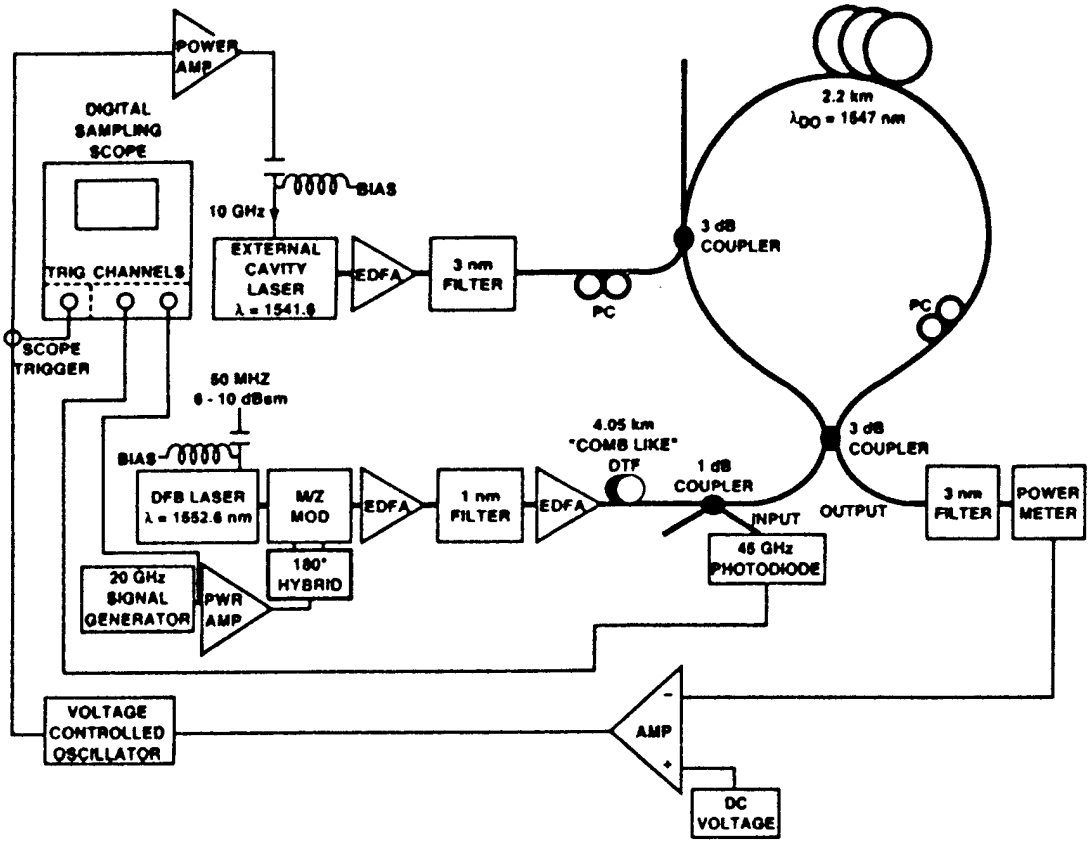

Figure 1. Experimental set-up.

The nonlinear optical loop mirror (NOLM) consists of 2.2 km of dispersion shifted fiber with a dispersion zero of 1547 nm. The control pulses are coupled into the NOLM by a wavelength independent 3-dB coupler. The polarization controller in the NOLM is adjusted so that in the absence of a control pulse (from the 10 GHz stream), a signal pulse (from the 40 GHz stream) is reflected at the input port. However, when a control and signal pulse are coincident in time, the signal pulse is transmitted through the output port. The NOLM acts as an all-optical AND gate.

In many cases, NOLM's have been configured as all-optical demultiplexers because they can be made relatively insensitive to timing jitter by utilizing the pulse walk through associated with polarization dispersion[7] and wavelength dispersion[8]. However, these same NOLM's can be used as bit phase sensors when control and signal pulse walk through is minimized. For example, when the signal and control wavelengths are equally spaced around the zero dispersion wavelength in the fiber, the group velocity for the two pulses in the loop is the same[9]. Then, any mismatch in timing between the two pulses will result in less signal power being switched out from the loop. In our scheme, an electro-optic PLL is constructed using the loop output power as a control signal for the VCO driving the harmonically modelocked external cavity laser.

Using the 10 GHz drive from the VCO as a trigger signal for the high-speed sampling oscilloscope, we measure the 20 GHz r.f. drive to the amplitude modulator and the 40 GHz optical pulse stream. Figure 3 (c,d) shows the measured electrical drive signal and optical pulse stream when the PLL is off. Note that there is no correlation between the 10 GHz

trigger and the 20 and 40 GHz waveforms. These traces have been averaged over many samples and are not a snapshot in time. However, when the PLL has locked the sources, the 20 GHz r.f. drive to the amplitude modulator (Fig. 3a) and the 40 GHz optical pulse stream (Fig. 3b) are synchronous with the 10 GHz drive to the modelocked external cavity laser and therefore to the trigger for the sampling scope. In our presentation, we will present autocorrelation data as well as sampling scope data that characterizes the switching operation of the NOLM when the sources are locked and unlocked. Also, we will discuss novel applications for the NOLM as a bit phase sensor.

In conclusion, we have demonstrated successful locking of a 10 GHz harmonically modelocked external cavity laser and a 40 GHz pulse stream generated using soliton compression of a Mach-Zehnder modulator and using a NOLM with zero pulse walk through as a phase comparator. The NOLM operates as an all-optical AND gate, with switching speeds limited only by the optical pulsewidth of the sources.

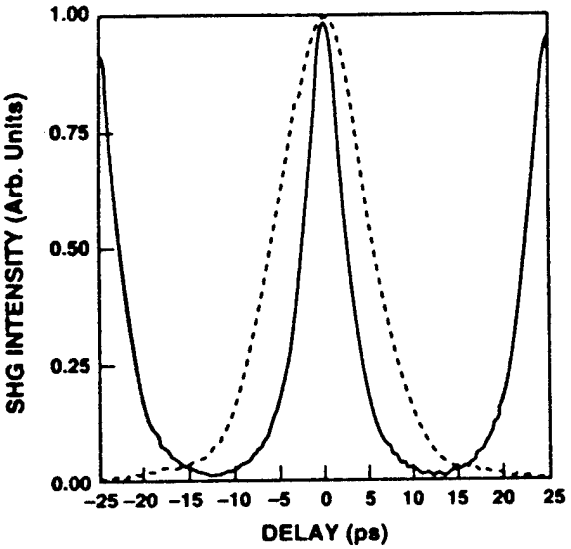

Figure 2. Autocorrelation traces for the 8 ps pulses in the 10 GHz pulse stream (dashed line) and the 3 ps pulses in the 40 GHz pulse stream (solid line).

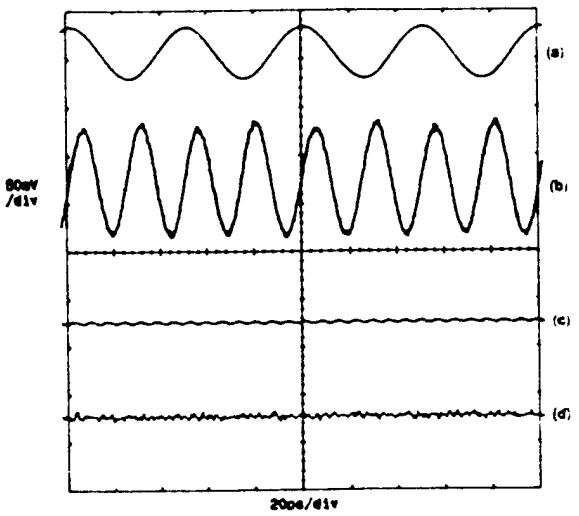

Figure 3. Sampling oscilloscope traces of the 20 GHz r.f. drive to the modulator (a) and the 40 GHz pulse stream (b) when the two laser sources are locked. When the sources are not locked, neither the r.f. drive (c) nor the pulse stream (d) are triggered.

REFERENCES

1. P.E. Barnsley, *IEE Proc. J*, **140**, p. 325, (1993).
2. A.D. Ellis et al., *Electron. Lett.*, **29**, p. 1323, (1993).
3. O. Kamatani et al., *Electron. Lett.*, **30**, p. 807, (1994).
4. S. Kawanishi et al., *IEEE J. Lightwave Technol.*, **11**, p. 2123, (1993).
5. S.P. Dijaili et al., *Appl. Phys. Lett.*, **55**, p. 418, (1989).
6. E.A. Swanson et al., *IEEE Photon. Technol. Lett.*, to be published in January, (1995).
7. J.D. Moores et al., *Opt. Lett.*, **16**, p. 138, (1991).
8. K.J. Blow et al., *Opt. Lett.*, **15**, p. 248, (1990).
9. M. Jinno et al., *IEEE J. Quantum Electron.*, **28**, p. 875, (1992).

An Optical Cell Synchronizer for Packet Switched Nodes

M. Burzio, P. Cinato, R. Finotti, P. Gambini, M. Puleo, E. Vezzoni, L. Zucchelli

CSELT - Centro Studi E Laboratori Telecomunicazioni
Via G. Reiss Romoli, 274
10148 Torino - ITALY

tel.: +39.11.2285.421
fax: +39.11.2285.085

Future high bit rate optical packet switched networks will be based on single or multiwavelength technology for transport, while the switching nodes, working in the optical domain, will operate on a cell basis, in a synchronous way. This will allow a fair resolution of contentions, through the use of optical buffers, and proper routing to the destination by means of space switching.

The synchronous operation of the optical packet switching nodes may imply stringent requirements on the timing of the packet arrivals at the node inputs, both at system start-up and following slow thermal variations in the fibers. For this reason cell synchronization must be provided at the node inputs, to align all incoming data flows to a local reference, as shown in fig. 1. This operation should be performed in the optical domain, to preserve the "transparency" of the whole node with respect to data bit rate and to overcome possible limitations of electronics at very high bit rates. Furthermore, in the case of a multistage switching node, the need for a "fine" synchronizer at the output of each switching module could arise, to recover cell timing fluctuations. Among the various constraints for the correct operation of an optical synchronizer a few must be underlined: (i) the cell start must be easily recognized, adopting a special format including a cell start identifier in the form of a coded bit sequence, as well as a guard band to allow setting of the O/E devices; (ii) at system start-up the transient towards the complete alignment must be as fast as possible, to avoid as far as possible data loss; (iii) the compensation range must be in the order or greater than one packet length; (iv) the time resolution must be compatible with the node specifications, but situations may occur in which a resolution << one bit duration would be necessary.

In this paper first experimental results obtained with the cell synchronizer structure proposed in [1] (patent pending) are reported, together with some implementation details. Fig. 2 shows a schematic of the synchronizer, which is composed by three main blocks: a coarse synchronizer, which is based on a cascade of switcheable optical fibre delay lines; a fine synchronizer, which exploits the chromatic dispersion in an optical fibre; and an electronic control. The control identifies the cell start and compares it with the local reference, driving the coarse synchronizer in a feed-back configuration and the fine synchronizer in a feed-forward configuration. The principle of operation of our system is explained in detail in [1]. The 64 byte long cell comprises a guard band and a four bit cell start identifier. These first experiments have been carried out at 622 Mbit/s. At the system start-up the algorithm implemented in the electronic control checks the position of the start word in several consecutive cells, to avoid false identifications. The fine synchronizer (fig. 4) is similar to that

described in [1]; however a 1.5 μm DBR laser with a more linear tuning characteristic has been used in the present work for the tunable wavelength converter (still based on a hybrid O/E/O approach); data reshaping followed by an external modulator have also been used. The delay range required by the fine synchronizer in this implementation is ± 400 ps: a fiber span with a total dispersion of ≈200 ps/nm has been used. The coarse synchronizer has been implemented using five low-loss thermo optic 2x2 switches (fig. 5), with fibre delay lines ranging from 400 ps to 6.4 ns; as no fast polarization independent 2x1 switch was available at the time of these experiment (e. g. an InP based DOS could be used [2]), a simple passive fiber coupler was used (which implies that there is data loss during the switching of the slow switches). Although the maximum achievable delay is less than a cell length at 622 Mbit/s (only for the temporary lack of some devices), all the same it has been possible to successfully demonstrate the principle of the synchronizer.

The electronic control (fig. 6) is based on four boards: the first one identifies the cell start, the second one filters the cell start identifier and calculates the delay with respect to the cell start reference, with 1.6 ns precision; the third one, which works in real time, controls the fine synchronizer driving the wavelength converter and calculates the delay between the cell and the synchronism in the range from 400 ps to 1.6 ns ; the last board receives the delay informations from the previous ones and provides the setting of the switches.

The test of the synchronizer has been performed by purposely delaying the data before entering the optical input of the synchronizer (a continuous flow of 64 byte long cells), generated by a 1.5 μm laser, with respect to the cell reference, and observing the output of the synchronizer on a sampling oscilloscope. Fig. 7 shows the result: the three traces represent a cell sync, before the synchronizer (upper trace), the output of the cell start recognizer (middle trace) and the data bits corresponding to the cell start identifier (1101 in this case, lower trace), By changing the data delay the result of fig. 8 is obtained: traces like those obtained in fig. 7 are superimposed, for various delays, up to 12.8 ns: a small "jitter" can be recognized in the data, due to the finite resolution and output power variations of the fine synchronizer, caused by the step wavelength tuning characteristic of the DBR laser in the Tunable Wavelength Converter. On the other hand, as expected, the cell start recognizer signal undergoes a jitter which is equal to $\pm T_m$, where T_m is the minimum delay in the coarse synchronizer,

In conclusion we have discussed some synchronization issues for an optical packet switched node, and presented experimental evidence of a first successful implementation of a cell synchronizer, operating at 622 Mbit/s.

References

[1] M. Burzio, P. Cinato, R. Finotti, P. Gambini, M. Puleo, E. Vezzoni, L. Zucchelli: "Optical cell synchronization in an ATM optical switch", Proc. ECOC'94, pp. 581-584, Firenze, Italy, Sept. 25-29, 1994.

[2] J. F. Venchant, M. Renaud, Ph. Jarry, A Goutelle, J. L. Peyre, M. Erman: "Fast, reconfigurable InP digital optical switches", Proc. OFC/IOOC'93, paper TuH2, pp. 30-31, San Jose, Ca, USA, February 21-26, 1993.

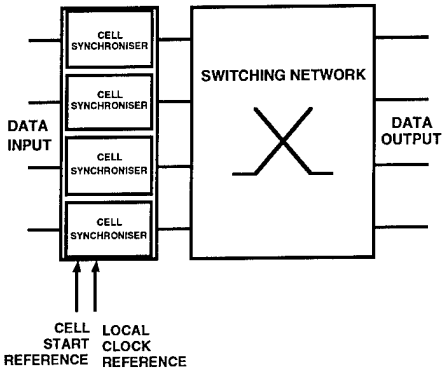

Fig. 1: Optical packet switched node with synchronizers.

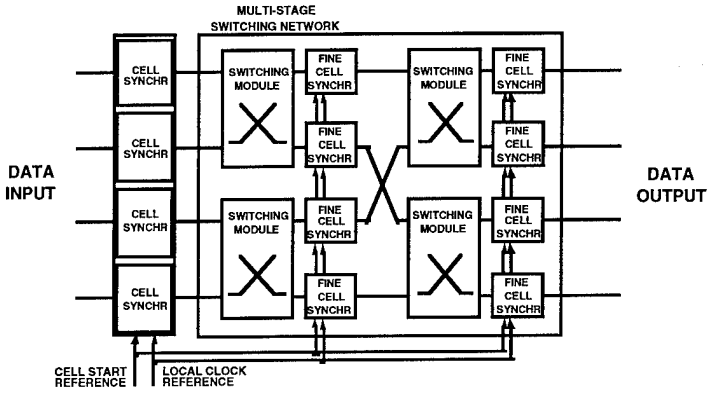

Fig. 2: Large size switching node with a multi-stage structure.

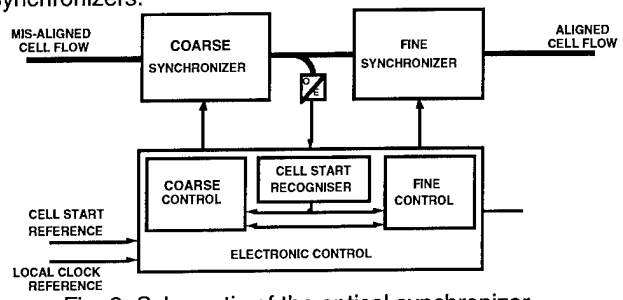

Fig. 3: Schematic of the optical synchronizer.

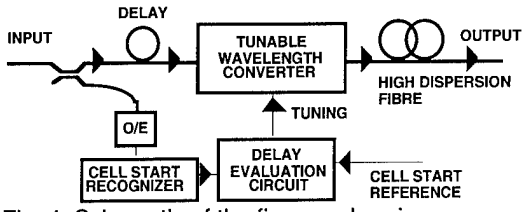

Fig. 4: Schematic of the fine synchronizer.

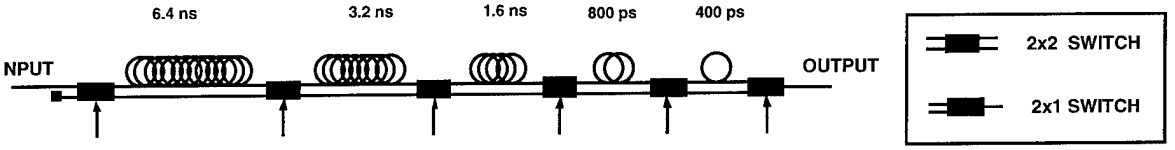

Fig. 5: Schematic of the coarse synchronizer.

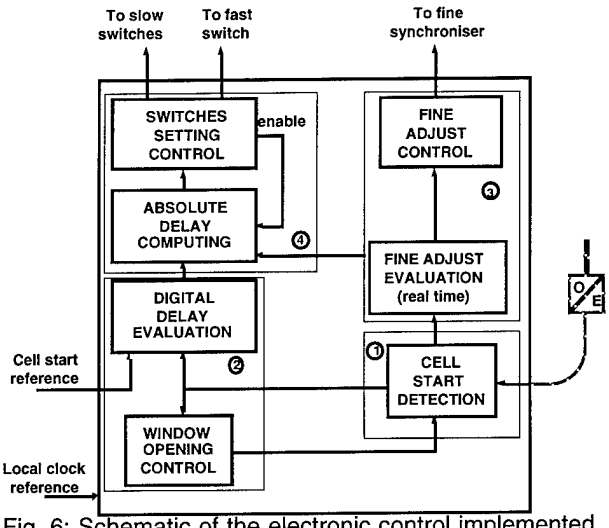

Fig. 6: Schematic of the electronic control implemented, with the four boards.

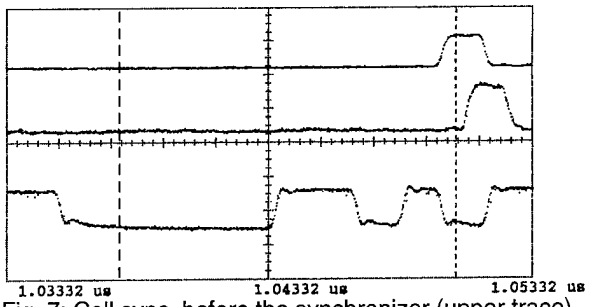

Fig. 7: Cell sync. before the synchronizer (upper trace), cell start recognizer output (middle trace) and output of the synchronizer (lower tace). Hor. scale: 2 ns/div.

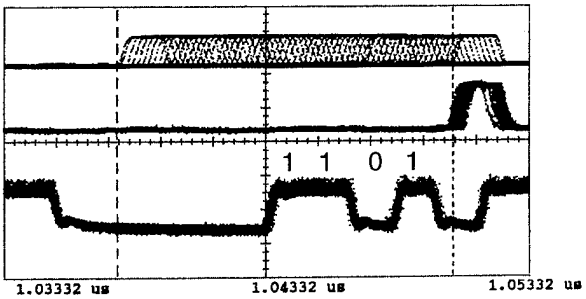

Fig. 8: As in fig. 7, but with several traces superimposed changing the input signal delay by 12.8 ns. Hor. scale: 2 ns/div.

Thursday, March 16, 1995

Operation of Photonic Networks

PThB 10:30 am-12:00 pm
Red Lion East

Charles Brackett, *Presider*
Bellcore

Management of Optical Networks

Sonny Johansson
Research Center System Switches
ELLEMTEL AB
Box 1505
S-125 25 Stockholm
Sweden

Anna Brodd, Kuno Elander
Ericsson Infocom Cunsultants AB

Management of optical network is an issue that is not very much discussed. Traditionally, we are only considering the transport aspects when optical networks are treated. We can define the transport view reaching from the basic generation of bits to the abstract level dealing with network functional architecture described by functions and reference points. These are all issues that tell us how to transport traffic between different locations.

The management view, on the other hand, is orthogonal to that of the transport view. Here we are interesting in how to transfer management information between the managing system and the optical nodes in order to ensure for the transport. We have to define: what management information that is required to route the traffic properly through the network, what eventreports that is received from the optical nodes when unambiguous occur, what action that should be taken to restore the transport in case of failure, and what should be monitored in order to guarantee the quality of the transport. This addresses questions on what information exchange that is needed between the management system and the optical nodes, which is defined by an management information model.

Before we through us in to the management world we have to start from the transport view, defining what network we should manage. This is accomplished by starting from the top-end defining a network functional architecture for the optical network layer similar to that what is defined for SDH, ITU-T G.803. Optical Trails and Optical Link Connections; Termination and Adaptation functions (see figure below) are examples of functional architectural components that have been defined during the work in RACE-MWTN.

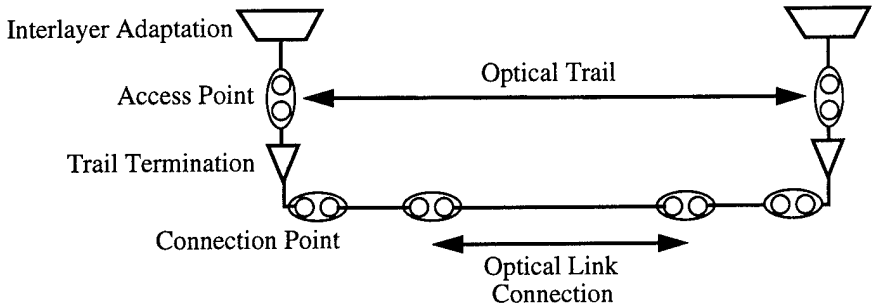

The network functional architecture is required when developing a network information model which defines the management view of the network in logical terms, Managed Objects (MOs). The ITU-T M.3100 provides a generic network information model and describes a standard set

of MOs and their properties, which are used when implementing the information model. In our case it was necessary to modify some MO (shaded in figure below), such as termination points for optical trails and optical link connections (optTTP and optCTP).

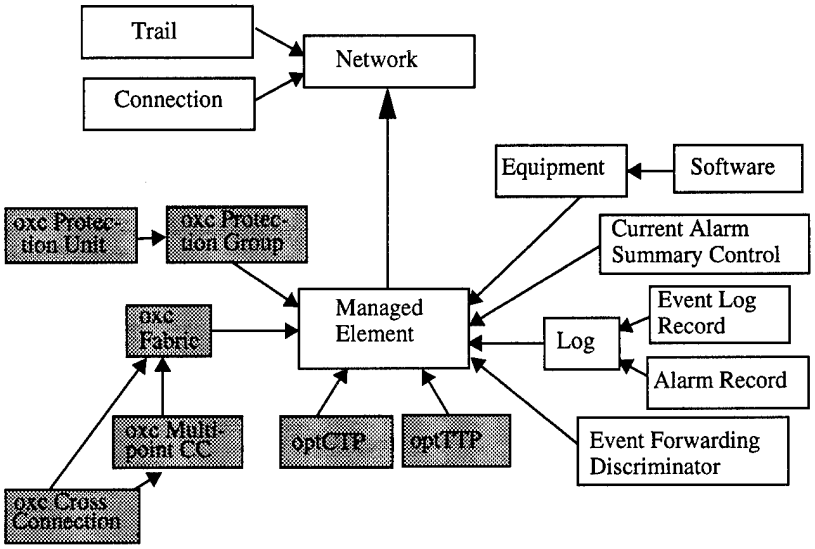

In the RACE-MWTN (R2028) we have been developing the demonstrator management system conforming the TMN standards (ITU-T M.3010). Two OXC nodes have been developed as Network Elements (NEs) communicating with our operations system (OS) over a Q3 interface.

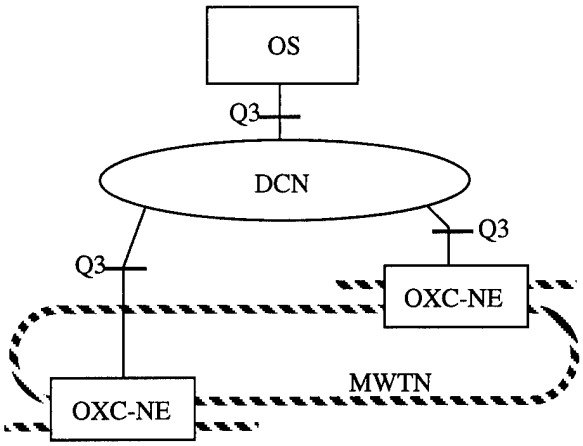

An OXC-NE is composed of optical devices included and a control system that present the OXC as a integrated NE to the Operations System. A TMN-Agent in the Network Element exchange management information with a TMN-Manager in the Operations System in accordance with the defined information model.

Acknowledge

RACE-MWTN (R2028), where this work was accomplished.

A Proposal and its Implementation Scheme of an Optical Network Management System

Tatsuya SHIRAGAKI, Naoya HENMI, and Masahiko FUJIWARA
Opto-Electronics Res. Labs., NEC Corporation
1-1, 4-chome Miyazaki, Miyamae-ku, Kawasaki, Kanagawa 216, Japan
Phone: +81-44-856-2310, E-Mail: shira@optsys.cl.nec.co.jp

Introduction Optical networks on which signals are routed and switched optically, are indispensable for achieving future large capacity and flexible communication networks. Some demonstration experiments have been carried out to show the feasibility of optical networks [1]-[4]. One of the most important issues in developing such networks is a network *Operation and Maintenance* (OAM) system. The present networks utilize an OAM system based on the SDH/SONET, in which OAM information is embedded in synchronous frames. Since, in the optical networks, some signals go through several nodes without any O/E and E/O conversions, OAM information cannot be obtained based on conventional schemes. An OAM implementation technology for optical networks should be put together, as some papers have pointed out [5],[6]. This paper proposes an OAM concept for optical networks. An implementation scheme for the concept is also proposed, and its feasibility is theoretically confirmed.

Basic Idea of a Proposed Optical Network OAM System In the optical network OAM concept, it is assumed that a conventional OAM system, such as that based on the SDH system, is utilized in an electrical layer. The OAM system for an optical network should complement the electrical layer system. Figure 1 is a schematic diagram of an optical network. In a certain node, an electric signal, which has been *Time Division* (TD) multiplexed and rearranged, is converted to an optical signal and enters a photonic switching network layer. In the photonic switching network, photonic *Wavelength Division* (WD) and *Space Division* (SD) switching technologies are used for routing the optical signal. Finally, the signal is converted to an electric signal, and demultiplexed into electrical-path-layer signals at some node. Between the two nodes where the O/E and E/O conversions are carried out, the contents carried by the optical signal are not changed while the signal is routed all-optically. This signal route defined by an optical signal should be identified to avoid mis-connection in the optical layer. Therefore, this should be one of the objects for an optical network OAM system. The authors define an *"optical path"* as this kind of an interval, as shown in Fig. 2. There can be two kinds of *optical paths*. One is defined by spatial (optical fiber) connection, and the other is determined by wavelength of the signal [7]. Since an optical signal is converted to an electrical signal at the end points of an *optical path*, some OAM information such as path identifier can be transported between a start point and an end point of an optical path. However, important information such as that regarding line-failure cannot be obtained efficiently by only monitoring optical paths' end points. The authors define an *"optical section"* as every interval between two consecutive optical nodes, to obtain and transport OAM information efficiently (Fig. 2). Indispensable optical network OAM information which should be transported in an optical section has been extracted referring to the SDH/SONET system. It should include *Automatic Protection Switching* (APS) information, optical cross-connecting information, and path identifiers as well as an order wire (OW) channel. The cross-connecting information is a type of information which uses *data communication channels* (DCC) in the SDH/SONET system. The APS between optical sections can be carried out by using photonic switching networks based on the OAM information monitored and transported for every optical section. Optical cross-connecting, which can rearrange the optical network flexibly, can also be carried out based on the information monitored at the end points of optical paths and optical cross-connecting information transported through each optical section.

Implementation of the Proposed Optical Network OAM Implementation of the proposed optical network OAM system is examined, considering the following general requirements;

- OAM information can be renewed at every node,
- OAM information transport means should have some survivability in itself.

We propose the system structure shown in Fig. 3 for realizing the proposed OAM system. In the configuration, the APS, cross-connecting information, and path identifiers which concern several fibers in an optical section as well as an OW channel are TD multiplexed into one signal at the sending node. The TD multiplexed signal is converted to an optical signal (an optical OAM signal) using a different wavelength from the main optical signals, and is distributed to several optical fibers. At the receiving node, after separating the optical OAM signals from main optical signals by WD demultiplexers, an optical selector segregates a single optical OAM signal. Using this structure, the OAM information can be renewed between every optical section. In addition, the number of transmitters and receivers for transporting OAM information will be reduced by using an optical divider and optical selector. Fault detection is also possible by simply monitoring the tapped optical OAM signals using low-speed fault-detectors placed in front of the selector. If a fiber is broken, a receiving node can select another fiber through which an optical OAM signal is transported. If the wavelengths in a 1.55 μ m band are used for the main optical signals, either a wavelength in the 1.3 μ m band or one in the 1.55 μ m band (other than used for the main optical signals) may be used for the optical OAM signal.

Evaluation of the Proposed OAM implementation The feasibility of the proposed OAM system has been evaluated theoretically. First, the required capacity for an OAM signal was examined, referring to the SDH/SONET system. The capacity for APS, DCC and OW are 128 kb/s, 768 kb/s and 64 kb/s, respectively, in the SDH/SONET system. This 768 kb/s DCC can deal with cross-connecting information for the approximately 50 paths in an SDH frame. Capacity for framing and identifiers are negligibly small. Required capacity for APS and optical cross-connecting was assumed to be proportional to the number of optical fibers involved. Capacity regarding optical cross-connecting is assumed to be at most to the extent of DCC capacity, because the number of optical paths (defined by wavelength) is considered to be less than the above described number of electrical paths (approximately 50). The calculated result for required capacity as a function of the number of optical fibers to be treated with an optical OAM signal is depicted in Fig. 4. Next, the loss budget for the optical OAM signal was estimated. An increase in the number of fibers to which an optical OAM signal is distributed, or an increase in the OAM signal capacity, will result in a decrease in loss margin for the system. The optical power level diagram was examined for two cases employing different devices as the optical selector; a Nx1 $LiNbO_3$ photonic switch (loss: 3.2 dB for a 4x1 switch) and a mechanical optical switch (loss: 0.5 dB). The optical receiver sensitivity was assumed to be -35 dBm at 622 Mb/s signal speed and inversely proportional to the required capacity for the OAM signal. A span loss of 20 dB (40 km) and system margin of 6 dB were assumed in the calculation. The capacity values limited by optical power level are also shown in Fig. 4. The calculated results show that the proposed optical network OAM system can handle OAM information of more than 16 fibers, each of which may include up to approximately 50 wavelength paths. This confirms the application feasibility of the proposed optical OAM system to practical systems.

Conclusion An *Operations and Maintenance* (OAM) system for optical networks with newly defined optical paths and optical sections has been proposed. An implementation scheme, in which the OAM signals relevant to several optical fibers are TD multiplexed and transported using different wavelength, was also proposed. The loss budget consideration for the optical OAM signal has demonstrated the application feasibility of the proposed scheme to practical systems.

References [1]T. Shiragaki et al., J. Lightwave Technol., vol.. 12, no. 8, p.1490, 1994. [2]T. Shiragaki et al., ECOC'93, ThP5.3. [3]T. G. Lynch et al., ECOC'92, ThA12.4. [4]S. Johansson, ECOC'92. WeA9.1. [5]R. S. Vodhanel et al., LEOS'94, ON4.1 [6]N. Wauters et al., ECOC'93, We3. [7]K. Sato et al., IEEE JSAC, vol. 12, no. 1, p.159, 1994.

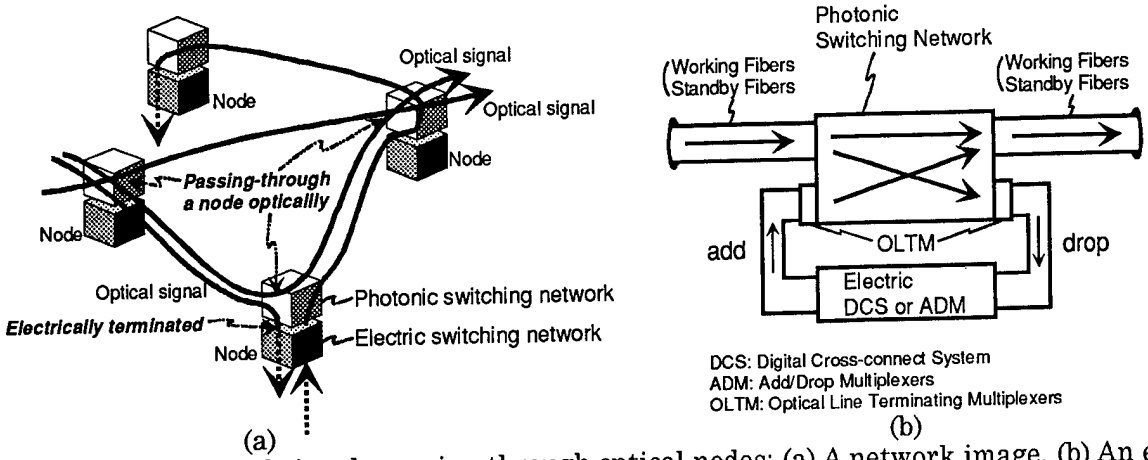

Fig. 1 Images of optical signals passing-through optical nodes: (a) A network image, (b) An example structure[2] for the network node.

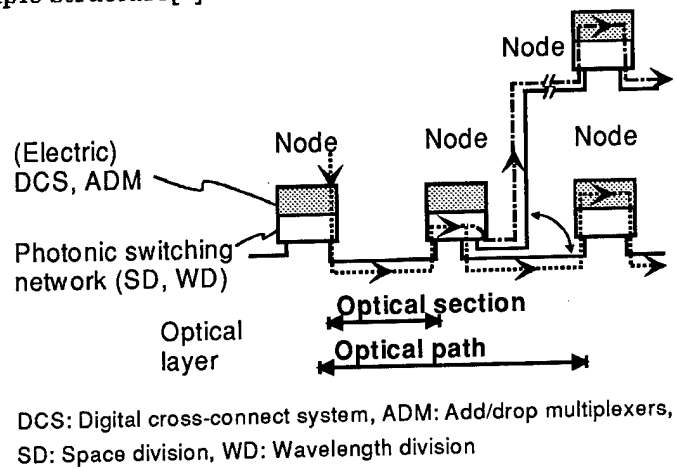

Fig.2 OAM layers structure for optical networks.

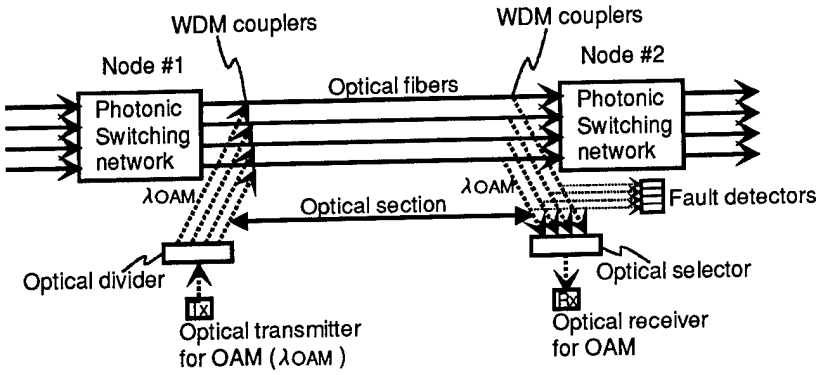

Fig. 3 Configuration of OAM implementation.

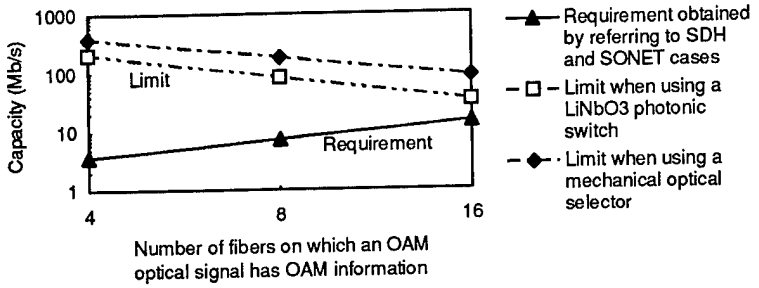

Fig.4 Required capacity for OAM and limited capacity for OAM by physical conditions.

An Optical Cross-Connect Architecture Incorporating Failure Recovery Using Reserved Wavelengths

S. Kuroyanagi, K. Hironishi, and T. Maeda
Fujitsu Laboratories Ltd.
1015 Kamikodanaka, Nakahara-ku, Kawasaki 211, Japan
Phone: +81-44-754-2623, Fax: +81-44-754-2741

Introduction

Optical path layer technologies are expected to be crucial in creating a flexible network architecture and expanding network capacity in broadband ISDN (B-ISDN) [1]. The optical cross-connect (OXC) is the main component in an optical transport network. OXC systems must offer a compact, economical switch architecture that allows effective modular growth. The OXC systems must also have robust network failure recovery, because large-capacity optical networks require a highly reliable optical path layer.

We modified our previously proposed wavelength-division (WD) switching network to allow modular expansion. We then compared the number of required optical devices in our switch with other structures. Using this switch, we also proposed an OXC architecture that provides failure recovery using reserved wavelengths.

OXC Switch Architecture

We already proposed a two-stage matrix WD switching network for photonic switching systems that implements tunable wavelength filtering and conversion [2]. Our network consists of two cascaded switch modules. Each crosspoint in the module has a switch element consisting of a wavelength filter and a wavelength converter. The photonic WD switching network switches the wavelength of the WD multiplexed (WDM) signals between two or more input-output paths call-by-call. The network is thus functionally the same as a virtual wavelength path (VWP) OXC which changes the wavelength link-by-link [1]. If the OXC allows modular growth for extra wavelengths and input-output links, we can increase its capacity as traffic increases. Our proposed architecture used a bus topology to split and combine the optical signals. However, a star topology is better for modular expansion than a bus topology. A star-topology WD switching network was recently proposed that is logically the same as our proposal (Fig. 1(a)) [3]. This network uses a star topology to split and combine the optical signals and allows modular growth in the number of wavelengths. We can also modify our proposal to allow modular expansion of the number of input-output links by using a star topology (Fig. 1(b)). This architecture can be expanded by adding modular units for more wavelengths and input-output links.

Besides being expandable, an OXC design must be low-cost and compact. Table 1 gives the number of optical devices required (not including splitters and combiners) for our structure (structure A) and for other proposed OXC [4,5,6] and WD switching network [7,8,9] structures (structures B to F). All the structures compared are non-blocking. As the table shows, our structure requires fewer optical devices than any other ($k \geqq 8$, $n \geqq 8$). Therefore, if we assume similar requirements for wavelength devices as for the optical switch (physical size, cost, and power consumption), our structure is lower-cost and more compact.

Failure Restoration

As network transmission capacity increases, link failures become a serious problem. Network restoration techniques are required to reroute a failed link to a normal link. Failure recovery using reserved wavelengths has been proposed [6].

We propose an OXC architecture that incorporates failure recovery based on reserved wavelengths.

We assume recovery that reroutes the path connection between two OXC nodes around link failures. Fig. 2 shows an example of path rerouting over reserved wavelengths for a single link failure. The link failure is between OXC-A and OXC-C. OXC-A reroutes the WDM signals from the working wavelengths to OXC-C through OXC-B using reserved wavelengths. The generic VWP OXC architecture consists of an OXC, an electrical XC, and an optical add/drop multiplexer (ADM) [6]. We divided the functions of the OXC into a routing block and a bypass block (Fig. 3). The routing block has three functions: First, to switch the wavelength and link position of the WDM signals from input links to arbitrary wavelengths and arbitrary links. Second, to switch the working wavelengths of WDM signals to reserved wavelengths and reroute the WDM signals to a normal link if a link failure occurs (OXC-A). Third, to return WDM signals arriving on reserved wavelengths to the working wavelength and route them to the required link (OXC-C). The bypass block passes WDM signals on the reserved wavelengths to the desired link without wavelength conversion (OXC-B).

Although the routing block also handles WDM signals on the reserved wavelengths, the total number of channels it switches is constant (kn). We can use our switch architecture shown in Fig. 1 as the routing block. However, this configuration increases the number of required wavelengths in the wavelength devices (Table 2). The bypass block requires a multi-wavelength filter (MWFIL) that can extract the reserved wavelengths, such as a wide band-pass filter or acousto-optic filter. Fig. 4 shows the structure of the bypass block using MWFILs. Type A consists of k^2 MWFILs. Type B consists of k MWFILs and k^2 optical gate switches (GSW). For a bypass, the MWFIL normally cuts off all incoming WDM signals and selects WDM signals with the reserved wavelengths. Evaluating feasibility based on power budget and signal-to-noise ratio (SNR) is an important technical issue for both the OXC and the optical transport network.

Conclusion

This paper outlined a switch structure that allows modular expansion to accommodate extra wavelengths and input-output links. This paper also proposed an OXC system, consisting of a routing block and a bypass block, that provides failure recovery based on reserved wavelengths. We think that our OXC is a promising architecture for developing a B-ISDN optical transport network.

References

[1]K. Sato et al., IEEE J. Select. Areas Commun., vol. 12, no. 1, pp. 159-170 (1994). [2]S. Kuroyanagi et al., Topical Meeting on Photonic Switching, 2C5 (1992). [3]H. -H. Witte, IEICE Trans. Commun., vol. E77-B, no. 2, pp. 147-154 (1994). [4]K. Sato, ECOC'94, pp. 919-926 (1994). [5]A. Jourdan et al., ECOC '94, pp. 563-566 (1994). [6]S. Okamoto et al., GLOBECOM '93, pp. 474-480 (1993). [7]M. Nishio et al., Topical Meeting on Photonic Switching, 14B-9(PD) (1990). [8]S. Suzuki et al., IEEE J. Lightwave Technol., vol. 8, no. 5, pp. 660-667 (1990). [9]B. Strebel et al., GLOBECOM '89, pp. 32-36 (1989).

Table 1 Number of required optical devices

	Filter		Converter		Switch (2x2, 1x2)	Total
	FFIL	TFIL	FCNV	TCNV		
Type A [2,3]	—	4nk	2nk	2nk	—	8nk
Type B [4]	nk	—	—	nk	nk^2	$2nk + nk^2$
Type C [5,7]	—	nk	nk	—	nk^2	$2nk + nk^2$
Type D [8]	4nk	6nk	6nk	—	—	16nk
Type E [9]	—	nk^2	nk^2	—	—	$2nk^2$
Type F* [6]	nk	—	nk	—	$(2n-1)(2nk + k^2)$	$4kn^2 + (2n-1)k^2$

Number of wavelengths: n Number of input-output links: k
FFIL: Fixed wavelength filter *: Clos network [ ]: Reference

Table 2 Number of required wavelengths

	Filter		Converter	
	FFIL	TFIL	FCNV	TCNV
OXC without recovery	—	Max [n, k]	k*	n
OXC with recovery	—	Max [2n, k]	k*	2n

Number of reserved wavelengths: n
*: Number of kinds of FCNV

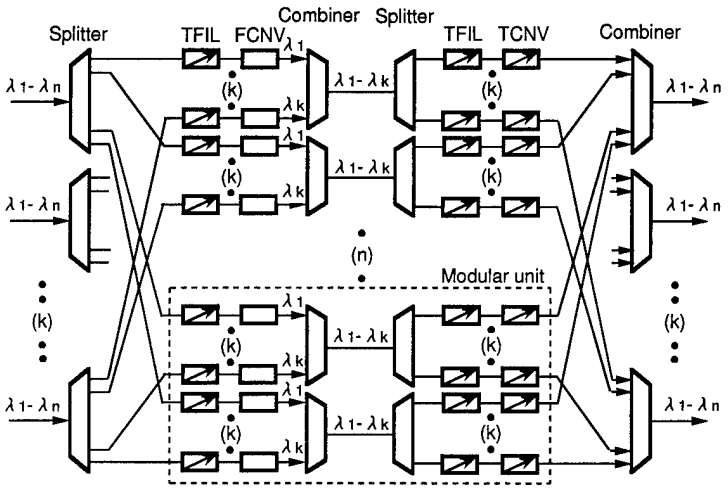

(a) Wavelength modular expandable switch structure

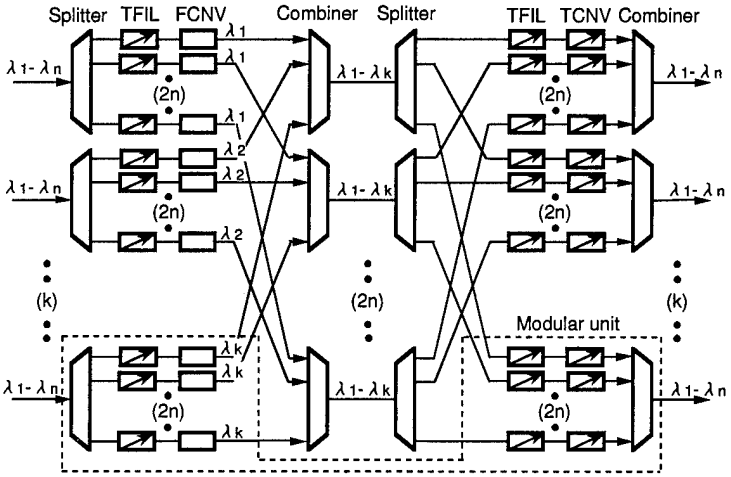

(b) Link modular expandable switch structure

FCNV: Fixed wavelength converter

TFIL: Tunable wavelength filter

TCNV: Tunable wavelength converter

Fig. 1 Modular expandable switch architectures

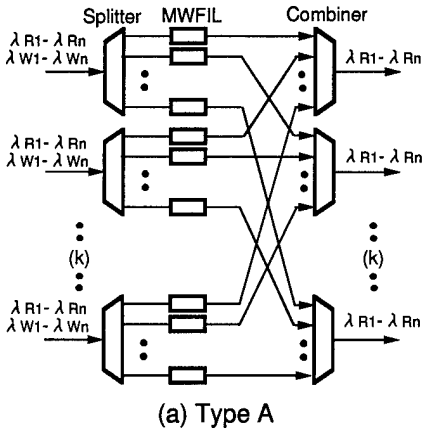

(a) Type A

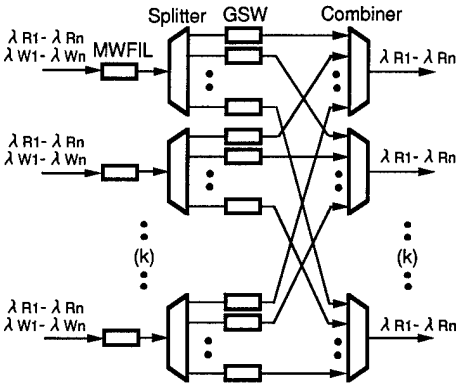

(b) Type B

MWFIL: Multi-wavelength filter

GSW: Gate switch

λ W1- λ Wn: Working wavelengths

λ R1- λ Rn: Reserved wavelengths

Fig. 4 Structure of the bypass block

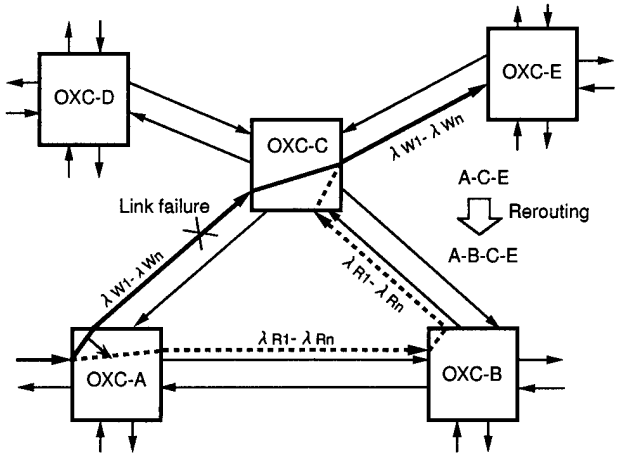

λ W1- λ Wn: Working wavelengths

λ R1- λ Rn: Reserved wavelengths

Fig. 2 Failure recovery using reserved wavelengths

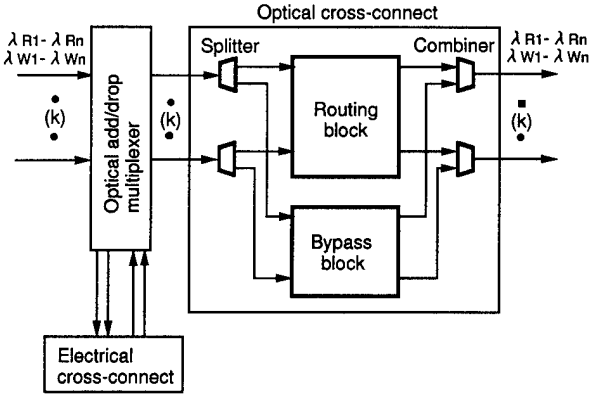

λ W1- λ Wn: Working wavelengths

λ R1- λ Rn: Reserved wavelengths

Fig. 3 Cross-connect architecture for failure recovery

Wavelength stabilization as a practical standard light source for wavelength division multiplexing system on 1.55μm

Yoshihiko Tachikawa, Yasuyuki Suzuki, Mamoru Arihara,
Takeshi Inoue, Shinichi Nakajima, Takaaki Hirata

Yokogawa Electric Corporation Optoelectronics Laboratory
2-9-32, Nakacho, Musashino-shi, Tokyo 180, Japan
Phone +81-422-52-5744 Facsimile +81-422-52-5928

Jun Ishikawa

National Research Laboratory of Metrology
1-4, Umezono 1-chome, Tsukuba-shi, Ibaraki 305, Japan
Phone +81-298-54-4045

Recent progress of communications requires the next generation of fiber optic communication systems such as wavelength multiplexing system (WDM) or optical time division multiplexing system (OTDM). For the demand on increase of transmission capacity, it is important to consider the wavelength dispersion of an optical fiber network and the gain spectrum of an erbium doped fiber amplifier. In order to realize above fiber optic systems, several wavelength standards are now under development.[1),2),3)] In this paper, we describe the construction and the specifications of a light source stabilized to an absorption line of hydrogen cyanide (HCN) gas on 1.55μm band.

Since it is well known that many absorption lines of HCN is on 1.55μm wavelength band, and the distance between neighboring absorption lines of an isotope of hydrogen cyanide such as $H^{13}C^{14}N$ is about 100GHz at optical frequency,[4)] we chose HCN gas for the wavelength stabilized light source as a standard material. The schematic diagram of the light source is shown in fig.1. The optical frequency from laser diode(LD) is modulated about ±5MHz by injection current with a small sinusoidal signal at 2kHz. To maintain the wavelength from LD to the center of an absorption line, two photodiodes(PD) and a divider are employed, and the output of the divider is synchronously detected by a lock-in-amplifier which output is fed back to the LD current. Fig.2 shows the short-term stability evaluated by the square root of the Allan variance for various averaging times τ in beat frequency fluctuation between two light sources. A square root of the Allan variance was obtained 2.5×10^{-10} for τ of 10s.

The absolute frequency and the long-term stability in optical frequency of a wavelength stabilized light source were evalu-

ated using a specially designed wavelengthmeter developed by National Research Laboratory of Metrology and Yokogawa Electric Corp..[5] Fig.3 shows the optical setup of the wavelengthmeter. The entire Michelson interferometer having a servo-controlled plain-moving mirror is put into a vacuum chamber and the reference laser is offset-locked by +100MHz to a standard He-Ne laser stabilized to the $^{127}I_2$,R(127),e-component. The frequency of the I_2-stabilized He-Ne laser has already been calibrated to within an accuracy of 6×10^{-11}. The optical frequency of the light source stabilized to the absorption line P(16) of $H^{13}C^{14}N$ was evaluated to be 192843.285GHz with the standard deviation less than 1MHz. The long-term stability in the frequency of one of our wavelength stabilized light sources is shown in Fig.4. The change in the frequency and the wavelength are less than 0.4MHz and 0.003pm over 2 years, respectively. Very small change has been achieved in the frequency characteristics of a wavelength stabilized light source using an absorption line of HCN.

As the result of the long-term stability evaluation, a light source stabilized to the absorption line of HCN is suitable for a wavelength reference in a WDM system and the other optical network systems.

References

1) Y. C. Chung, IEEE J. lightwave technology, vol.6, no.6, pp.869-876, 1990.
2) Y. Sakai, S. Sudo and T. Ikegami, IEEE J. quantum electron., vol.28,no.1,pp.75-81, 1992.
3) S. Yoshitake et al., SPIE vol.1837 pp.124-133, 1992
4) H. Sasada and K. Yamada, Appl. Optics. vol.29,no.24, pp.3535-3546, 1990.
5) J. Ishikawa and H. Watanabe, IEEE Trans. Instrum. Meas., vol.42, no.2, pp.423-425, 1993.

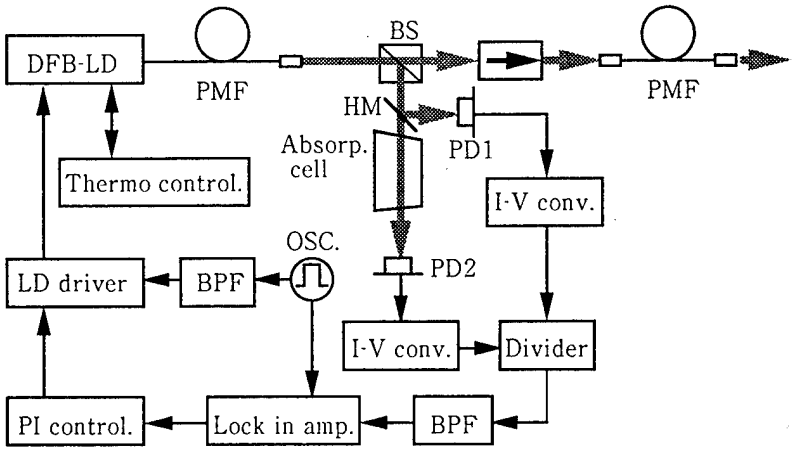

Fig.1 The schematic diagram of a wavelength stabilized light source.

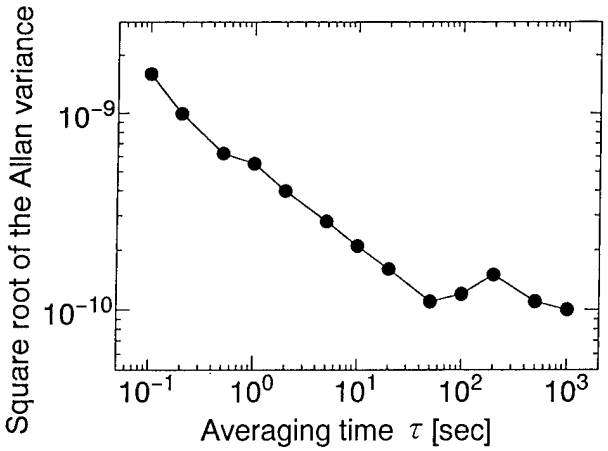

Fig.2 Short-term stability evaluated by the square root of Allan variance in beat frequency fluctuation between two light sources.

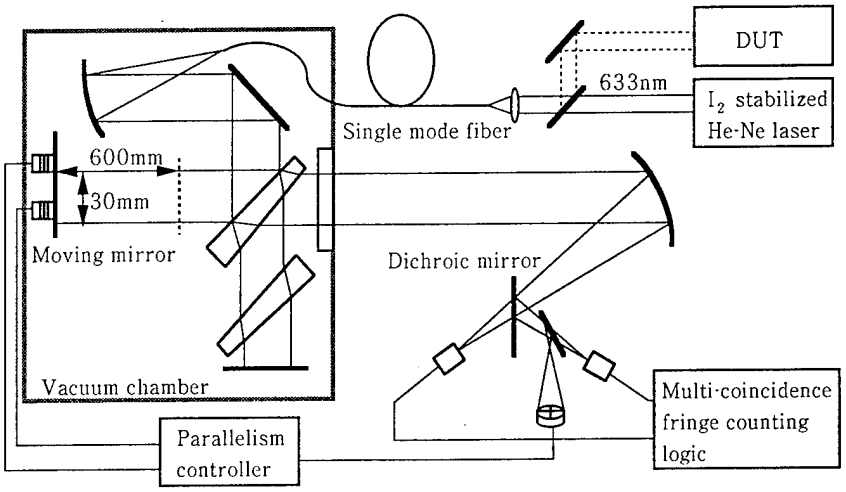

Fig.3 Optical setup of wavelengthmeter having a servo-controlled plain-moving mirror.

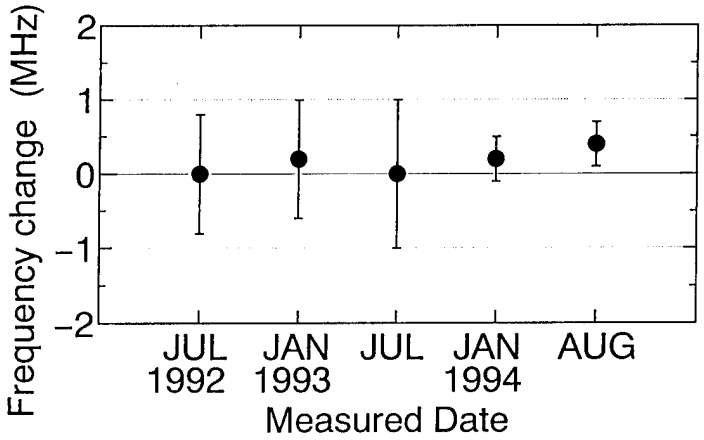

Fig.4 Long-term stability in the frequency characteristics of a wavelength stabilized light source.

Thursday, March 16, 1995

Packet-Switched Photonic Networks: 2

PThC 1:30 pm-3:00 pm
Red Lion East

Robert Leheny, *Presider*
ARPA

Photonics and ATM Switching

Jacques Dupraz
Alcatel
Rte. de Nozay, Marcoussis, F-91460, France

ATM in switching and optics in transmission are the key technologies of future broadband networks. This paper discusses the problems associated with the introduction of photonics in ATM switching from a technical viewpoint.

Photonic Switching of Optical Interconnects in Large Telecom Nodes

Magnus Buhrgard

Research Center System Switches
ELLEMTEL Telecommunication Systems Laboratories
Box 1505, S-125 25 Stockholm, Sweden
Telephone: +46 8 727 36 67

1 Introduction

A large scale introduction of broadband services would put challenging demands on the telecom transport network. The rapid development in optical transmission will most likely meet the demands in this area, whereas the potential bottlenecks are found in the transport network nodes. New technologies are needed to handle the large traffic through the nodes more efficiently.

There is a continuous development towards a higher degree of integration in switching hardware, especially for integrated circuits. However, the demand for considerably higher capacity in broadband telecom nodes will still result in a large amount of hardware. Interconnection between different parts of the switch fabric will be increasingly difficult as the bandwidth increases. Optical Interconnects (OIC) are well suited for carrying high speed data streams within a switch node. It is expected that OICs will be used e.g. in large ATM switches for transferring of signals between cabinets. The bandwidth that has to be supported between two cabinets can be tens of Gigabit/s. The OICs are not optically connected to the fiber transmission lines used between switch nodes, i.e. OICs have to be efficient enough to compete with coaxial cables on equal terms.

The next step would be to introduce photonic switching of OICs for even larger switches. In this case the optical domain is already introduced in the switch and a photonic switch element can be used directly to switch data streams between OICs in contrast to an electronic switch element which has to be combined with electro-optical conversion. The requirements on the photonic switch elements are less demanding as compared to switching of fiber transmission lines. The optical power budget is usually larger and dispersion effects can be disregarded.

The ideal task for photonic switching is infrequent and slow space switching of high bit-rate signals. The switching should be controlled by electronics and not have to be synchronized to the bitstreams which are switched nor require any memories. It is also advantageous if wavelength multiplexing can be utilized since it introduces a new dimension in photonic switching. Examples of how these types of photonic switching can be utilized to obtain large flexible broadband switch nodes are described in this paper.

In paragraph 2 suitable applications are presented. In paragraph 3 an ATM-switch, with Terabit/s capacity, is outlined as a more detailed example.

2 Suitable applications for photonic switching

There are two applications where OICs are likely to be used and where photonic switching can add further advantages: A) Between SONET/SDH transmission equipment and a switch or cross-connect; B) Within a large switch or cross-connect.

A1 Redundancy: A group of SONET/SDH Line Terminals (LT) are connected to a group of Exchange Terminals (ET), instead of a one-to-one relation between LTs and ETs. A simplified example

which illustrates the application is shown in Figure 1. This arrangement maintains full throughput if one of the ETs fails and reduced throughput if one of the switches fails.

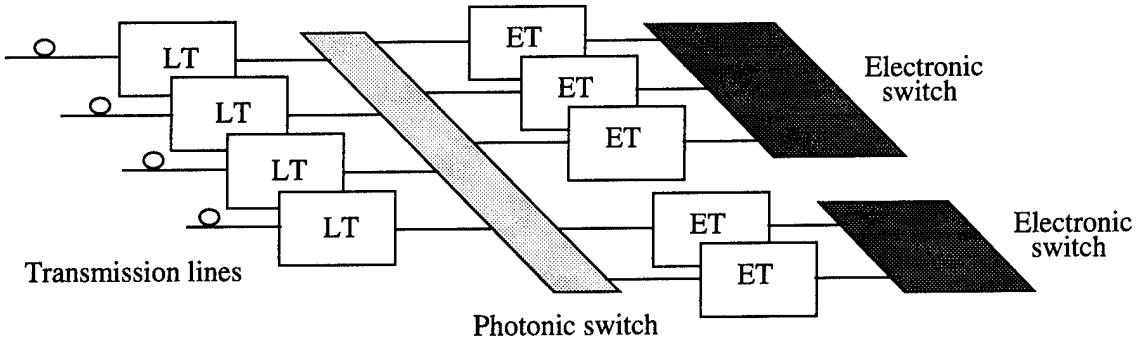

Figure 1 Redundancy through photonic switching

A2 Flexibility: Both ATM-switching and circuit-switching use SDH/SONET for transmission. The two switch modes will most likely coexist in future telecom networks. Photonic switching can connect the transmissions lines to the different switch types according to the changing traffic behaviour. This will increase the flexibility in the network.

B Within a switch: Photonic switching can be used if the switch architecture has a block with pure space switching which only requires relatively slow switching. This may seem as severe restrictions but it is quite possible to design efficient switch architectures using such blocks. An example is described below.

3 A Terabit/s ATM switch with photonic switching

Switch architecture: Photonic switching is used to connect different ATM access units, see Figure 2. The bandwidth allocated between the units will change in response to changes in traffic. The switch has a three stage structure, where the first stage, *the input stage*, is partitioned equally between the access units. This is also the case for the third stage, *the output stage*. These stages are both using electrical switching, whereas the second stage is performed by the photonic switch fabric.The photonic switch fabric routes 2.5 Gb/s cell streams in the optical domain. Changes in the routing can be done in the millisecond time scale i.e. the photonic switch acts as a cross-connect and does not have to switch individual ATM cells.

The ATM access unit is composed of two parts. It has one part which belongs to the input stage of the switch, where the inputs are connected to device boards with different speeds and the outputs holds the transmitter end of optical interconnects carrying ATM cell streams at 2.5 Gb/s. The purpose of this part is to route the cells to the correct output and synchronize them to other cells which have been routed to the same output. The other part of the access unit belongs to the output stage of the switch. It has optical interconnect receivers at the inputs and the outputs are connected to the same device boards as the input stage part. The purpose of the output stage part is to route the incoming cells to the correct device board. The output stage part is equipped with ATM cell buffers which are used to resolve congestion at the outputs.

Both the input stage part and the output stage part are complete switches, i.e. ATM cells can be routed from any input to an arbitrary output. This gives the flexibility needed to obtain a non-blocking three stage switch structure. Up to 16 ATM access units can be connected to the photonic switch fabric which gives a total switch capacity of 1.25 Tb/s.

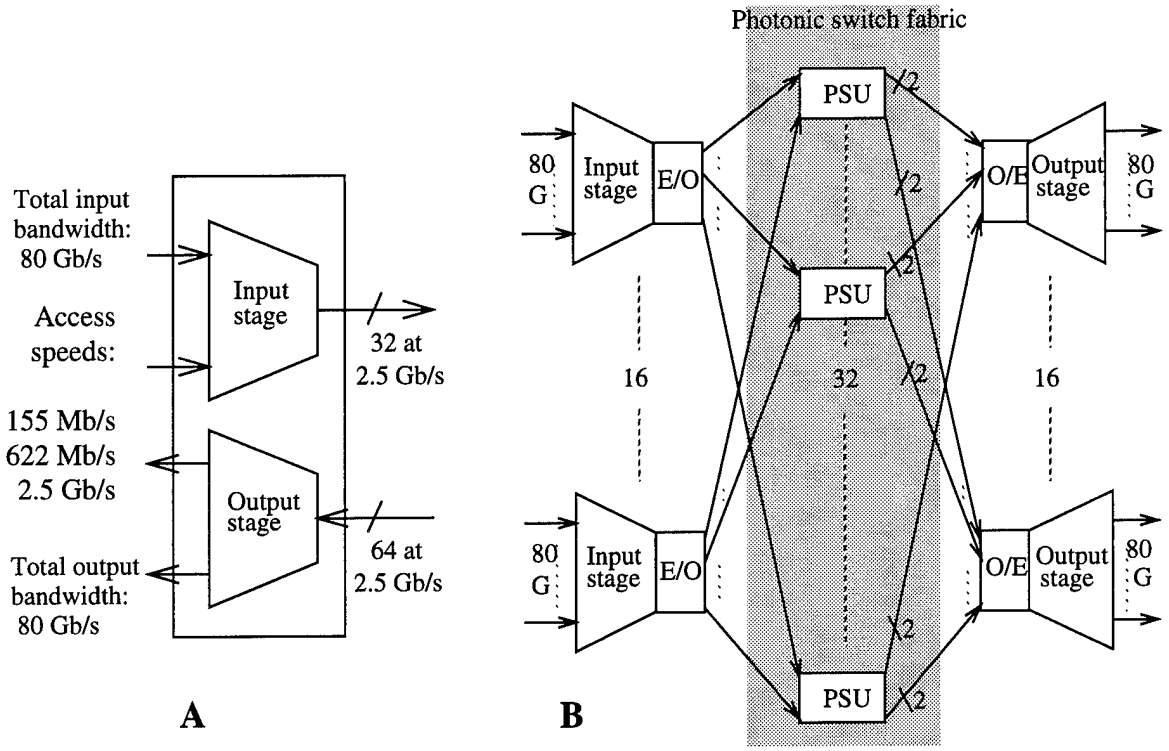

Figure 2 A: Schematic picture of the ATM access unit
B: The photonic switch fabric in its context, PSU: Photonic Switch Unit.

System characteristics: Following the ATM standard, traffic treated by the switch is connection oriented, i.e. a connection is established between the end users before ATM cells are sent and routed through the switch. Cells belonging to a certain connection are always routed in the same way through the switch. The main characteristics of each connection is stored in the management system which is associated with the switch. Based on that information e.g. peak bandwidth, burst duration, a rough estimate of how the available bandwidth between the access units should be divided can be made. The estimate is continuously updated as existing connections are closed and new ones are established. The optical paths through the photonic switch fabric are created in accordance with the estimate and can be changed by the management system when needed. The photonic switch fabric is designed to be non-blocking to ensure that the estimated bandwidth allocation always can be carried out.

The photonic switch fabric: Figure 2B shows the structure of the photonic switch fabric and its connections to the input and output stages of the switch. The photonic switch fabric is composed of 32 photonic switch units (PSU). Each PSU has 16 inputs and 32 outputs. It is a 16 x 16 switch matrix with a 1:2 passive split at each matrix output. Only space switching is performed in the photonic switch fabric. The 1:2 passive splits are introduced to obtain a more flexible bandwidth allocation between ATM access units. That feature is not explained in this summary.

Non-blocking through WDM: In order to fulfil the requirements on a non-blocking switch network wavelength division multiplexing (WDM) is used. The optical transmitters in the input stage can emit either of two different wavelengths and the receivers in the output stage can select either of them. The PSU is not wavelength selective, hence the WDM is only performed in the input and output stages. It is possible to omit the WDM scheme, but then the number of inputs and outputs in the ATM access units have to be doubled and the photonic space switch has to be expanded accordingly.

A Novel Photonic Architecture for High Capacity ATM Switching Applications

D. Chiaroni*, C. Chauzat, D. De Bouard, S. Gurib, M. Sotom, J.M. Gabriagues
* Alcatel CIT - Centre de Villarceaux, 91625 Nozay Cedex, France
Alcatel Alsthom Recherche, Route de Nozay, 91460 Marcoussis, France

Introduction

More and more, the capacity of telecommunication networks will have to be increased so as to meet the future needs of the customers in terms of bandwidth. ATM has been identified as a standard switching technique for the future broadband network. For these reasons an optical ATM switching architecture [1] has been proposed and recently demonstrated with the build up of a 4x4 switching matrix operating at 2.5 Gbit/s.

Tremendous progress has been achieved in the field of the switching components. The all optical wavelength converters [2], multiwavelength optical gates and wavelength channel selectors [3] are as many key components enabling the implementation of future photonic ATM switching architectures.

In this paper, we describe a new optical switching architecture relying on the same principles as those used for the previous demonstrator [4] but arranged in a different way, following the so-called broadcast-and-select scheme. First experimental results obtained at a bit rate of 2.5 Gbit/s are also reported.

The optical ATM switch architecture

The switching architecture relies on the use of wavelength encoding to achieve cell routing and the exploitation of optical Fiber Delay Lines (FDLs) accessed by fast optical gates to perform cell buffering and time switching. The NxN matrix, described in figure 1, is basically composed of three main blocks, namely the cell encoder, the cell buffer and the cell selector.

- The wavelength encoding block consists of a set of N All Optical Wavelength Converters (AOWCs), one per input and each being assigned one fixed wavelength.
- The buffering and time switching block includes M Fiber Delay Lines (FDLs) and a space switch using Semiconductor Optical Amplifier Gates (SOAGs).
- The wavelength selection block is based on a set of N Wavelength Channel Selectors (WCSs) built up with optical demultiplexers and SOAGs.

The principle of operation can be depicted as follows. Each incoming cell is assigned one wavelength by means of a wavelength converter identifying its input port, and then fed into the cell buffer. All cells are experiencing all possible delays achievable within the buffer. The role of optical gates of the buffer associated to each output of the switch is to select one timeslot corresponding to the appropriate delay, as determined from actual traffic conditions at the input. All signals, at all available wavelengths are gated simultaneously. Finally the wavelength selector only discriminates one outgoing cell at a time, on the basis of its encoding wavelength, i.e. its input address. One of the main advantages offered by the proposed architecture is that multicasting is provided easily, as the same wavelength can be selected at any time at any output port. This should be of prime importance to meet the requirements of future applications and services.

Three key devices are required for the implementation of this architecture, namely the AOWC, the SOAG and the WCS.

- The AOWC can be based on a SOA operated under cross-saturation regime [2]. This device has proven to be easy to use thanks to its polarisation and wavelength insensitivity and could moreover accommodate very high bit rates. By adopting a contra-directionnal launching configuration, the device can cope with an input wavelength identical to the ouptut one.
- Both the buffer and the SOAGs are to be operated in a multi-wavelength regime. To avoid interchannel cross-modulation which might occur in conventional SOAs, clamped-gain SOAs [5] are required, which maintain the gain at a constant value. Dynamic ranges of input power well above 12 dB have been recorded at 2.5 Gbit/s on first samples tested in our laboratory, allowing a capacity of 16 channels in such an architecture.
- The WCS could be realised by combining one optical demultiplexer to separate the wavelengths, a set of SOAGs to achieve the cell selection and one multiplexer to recombine the selected cells towards one common output port. This device takes advantage from the fast switching capability of the SOAGs. Previous preliminary experiments at 2.5 Gbit/s have shown that such a device can cope with a 2-bit guardband with a negligible penalty [6].

Experimental results and discussion

A first experimental set-up operating at 2.5 Gbit/s was assembled and equipped so as to experimentally simulate switching matrices with various sizes. The hardware actually implemented is represented with thick lines in figure 1. Each incoming optical signal experiences a transmission path throughout the switching matrix, which is to some extend independent from the size of the switch. Contrary to what occurred in the previously proposed architecture, each signal does not suffer from any accumulation of extra noise generated by amplifier gates other than those involved. The only limitations of size are imposed by both the input power and the dynamic range of the SOA gates.

The figure 2a shows the Bit Error Rate (BER) performance as a function of the switch size (4x4 and 16x16) when only one channel is launched into the switch. A 0.7 dB penalty was recorded for a 4x4 switch with respect to the back-to-back and no additional penatly has been measured increasing the switch size to 16x16.

The figure 2b shows the BER evolution for both sizes when feeding the switch with an additional source simulating the presence of the 3 or 15 missing channels. A less than 1 dB penalty has been recorded in both configurations with less than 0.5 dB variation on the sensitivity due to the switch size increase.

The present architecture takes advantage of components with fast switching times. The switching functions are essentially located in SOA devices. When electrically driven, the switching time is below 800 ps (rise time + delay). Thus, the guard band can be limited to only two bits. The integration can be easily effective with an optical gate array technique [7]. The integration is also possible in the WCS [3,7] which offers attractive perspectives.

Keeping in mind that the guard band can be reduced to only two bits at 2.5 Gbit/s, the upgrade to bit rate as high as 10 Gbit/s is quite realistic (one byte for the guardband). The number of inputs is limited currently to 16 but can be iincreased by an optimisation of the SOAGs. With a sufficiently high input power in the first stage (after the first multiplexer) the output optical signal-to-noise ratio would be high enough to allow the cascade of elementary modules.

Conclusion

The new optical ATM switch architecture takes advantage of new optoelectronic components capable of fast switching. Experiments at 2.5 Gbit/s using a wavelength channel selector [6] have shown the ability to reduce the guard band to only two bits at 2.5 Gbit/s with no extra penalty due to the switching regime. Theoretical predictions have shown a favorable optical signal-to-noise ratio (more than 19 dB in a 0.5 nm filter bandwidth) at each output of the switching matrix. Experimental tests on one optical path through the matrix in transmission regime at a bit rate of 2.5 Gbit/s have led to a penalty lower than 1 dB compared to the back to back in a 16x16 configuration. No more than 0.5 dB penalty has been recorded between the 4x4 and the 16x16 configuration. Finally the number of channels simulated by turning on or off an extra source simulating the presence of 16 channels and by adjusting the channel powers did not introduce any significant variation of the transmission performance. Thanks to the high performance obtained and its capability for broadcasting, the novel photonic ATM switching architecture seems very promising for future broadband applications.

References

[1] D. Chiaroni et al. "Rack-mounted 2.5 Gbit/s ATM photonic switch demonstrator", ECOC'93, Montreux, Switzerland, post-deadline paper ThP12.7.

[2] K. Stubkjaer et al. "Semiconductor Optical Amplifiers as Linear Amplifiers, Gates and Wavelength Converters",ECOC'93, Montreux, Switzerland, paper TuC5.1.

[3] M. Zirngibl et al. "Digitally Tunable Channel Dropping Filter/Equalizer Based on Waveguide Grating Router and Optical Amplifier Integration", IEEE Photonics Technology Letters, Vol. 6, No. 4, April 1994, pp 513-515.

[4] J.M. Gabriagues and J.B. Jacob. "OASIS : A High-speed photonic ATM switch Results and Perspectives", accepted for communication to ISS'95.

[5] G. Soulage et al. "Clamped Gain Travelling Wave Semiconductor Optical Amplifier as a Large Dynamic Range Optical Gate", ECOC'94, Firenze, Italy, paper Tu.P.20.

[6] D. Chiaroni et al. "Wavelength Channel Selector with Subnanometric Resolution and Subnanosecond Switching Time", ECOC'94, Firenze, Italy, paper We.A.4.4.

[7] D. Leclerc et al. "High Performance Semiconductor Amplifier Array for self-Aligned Packaging using Si V-Groove Flip-Chip Technique", ECOC'94, Firenze, Italy, paper Th.B.4.4.

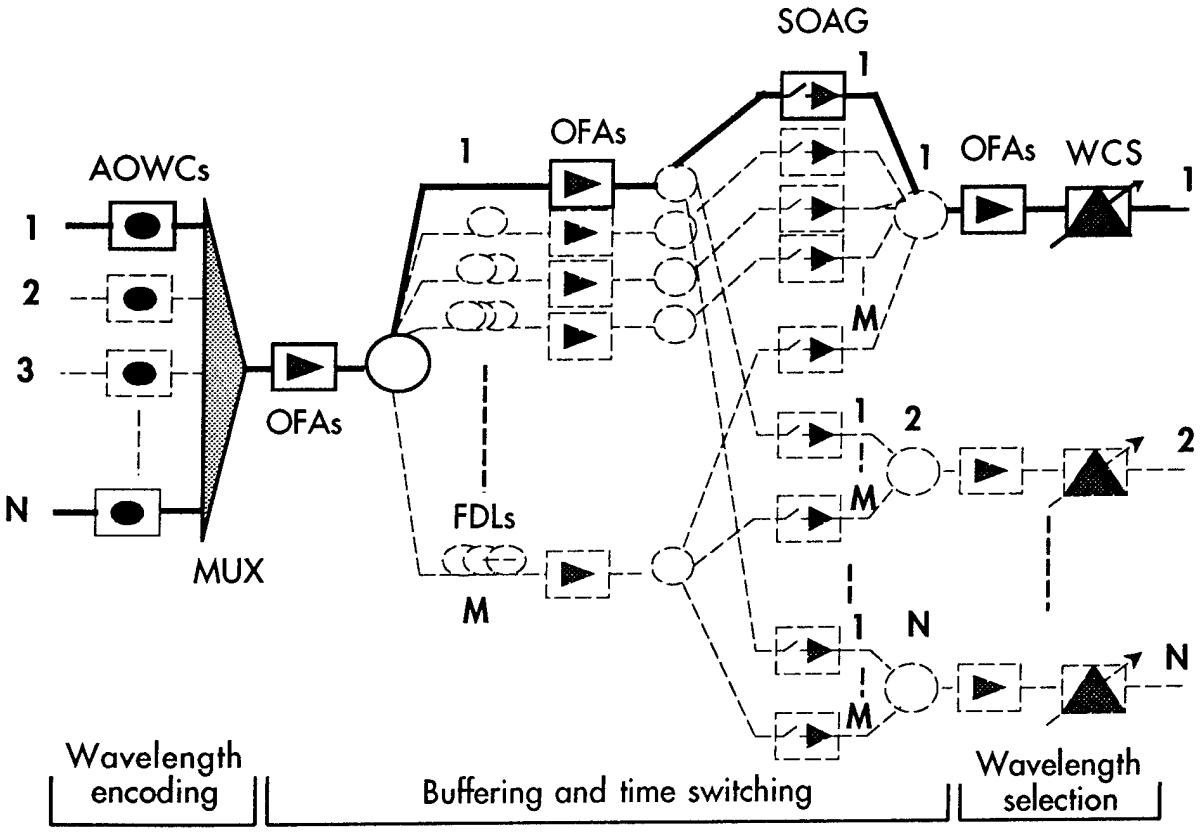

Figure 1 : The ATM switching architecture in a N x N configuration containing a M position buffer.
The thick lines indicate the optical path actually implemented and tested.

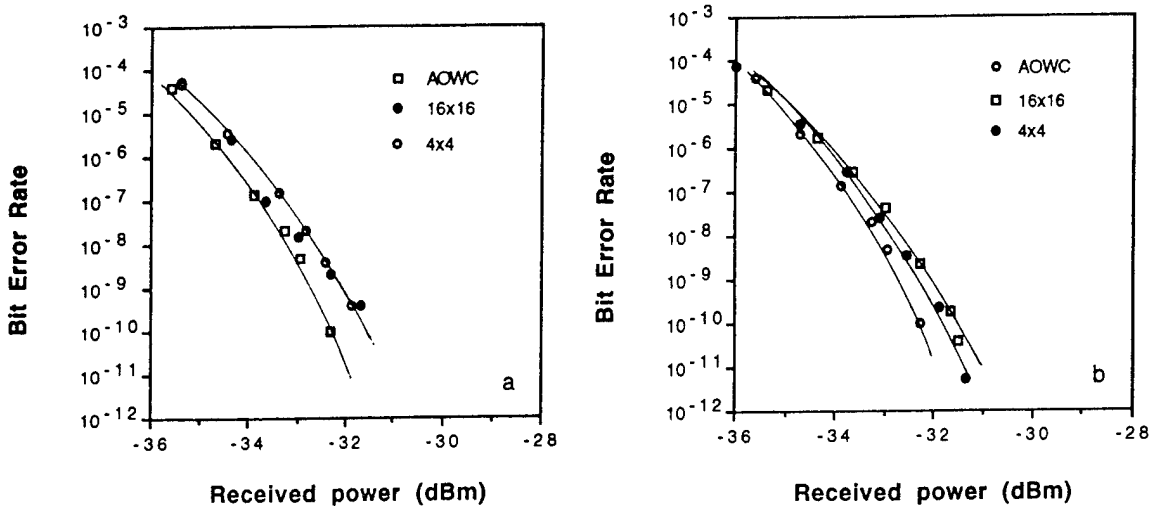

Figure 2 : Transmission tests at 2.5 Gbit/s for different sizes N=4 or 16
a : when only one channel is launched into the switch.
b : when feeding the switch with an additional source in order to simulate the presence of 16 channels.

Fanout, Replication, and Buffer Sizing for a Class of Self-Routing Packet-Switched Multistage Photonic Switch Fabrics

Ashok V. Krishnamoorthy and Fouad E. Kiamilev*

AT&T Bell Laboratories
Advanced Photonics Research Department
Holmdel, NJ 07733
*University of North Carolina at Charlotte
Department of Electrical Engineering
Charlotte NC 28223

We present the Stretch multistage switch; a class of self-routing multistage interconnection networks that provides a continuous performance-cost tradeoff between two of its degenerate forms: the Knockout switch[1] and the Tandem banyan network[2]. Stretch networks utilize simple destination tag routing and can be designed to achieve low delay and arbitrarily low blocking probabilities for random, permutation, and non-uniform traffic without using internal buffers in the switches. These qualities make them useful for both fast packet (ATM) switching and multiprocessor architectures. The flexibility of the architecture helps the designer to accommodate user requirements in terms of packet loss probabilities while allowing the structure of network to be driven by technology considerations. The advantages of the Stretch multistage switching fabric come to bear in cases where the number of channels is very large and the ability to use fanout in the network is available. These considerations make it a good candidate for a photonic implementation. In this paper, we discuss the design of switch fabric and suggest a possible photonic switch implementation.

There are two primary sources of packet loss in fast packet switches: internal link contention (ILC) and output port blocking (OPB). The former occurs when two or more packets contend for the use of the same interconnection link within the network. The latter occurs when more than one packet attempts to exit the switch on the same output port. According to the Knockout principle[1], a ceiling on the packet loss probability can be achieved by incorporating a fixed number of buffers per output port. The knockout switch uses a fully connected switch architecture (N^2 links and switches) to eliminate ILC and a fixed number of buffers per output port to limit OPB. However, for large numbers of interconnected channels or ports, architectures that limit the bisection width of the network to NF (with $F < LogN$) are preferable. At the other end of the performance/cost spectrum, a Tandem banyan switch minimizes the bisection width and the number of links and switches; it uses multiple banyan networks placed back-to-back to reduce ILC, and output buffers to limit OPB. But, for delay sensitive applications, and for non-uniform "hot-spot" traffic, the need to reduce ILC in Tandem banyan networks becomes apparent.

The "Stretch" network was designed to provide a tradeoff between the Knockout switch and the Tandem banyan in terms of ILC. In physical terms, this is accomplished by trading the bisection width of the network versus the number of switching stages (depth). Stretch networks incorporate fanout stages similar to extended generalized shuffle (EGS) networks[3], concentrating fanin stages similar to the knockout switch[1], and cascaded back-to-back networks similar to the Tandem banyan network[2]. The fanout stages enable partial contention-free routing to one of F pipes; the fanin stages provide buffering and concentration of outgoing packets, and the back-to-back extended banyan networks provide low contention routing. A Stretch switch is characterized by a number of parameters: N,F,K,P,R, and T[4,5]. N denotes the number of input/output channels . F is the maximum fanout or fanin. K is the number of input/outputs of the switching element used in the switching and routing stages. P is the number of packet buffers per output channel. R is the number of back-to-back replications of the unipath Stretch[N,F,1] network, and T is the

number of Stretch[N,F,R] networks used in parallel.

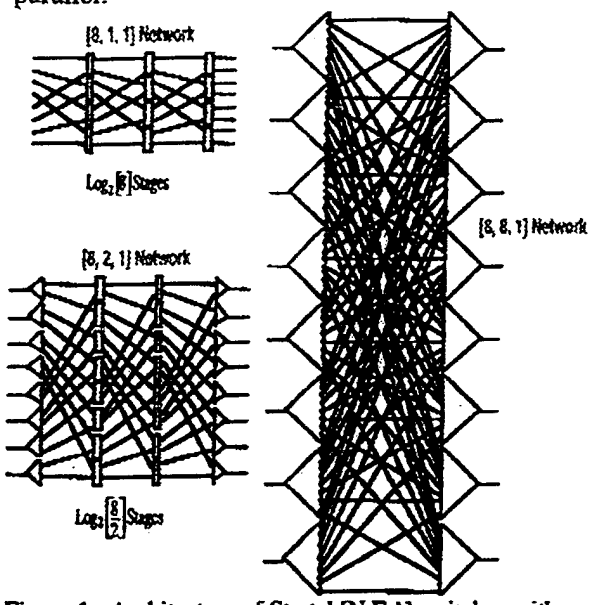

Figure 1: Architecture of Stretch[N,F,1] switches with F=1, 2, and 8 respectively. The bisection width of the network is NF. The fanout stage provides contention-free routing to one of F logical "pipes" using the first Log_2F bits of the destination addresses for each of the N input packets. The remaining $Log_2(N/F)$ bits are consumed in the switching stages that route packets to the correct output concentrator.

The basic unipath Stretch[N,F,1] switch is shown in figure 1. At one extreme (F=N), the Knockout switch is fully connected and contention-free. At the other (F=1), the well known banyan network achieves maximum connection multiplexing but suffers a high degree of internal link contention. In a unipath Stretch[N,F,1] switch, the number of logical routing stages remains the same (Log_2N) regardless of the fanout; this enables simple destination-based routing techniques to be used. These unipath stretch networks may then be cascaded back-to-back to achieve low contention (Figure 2), or in parallel ($T \geq 1$) to achieve tolerance to faults and reduced effective loading. Output port contention is alleviated using a finite number of buffers at each output channel, according to the Knockout principle[1]. Note that the parameters T, R, and F can also be implemented in the time domain, leading to the notion of a "time-dilated" Stretch network. A common feature of all Stretch networks is that each stage of the networks uses a simple perfect-shuffle interconnection, or any of the topologically equivalent connection patterns[6].

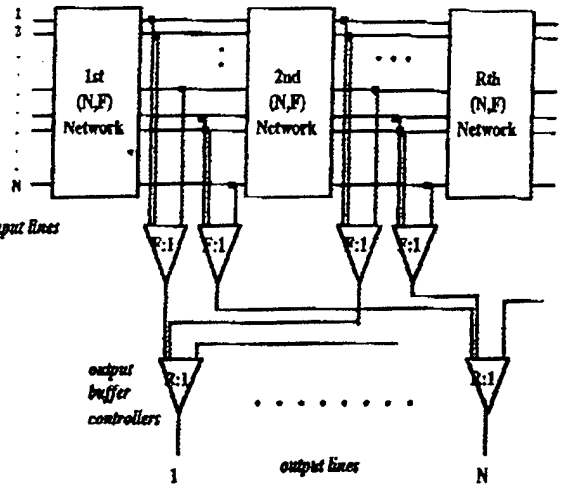

Figure 2: Architecture of a Stretch[N,F,R] switch. Input packets are routed without contention to one of F pipes. Once in a pipe, packets that suffer contention on the last $Log_2(N/F)$ bits of their destination address in the first [N,F,1] network are subsequently routed to their correct destinations in the following ($R \geq 1$) networks. Subsequent networks in the chain do not require fanout stages. Buffers placed at each output port of the network collect, store, and forward all correctly routed packets.

We have analyzed the performance of the network under uniform traffic, and performed extensive simulations of the performance of the Stretch[N,F,R] switch under uniform, permutation and "hot-spot" traffic. Figure 3 shows the probability of packet loss due to internal link contention of the new switch architecture under fully-loaded uniform and permutation traffic. The case where F=1 corresponds to the Tandem banyan network. Note that a relatively small amount of fanout provides a much better scaling in terms of cell loss rates versus the number of banyan networks (R) placed end-to-end. Figure 4 shows the performance of the network under fully loaded, non-uniform, 1% "community-of-interest " (COI) traffic. This occurs when all input ports send 1% of their input packets to a specific output port. The remaining traffic is uniform. For this type of traffic, fanout is essential to alleviate "hot-spots," that can severely congest the network. We have also investigated the effect of limiting the number of packet buffers per output port. For a specific traffic type, this sets a floor on the packet loss probability due to OPB; further improvement of ILC by increasing F and R does not reduce the overall cell loss rate. For instance with fully loaded, uniform traffic in a network with 1024

channels, P=4 limits the cell loss rate to approximately 10^{-2}; P=6 limits it to 10^{-4}; and P=8 to 10^{-6} etc. In our presentation, we will discuss designs that balance cell loss rates due to each of these factors, for different traffic types and loading.

The correct parameterization of a Stretch network in terms of the F, R, K, P, and T values, is dependent on traffic characteristics, performance requirements, and technology cost considerations. As figure 3 indicates, multiple Stretch network configurations exist to satisfy a given set of performance requirements and traffic types; this enables the architecture to be tailored to capitalize on the strengths of a particular technology. For a smart pixel implementation of such a switching fabric, the required number of channels, the maximum acceptable loss rates, and the traffic types and loading of traffic of traffic are typically specified by the end user. Device and system considerations dictate the clock speed, the power budget, system losses, the appropriate switching element size, and the maximum available fanout per stage (which in turn depends on the receiver sensitivity). These will typically set an upper limit to bisection width of the network (NF channels). The parameters R and P can then be tuned to meet performance specifications. The architecture can be made "growable" or scalable, and also fault tolerant, by placing several (T) such Stretch[N,F,R] in parallel. Scalability and modularity can also be achieved by designing the network at lower line speeds (high effective loading) and by tuning up the line speeds (lower effective loading).

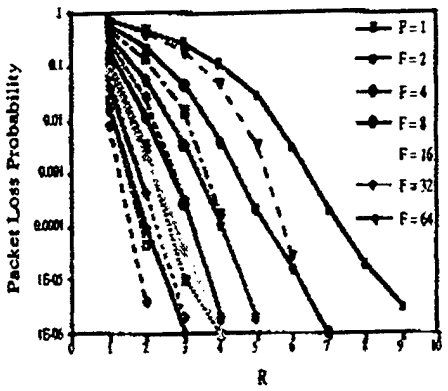

Figure 3: Packet loss probability under uniform (solid lines) and permutation (dotted lines) traffic for a Stretch[1024,F,R] switch. Packets that suffer contention on the last $Log_2(N/F)$ bits of their destination address are subsequently routed to their correct destinations in the following networks.

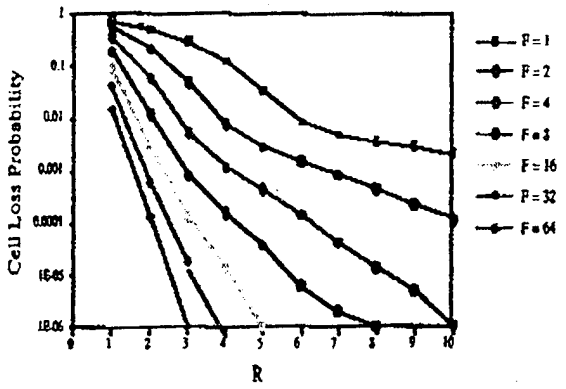

Figure 4: Packet loss probability under 1% "community of interest" traffic superimposed over uniform traffic (99%) for a fully loaded Stretch[1024,F,R] switch. The effect of adding fanout to the network is more pronounced for non-uniform traffic patterns.

References:

1. Y-S. Yeh, M. G. Hluchyj, and A. S. Campora, *IEEE Journal Selected Areas Communication*, Vol. 5, No. 8, pp. 1274-1282, October, 1987.

2. F. A. Tobagi, T. Kwok, and F. M. Chiussi, *IEEE Journal Selected Areas Communication*, Vol. 9, No. 8, pp. 1173-1193, October, 1991.

3. T. J. Cloonan, G. W. Richards, F. B. McCormick, and A. Lentine, Technical Digest, *OSA Topical Meeting on Photonic Switching*, Salt Lake City, March 1991.

4. A. V. Krishnamoorthy, F. Kiamilev, and S. Esener, "A new class of packet-switched extended-generalized shuffle networks," *Technical Digest*, OSA annual meeting, September 1992, Albuquerque, USA..

5. A. V. Krishnamoorthy and F. Kiamilev, "Stretch[N,M,F,R,T] networks: a class of packet-switched multistage interconnection networks," US Patent filed, December 1993.

6. L. Bhuyan and D. Agrawal, "Generalized shuffle networks," *IEEE Transactions on Computers*, Vol. C-32, No. 12, Dec. 1983.

An Efficient Signal Distinction Scheme for Large-scale Free-space Optical Networks Using Genetic Algorithms

Ahmed Louri, Hongki Sung, Yoonkeon Moon, and Bernard P. Zeigler
Department of Electrical and Computing Engineering
The University of Arizona, Tucson, AZ 85721
Phone: (602) 621-2318, Fax: (602) 621-8076
E-Mail: louri@ece.arizona.edu

1 Introduction

Free-space optical interconnection networks can be classified into two types, *space variant* and *space invariant*, according to the degree of space variance [1]. The degree of space variance determines the network's complexity and regularity. A totally space variant network allows a completely arbitrary interconnection between nodes, whereas a totally space invariant network has a definite, regular structure with all the nodes having the same connection patterns. In terms of physical implementations, the degree of space variance can be interpreted as the degree of sharing beam steering optics among the nodes of a given network. In other words, all nodes in a totally space-invariant network can share a single beam steering optics (considering multiple fanouts as one steering optics) to realize the given network topology, whereas, in a totally space variant network, each node requires a distinct beam steering optics. This is one of the reasons why space variant networks require complex optical implementations that often result in low interconnection density and high cost.

However, space invariant networks require mechanisms for distinguishing the origins of incoming beams (or signals) detected at the node since several signals may arrive at the same time if the node degree of the network is greater than one. We can distinguish the origins of the incoming signals if each signal has unique wavelength (wavelength division multiplexing) or each signal arrives at uniquely assigned timeslot (time division multiplexing). For an N-node network, this would require up to N different wavelengths or N timeslots. Therefore, for a large-scale interconnection network, the requirement for the prohibitively large number of wavelengths makes such solutions impractical since the number of wavelengths from the currently available light sources is very limited. Similarly, the use of large number of timeslots would result in unacceptably large communication latency. It should be noted that the incoming signal distinction problem can be easily solved in space variant networks since we can have each incoming beam hit on a difference detector within the receiving node. This can be done easily in totally space variant networks because each incoming signal has its own beam steering optics. The incoming signal distinction by the use of a unique detector for each incoming signal is based on the concept of space division multiplexing. In a totally space-invariant network with N nodes, a trivial space division multiplexing scheme always exists if each node has $N-1$ detectors. In this paper, we present a method for reducing the required number of detectors per node for incoming signal distinction in a space-invariant network.

2 Motivation

Let us consider an example network of a linear array with 4 nodes as shown in Fig. 1. Fig. 1.a shows the topology of the 4-node linear array and Fig 1.b presents a side view of a totally space invariant optical implementation. A beam steering optics is responsible for generating two fanouts, one fanout to the right neighboring node and the other to the left neighboring node. We can see from the figure that all nodes have the same connection pattern and, con-

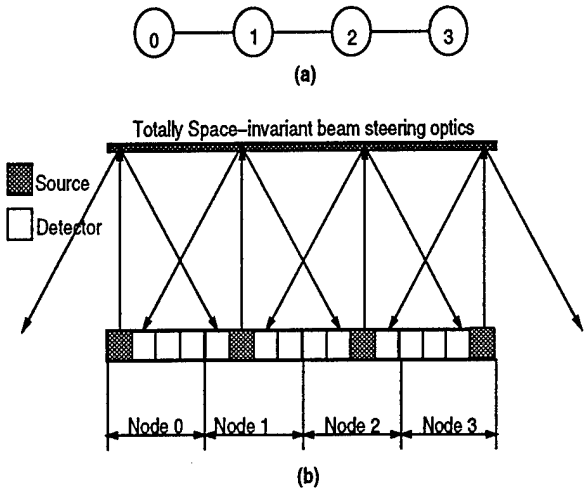

Figure 1: An example network of a 4-node linear array. (a) the topology. (b) A totally space-invariant optical implementation. Each node is connected to neighboring nodes on both side except nodes on extreme ends.

sequently, can share a single beam steering optics to provide all the required optical links. The source position of each node is different from those of the others so that the incoming signals can be distinguished by the positions of the detectors. Similar straightforward spatial encoding of source positions at the nodes is used in the design of optical hypercube networks [2, 3].

However, such straightforward encoding scheme requires too many unused detectors for large-scale networks. For an N-node network with node degree k, only k different signals may simultaneously arrive at a node since the node is connected to k nodes. Thus, in the space division multiplexing technique, only $k+1$ (k detectors and 1 source) pixels per node are utilized and the remaining $N-k-1$ pixels are wasted. This area waste is significant if $N >> k$. For example, the straightforward spatial encoding in a ten-dimensional hypercube network would result in $(1024 - 11 = 1013)$ unused pixels per node, which is not acceptable.

In what follows, we present a novel scheme which can greatly reduce the total number of unused pixels.

3 Proposed Signal Distinction Scheme

An efficient signal distinction scheme is to find the minimum number of detector pixels per node required for the incoming signal distinction in a given network. This problem can be re-stated if we represent a given network as a graph where a vertex and an edge represent a node and a link, respectively. Let V (E) represent the set of vertices (edges) in a graph, G.

Problem: Given a graph $G = (V, E)$, a positive integer $K \leq |V|$, which is a representation of a network, is G K-colorable? i.e., does there exist a function $f : V \rightarrow 0, 1, \cdots, K-1$, for all i and j, such that $f(i) \neq f(i_1) \neq f(i_2) \cdots \neq f(i_j)$ where i_j represent all neighbors of node i.

The above problem is NP-complete since it can be reduced into the *Graph K-Colorability* problem which is known as NP-complete [4]. In general, NP-complete problems are very hard to solve unless the problem size is small enough. Using genetic algorithms (GAs), we solved the above modified colorability problem to get efficient signal distinction schemes for the mesh, the hypercube, and the binary de Bruijn networks [5].

GAs were developed to study the adaptive process of natural systems and to develop artificial systems that mimic the adaptive mechanism of natural systems [6]. GAs can also be applied to various optimization problems such as the traveling salesman problem. In a given problem, a set of potential solutions (called a population of individuals) to the problem is initially created at random. Each solution is evaluated to give some measure of its fitness. Then a new set of solutions (next generation of the population) is formed by selecting better (fitter) solutions. Some of the new solution set undergos transformation by means of *genetic* operators such as *mutation* and *crossover*. The mutation is an operation which alters a small part of a solution. The crossover creates new solutions by combining parts from several other solutions. The probabilities of the mutation and the crossover are control parameters which affect the convergence rate of GAs. Thus, GAs use the notion of survival of the fittest by passing good genes (potential solutions) to the next generation and combining different genes to explore new search points.

We used a new type of GAs, called the Enhanced Parallel Genetic Algorithm (EPGA) [7], since we were unable to get solutions using conventional simple GAs as the network size grows. Using the concept of the Hierarchical GA [8], the running time of the EPGA was significantly reduced. Details of the EPGA are beyond the scope of this paper and interested readers should refer to [7]. Table 1 shows the minimum number of distinct colors or number of distinct pixels required using the EPGA for the mesh with wraparound connections, the hypercube, and the binary de bruijn networks. A number in the parenthesis indicates the theoretical optimal number of pixels per node which is equivalent to the node degree (optimal number of detectors) plus 1 (one source).

Network Size	Hypercube	Mesh	de Bruijn
16 nodes	8 (5)	8 (5)	7 (5)
64 nodes	11 (7)	8 (5)	9 (5)
256 nodes	18 (9)	8 (5)	9 (5)
1,024 nodes	26 (11)	9 (5)	11 (5)

Table 1: Minimum number of pixels (a source and multiple detectors) per node required for a given size network. Note that node degree of the hypercube increases logarithmically with respect to the network size, whereas those of the mesh and the binary de Bruijn are constant. A number in the parenthesis indicates the theoretical optimal number of pixels. The mesh is assumed to have wraparound connections.

For example, for a 256-node hypercube (8-dimensional hypercube), the proposed scheme requires only 18 pixels for the space division multiplexing technique, whereas the straightforward space division multiplexing technique would require as many as 256 pixels per node.

Fig. 2 demonstrates an example of the source position encoding, found by the proposed scheme, for the four-dimensional hypercube network with 16 nodes. The beam steering optics for the totally space-invariant optical implementation of such networks is based on [2].

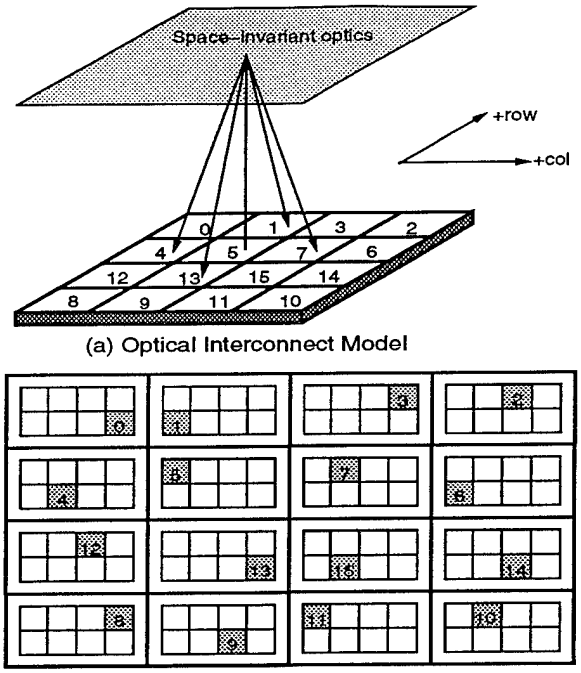

(a) Optical Interconnect Model

(b) Spatial encoding of source pixel positions

Figure 2: (a) A 3D model of totally space-invariant beam steering optics for implementing optical hypercube networks [2]. The beam steering optics generates 8 fanouts of which amounts of spatial shifts are $\pm 1col$, $\pm 1row$, $\pm 3col$, and $\pm 3row$, respectively. (b) Spatial encoding of source pixel positions in a 4-dimensional hypercube network with 16 nodes. Each node has 8 pixels; a source and 7 detectors. A dark pixel represents a source and the position of the source pixel is the spatial encoding of the corresponding node address as indicated by a number. White pixels represent detectors.

A dark pixel and a white pixel represent a source and a detector, respectively. Note that the node address is spatially encoded by the position of the source pixel. The corresponding address is indicated by a number in the source pixel. For a four-dimensional hypercube network, the proposed scheme requires 8 pixels per node which is a 50% saving compared to 16 pixels per node required by the straight forwarding encoding scheme.

4 Discussions

A free space space-invariant design approach is simple to design and can provide higher interconnect density compared to the space-variant approach. However, the space-invariant design utilizes given power less efficiently than the space-variant approach. In addition, the space-invariant approach often results in low resource utilization for distinguishing incoming signals; i.e., the approach may require many unused detectors when space division multiplexing technique is used for signal distinction. In this paper, we have presented an efficient scheme for distinguishing incoming signals. We first formulated the problem as a modified graph colorability problem and solved it using a new type of genetic algorithm called the Enhanced Parallel Genetic Algorithm. The proposed scheme significantly reduces the number of the unused detectors, which enables the use of space division multiplexing technique in large-scale optical networks.

The proposed signal distinction scheme can also be used in wavelength division multiplexing and/or time division multiplexing techniques by considering the spatial positions as distinct wavelengths or timeslots, respectively. With wavelength or time division multiplexing techniques, each node has a single detector unlike the multiple detectors with the space division multiplexing technique. A receiving node distinguishes the origin of the incoming signal by identifying the wavelength of the signal or the timeslot the signal occupies.

References

[1] G. E. Lohman and K. H. Brenner, "Space-invariance in Optical Computing Systems," *Optik*, vol. 89, pp. 123–134, 1992.

[2] A. Louri and H. Sung, "Efficient Implementation Methodology for Three-dimensional Space-invariant Hypercube-based Free-space Optical Interconnection Networks," *Applied Optics*, vol. 32, pp. 7200–7209, Dec. 1993.

[3] Y. Sheng, "Space Invariant Multiple Imaging for Hypercube Interconnections," *Applied Optics*, vol. 29, pp. 1101–1105, 1990.

[4] M. R. Garey and D. S. Johnson, *Computers and Intractability: A Guide to the Theory of NP-Completeness.* New York, NY: W. H. Freeman and Company, 1979.

[5] J.-C. Bermond and C. Peyrat, "De Bruijn and Kautz Networks: a Competitor for the Hypercube?," in *Proceedings of the First European Workshop on Hypercube and Distributed Computers*, Rennes, France, pp. 279–293, Elsevier Science Publishers, Oct. 4-6 1989.

[6] J. H. Holland, *Adaptation in Natural and Artificial Systems: an Introductory Analysis with Applications to Biology, Control, and Artificial Intelligence.* Ann Arbor, MI: University of Michigan Press, 1975.

[7] B. P. Zeigler and Y. Moon, "An Enhanced Parallel Genetic Algorithm With A Novel Selection Strategy," *submitted to IEEE Trans. Parallel and Distributed Systems*, 1994.

[8] J. Kim, "Hierarchical, Asynchronous Parallel Genetic Algorithms For Simulation-Based System Design," Ph.D. dissertation, University of Arizona, Tucson, AZ, 1994.

Thursday, March 16, 1995

Optoelectronic Devices for Photonic Switching

PThD 3:30 pm-5:00 pm
Red Lion East

H. Venghaus, *Presider*
Heinrich Hertz Institute, Germany

Semiconductor Guided-Wave Switching

J.E. Zucker
AT&T Bell Laboratories
101 Crawford Corner Road
Holmdel, NJ 07733

Recently a systems pull from new fiber-optic networks has spurred development of custom semiconductor switches using novel materials, fabrication methods, and sophisticated optical design tools.

TRANSMISSION EXPERIMENTS ON FULLY PACKAGED 4x4 SEMICONDUCTOR OPTICAL AMPLIFIER GATE SWITCH MATRIX

Claus Popp Larsen¤ (Tel: +46 8 757 5446), Erland Almström* (Tel: +46 8 727 4343)
Wim van Berlo+, Jan-Erik Falk+, Fransesco Testa$, Lars Gillner, Mats Gustavsson

Fiber Optics Research Center, Ericsson Components AB, S-164 81 Stockholm, Sweden
¤also with L.M.Ericsson A/S, Denmark and EMI at the Technical University of Denmark, Denmark
*ELLEMTEL AB, Box 1505, S-125 25 Älvsjö, Sweden and
Lab. of Photonics at the Royal Institute of Technology, Sweden
+Opto and Microwave Electronics Division, Ericsson Components AB, S-164 81 Stockholm, Sweden
$Ericsson Telecommunicazione S.p.A. R&D Div., I-00040 Rome, Italy

INTRODUCTION It is today commonly acknowledged that the optical switch will be a key component in future optical communications networks [1,2,3]. Apart from requirements such as high flexibility and transparency to bit rate and format, optical switches must be able to support wavelength division multiplexed (WDM) networks and already existing components as especially erbium doped fibre amplifiers (EDFA's). Several designs have been suggested and implemented including both lithium-niobate [4] and semiconductor based [5] devices. Among the latter, loss-compensating components [6,7] are believed to be advantegeous, since the switch architectures will probably get rather extended. The main disadvantage compared to switches without amplification is that a limited dynamic range is obtained due to the semiconductor gain medium. The switch evaluated here (see fig 1) is a monolithic strictly non-blocking device based on semiconductor optical amplifier (SOA) gates in InGaAsP/InP, operated in the 1550 nm window [8]. Publications of optical switches have so far mainly dealt with unpackaged components. Performance has often been measured with a cw source as to achieve gain optimisation. In this paper, extensive bit error rate (BER) measurements on fully packaged InP switches are presented concerning dynamic range and dependence upon polarisation of the incoming signal. The system has been optimised for low BER rather than maximum gain. Furthermore, cascading of several switches and a WDM experiment demonstrate the usefulness of this component in future optical WDM networks, and theoretical simulations investigate dependence of reflections and bit rate.

EXPERIMENTS The experimental set-up shown in fig 2 compromises a DFB laser, two EDFA's working as booster and preamplifier, respectively, one attenuator to control input power to the switch and one attenuator to adjust received power at the detector, a polariser to control the state of polarisation before the switch, a multicavity filter with a FWHM = 2 nm and an APD receiver. Pseudorandom data with a word length of 2^{23}-1 and NRZ coding was used both for 622 Mb/s and 2.488 Gb/s. Reference measurements were made with the switch replaced by a connector, i.e. both EDFA's were included, which gave a maximum penalty of 0.2 dB compared to back-to-back.

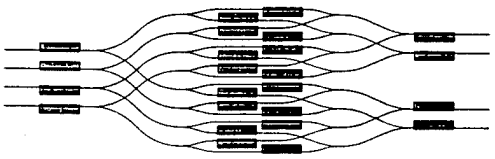

Fig 1: Diagram of the integrated 4x4 switch with 4 input amplifiers, 16 gate amplifiers and 4 output amplifiers [8]

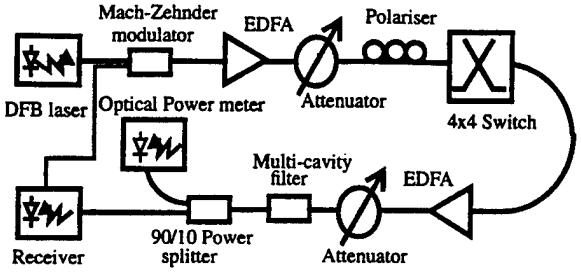

Fig 2: Experimental set-up for evaluation of 4x4 switch at single channel and one through-pass transmission

Two 4x4 switch matrices were used in the experiments. Because they are based on SOA's, they have an optimal operation point, concerning quality of transmission, depending on the input power to the switch (P_{in}) and the gain in each SOA, i.e. the bias currents. Reflections between the active and passive waveguides in the structure (internal reflections) and at the end facets of the chip (external reflections) narrow the dynamic range

which furthermore complicates optimisation. Compared to the situation where the amplifiers for a given P_{in} and bias currents are driven into saturation as to get maximum output power, the gain in this case is about 5 dB less, but on the other hand, very limited transmission of information is possible at gain optimisation. Due to polarisation sensitivity, the optimal polarisation is launched into the switches in all the experiments, except in the case where polarisation dependency is determined. Here a measurement for 'worst case' polarisation is carried out, meaning that the polarisation is rotated 90° compared to optimal polarisation.

In fig 3 the dynamic range and polarisation dependence for the switch are depicted at 622 Mb/s. Power penalty is plotted as a function of P_{in}. The bias current to each individual amplifier is optimised with respect to BER at optimal polarisation. Power penalty is the sensitivity compared to the reference measurement mentioned in the previous section. For low input powers the penalty arises from spontaneous emission, and for high input powers the gain saturation will allow a space more gain than a mark, thus reducing the extinction ratio, which in turn increases the penalty. It is observed that within a power penalty of 2 dB, the dynamic range for the switch is larger than 20 dB.

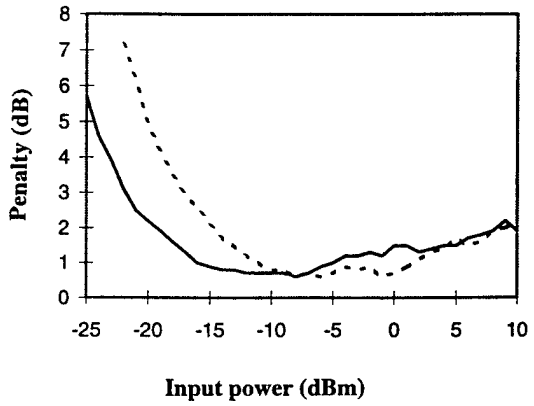

Fig 3: Power penalty against P_{in} for different states of polarisation at 622 Mb/s for BER=10^{-9}. Optimum polarisation (solid lines) and 'worst case' polarisation (dashed lines)

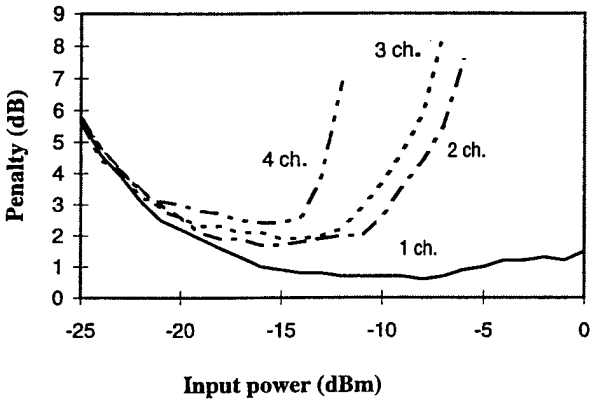

Fig 4: Power penalty against P_{in} pr. channel at WDM transmission at 622 Mb/s for BER=10^{-9}

Concerning polarisation, the most significant difference is that the 'worst case' curve at low input powers is shifted 3 dB towards larger input powers. This can be understood as an attenuation of the signal, because while operating at the worst polarisation state, the signal sees less gain. If 1 dB polarisation dependence can be accepted, the device is polarisation independent concerning transmission quality within a dynamic range of more than 20 dB. The unsaturated fibre-to-fibre gain at optimum polarisation is ~ -2 dB.

The switch is capable of transmitting multiple wavelengths simultaneously, as shown in fig 4. The experiment was carried out for random modulation of the channels at 1552, 1556 and 1560 nm, while 1548 nm was the channel under test. Bit rate was 622 Mb/s. For three wavelength transmission, the 1560 nm channel is excluded, and for two wavelength transmission the 1556 nm channel is also excluded. If 3 dB power penalty is acceptable, 4 wavelength channels can be transmitted simultanously over an input power range of 7 dB. For low values of P_{in}, the curves are identical which has been expected, since no additional spontaneous emission is generated. For large values of P_{in}, however, the switch is saturated quicker, depending on the number of channels involved. Furthermore, cross gain modulation may distort the signal even more.

Fig 5 shows the results from the numerical simulations. The model in [9] has been modified to take into account the dynamic processes in the InP SOA's. Internal reflections, external reflections and the SOA refractive index dependence on electron density have been included. As the bit rate is increased (from long-dashed to solid line), the influence of the reflections increases. The theoretical results are in qualitative agreement with the measurements.

Even though a higher bit rate further restricts signal transmission, it is indeed possible to cascade switches at 2.488 Gb/s. In fig 6 is shown a transmission experiment through 3 paths in a switch and a total fibre length of 2x80 km in the Stockholm Gigabit Network (SGN). The SGN is an experimental network consisting of several

nodes in the Stockholm area, interconnected by installed standard single mode fibre. Power penalty compared to back-to-back was mainly arising from spontaneous emission from the the InP switches and the EDFA's. Crosstalk, which is lower than -30 dB in the switch, is believed not to cause any noticeable power penalty. Despite the fact that the polarisation and the input power to the switch were not optimised, the power penalty for one pass through the switch and 80 km of fibre is only 1.0 dB, 2.4 dB for two passes and 160 km of fibre and 4.7 dB for three passes and 160 km of fibre.

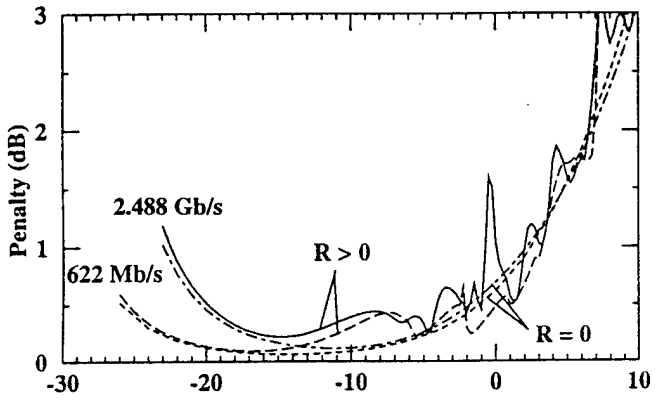

Fig 5: Calculated power penalty at BER = 10^{-9} as function of input power at 622 Mb/s and 2.488 Gb/s with (R>0) and without (R=0) reflections. The unsaturated switch matrix gain is -2.3 dB.

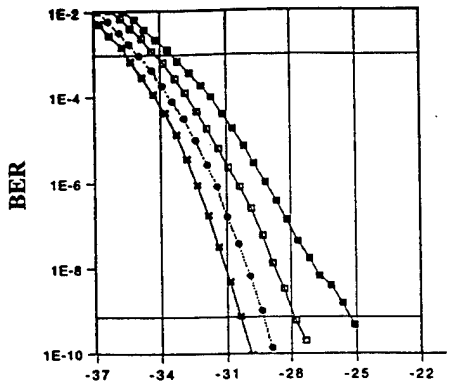

Fig 6: BER curves for transmssion in the SGN through a switch at 2.488 Gb/s for λ=1548 nm. The curves represent from left to right: Back-to-back; one pass and 80km of fibre; two passes and 160 km of fibre; three passes and 160 km of fibre.

CONCLUSION Transmission experiments were carried out for fully packaged InGaAsP/InP 4x4 semiconductor optical amplifier gate switches. Within a power penalty of 2dB, the switch has an input power dynamic range well beyond 20 dB at BER = 10^{-9} for 622 Mb/s, no matter which polarisation. In WDM transmission with four equally spaced channels from 1548 - 1560 nm, we measure 3 dB of penalty within a dynamic range of 7 dB. Theory predicts smaller dynamic range and increased sensitivity towards reflections for higher bit rates. However, it was possible to go three times through an InP switch and through 160 km of fiber at 2.488 Gb/s in the SGN with a penalty of 4.7 dB at BER = 10^{-9}. In all experiments the switches co-existed with EDFA's in the system without any problems. This proves promising for future WDM network applications.

The two perhaps most serious problems with the switches at the moment are polarisation dependency and internal and external reflections. These problems can however be reduced by a modified switch design.

ACKNOWLEDGEMENTS This work was accomplished within the RACE R2028 (MWTN) project.

REFERENCES

[1] G.R.Hill *et. al.*, J. Lightwave Technol. **11**, 667 (1993)
[2] S.Johansson *et. al.*, J. Lightwave Technol. **11**, 688 (1993)
[3] M.Fujiwara, ECOC'91, Paris, France, Vol 1, 97
[4] P.Granestrand *et. al.*, IEEE Photon. Technol. Lett. **6**, 71 (1994)
[5] R.Krähenbühl *et. al.*, ECOC'94, Firenze, Italy, Vol. 2, 511
[6] M.Gustavsson *et. al.*, Electron. Lett. **29**, 1083 (1993), correction Electron. Lett. **29**, 1310 (1993)
[7] T.Kirihara *et. al.*, OFC'94, San Jose, USA, Vol 4, 55.
[8] M.Gustavsson *et. al.*, Electron. Lett. **28**, 2223 (1992)
[9] L.Gillner, IEE Proc. J. **140**, 309 (1993)

Low-voltage electroabsorption in InGaAsP/InP multiple-quantum-well electron transfer structures

Ulf Olin[a], *Dana Varga*[b], *Krister Fröjdh*[c], *Johan Wallin*[b], *Gunnar Landgren*[b]

a) Institute of Optical Research, S-100 44 Stockholm, Sweden, Phone: (+46-8)-7911325

b) Laboratory of Photonics and Microwave Engineering, Department of Electronics, Royal Institute of Technology, Electrum 229, S-164 40 Kista, Sweden

c) Department of Physics II, Royal Institute of Technology, S-100 44 Stockholm, Sweden

Fast low-chirp electro-optic modulators are essential for applications as external modulators in long-haul communication systems. For integration with high-speed drive electronics, the modulation voltage should be restricted to preferably the sub-volt region. Barrier reservoir and quantum well electron transfer structures (BRAQWETs) have shown a great promise for these applications, due to its large electro-refractive effects[1] and fast intrinsic speed, which make them particularly suitable for high-speed Mach-Zehnder interferometric amplitude modulators[2].

In this paper we describe experimental results concerning a comparison between BRAQWETs with one quantum well per period and BRAQWETs with several quantum wells per period. The advantage of using several quantum wells per period is that the voltage drop over one period is nearly independent of the number of quantum wells. Thus, larger electro-absorptive effects should be obtained for a structure with several quantum wells per BRAQWET period as compared to a structure with an equal total number of quantum wells, but with just one quantum well per period. However, previous results have shown that band-bending could cause a non-uniform phase space

filling of the quantum wells in the BRAQWET period[3], thus reducing the usefulness of this approach.

The InGaAsP/InP structures shown in Fig. 1 were grown by metalorganic vapour phase epitaxy (MOVPE). Structure 1a consists of five periods with one quantum well per period, whereas structure 1b consists of one period with five quantum wells. After the epitaxy, round mesa structures, with a diameter of 500 μm, were formed.

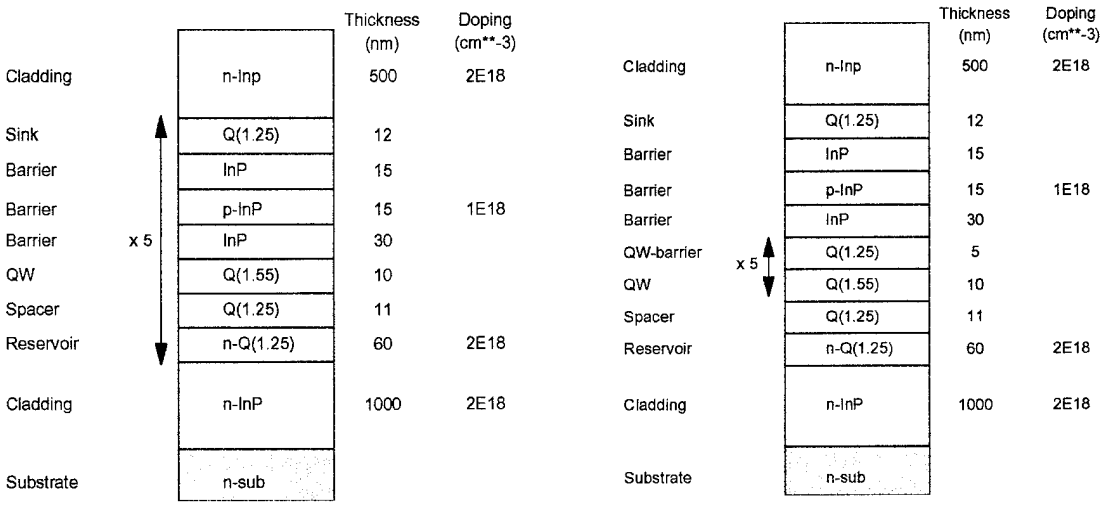

Figure 1. Schematic layouts of the BRAQWETs structures. Structure 1a is shown to the left and structure 1b to the right.

Fig. 2 shows the differential transmission spectra for structure 1a. For positive applied voltages the spectra are nearly unipolar, which is characteristic for phase space filling effects due to electron transfer, whereas for negative applied voltages the quantum confined Stark effect is seen. The differential transmission spectra for structure 1b (Fig. 3) show that the maximum differential transmission change due to electron transfer is the same as for structure 1a. This transmission change is, however, obtained at a considerably smaller applied voltage. Thus, this shows that it should be possible to reduce the drive voltage for electro-optic electron transfer devices, by using several quantum wells per BRAQWET period. The detailed mechanisms for this enhanced

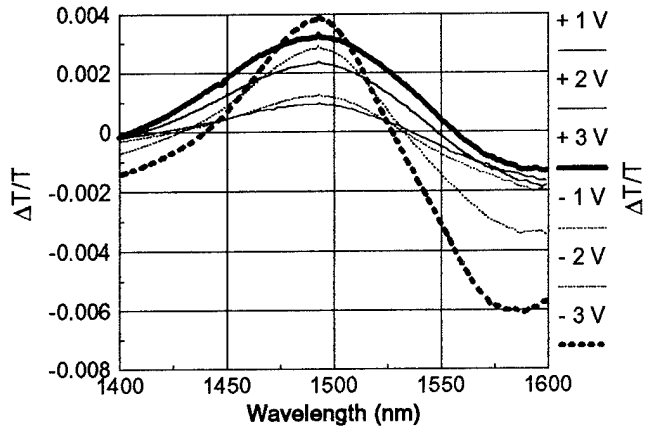

Figure 2. Differential transmission spectra for structure 1a.

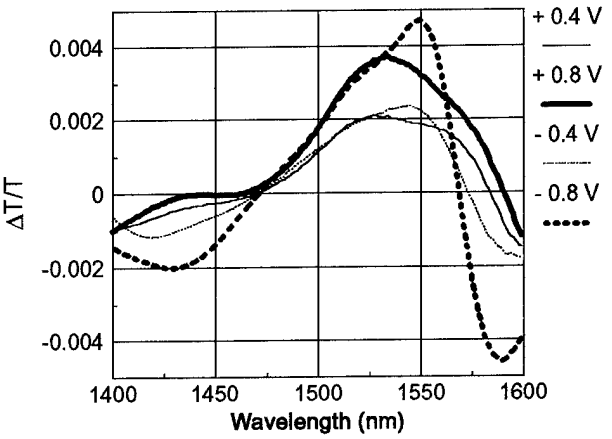

Figure 3. Differential transmission spectra for structure 1b.

electroabsorption are currently not fully understood. Further experimental and modelling results will be presented at the conference.

References

1. J.E. Zucker, T.Y. Chang, M. Wegener, N.J. Sauer, K.L. Jones, and D.S. Chemla, "Large refractive index changes in tunable-electron-density InGaAs/InAlAs quantum wells," IEEE Photonic. Technol. Lett. **2,** 29-31 (1990).

2. J.E. Zucker, K.L. Jones, T.Y. Chang, N. Sauer, B. Tell, K. Brown-Goebeler, M. Wegener, and D.S. Chemla, "Compact low-voltage InGaAs/InAlAs multiple quantum well waveguide interferometers," Electron. Lett. **26,** 2029-2031 (1990).

3. N. Agrawal, F.W. Reier, C. Bornholdt, C.M. Weinert, K.C. Li, P. Harde, R. Langenhorst, G. Grosskopf, L. Berger, and M. Wegener, "Electroabsorption and saturation behavior of InGaAsP/InP/InAlAs multiple superlattice electron transfer optical modulator structures," Appl. Phys. Lett. **63,** 1110-1112 (1993).

Vertical Cavity X-Modulators

J. A. Trezza, J. Powell, M. Morf, and J. S. Harris, Jr.
Solid State Laboratories, Stanford University, Stanford CA, 94305
(415) 723-1926

Recently, we have experimentally developed two types of ideal optoelectronic switches using Fabry-Perot vertical, III-V semiconductor structures. Zero chirp reflectivity modulators operate as *pure optical amplitude* switches;[1] vertical cavity phase flip modulators (VCPPM) operate as *pure optical phase* switches.[2] The later display large intensity output in both of the device's states and switching occurrs by altering phase between 0° and 180°. In this work we describe a photon conserving, reversible intensity switch. In this device, known as an X-modulator, the incident power is either transmitted through or reflected from the device. Reversibility indicates that the device is designed so that the outputs for light incident from both the top and bottom of the structure are nearly identical. The device ideally does not modify total amplitude or phase, but merely *routes* incident photons. Thus the X-modulator provides the third of the three desirable optical modulators: amplitude modulator, phase modulator, direction modulator. By being both conservative *and* reversible, the device is uniquely capable of performing complex optical switching, routing, and logic.[3] The device is essentially a vertical cavity, electro-optical realization of an X-gate (sometimes referred to as a Fredkin Gate) which is a primitive structure into which all logic functions can be decomposed. The first experimental device, when switched with an applied bias of 40V, modulates from (T ~ 60%, R~ 6%) to (T ~ 6%, R~ 60%). We will discuss individual device design including the optimization of the device parameter space: lower voltage, optical bandwidth, modulation ratio, insertion loss, and how to match these devices to electronics. In addition, theoretical and experimental results of stacked devices and the use of graded buffers to reduce electric field requirements will be explained as will issues such as device crosstalk in cross bar switches.

The X-modulator consisted of asymmetric *p-i-n* Fabry-Perot cavity here containing top and bottom mirrors of 10 and 12.5 period GaAs/AlAs quarter wave stacks surrounding an undoped cavity of 45, 75Å $In_{0.2}Ga_{0.8}As$ quantum wells. The bottom of the wafer was antireflection coated with SiN_x. Numerical device modeling was performed.

Figure 1 shows the theoretical prediction before growth and the experimental results of this device taken with light incident from both the top and the bottom of the device. The characteristics using bottom incident light is within 1.5% of the characteristics using top incident light. We note that our structures used 200Å GaAs barriers to eliminate strain induced material degradation caused by the 45 strained quantum wells. By using graded

buffers[4] to improve the material, 20% indium content (or greater) quantum wells with 35Å barriers have been shown to be an acceptable material . This reduces voltage by 40%.

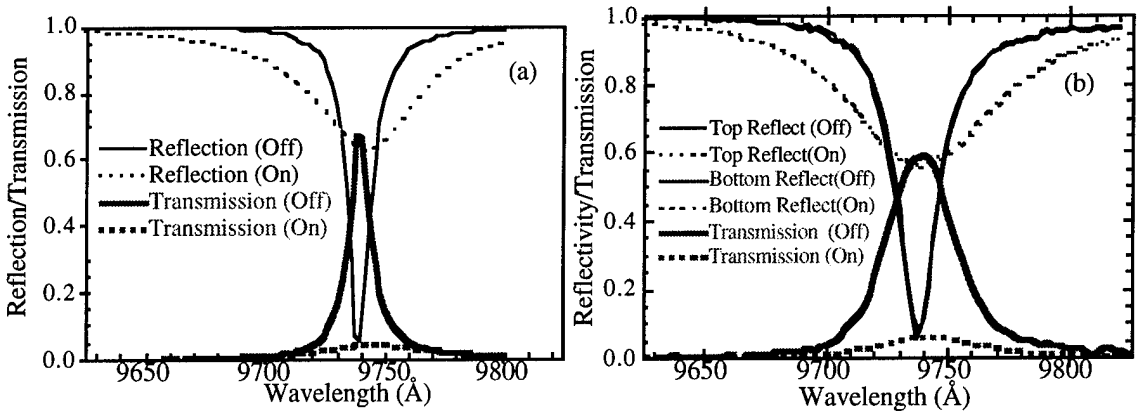

Figure 1: (a) Theoretical and (b) experimental curves for reflection and transmission spectrum of the X-modulator. "On" indicates response with and applied electric field

Fabry-Perot devices are optically characterized primarily by voltage, optical bandwidth (OB), modulation ratio (MR), change of reflectivity (DR) (related to insertion loss), and reflected phase. Modulation ratios well over 1000, and voltages of 5V are possible with changes in reflectivity above 60%. (multiply voltage by 0.6 if using graded buffer layer technique). In general:

- For a fixed voltage, as MR increases, DR increases and OB decreases.
- For a fixed DR, as voltage increases, OB increases and MR decreases.
- For a fixed MR, as voltage increases, OB increases and DR decreases.

Through design we control: front and back mirror reflectivities, cavity length, distance (in wavelength) of zero bias exciton peak from the Fabry-Perot peak, and maximum and minimum exciton absorption.

We theoretically predicted and experimentally verified the optical properties of two stacked 200μm x 200μm square X-modulators (shown schematically in the Figure 2 inset). Light incident at 21° off normal incidence was used, which imparted a 50Å blue shift to the Fabry-Perot resonance wavelength. Inputs A, B, and C represent optical inputs for this device while D and E are electrical inputs. For our measurements, only A was an 'on' optical signal making the effective outputs: *D*, *D*E, and *DE* for outputs 1, 2 and 3 respectively. Output '1' represents the single device reflectivity response and was similar to that of Figure 1b. Figure 2 shows the logic high and some of the various logic low levels at the Fabry-Perot wavelength for the outputs 2 and 3, given the different combinations of the electrical inputs. The device can be thought of as performing logic, or as simply a structure for routing optical beams to three output paths. Stacked wafers,

containing 2-D arrays of devices would be able to perform extremely efficient complex switching, routing and logic.

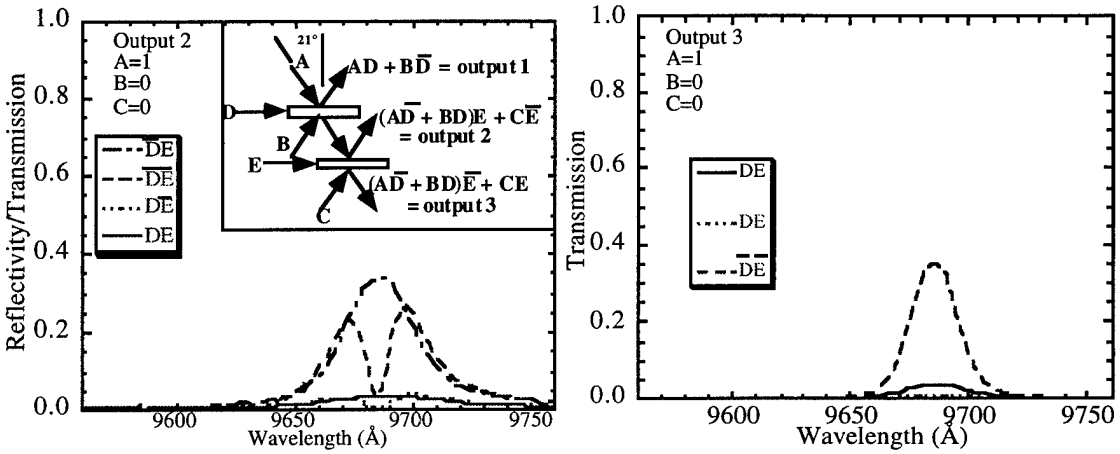

Figure 2: Measured signal versus wavelength for output 2 and output 3 (shown schematically in inset) of a dual stacked X-modulator system. Output 1 is similar to the plots shown in Figure 1 with the appropriate wavelength shift.

We also investigate and discuss the design aspects of the angular dependence of the 'off' state reflectivity for both TE and TM light incident on an X-modulator. Because the cavity mode shifts, but the exciton absorption wavelength does not, for incident angles in excess of 21°, the contrast ratio will begin to degrade and a TE-TM split will be observed. Devices can be designed for use at larger angles, though, by fabricating with a wider cavity. Note that TE and TM modes for non-normal incident light interact with heavy hole excitons differently. This must be considered.

In conclusion, we have designed, fabricated and tested vertical cavity X-modulators: a structure which allows for both reversible and conservative switching. Initial X-modulator results display changes in reflection and transmission of over 55% each. The devices were fabricated to accept incident light from both the bottom and top of the structure, making them reversible. In addition, we have discussed optimization conditions, results for multi-device configurations, and angular input issues. We believe that X-modulators will have a significant impact on efficient switching, 3-D array optical routing and logic.

---

[1] J. A. Trezza, B. Pezeshki, M. C. Larson, S. M. Lord, and J. S. Harris, Jr., Appl. Phys. Lett **63**, 452 (1993).
[2] J. A. Trezza, J.S. Harris, Jr., J. Appl. Phys **75,** 4878 (1994).
[3] E. Fredkin, T. Toffoli, International Journal of Theoretical Physics, **21**, 3 (1982).
[4] S.M.Lord, B. Pezeshki, J.S. Harris, Jr., Opt. And Quant. Elect. **25**, 5953 (1993).

Bit Error Rate Studies of Diode-Clamped FET-SEED Optical Receivers

T. K. Woodward[a], *A. L. Lentine*[b], *L. M. F. Chirovsky*[c]

AT&T Bell Laboratories

[a] *Holmdel, NJ 07733,* [b] *Naperville, IL 60566,* [c] *Murray Hill, NJ 07974*

The use of optics has been proposed as a technique to improve the performance of a variety of switching systems. In one scenario, large numbers of optical receivers and transmitters would be directly integrated onto semiconductor processing elements, as a means to reduce the communication problems of such elements.[1] In such a scheme, the receiver unit is particularly worthy of careful study, since it carries with it certain constraints on area and power consumption that are not generally present in other types of optical receivers. Accordingly, we have studied of the bit-error rate (BER) performance of one type of receiver being used in such systems, the diode-clamped optical receiver. This receiver is a high-impedance FET-based digital receiver whose basic operation has been described previously.[2, 3]

The circuit with which we are concerned is shown in schematic form in Fig.1. All gate lengths were nominally 1 μm, except for a 2 μm length in the source follower, and FET widths are indicated in the schematic. The circuit, excluding the off-chip driver element, fits entirely within a 90 x 60 micron area, and the power consumption is in the 2 mW range.[4] These figures are in keeping with the buffered FET logic (BFL) FET-SEED technology in which the receiver is presently realized. However, lower power consumption would be possible in alternate technologies such as GaAs direct coupled FET logic (DCFL) or in Silicon CMOS logic. The measurements described here were made with directly modulated commercial laser diodes (Hitachi 8318 40 mW) at 850 nm driven from pattern generator with a pseudo-random-bit sequence (PRBS) of $2^{23} - 1$ length. The signal output from the receiver was sent directly to an oscilloscope to observe eye patterns and output levels, or was boosted with a commercial amplifier (Veritech 3k10p) and input to a BER analyzer (Hewlett Packard 71603B).

The operation of the receiver depicted in Fig.1 is shown in Fig.2 at 1 Gb/s. The signal amplitude is determined by the current generated in the source follower. The logic swing driving the source follower should be roughly from -0.5 V to +0.9 V.[4] Since the output is terminated to ground, the total available

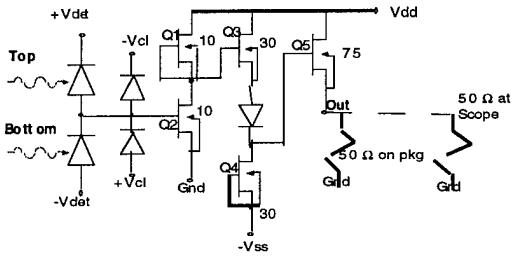

Figure 1: Schematic of the Receiver circuit being tested. Typical biasing conditions were Vdd = 2. 5 V, Vss = -1. 5 V, ± Vdet = ±6. FET widths in microns are indicated.

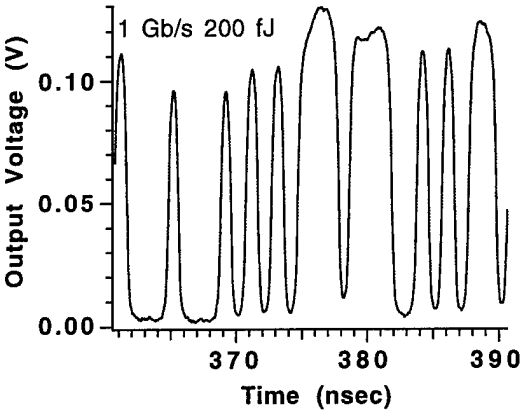

Figure 2: Output voltage signals from the receiver at 1 Gb/s. Output levels are consistent with logic-level voltages input to the source follower.

voltage variation is 0.9 V. Given the likely current drive capacity of the 75 μm wide FET forming the source follower (< 3.5 mA) and the parallel termination at both the source and oscilloscope, we conclude that the observed 100 mV output voltage swing is consistent with a logic-level input to the off-chip driving element.

The clamping diodes play a key role in determining the sensitivity and speed of this receiver, since they determine the permitted input voltage swing. For a given input power, a certain current is developed in the photo-detectors, which is balanced

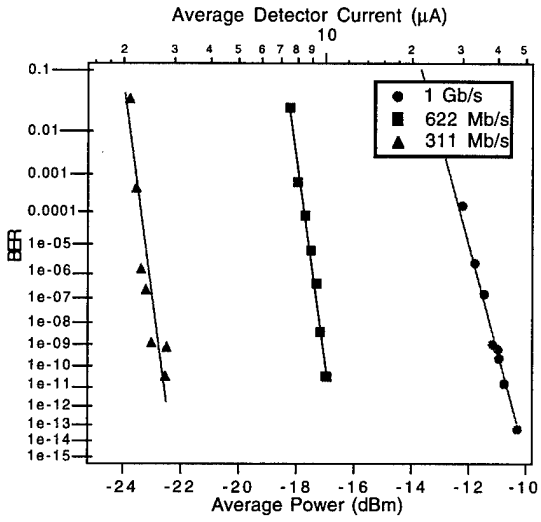

Figure 3: BER vs received power (bottom axis), and average detector current (top axis) for operation with fixed clamping voltages of about ±0. 6 V.

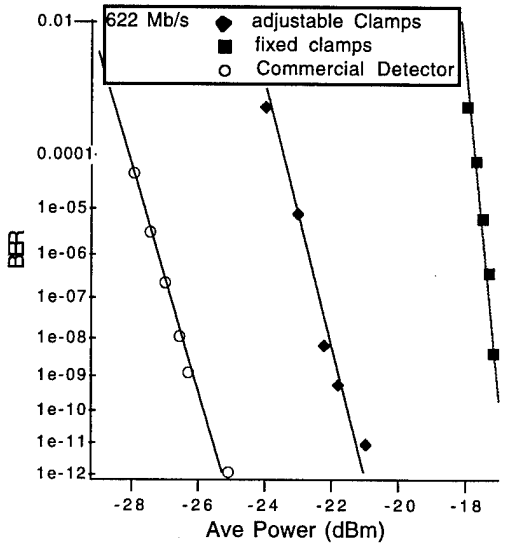

Figure 4: BER vs received power (bottom axis) at 622 Mb/s for operation with fixed clamps, adjustable clamps, and a commercial detector looking at one of the two signal lasers.

at a particular voltage by a current through one of the clamping diodes. For each diode, these voltages can be added to find the maximum-input-voltage swing ΔV_{max}. Subtracting from this the net forward clamping voltage ΔV_{cl} yields ΔV_{req}; the input-voltage swing required to reach the clamping voltages. In fact, we find that when the BER is studied as a function of clamping voltage at a given optical power a low error rate is obtained when ΔV_{req} is somewhat smaller than what the optical pulse energy can induce. The possible voltage swing that the light can induce is found from $\Delta V_{poss} = S\Delta E/C$, where S is the responsivity of the detector (0.5 A/W), C is the input capacitance ($\sim$ 50 fF), and ΔE is the input optical pulse energy.[2]

In Fig.3, we present one way of studying the BER sensitivity of this receiver, in which we fix the clamping voltages at $\sim \pm 0.6V$ (which is nearly optimum for 1 Gb/s operation) and vary both the bit rate and the optical power levels in the set and reset beams (holding both equal at all times). We find that floor-free performance is obtained to at least 1×10^{-14}. Second, we find that the receiver can operate with low error rates at 1 Gb/s, which is remarkable given the extreme simplicity of the receiver. We find further that the sensitivity improves as the bit rate is decreased, which is partially explained by the fact that this receiver switches on the optical *energy* and not the optical power. There are additional factors as well, which become apparent when one determines the optical pulse energy required for a BER of 1×10^{-9}. From Fig.3, these values are 32 fJ, 62fJ, and 153 fJ for 311 Mb/s, 622 Mb/s, and 1 Gb/s, respectively. The decrease in energy at lower bit rate can be explained by considering the following. First, a reduced current translates into a reduced ΔV_{req} (the input voltage swing determined by the clamping diodes), since the clamping diodes will equilibrate at lower voltages. We can compute ΔV_{req} from an I–V curve of a clamping diode and the total clamping voltage of 1.2 V.[2] We find ΔV_{req} and ΔV_{poss} for the three bit rates to be 0.66 V and 1.53 V for 1 Gb/s, 0.46 V and 0.62 V at 622 Mb/s, and 0.33 V and 0.32 V at 311 Mb/s. These numbers illustrate the second effect, which is due to the speed improvement that can be obtained if the required voltage swing is accomplished at the start of the bit period, and causes the receiver to operate over-clamped at high-bit rates with non-return-to-zero (NRZ) format. Therefore, only part of the optical pulse energe one measures is actually being used to produce ΔV_{req}. Finally, pattern-dependent noise in the laser modulation source cannot be discounted, as this also becomes worse as data rates increase.[2, 3]

A second means of studying the sensitivity of this receiver is to permit the clamping diodes to be adjusted at each power and bit rate to optimize the

BER. This is shown in Fig.4, along with the fixed clamp data for 622 Mb/s from Fig.3, as well as the single-beam performance of a commerical detector (Antel ARX-SA). We see that the slope of the BER curve differs for fixed or adjustable clamps. Further, the slope of the BER curve with adjustable clamps is nearly the same as for a commercial analog detector. The latter result implies that the noise sources limiting the performance of the receiver when the clamps are adjusted for optimal performance are no different than for an analog receiver. On the other hand, when the clamps are not adjusted, a different sort of behavior arises, which can be explained by the presence of the clamping diodes as a nonlinear load element, causing a stronger-than-normal dependence of the signal-to-noise ratio on received power. In other words, errors accumlate very rapidly once the signal strength falls below that needed to reach ΔV_{req}. In a sense, ΔV_{req} forms a decision threshold at the input of the receiver and exemplifies the digital nature of the circuit.

Finally, an important caveat to these studies needs to be mentioned. That is, low BER measurements may be obtained from this receiver with very small signal swings, because off-chip amplification is used to boost the signal to levels sufficient for the error rate detector to operate. While this *does* define the ultimate sensitivity level of the receiver, it does *not* imply that it will be possible to use this receiver in a smart pixel application at such a power level. Such applications generally require a logic-level voltage at the output of the receiver (just before the source follower in Fig.1). For example, consider Fig.5 and Fig.6, which compares two cases of 622 Mb/s operation. For the lower-power operation (Fig.6), the output signal swing is small, indicating that logic levels are not being generated at the source follower. For this signal level to be usable on the chip, additional amplification stages would be required. This represents an additional cost in area and power consumption that might or might not be acceptable in a given system. However, if the clamping voltage is relaxed, full logic swing is possible, as evidenced in Fig. 5, which was obtained with 50 fJ, instead of 21 fJ.

In conclusion, we have reported some results from the BER testing of a diode-clamped receiver. We have confirmed the fundamentally digital nature of the receiver and demonstrated that it can be operated with low error rates to 1 Gb/s.

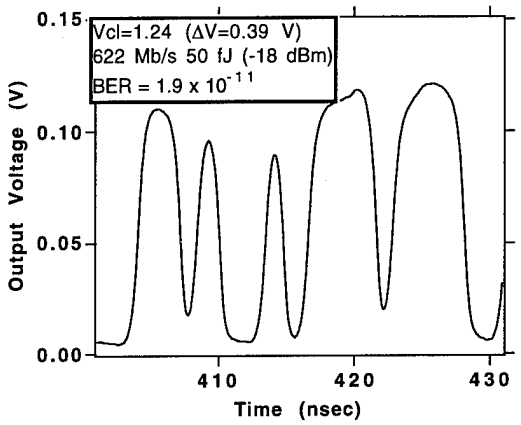

Figure 5: Output signal levels for 622 Mb/s at a relaxed clamping voltage capable of generating logic levels at the input to the final stage source follower in the receiver.

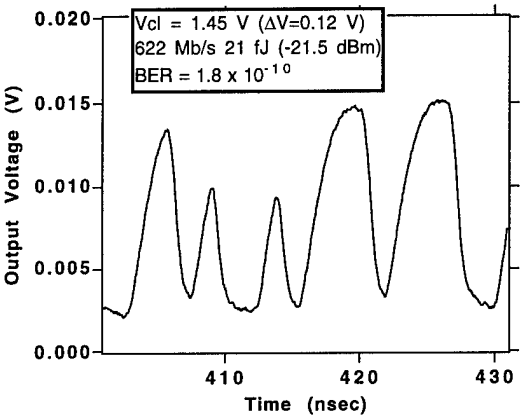

Figure 6: Output signal levels for 622 Mb/s near the ultimate sensitivity level of the receiver indicating that logic levels are not being generated at the input to the final stage source follower.

[1] see, for example F. B. McCormick, et. al. *Applied Optics*, **33**, pp. 1601-1618, 1994.

[2] T. K. Woodward, A. L. Lentine, Leo M. F. Chirovsky, *IEEE J. Quantum Electr.*, **30**, p. 2319-2324, Oct. 1994.

[3] A. L. Lentine, L. M. F. Chirovsky, T. K. Woodward, *IEEE J. Quantum Electr.*, **30**, pp. 1167-1171, 1994.

[4] a receiver with 10 micron wide source follower was studied in T. K. Woodward, et. al. To Appear in *IEEE Electron Dev. Lett.*

Friday, March 17, 1995

Transport Network Switching and Routing: 2

PFA 8:30 am-10:00 am
Red Lion East

Sonny Johansson, *Presider*
Ellemtel Telecommunication Systems Laboratories, Sweden

Review of ARPA-sponsored WDM Networking Projects

Charles A. Brackett
Bellcore
331 Newman Springs Road
Red Bank, NJ 07701

The concepts and progress of current ARPA-sponsored WDM networking projects will be reviewed, with emphasis on what has been learned and where new challenges lie.

A Comparison of Coherent Crosstalk Induced BER Floors in Four Types of $N \times N$ Space Photonic Switches

D. J. Blumenthal †, P. Granestrand ‡ and L. Thylen ‡†

† Microelectronics Research Center
School of Electrical and Computer Engineering, Georgia Institute of Technology
Atlanta, GA 30332, Tel: (404) 853-9448

‡ Fiber Optics Research Center , Ericsson Components, AB
S-16481 Stockholm, Sweden

‡† Laboratory of Photonics and Microwave Engineering
Department of Electronics, Royal Institute of Technology, Electrum 229
S-164 40 Kista-Stockholm, Sweden

1 Introduction

The all-optical multiwavelength network is a prime candidate for the future "information highways". In order to make these networks a practical reality, a number of questions need to be answered in terms of specifying components and subsystems. A critical issue involves bit error rate (BER) floors that degrade the normal statistical BER performance curves.

In this paper we consider the BER floors induced by coherent crosstalk in photonic switch arrays, e.g., in a switch in an optical cross connect [1], which route information from different optical sources of nominally the same wavelength. It has been shown that BER floors can develop due to coherent crosstalk in passive-splitting/active-combining switches [2]. Here, we extend this analysis to compare the crosstalk requirements for four different $N \times N$ switch array architectures. Incoherent crosstalk requirements have been analyzed for $N \times N$ photonic switches [3]. The optical fields entering a photonic switch from geographically different optical sources will overlap within the receiver bandwidth with a certain probability. If these signals coherently mix at a switch output due to crosstalk within the switch array, the received signal will fluctuate and cause bit errors.

2 Coherent Crosstalk in $N \times N$ Switches

We consider an $N \times N$ switch where $N-1$ inputs contribute to the coherent crosstalk at the i_{th} output channel and on-off intensity modulation is used. The instantaneous optical field at the i_{th} switch output can be written to include the statistical nature of the crosstalk sources:

$$U^{(N)} = \sqrt{S}\left[\cos\omega_0 t + \sum_{n=2}^{N} a_n P_n \cos\left(\omega_n t + \theta_n\right)\right] \tag{1}$$

where a_n, the 'crosstalk coefficient', is a function of crosstalk, switch structure and setting of undefined switch elements. $S/2$ is the instantaneous power in a "one" bit, ω_0 is the instantaneous frequency of the Nth channel, ω_n is the instantaneous frequency of one of the $N-1$ crosstalk channels, and θ_n is the instantaneous phase of one of the $N-1$ crosstalk channels relative to the i_{th} channel. The P_n are random numbers that specify if the crosstalk signals are ones or zeroes. Worst case coherent crosstalk occurs when ones are present at the other $N-1$ inputs and can affect the 2nd order statistics of the BER (i.e., burstiness of the errors). Taking into account the arrival statistics of ones and polarization states across the switch inputs will improve the BER averaged over a long sequence of bits and is the subject of work to be published.

We assume that bits are time aligned at all switch inputs, that the instantaneous optical phases change only once per bit interval (this assumption is valid when the laser line widths are equal to the bit rate), and that $\omega_0 - \omega_n$ lies within the low pass filter function of the receiver (denoted LP[..]). The instantaneous intensity at the i_{th} switch output is given by:

$$Q^{(N)} = \mathrm{LP}\left[\left|U^{(N)}\right|^2\right] = S\left(1/2 + \sum_{n=2}^{N} a_n P_n \cos\theta_n + \sum_{n=2}^{N}\sum_{m=2}^{N} a_n a_m P_n P_m \frac{1}{2}\cos(\theta_n - \theta_m)\right) \quad (2)$$

The expectation value of $Q^{(N)}$ is $S/2$ and the optimum threshold is $S/4$. A coherent bit pattern dependent error occurs if $Q^{(N)} < S/4$. To investigate first order effects, we optimistically drop the double sum term for these calculations. However, it is important to note that these terms can contribute significantly to coherent signal degradation. In this approximation, the error condition is $\sum_{n=2}^{N} a_n P_n \cos\theta_n \leq -\frac{1}{4}$.

The instantaneous field amplitude equations for the switch architectures are given below (these architectures are defined in [3]). In the Passive-Splitting/Active-Combining Switch (PSAC) we assume that non-defined switch states are *not* set to 3 dB-state, but are set arbitrarily. For the Active-Splitting/Passive-Combining Switch (ASPC) case, we assume that the 'undefined' switch elements are in the 3 dB state. For the Active-Splitting-Active-Combining Switch (ASAC) case, worst case input-output point-to-point combinations are assumed. For the GAA case, E is equivalent to C when used as a relative power leakage in a gate. In all cases, crosstalk in waveguide crossovers is ignored (otherwise implementation specific issues must be taken into account).

$$U^{(N)}_{\mathrm{PSAC}} = \sqrt{S}\left\{ cos\omega_0 t + \sum_{i=1}^{log_2 N}\sum_{j=1}^{\binom{log_2 N}{i}} C^{i/2}\cos\phi_{ij}\right\} \quad (3)$$

$$U^{(N)}_{\mathrm{ASPC}} = \sqrt{S}\left\{\cos\omega_0 t + \sqrt{C}\sum_{i=1}^{log_2 N}\sum_{j=2^{i-1}+1}^{2^i} 2^{-(i-1)/2}\cos\phi_{ij}\right\} \quad (4)$$

$$U^{(N)}_{\mathrm{ASAC}} = \sqrt{S}\left\{\cos\omega_0 t + C\sum_{i=1}^{log_2 N}\sum_{j=1}^{2^{i-1}}(1/2)^{i-1}\cos\phi_{ij}\right\} \quad (5)$$

$$U^{(N)}_{\mathrm{GAA}} = \sqrt{S}\left\{\cos\omega_0 t + \sqrt{E}\sum_{i=2}^{N}\cos\phi_i\right\} \quad (6)$$

3 Simulation Results and Crosstalk Bounds

The total optical field, including primary and crosstalk signals, at a primary output port was numerically simulated for each switch type using Eqns. 3 to 6. ϕ is uniformly distributed over the interval $[0, 2\pi]$. The BER is calculated by testing the error condition over M time slots with the phase randomized across all switch inputs and in time and weighted by the appropriate crosstalk coefficients.

The curves in Fig. 1a show the calculated BER as a function of switch crosstalk for $N = 32$ with $M = 10,000$. A critical crosstalk value is reached where the BER due to coherent crosstalk approaches zero rapidly. To the left of this point, standard noise contributions will result in the typical BER curve. For switches with crosstalk values to the right of this point, the BER will hit a BER floor.

To eliminate the BER floor under the constraint that even if the phases at all switch inputs are $-\pi$ out of phase with the primary signal, we set the condition that $\sum_{n=2}^{N} a_n < 1/4$. The following equations describe this constraint on C as a function of N for the four switch types and are plotted in Fig. 1b. Eqn. 7 is an approximation for $N \geq 4$.

$$\mathrm{PSAC} \rightarrow C^{1/2} log_2 N + C log_2 N(log_2 N - 1)/2 < 1/4 \quad (7)$$

$$\mathrm{ASPC} \rightarrow \sqrt{C}(\sqrt{N} - 1)/(\sqrt{2} - 1) < 1/4 \quad (8)$$

$$\mathrm{ASAC} \rightarrow C log_2 N < 1/4 \quad (9)$$

$$\mathrm{GAA} \rightarrow \sqrt{E}(N - 1) < 1/4 \quad (10)$$

4 Conclusions

We have calculated the coherent crosstalk BER floor for four types of photonic switch structures, passive-split/active-combine, active-split/passive-combine, active-split/active-combine, and gated-amplifier array. This crosstalk is due to coherent mixing of primary and crosstalk signals at a given switch output, resulting in a

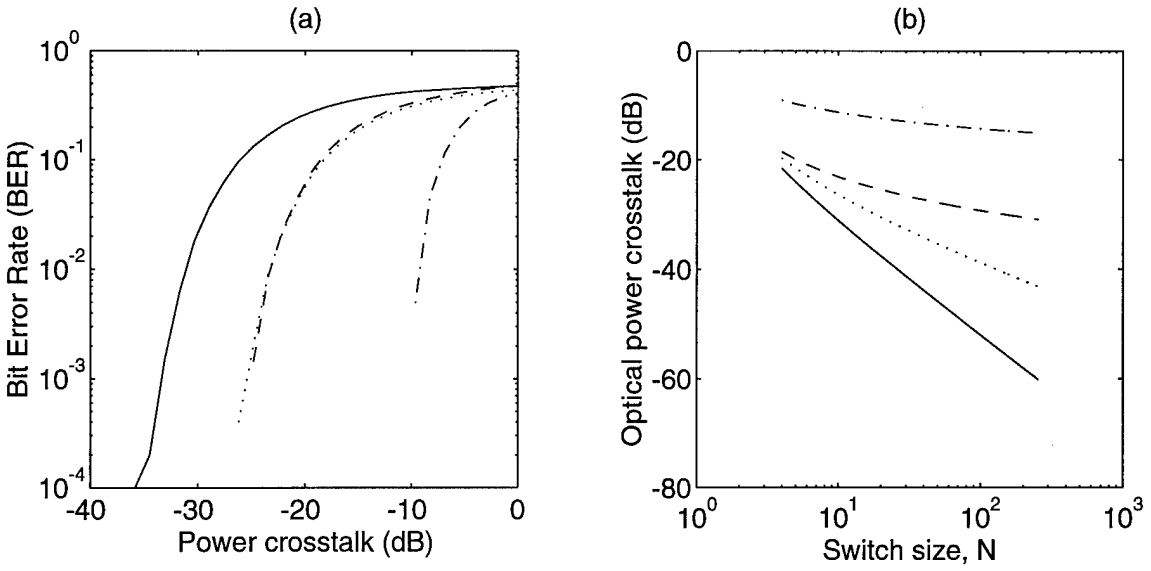

Figure 1: (a) Dependance of BER on switch crosstalk due to coherent effects for four different switch types with N=32, (b) worst case crosstalk bounds for no BER floor as a function of N. Figure legend: ASPC = "..." PSAC = "- -" ASAC = "-.-" GAA = "—"

closure of the eye pattern. The size dependent bounds on crosstalk for low BER operation were calculated using statistical numerical simulations and show the presence of a BER floor. Bounds on crosstalk as a function of switch size were also investigated. It is seen that as the switch size increases, lower crosstalk elements are required. The switch type that is most yielding to crosstalk requirement is the ASAC structure, while the type that is most demanding on the crosstalk is the GAA. For small switch sizes N, there is a higher probability that the phases at all inputs can align to the worst case and the lower bound curves may be a more accurate design guide. For larger switches, the worst case occurs with extremely low probability, and the statistically generated curves may serve as an accurate guide. The interpretation of BER must be approached carefully, as the BER measured over a long string of bits only characterizes the first moment (average) of the BER. The pattern dependency of coherent crosstalk can generate conditions where the errors are bursty by nature, thereby causing periodic BER floors to occur. It is therefore important to consider the arrival statistics of the deterministic bit errors. Also, taking into account the arrival statistics of 'ones' and 'zeros' in addition to the polarization states will also reduce the probability of the worst case situation occurring.

5 Acknowledgments

This work was supported in part by the National Science Foundation under a National Young Investigator (NYI) grant and partially carried out under the RACE MWTN (R2028) project. The Laboratory of Photonics and Microwave Engineering acknowledges support from the Swedish Board of Technical Development (NUTEK).

References

[1] G.R. Hill, et.al., "A Transport Network Layer Based on Optical Network Elements," *J. Lightwave Technol.* , vol. 11, no. 5/6, May/June, 1993.

[2] D.J. Blumenthal and L. Thlyen "Coherent crosstalk induced BER floors in $N \times N$ space photonic switches," *LEOS Summer Topical Meeting on Optical Networks and Their Enabling Technologies*, Postdeadline paper, July 11-13, 1994.

[3] R.A. Spanke, "Architectures for Guided-Wave Optical Space Switching Systems," *IEEE Comm. Mag.*, vol. 25, no. 5, pp. 42-48, May, 1987.

[4] M. Gustavsson, B. Lagerstrom, L. Thylen, M Janson, L Lundgren, A. -C. Morner, M. Rask, B. Stoltz, "Monolithically integrated 4×4 laser amplifier gate switch arrays", *Proc OSA Topical Meeting on Optical Amplifiers and their Applications*, (1992), paper PD9.

Dualities among "Space," "Time" and "Wavelength" in All-Optical Networks *

Hisashi Kobayashi†
Department of Electrical Engineering
Princeton University
Princeton, NJ 08544
e-mail: hisashi@princeton.edu

Ivan P. Kaminow
Crawford Hill Laboratory
AT&T Bell Laboratories
Holmdel, NJ 07733
e-mail: ipk@hoh-1.att.com

All-optical networks (AONs) are emerging as the next generation broadband networks for both wide-area and local-area networks. In order to fully exploit the enormous bandwidth that optical channels can provide, it is essential to make the best use of WDM (wavelength division multiplexing), TDM (time division multiplexing) and SDM (space division multiplexing). A device called "wavelength grating router (WGR)" [3, 4] (also known as $N \times N$ multiplexer) has been developed to provide interconnections in an AON, allowing wavelengths to be reused in different parts of the network [1]. Figure 1 (a) gives a schematic diagram of the $N \times N$ static WGR, in which the number of wavelengths F is equal to the number of ports N. Figure 1 (b) is an equivalent representation of this device in terms of an array of wavelength multiplexers D_w and that of wavelength multiplexers M_w [2].

If we represent the $N \times N'$ WGR by the N array of demultiplexers $(1 \times F)$ followed by the N' array of multiplexers $(F \times 1)$, and if we insert an F array of space switches $(N \times N')$ between them, we obtain a generalized structure of what is called a "dynamic router" [1], as shown in Figure 2 (a). The f-th S switch $(f = 0, 1, \cdots, F-1)$ performs space switching on signals that are carried by wavelength λ_f. The degree of connectivity is now increased to $C = NN'F$. Note that the total number of circuit connections (point-to-point) that can be supported simultaneously is still $\min\{N, N'\}F$: the insertion of the F spatial switches increases the total number of realizable connections, but many of these connections interfere at the output ports.

Figure 2 (b) represents its time-domain counterpart, where the input signals are TDM signals. If the T space switches are realized by one space switch that is time shared, the resulting structure is what is known as a *time-multiplexed space* (TMS) switch. If we insert an array of TSIs $(T \times \tau)$ between the arrays of demultiplexers and space switches, and another array of TSIs $(\tau \times T')$ between those of space switches and multiplexers, we will obtain what is known as a T-S-T switch, as shown in Figure 3 (b). Note that the T, T' and τ can be different, but it is necessary that $\tau \geq T + T' - 1$ for the switch to be nonblocking.

The wavelength counterpart of the T-S-T is given by the structure of Figure 3 (a). The $F \times \Phi$ switch, W, is the wavelength counterpart of the TSI switch, hence may be called a *wavelength*

*Supported by a grant from ARPA to the AON (All-Optical Network) Consortium
†A Consultant to AT&T

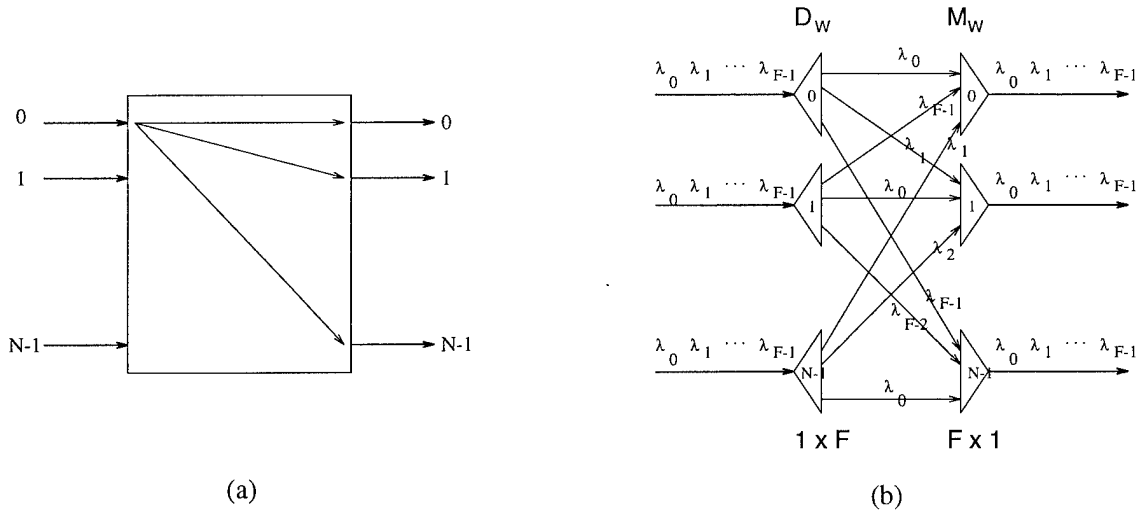

Figure 1: (a) $N \times N$ wavelength grating router (or static wavelength router); (b) Demultiplexer-multiplexer representation of the $N \times N$ WGR

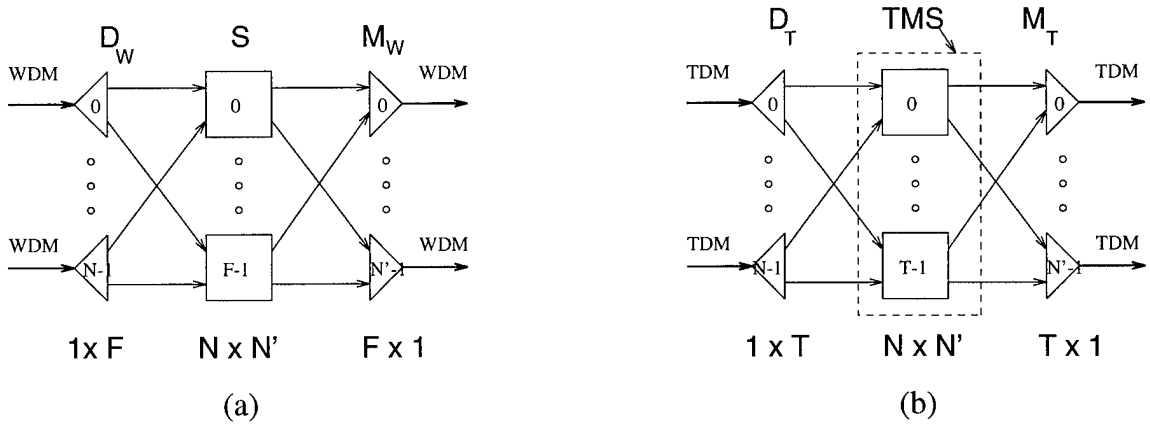

Figure 2: (a) Dynamic wavelength router; (b) Time multiplexed space (TMS) switch

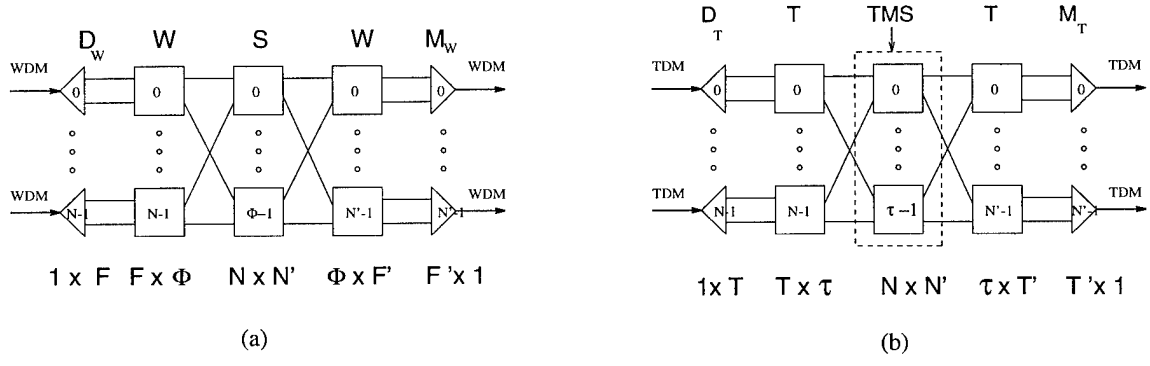

Figure 3: (a) W-S-W switches with WDM signals; (b) T-S-T switches with TDM signals

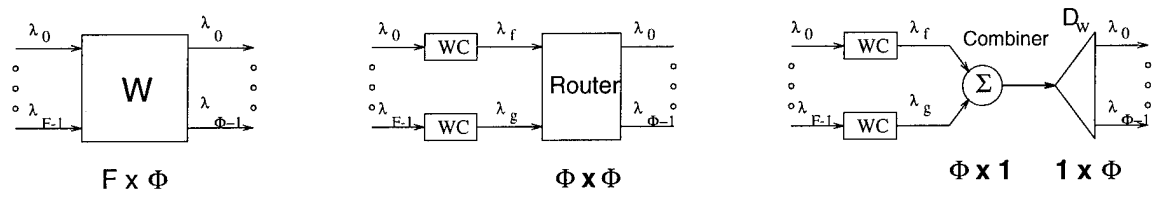

(a) (b) (c)

Figure 4: (a) Wavelength interchanger; (b) Wavelength converters followed by a "router"; (c) Actual implementation example

interchanger or wavelength division switch (WDS). It can be implemented by using an array of wavelength converters, WCs, (also called frequency changers), followed by a router, whose outputs ought to be in the right order, i.e., $\lambda'_0, \cdots, \lambda'_{\Phi-1}$, independent of the ordering at the inputs $\lambda'_f, \cdots, \lambda'_g$, as shown in Figure 4 (b). Note that Φ can be different from F, the number of input wavelengths. Furthermore, and the set $\{\lambda_0, \lambda_1, \cdots, \lambda_{F-1}\}$ can be completely different from the set $\{\lambda'_0, \lambda'_1, \cdots, \lambda'_{\Phi-1}\}$. The latter set is locally defined within the individual W switch. The $\Phi \times \Phi$ "router" in Figure 4 (b) is a "logical" router in the sense that only $F(\leq \Phi)$ input ports are active at any given time. One way to realize this "router" is to have a wavelength "combiner" followed by a grating-based multiplexer $(1 \times \Phi)$, as shown in Figure 4 (c).

Finally we extend the above results to the case, where input signals are combined TDM/WDM. We discuss appropriate versions of the above router/switches. The outputs from D_w, i.e., the inputs to the S, are TDM signals. Therefore, we discuss different cases, depending on whether each of the S and W switches may be time-multiplexed or not. If W switches (i.e., their WC components) can tune to different wavelengths at different time slots, then we can construct what may be termed a *time-multiplexed wavelength* (TMW) switch.

In a separate paper [5] we discuss achievable performance of these devices, in terms of *call blocking probability* and discuss how the availability and unavailability of TSI and "wavelength interchanger" will impact the capability of AONs.

References

1. S. B. Alexander et al. (1993). "A Precompetitive Consortium on Wide-Band All-Optical Networks." *Journal of Lightwave Technology* **11**(5/6):714-735, May/June, 1993.

2. C. Bracket (1990). "Dense Wavelength Division Multiplexing Networks: Principles and Applications," *J. of Selected Areas in Communications*, **8**, 6, pp. 948-964, August 1990.

3. C. Dragone (1991). "An NxN Optical Multiplexer Using a Planar Arrangement of Two Star Couplers." *Photon. Tech, Lett.*, **3**:813-815, Sept. 1991.

4. B. Glance, I. P. Kaminow, and R. W. Wilson (1994). "Applications of the Integrated Waveguide Grating Router." *Journal of Lightwave Technology* **12**(6): 957-962, June 1994.

5. H. Kobayashi, B. L. Mark and Y. Osaki (1994). "Call Blocking Probability of All-Optical Networks," To appear in *Proc. IEEE BSS'95*, Poznan, Poland, April 1995.

Mechanical Optical Fibre Cross Connect

Sven Sjölinder, Ericsson Cables AB, Network Products Division, S-172 87 Sundbyberg, Sweden. Tel no +468 764 3108, fax +468 985 503

Introduction

Cross connect in the physical layer of the optical network is needed of several reasons. They may vary from operator to operator depending on the network architecture. The main reasons in many cases are installation of new terminals and service work on the fiber line. The cross connection is made at the ODF (=optical distribution frame) points in the network. The ODF:s are frequent and placed at the nodes in the network. To upgrade the network and install a new terminal, the appropriate connections are made manually at the ODF. To reduce labour cost and time Ericsson suggest to introduce a remotely controllable ODF. The remote control is made from anywhere in the network from a portable PC. With an remotely controllable ODF the documentation of the fiber network configuration may be made automatically and always be kept updated.

In an urban area the fiber number may soon become in the range 100-1000 at each node. Hence, an important qualification for an optical cross connect is to accommodate a large number of ports. Also, the switching principle to avoid entanglement of the fibres is important. The switching time is of less care since manual actuation is accepted today in most applications. The main function for a space switch for rerouting is to decrease labour cost by being remotely controllable and thus making the travels to the nodes unnecessary.

Design and Performance of the Fibre Cross Connect, FXC

The cross connect fabricated comprises electrical motors which move an optical fibre connector on a matrix base plate. Both sides of the matrix plate is used. The motors move the fibre to a certain position in the matrix. Each connector is only allowed to be moved in a linear direction. The directions on the two sides are perpendicular to each other, forming a crossbar system. The principal is seen in figure 1. In this way all possible combinations can be set up independent of the position of other connectors. The connection (mating) function is made by motors assembled together with the connectorized fibres in the "locomotives". Each locomotive thus contain two motors. The fabricated FXC is shown in figure 2.

Standard optical connectors are used. They are of flat angled type i.e. no physical contact is achieved between the glass surfaces of the two fibres. The design was chosen to get low wear on the fibres end surfaces and long lifetime of the connectorized fibres. The connector is a ceramic ferrule with 6^0 angle, assembled in a v-groove. The ferrule and the V-groove form a block handled by the motor. After mating of the blocks, a force is applied to press the two mating ferrules closely together. This principle has shown excellent performance. No wear or dirt problems at all has been measured during the first 2700 matings, figure 3. The matings were performed without cleaning of the ferrules. A variation of optical

loss of up to 0.8dB is seen. The variation is caused by interference. It is in accordance with theoretical predictions assuming 4% fresnel loss. In this way outermost wear and dirt resistance is achieved , the glass surfaces never touch each other and optical loss and back reflection is kept well within limits during all the 2700 operations. Maximum loss is 1.67 dB. It is the sum of two connections (the cross point and one interface) and the fresnel loss variation. The return loss is always better than -40dB.

Reliability

The advantage of a mechanical fibre cross connect is reliability. Most important is that the connections are mechanical and passive and hence not relying on continuos power supply. The connections will stay in operation even at power failure. Power is only needed for switching. The design is made to have a reference point so even if a serious damage to electronics erase all memory it is possible to remotely define a position for the locomotive by ordering it to move to its reference point.

Summary

An fiber optical cross connect, FXC, based on mechanically movements of fiber connectors has been fabricated and tested. It is demonstrated that 2700 switching operations can be made without cleaning of the ferrules. It is operated from an PC (personal computer) and can switch any of N incoming fibres to any of M outgoing fibres in a non blocking way.

References

1. M.Tachikura, T.Katagari, H. Kobayashi, Strictly Nonblocking 512×512 Optical Fiber Matrix Switch Based on Three-stage Clos Network. IEEE Phot. tech. Let. Vol.6, No.6, June 1994 p.764.

2. G.A. Pesavento, Building Optomechanical Switching systems, Lightwave, Jan 1991.

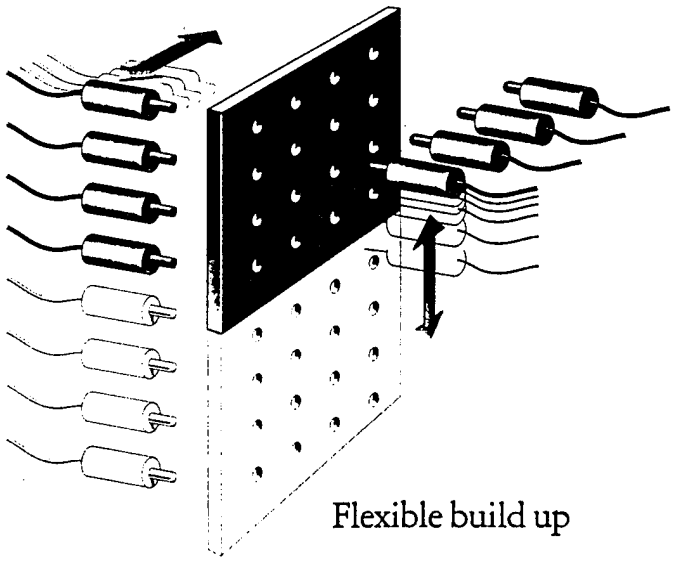

Figure 1: Basic principle of fiber optic cross connect, FXC.

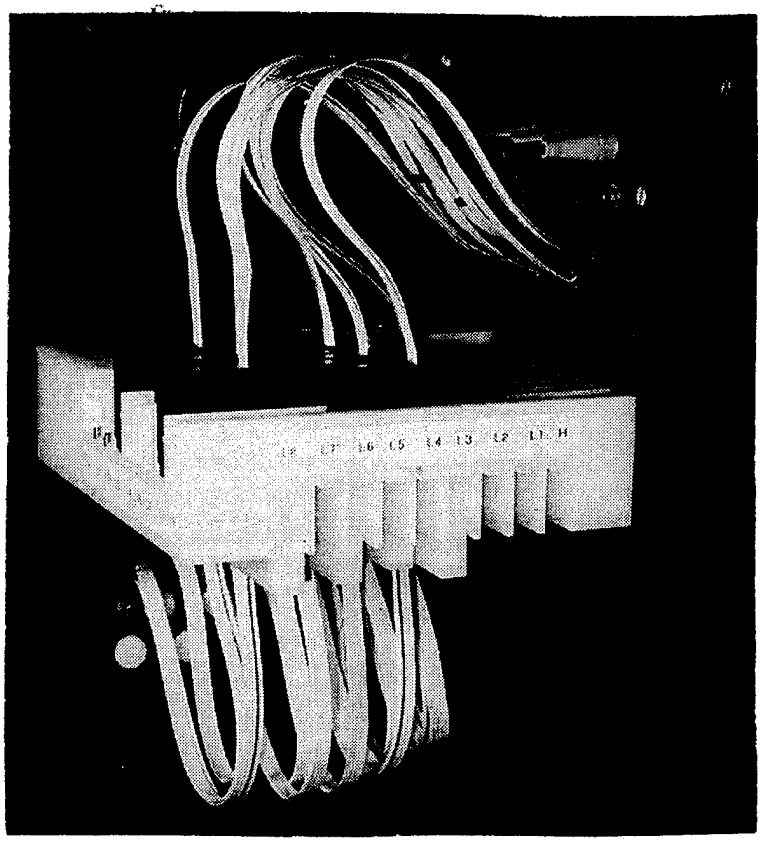

Figure 2: A picture of the FXC fabricated.

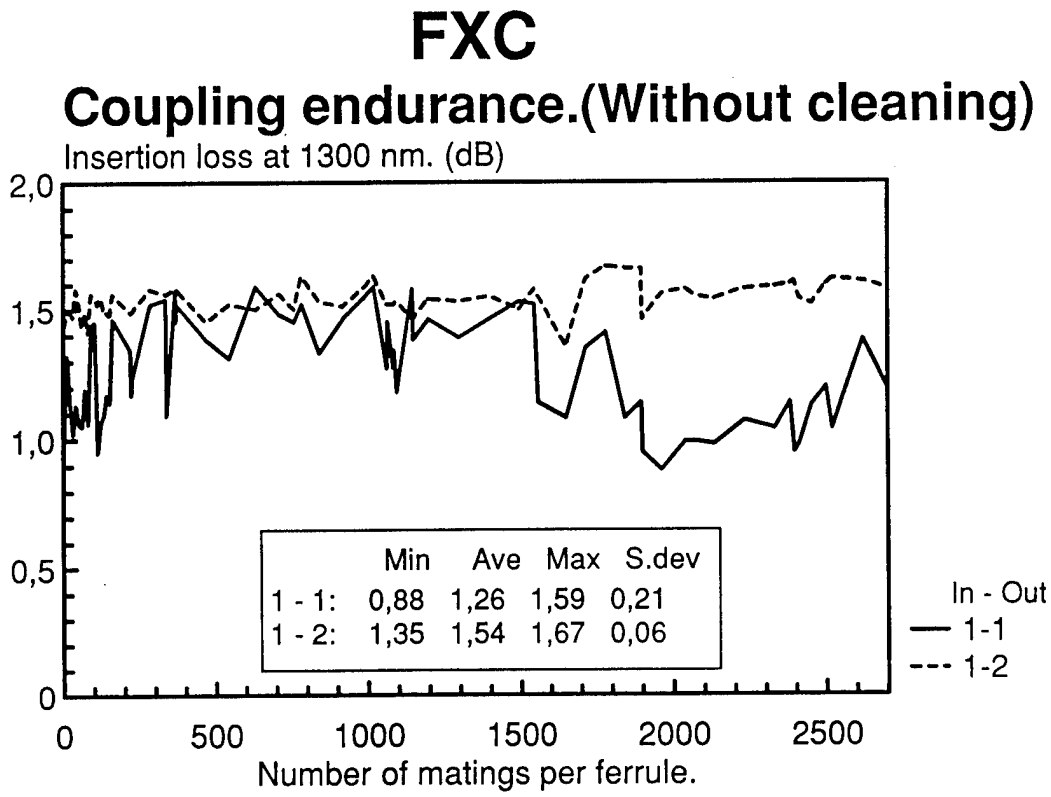

Figure 3: Optical loss versus number of matings for two connections.

THERMAL CONSIDERATIONS IN THE DESIGN OF OPTO-ELECTRONIC DEVICE MOUNTS

D.B. Buchholz, A.L. Lentine, R.A. Novotny
AT&T Bell Laboratories, 2000 N. Naperville Rd., Naperville, IL 60566
(708) 979-2809, FAX (708) 713-7951

For some optoelectronic devices, the optical characteristics of the device are a strong function of the device temperature. An example of this is the self-electro-optic effect device (SEED).[1] SEEDs make use of the shift in wavelength of the exciton absorption maxima that occurs as a function of a changing electrical field across multiple quantum well material.[2] For a typical device, the absorption maxima must be shifted by 3 to 5nm to obtain good contrast between the absorptive and reflective states. A change in the device temperature, however, can also change the location of the exciton absorption maxima.[3] For GaAs/AlGaAs devices the absorption maxima shifts approximately 0.28nm/°C.[4] Thus, it becomes necessary to carefully design the SEED mount to minimize the temperature gradient and, therefore, this temperature induced shift across the chip.

In this paper we have used finite element analysis (FEA) to model mounts for a 16x16 array of FET-SEED switching nodes. By careful mount design, the calculated temperature spread could be held to 1°C even when the power density was 40W/cm^2 over the 0.15cm^2 active chip area; a 6W chip. We have also used the temperature dependence of the exciton absorption maxima to map the temperature of an existing 4x4 array of FET-SEED switching nodes[5], operating at a power density of 49W/cm^2 and found the results in good agreement with those obtained by FEA.

Two fundamental tasks exist in the thermal management of a chip; not only is it necessary to prevent the entire chip from heating to a point where thermal effects degrade the overall performance but it is also necessary to maintain the temperature of multiple locations on the chip to nearly the same temperature.The exact amount of temperature variation that can be tolerated (ΔT) will depend on the application but in general it will fall into the range of 1 to 4°C. It is not necessary to hold the entire chip to this temperature range but only specific devices on the chip, such as all the optical output modulators. The temperature variation of interest is the difference between the hottest and coolest of these devices, as shown in Figure 1, not the overall temperature spread or the temperature differential of a single node. The temperature profile depicted

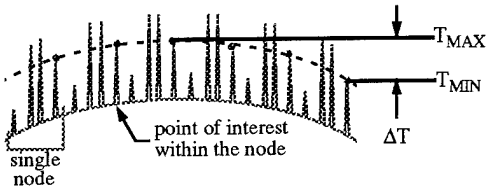

Figure 1
Sematic 1D Temperature Profile
SEED Node Array

in Figure 1 is representative of that which one would expect in a regular array of nodes. The chief cause of temperature variation between equivalent devices on the chip is the spreading of heat to the predominately passive regions around the periphery of the chip where the electrical I/O bond pads are located.

The design of a SEED mount must, therefore, contain an analysis of the temperature variation between the equivalent critical optoelectronic components on the chip. The testing of the mounted chip must contain an analysis to verify the temperature variation between these components. The first of these two tasks can be accomplished by finite element analysis and will be discussed later. The second of these two tasks can be accomplished using the same physical phenomena that makes attention to temperature variation necessary, namely the shifting of the exciton peak location. The experimental setup used in this study is shown in Figure 2. The chip, a 4x4 array of 210um x 210um FET-SEED switching nodes[5], was held at

a constant temperature with a thermal electric cooler (TEC). A laser light source, λ=850nm, and

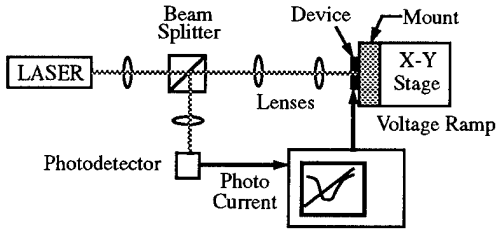

Figure 2
Experimental Setup

lens system was used to illuminate a single SEED modulator. The reflected light was focused on a photodetector. A bias voltage ramp was applied to the modulator and the photocurrent of the reflected light measured as a function of the applied bias. The minimum photocurrent corresponds to the absorption maxima. Next, the temperature of the entire chip was changed by adjusting the TEC. The change in bias voltage at which the absorption maxima occurred, for the same modulator, was noted. In this manner a ΔV verses ΔT curve was constructed. Finally an X-Y stepper stage was used to move the laser illumination to different modulators and the bias voltage at which the absorption maxima occurred noted as a function of chip location. A finite element analysis (FEA) program was used to model the temperature profile of the measured device. The device mount is depicted in Figure 3. The thermister used to control the TEC, was

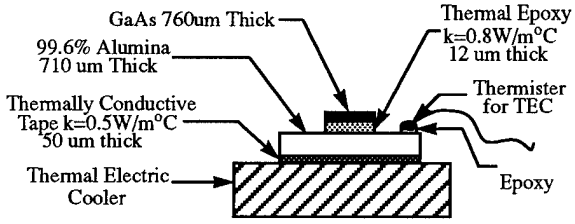

Figure 3
Thermal Model for FEA

not part of the thermal model but is included to further define the experimental setup. The thermistor was held at 20°C. The chip was powered to 350mW and the power was assumed to be distributed evenly over the 840um x 840um active area of the array (49W/cm^2). The overall chip size was approximately 2.8mm square and the ceramic was 7.5mm square. Figure 4a is a plot of the measured temperature for four different modulators on the chip. Figure 4b is a plot of the isotherms on the

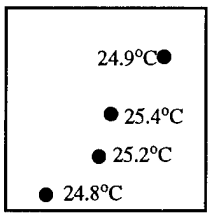

Figure 4a
Experimentally Determined Temperature Profile
4x4 SEED Array

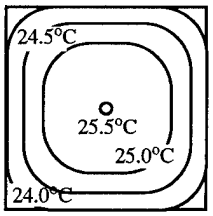

Figure 4b
Finite Element Analysis Temperature Profile
4x4 SEED Array

active area of the chip surface as predicted by the FEA program. The thickness of the thermal epoxy used to affix the device to the ceramic was an estimate and could easily account for the minor differences between the model and the experimental measurements.

The chip just examined had a temperature variation across the active area on the order of 1.5°C, which for most applications would be acceptable. As mentioned, the chip was a 4x4 array of SEED nodes. For a chip of this size, even the center nodes are close to the non-active boarder regions and the effect of thermal spreading is therefore minimized. The temperature distribution for a 16x16 array of 240um x 240um FET-SEED switching nodes, operating at 6.3W (40W/cm^2 over a 0.15cm^2 active area) mounted the same as the 4x4 array, is shown in Figure 5. Not only does the overall temperature

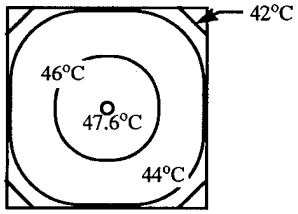

Figure 5
Finite Element Analysis Temperature Profile
16 x 16 Node SEED Array

of the chip rise but the temperature variation increases to 5°C. Again, the chief cause of the temperature variation is heat spreading into the inac-

tive boarder regions of the chip; the active chip area is 3.84mm x 3.84mm and the overall chip size is 4.32mm x 4.32mm. A mount for the 16x16 node array was designed that would counter the effects of the heat spreading, as shown in Figure 6. An

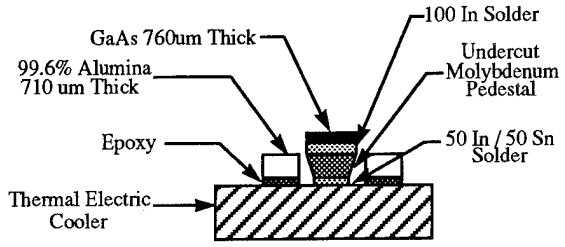

Figure 6
Heat Confining Chip Mount

opening is cut in the ceramic used for the device interconnect and the device is mounted on a molybdenum pedestal that tapers down as it approaches the TEC. The taper in the pedestal counteracts the effect of the inactive chip periphery and the temperature spread is reduced to approximately 1°C, as shown in Figure 7. The decrease in

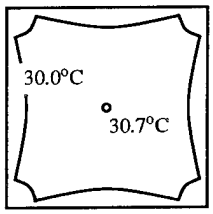

Figure 7
Finite Element Analysis Temperature Profile
16 x 16 Node SEED Array
With Heat Confining Chip Mount

the overall chip temperature is due to the use of solder for the two bonds in the thermal path instead of organic adhesives. The use of low temperature solders is required because of temperature limitations imposed by the TEC.

In conclusion, we have mapped the temperature across the active area of a SEED array by calibrating the exciton peak shift, of the GaAs-AlGaAs quantum well modulators, as function of temperature. We have compared the measured temperature profile to one modeled by finite element analysis and found them in good agreement. Using the finite element analysis program, we have shown that with proper design of the chip mount, areas of equivalent optoelectronic functions can be held at a uniform temperature, $\Delta T \sim 1^{\circ}C$, even for large high power density devices.

This work was partially sponsored by ARPA under Air Force Rome Labs contract number F30602-93-C-0166.

References

[1]D. A. B. Miller, D. S. Chemla, T C. Daman, A. C. Gossard, W. Weigmann, T. H. Wood, C. A. Burrus, "Novel hybrid optically bistable switch: The quantum well self-electro-optic effect device," Appl. Phys. Lett. **45**, pp. 13-15 (1984)

[2]D. A. B. Miller, D. S. Chemla, S. Schmitt-Rink, "Electric Field Dependence of Properties of Semiconductor Quantum Wells: Physics and Applications", in *Optical Nonlinearities and Instabilities in Semiconductors*, H. Haug Ed., Academic Press, Inc., 1988

[3]S. M. Sze, *Physics of Semi Conductor Devices*, 2nd Ed., John Wiley and Sons, 1981 pp.15

[4]R. A. Novotney, "Parallel optical data links using VCSELs," Proceedings SPIE, vol. **2147,** *Vertical-Cavity Surface-Emitting Laser Arrays,* pp. 140-149 (1994)

[5]D.B.A. Miller, M.D.Feuer, Y.T. Chang, A.S.C. Shunk, J.E. Henery, D.J. Burrow, D.S. Barrow, D.S. Chemla, "Field-Effect Transistor Self-Electrooptic Effect Device: Integrated Photodiode, Quantum Well Modulator and Transistor," IEEE PTL, **V1**, N3, March 1989

Friday, March 17, 1995

Photonic Network Components

PFB 10:30 am-12:30 pm
Red Lion East

Takeshi Ozeki, *Presider*
Sophia University, Japan

Recent Advances in Planar Lightwave Functional Devices

Kaname Jinguji, Koichi Takiguchi, and Masao Kawachi

NTT Opto-Electronics Laboratories
Tokai-mura, Naka-gun, Ibaraki-ken, 319-11, Japan
E-mail: jinguji@nttiba.ntt.jp

1. Introduction

Optical frequency-division-multiplexing (FDM) systems have been widely studied in order to achieve large-capacity optical networks. The key components in this field are optical functional devices such as multi-frequency-channel selectors[1] and band-pass optical filters. Recently, we have developed a circuit synthesis algorithm[2] by analogy with electrical digital filters. We first briefly review the evolution of silica-based planar lightwave circuits (PLCs)[3]. Then we describe the new generation of PLCs, including programmable optical filters[4], designed using the synthesis algorithm.

2. Evolution of silica-based PLCs

Various PLCs have been developed based on low-loss silica waveguides on silicon substrates. The PLCs can be classified into four generations in terms of their evolution as shown in Fig.1. The first generation includes simple Y branches and directional couplers. Most of these devices function simply as power splitters. A 1xN splitter (N=4, 8, 16, 32) formed by connecting Y-branches is now commercially available. The second generation includes Mach-Zehnder (MZ) interferometers[5] and ring resonators which have been designed by analogy with microwave or milimeter-wave filters. This generation of PLCs is equipped with thermo-optic (TO) phase shifters to control the optical phases. This enables them to perform higher functions. MZ interferometers in particular can perform various lightwave functions depending on the path difference ΔL between the two directional couplers. These functions include optical switching, wavelength-insensitive coupling, and optical multiplexing/demultiplexing in wavelength-division multiplexing (WDM) and FDM communications. The third generation includes NxN star couplers and arrayed-waveguide grating (AWG) multiplexers. This type is equipped with free-space radiative slab waveguides. AWG multiplexers are expected to be the key components in constructing wavelength-addressed network or switching systems. The fourth generation, which has recently been the subject of intense study, is the major concern of this paper. The feature of this generation is that their circuit parameters are designed from desired filter characteristics based on a synthesis algorithm as shown in Fig. 2. The synthesis methods and functions of this new generation of PLCs are described in the following section.

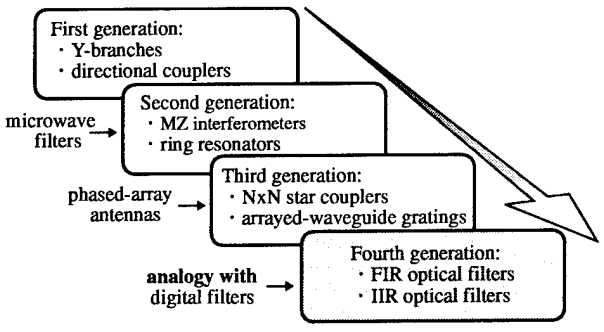

Fig.1 Evolution of silica-based PLCs

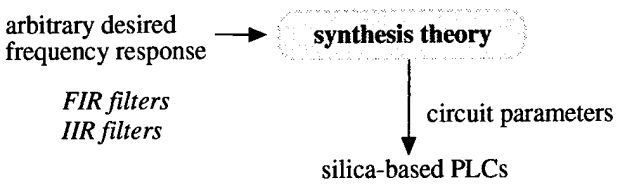

Fig.2 Feature of the fourth generation

3. Synthesis of optical filters

(1) Classification of optical circuits

Optical circuits can be regarded as delay-line systems constructed using optical branches, delays, and combiners. This means that optical circuits have the same transfer characteristics as electrical digital filters. Optical circuits can be classified into two classes by reference to the classification of digital filters. One is a finite-impulse-response (FIR) type which has no recursive delay-lines, and the other is an infinite-impulse-response (IIR) type which has recursive delay-lines. For example, MZ interferometers are FIR type and ring resonators are IIR type. We succeeded in developing synthesis algorithms adaptable to both FIR and IIR types with two-port configurations by analogy with digital filters. We deal only with two-port circuits, because two-port filters have the advantage that 100%-transmittance filtering and a pair of power-complimentary optical outputs are automatically realized as a natural consequence of the two-port circuit configuration.

(2) Synthesis of two-port FIR optical filters

The circuit configuration of a two-port FIR optical filter is shown in Fig.3. An N-order FIR optical filter is constructed by using N unit elements each composed of one directional coupler and one delay-line with one phase shifter. The loss-less transfer characteristics of this filter are expressed by the following 2x2 unitary matrix:

$$S=\begin{pmatrix} H(z) & jF_*(z) \\ jF(z) & H(z) \end{pmatrix}$$

$$H(z)=(\sum_{k=0}^{N} a_k z^{-k})z^{\frac{N}{2}},\quad F(z)=(\sum_{k=0}^{N} b_k z^{-k})z^{\frac{N}{2}} \qquad (1)$$

where z denotes $\exp(-j2\pi f/f_{FSR})$ and f_{FSR} indicates the free spectral range. The expansion coefficients a_k and b_k are complex.

Our design algorithm includes the four design processes outlined below. In order to obtain the optimum circuit parameters from a desired cross transfer function $F_0(z)$, it is necessary:

1) to decide the unit delay-time difference $\Delta\tau$ from a desired frequency period, and obtain the complex expansion coefficients b_k of F(z) from a desired transfer function $F_0(z)$ by using a proper approximation method for digital filters,

2) to normalize the obtained complex expansion coefficients so as to get the maximum transmittance of 100%,

3) to calculate H(z) from F(z) by using the unitary condition of the S matrix,

4) to resolve the total transfer matrix S into the product of the unit element matrices such as

$$S=S_N S_{N-1}\cdots S_k\cdots S_2 S_1 S_0 \qquad (2)$$

by considering the unitary condition of each basic transfer matrix S_k and calculate the phase shift value θ_k at each tunable coupler and the phase shift value φ_k of each tunable phase shifter from each resolved basic transfer matrix.

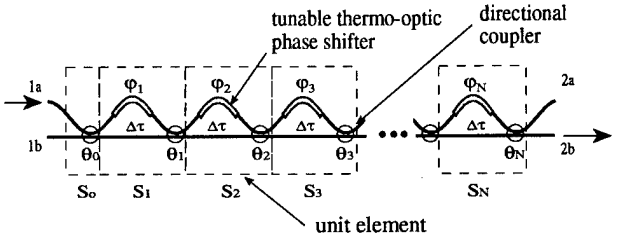

Fig.3 Circuit configuration of a two-port FIR optical filter

Figure 4 shows a multi-channel selector for use in an optical FDM highway switch. The selector can select several channels from many multiplexed frequency channels. In this design example, three frequencies, f_1, f_3, and f_7, are selected.

Figure 5 shows a linear-phase Chebyshev filter for use in optical FDM communication. This filter provides band-pass filtering with equal ripples and linear-phase characteristics simultaneously.

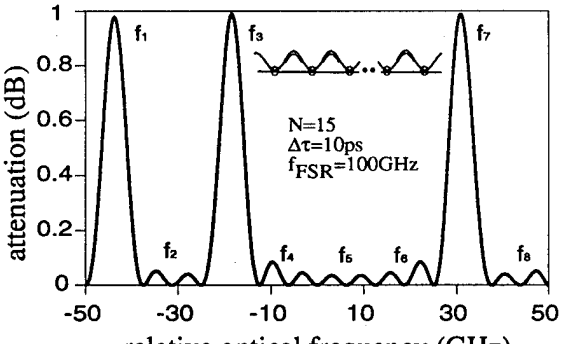

Fig.4 Multi-frequency-channel selector using a two-port FIR filter

Evolution of Fiber Arrays for Free Space Interconnect Applications

Nagesh Basavanhally, Richard Borutta, Randall Crisci, Casimir Nijander and Laurence Watkins

AT&T Bell Laboratories
Engineering Research Center
Princeton, NJ 08540

1. Introduction

Photonics technology involving parallel processing architecture is becoming extremently important for large scale information movement. The obvious reasons are high bandwidth of optical media, the lack of light beam interference and the possibility of high density interconnections. Free space optical interconnection [1] [2] [3] offers the potential for large number of interconnections. Such free space interconnect schemes are being considered for large VLSI systems and photonic switching systems. These systems require fiber arrays for bringing in and taking out optical signals from the computing or switching environment. The positioning accuracies of the fibers in such arrays vary from one to ten micrometers (microns) depending on the systems' architecture. In this paper, we will present the opto-mechanical challenges that are presented during design and fabrication of 2-D fiber input array, and alignment and attachment of microlens arrays to fiber bundle.

2. 2-D Fiber Array

Fiber bundles are needed for inputting pulsed optical signals onto the free space optical fabric. Fiber bundles consist of fibers (typically 125±1 μm in diameter) spaced in a two dimensional array with known x and y spacing. The variation in the pitch of the fibers can range from 2 μm for single mode fiber arrays to 10 μm for multimode fiber arrays, depending on the system architecture and application. The x-y location of the light from the fiber depends on two factors: (1) the location of the fiber and (2) the concentricity of the fiber core. Another important parameter is the deviation from perpendicular of the fiber to the spacer. It is important that all beams emerging from the fibers propagate in the same direction colinear to the optic axis of the system fabric. Such system requirements translate into fabrication of precision mechanical elements.

Single-crystal silicon have long been used for locating fibers. Figure 1 shows preferentially etched grooves in silicon that have been used for splicing arrays of fiber.[4] [5] Very precise grooves can be etched in silicon by lithographically defining the groove patterns in photoresist and then etching them with a preferential chemical etch into silicon. This results in grooves with a trapezoidal cross-section. The groove width and depth can be fabricated to about 1 μm tolerance. For stacking these chips to form a two dimensional array, the silicon wafer needs two sided lithography and has to be etched from both sides. Although high dimensional accuracy between grooves can be realized, stacking the chips will require tolerances on the wafer thickness to be less than 1 μm. Maintaining this tight tolerance on wafer thickness is a very difficult task to achieve. Since the fibers lay in the grooves, the fiber angle and hence the emerging beam angle is controlled by the flatness of the silicon wafers.

An alternate way of building fiber bundles is by inserting fibers in substrate with precisely etched holes.[6] [7] [8] [9] Precisely located holes can be etched in a <100> silicon wafer.[10] As shown in Figure 2, the sides of the holes would be tapered because they would be defined by the <111> crystal planes. The sloping sides also limit the spacing between the fibers. As an example, for a .51 mm (20 mil) thick wafer, the minimum hole separation that can be obtained is ≈850 μm. Etching holes from both sides of the wafer reduces the minimum separation to half the above value. However, this method requires precise alignment of masks for the two sided lithography. The location of the fiber depends on location of the hole in the spacer and the clearance between the fiber and the hole.

Silicon with <110> orientation could be used for fabricating substrates with holes that have vertical walls.[11] This orientation silicon ends up with parallelogram shaped holes as shown in Figure 3.

Other types of substrate that are suitable for etching holes are photosensitive glass materials such as Fotoform® made by Corning Inc. and thin brass stock as shown in Figure 4. It can be seen that the brass gives a smoother etched surface compared to Fotoform material. Since the thickness of brass substrates is of the order of 100 μm, a backing substrate such as Fotoform® glass is needed to strengthen the structure.

Table 1 compares the tolerances on hole locations and their diameter. Depending on the system requirements and the type of fiber, either single mode or multimode fiber being used, one can choose the appropriate substrate.

TABLE 1

SPACER MATERIAL AND FABRICATION TOLERANCE

MATERIAL	HOLE SPACING TOLERANCE (μm)	HOLE SIZE TOLERANCE (μm)	APPLICATION
FOTOFORM® GLASS	±6	±5	MM Fiber
BRASS	±3	±3	SM/MM Fibers
SILICON	±0.5	±2	SM/MM Fibers

2.1 Basic Design

Figure 5 shows the concept for constructing a fiber array. Two substrates (in this case Fotoform® glass) are aligned, stacked one above the other using precision sapphire spheres and epoxy bonded. Stacking the substrates serves two purposes. First, it keeps the fibers in vertical position after insertion and second, a lead-in can be provided by tapering the back substrate for ease of insertion. The substrate shown in Figure 4 was used in this particular design. The fiber bundle was fabricated by inserting fibers through the holes in the stack, epoxying the fibers in place and polishing the ends.

It is obvious that forming large 2-D arrays by manually inserting fibers without damaging them can be tedious. Hence an assembly apparatus was developed for inserting 12 to 18 fibers at a time into substrates.

One of the main concerns in any fiber integrated component is the fiber breakage during fiber handling. Another concern when fabricating large fiber bundles is the development of cracks during polishing.

These problems can be somewhat overcome by using a modular approach—a manufacturable one—as shown in Figure 6.[12] Here, linear fiber arrays are precisely placed next to each other by plugging them into a cage to form a fiber array. The penalty one pays for using this approach is the distance between arrays, which is dictated by the thickness of individual arrays. The distance between the arrays is controlled to lithographic accuracies, using two etched silicon spacers. The fine adjustment of the orientation is controlled by incorporating a flexure spring within the cage. Figure 7 shows the alignment that can be realized in such a modular approach.

3. Alignment and Attachment of Microlens Array to Fiber Array

One of the key elements in stacked planar optics[13] is precisely aligned 2-D microlens arrays. These lenses are fabricated to photolithographic tolerances on planar wafers. Literature[14] shows its wide range of uses in different system architectures. In this section we will discuss some of the possible ways of *passively* aligning these microlenses to fiber arrays.

Since the Fotoform® and brass substrates shown in Figure 4 are fabricated using photolithography steps, it is conceivable to incorporate mechanical alignment features in these substrates. Figure 8 is a

photograph of a microlens array attached to a linear MM fiber array (MAC™) using a photochemically etched brass holder. Microlens to fiber alignment has been obtained by using the alignment pins as the guide for the brass holder. Figure 9 shows the concept of attaching microlens array onto a 2-D fiber array. Alignment microlenses, which were fabricated lithographically along with the microlens array, were used to attach the microlens array to a brass substrate holder. The holder in turn is aligned and attached to the fiber array using precision glass ball lenses. These ball lenses can be obtained with diameter tolerance held to ±1 micron. Figure 10 shows a photograph of a microlens array attached to a two dimensional fiber array.

4. Summary

We have presented the challenges involved in the design, fabrication and assembly of fiber arrays. Various 2D fiber arrays with different number of fibers have been fabricated and used in electro-optic system applications. Also, the precision part requirements and fabrication to meet system requirements such as aligning microlens arrays onto fiber bundle, have been illustrated.

Current work involves expanding the modular fiber array into a 4 x 72 matrix. The results of this array will be presented at the conference.

REFERENCES

1. McCormick, F.B. et al., 1990, "A Free Space Cascaded Optical Logic Demonstration," *Applications of Optical Engineering: Proceedings of OE/Midwest '90, Proceedings of the SPIE* , Vol 1396.
2. Novotny, R.A., Kerbis, E., Brubaker, J.L., Basavanhally, N., and Freund, J., 1991, "Two-dimensional Fiber Optical Data Link Using Self-electrooptic Effect Device Modulators and OEIC Detectors," *OSA Annual Meeting.*
3. Jahns, J., Lee, Y.H., and Jewell, J.L., 1990, "Optical Interconnects Using Microlasers and Planar Optics," *International Topical Meeting on Optical Computing, Proceedings of the SPIE* , vol 1359.
4. Schroeder, C.M., 1978, "Accurate Silicon Spacer Chips for an Optical Fiber Cable Connector," *Bell System Technical Journal,* 57, pp 91-97.
5. Miller, C.M., 1978, "Fiber Optic Array Splicing With Etched Silicon Chips," *Bell System Technical Journal,* 57 (1), pp 75-90.
6. Basavanhally, N.R., et al., 1992, "Optical Fiber Alignment Method," US Patent No. 5,135,590.
7. Basavanhally, N.R., et al., 1993, "Optical Fiber Alignment Apparatus Including Guiding and Securing Plates," US Patent No.5,185,846.
8. Basavanhally, N.R. and Watkins, L.S., 1992, "Opto-Mechanical Alignment and Assembly of 2D-Array Components," Proceedings of the ASME Winter Annual Meeting, EEP-Vol.2, PED-Vol.60.
9. Proudley. G.M., et al., 1994, "Fabrication of two-dimensional fiber optic arrays for an optical crossbar switch," Optical Engineering, Vol. 33, No. 2, pp 627-635.
10. Petersen, K.E., 1982, "Silicon as a Mechanical Material," *Proceedings of the IEEE,* Vol. 70, No. 5.
11. JPL Invention Report NPO-16562/6062., 1987, "Deep, Precise Etching in Semiconductors," *NASA Tech Brief,* Vol. 11, No. 3.
12. Basavanhally.N.R., "Optical Fiber Alignment Apparatus," US Patent Pending.
13. Iga, K., Oikawa, M., et al., 1982, "Stacked Planar Optics: An Application of the Planar Microlens," *Applied Optics,* Vol. 21, No. 19.
14. Oikawa, M., Nemoto, H., et al., 1991, "Light Coupling Characteristics of Planar Microlens," Miniature and Micro-Optics: Fabrication and System Applications, *SPIE,* Vol. 1544.

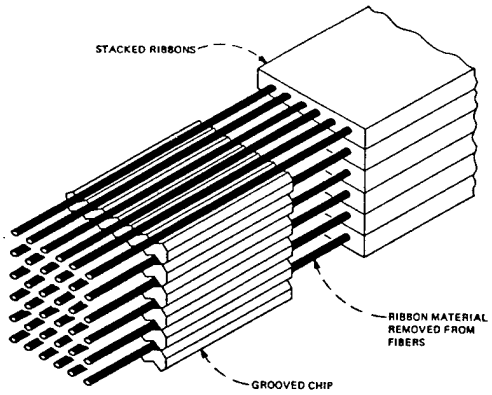

Figure 1: Stacking of Fiber Ribbons Using Silicon Alignment Chips
© 1978 AT&T. Reprinted with permission.

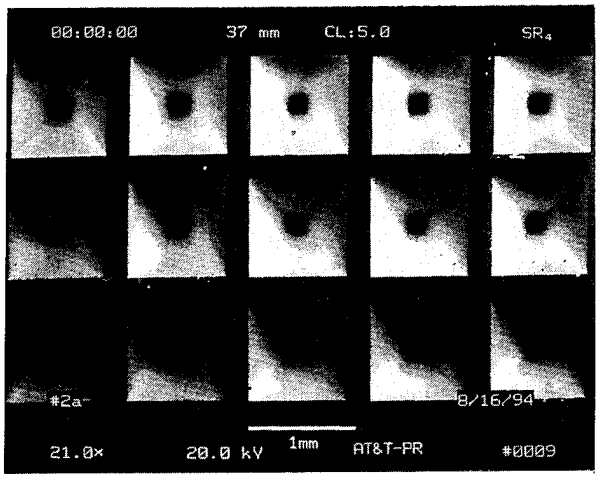

Figure 2: Etched Holes in <100> Silicon Substrate

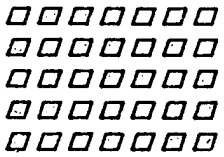

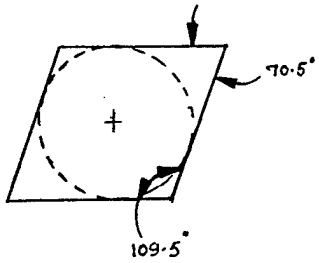

Figure 3: Schematic of Etched Holes in <110> Silicon

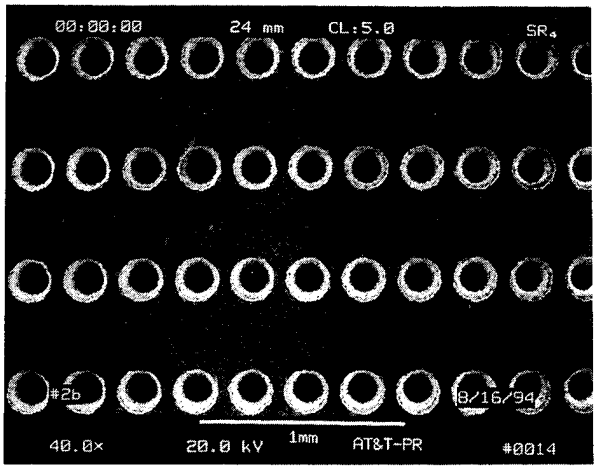

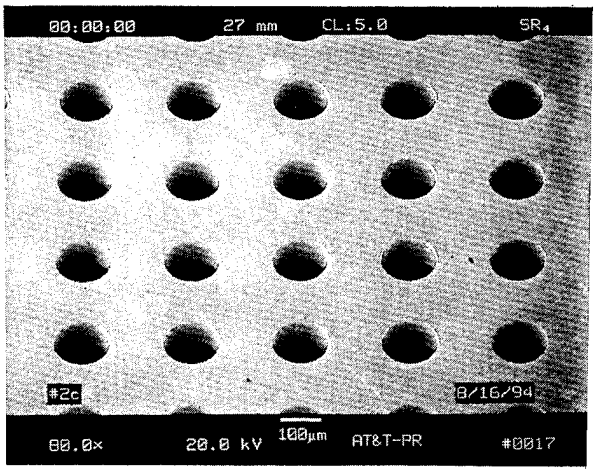

Figure 4: Etched Holes in Fotoform® and Brass Substrates

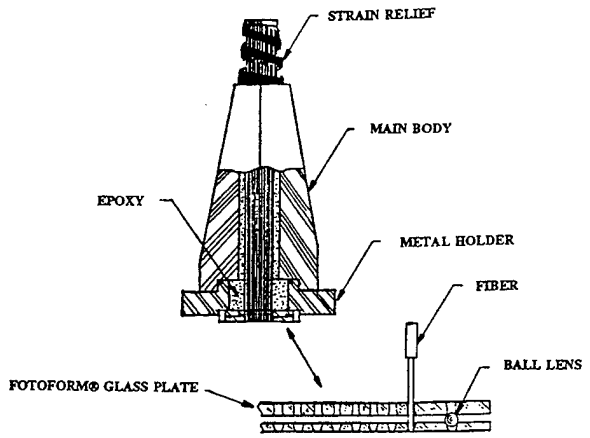

Figure 5: 2D-Fiber Bundle Design

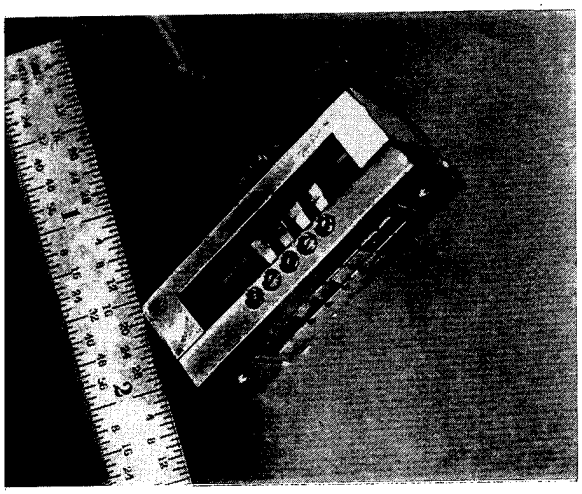

Figure 6: 2D-Fiber Bundle—a Modular Approach

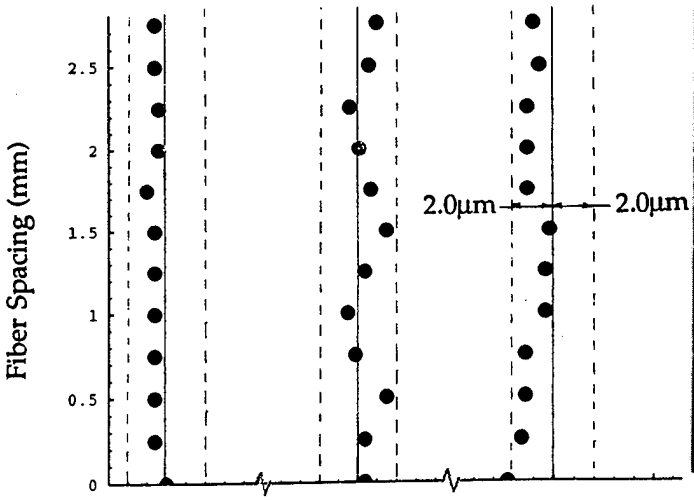

Figure 7: Typical Dimensional Accuracy of Modular Fiber Bundle

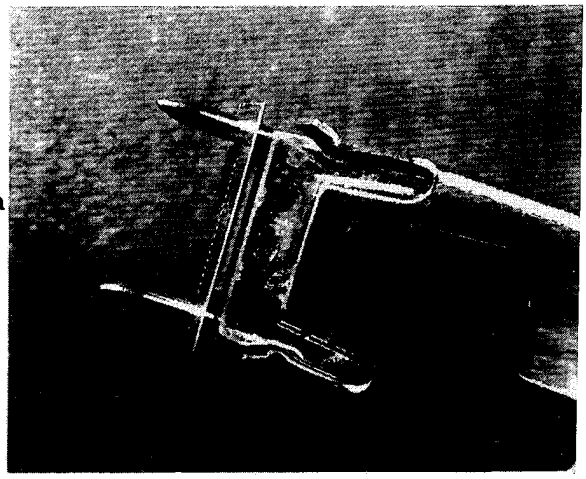

Figure 8: Microlens Array Attached to a Linear Fiber Array

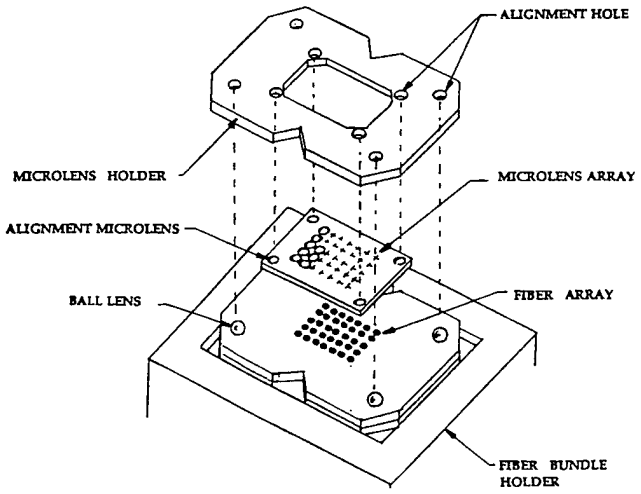

Figure 9: Schematic of Microlens Attachment on to a 2D-Fiber Bundle

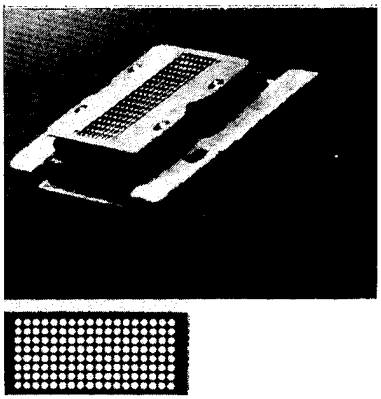

Figure 10: Photograph of Fiber Bundle with Microlens Attached

Optical Beam Routing through Time-Domain Spatial-Spectral Filtering

W. R. Babbitt
Department of Electrical Engineering, FT-10
University of Washington, Seattle, Washington 98195

T. W. Mossberg
Department of Physics, University of Oregon
Eugene, Oregon 97403
(503) 346-4779 [twmoss@oregon.uoregon.edu]

Recent years have seen the development of a variety of techniques for the storage and processing of optical data streams in materials with [1-10] and without [11-12] intrinsic frequency selectivity. These techniques are characterized by very high bandwidth and relatively large time-bandwidth product. It is known, that the optical processes responsible for the storage and/or processing of temporal waveform data frequently also lead to the storage of spatial waveform information [13,14]. It has been demonstrated, for example, that sequences of images can be stored.[5,7,8] An area that is relatively unexplored, however, relates to the possible interactions between stored temporal and spatial information. We explore one example of how the temporal and spatial information stored within a material can interact and lead to a novel functionality, i. e. the passive routing of optical beams along one of many possible temporally encoded directions.

Consider an active material that exhibits inhomogeneous absorption line broadening, and assume that the absorptivity of this material can be modified in proportion to the total energy fluence per unit volume and unit frequency to which it is exposed. The absorption modification may occur by any of the mechanisms that lead to persistent spectral holeburning [15]. Let the material's spectral resolution be denoted by $\Delta\upsilon_h$ and its total bandwidth by $\Delta\upsilon_i$. Suppose that the active material is exposed to two successive optical programming beams of finite duration, $E_1(\vec{r},t)$ and $E_2(\vec{r},t)$, which we denote according to their temporal order. We assume, for simplicity only, that these beams are plane waves which propagate in the respective directions $\hat{k}_1$ and $\hat{k}_2$. Thus, the electric field of beam ε ($\varepsilon = 1,2$) can be represented as

$$E_\varepsilon(\vec{r},t) = \int_{-\infty}^{\infty} E_\varepsilon(\nu)\exp\left[-2\pi i\nu(t-\vec{r}\cdot\hat{k}_\varepsilon/c)\right]d\nu, \qquad (1)$$

where $E_\epsilon(\nu)$ is the Fourier transform of beam ε at the origin ($E_\epsilon(0,t)$). The total optical energy fluence seen by the material as a function of spatial and spectral position is proportional to

$$|E_{tot}(\vec{r},\nu)|^2 = |E_1(\nu)|^2 + |E_2(\nu)|^2 + \left\{E_2(\nu)E_1^*(\nu)\exp\left[-2\pi i\nu\vec{r}\cdot(\hat{k}_2-\hat{k}_1)/c\right] + \text{c. c.}\right\}. \qquad (2)$$

The interference terms at the right of Eq. 2 contain detailed information on the spectral and spatial behavior of the electric fields of the two incident beams. In the simple plane wave case considered, the interference terms consist of relatively simple spatial gratings distributed in a potentially complex fashion in frequency space.

Suppose that material is illuminated after programming by a plane-wave data beam (beam 3) of unit wavevector $\hat{k}_3=\hat{k}_1$. By virtue of the spatial-spectral gratings created during programming, the material now acts as a spatial-spectral filter and deflects specific spatial-spectral components of the data beam in the direction $\hat{k}_2$. Assuming that the total time interval spanned by the two programming beams is considerably shorter than $\Delta\upsilon_h^{-1}$ and that the spectral bandwidths of all the beams are less than $\Delta\upsilon_i$, we can write the temporal and spatial structure of the deflected beam as

$$E_{def}(\vec{r},t) \propto \int_{-\infty}^{\infty} E_3(\nu)E_2(\nu)E_1^*(\nu)\exp\left[2\pi i\nu(t-\vec{r}\cdot\hat{k}_2/c)\right]. \qquad (3)$$

Equation (3) assumes that the intensity of the beams remains low enough so that the active material continues to respond

linearly. The temporal envelope of the deflected field may also be expressed as the convolution of the second programming beam with the cross-correlation of the first programming beam and the data beam. Since frequency-selective materials frequently have inhomogeneous absorption bandwidths in excess of 10 GHz, the correlators and convolvers based on these material possess similarly high bandwidths.[6]

Routing can be accomplished in the following manner. In the programming phase, the material is illuminated by multiple pairs of programming beams. The first beam of each pair propagates in the common direction $\hat{k}_1$ and has a unique routing address encoded onto its temporal waveform. The second beam in each pair propagates in a unique direction (say $\hat{k}_2^{(i)}$) along which correctly addressed data is to be routed. Temporally, this second programming beam consists of a simple short pulse. In the routing phase, a continuous data stream is made incident on the programmed material so that $\hat{k}_3=\hat{k}_1$. Whenever a temporal segment of the data stream reproduces the address of preprogrammed output channel (i), a pulse with the same temporal character as the second programming pulse is deflected into the direction associated with channel (i), i. e. $\hat{k}_2^{(i)}$. It follows that bits within the data stream can be routed into direction $\hat{k}_2^{(i)}$ by preconvolving them with the $\hat{k}_2^{(i)}$ address sequence. Data can be sent to any of the programmed directions by preconvolving it with the address corresponding to the desired direction.

A schematic depiction of the programming and routing process are shown in Figure 1. In part (a), a series of n pairs of programming pulses are made incident on a frequency-selective router material to write the spatial-spectral gratings necessary for routing. In part (b), a data stream having the succession of addresses shown in the top trace enters the router along the common programming direction. When the data stream contains the address A(i) (i = a,b,c), a pulse of light is generated in the direction $\hat{k}_2^{(i)}$ as shown in the lower three traces.

We have used Eq. 3 to simulate the light intensity as a function of time deflected into the three different output directions shown in Fig. 1b when using a specific set of address codes A(a), A(b), and A(c). The address codes, convolved data stream, and output signal intensities are shown in Fig. 2. The addresses used are 16-bit-long, random, binary-phase codes. They were used to simply demonstrate the routing effect and do *not* represent the optimal address codes. Nevertheless, crosstalk between the output channels is small. A variety of different addressing schemes are possible and may be in the form of amplitude, phase, and frequency modulation.

Up to now, we have discussed implementation of the router device using frequency-selective active materials. Following Eq. 2, it was pointed out that the programming material was recorded in the form of spatial-spectral gratings. Owing to the frequency-selectivity of volume holograms, this same information can be stored in frequency insensitive holographic materials, e. g. photorefractives. The ability of volume holographic materials to store temporal waveform information has been noted and subjected to limited demonstration.[12] The frequency-selectivity available in cm-scale storage materials (on the order of several gigahertz) is, however, much weaker than in the case of the cryogenic intrinsically frequency-selective materials (on the order of several kilohertz). This means that the address codes in the data stream must be very brief (less than ≈100 psec total duration for cm-scale gratings). This short timescale may, however, be entirely consistent with relatively near term optical transmission capability. The advantage of volume holographic implementation is of course the relative robustness and room temperature operation of the active material.

In summary, we have proposed using the frequency selectivity of both intrinsically frequency-selective materials and frequency-insensitive volume holographic materials to simultaneously perform the temporal and spatial processing required to passively route appropriately encoded data along chosen paths. The flexibility of the proposed router to accept phase, amplitude, and frequency encoded addresses enables a variety of implementation options. The high bandwidth capabilities of these frequency-selective materials (tens to thousands of gigahertz) enables full utilization of the bandwidth capabilities of fiber optics. We will discuss details of this method. We gratefully acknowledge support of the Air Force Office of Scientific Research under contracts F49620-92-J-0384 and F49620-93-1-0513.

1. T. W. Mossberg, Opt. Lett. **7**, 77 (1982); **17**. 535 (1992).
2. Y. S. Bai, W. R. Babbitt, N. W. Carlson, and T. W. Mossberg, Appl. Phys. Lett. **45**, 714 (1984). 3. Y. S. Bai, W. R. Babbitt, and T. W. Mossberg, Opt. Lett. **11**, 724 (1986).
4. M. Mitsunaga, R. Yano, and N. Uesugi, Opt. Lett. **16**, 1890 (1991).
5. B. Kohler, S. Bernet, A. Renn and U. P. Wild, Opt. Lett. **18**, 2144 (1993).

6. W. R. Babbitt and J. A. Bell, Appl. Opt. **33**, 1538 (1994).
7. M. Mitsunaga, N. Uesugi, H. Sasaki, and K. Karaki, Opt. Lett. **19**, 752 (1994).
8. X. A. Shen, E. Chiang and R. Kachru, Opt. Lett. **19,** 1246(1994).
9. P. Saari, R.Kaarli, and A. Rebane, J. Opt. Soc. Am. B **3**, 527 (1986); P. Saari, R. Kaarli, and M. Ratsep, J. of Luminescence B **56**, 175 (1993).
10. M. Mitsunaga, Opt. and Quantum Electronics **24**, 1137 (1992).
11. H. Y. S. Li and D. Psaltis, Appl. Opt. **33**, 3764 (1994) and references therein.
12. Yu. T. Mazurenko, Appl. Phys. B **50**, 101(1990).
13. N. W. Carlson, W. R. Babbitt, and T. W. Mossberg, Opt. Lett. **8**, 623 (1983).
14. M. K. Kim and R. Kachru, Opt. Lett. **12**, 593 (1987).
15. *Persistent Spectral Hole-Burning: Science and Applications,* W. E. Moerner, Ed., Springer-Verlag, New York (1988).
16. M. Zhu, W. R. Babbitt, and M. C. Jefferson, manuscript in preparation.

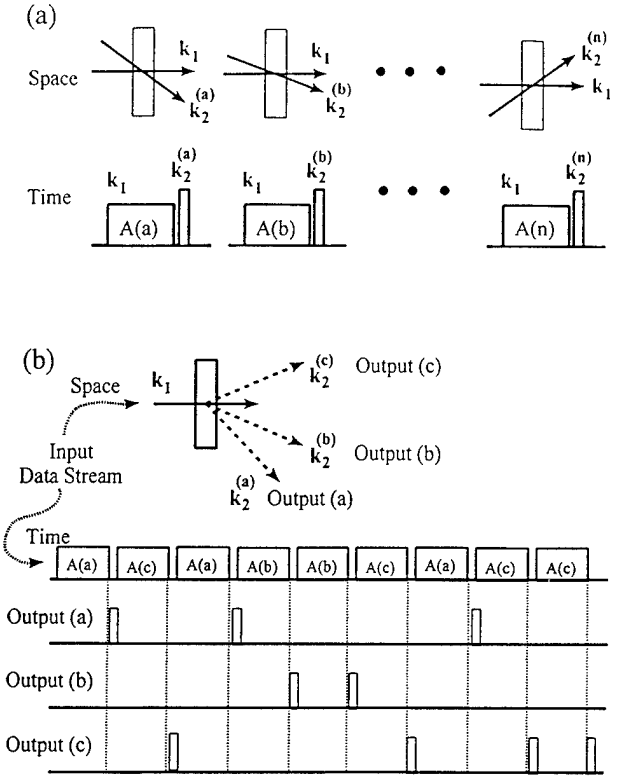

Figure 1

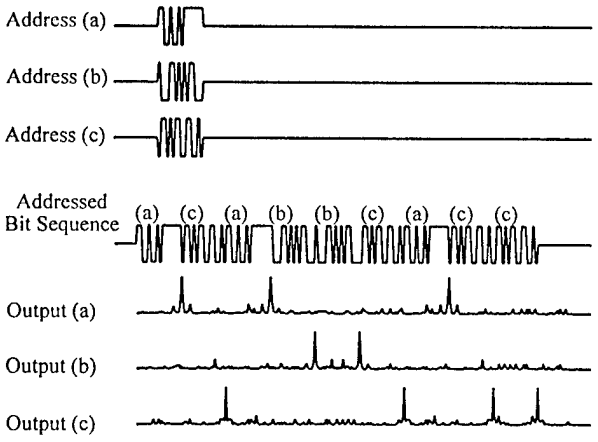

Figure 2

Figure 1. Router Method. (a) A frequency-selective router material is exposed to a series of n pairs of programming pulses. The programming pulses have the spatial orientations and temporal characteristics shown in the first and second rows, respectively. (b) A data stream is incident on the programmed router material and temporally addressed bits (first trace) are routed into the three output directions shown. Light intensity scattered into the three output directions is shown schematically in the bottom three traces.

Figure 2. Simulation of router performance with the data stream shown in Fig. 1b and the specific address codes shown in the top three traces. The last four traces duplicate the corresponding traces in Fig. 1b. Even with the unoptimized address codes chosen, crosstalk between the output channels is quite small.

Multi-functional Surface-Emitting Laser-Based Integrated Photonic/Optoelectronic Switch For Parallel High-Speed Optical Interconnects

Y. C. Lu, Julian Cheng
University of New Mexico, Center for High Technology Materials
EECE Building, Room 125, Albuquerque, NM 87131
J. C. Zolper, J. Klem
Sandia National Laboratories, Albuquerque, NM 87156

The monolithic integration of vertical-cavity surface-emitting lasers (VCSELs) with active electronic devices combines the optical source array and its driver circuits into a single IC technology, which is useful for parallel high-speed optical interconnects. Another motive for the integration of VCSELs with high speed electronics is to provide an optical switching network with a simple optoelectronic interface that allows individual electronic computer processors to communicate with each other through parallel optical channels. A dynamically reconfigurable optical switching network[1-2] can simultaneously route optical data between many different electronic processors as they perform parallel processing sequences using shared resources. Each switch of the network must provide an optical link to all the other nodes, as well as an optical $\Leftrightarrow$ electrical interface to an electronic processor. Each switch must thus perform both the optical and optoelectronic switching functions in order to convert data between various combinations of electrical and optical input/output (I/O) formats.

We describe a multi-functional optical/optoelectronic switch based on the monolithic integration of a novel, three-terminal AlGaAs/GaAs heterojunction bipolar phototransistor (HBPT) with a vertical-cavity surface-emitting laser(VCSEL), which can perform a variety of optical and optoelectronic switching functions. It can transform either optical or electrical input data into an optical or electrical output format at a data rate of 350 and 500 Mb/s, respectively. It also provides a convenient platform for combining electrical and optical input data packets into a common output format. This flexible switch can be used to construct a reconfigurable, three-dimensional switching fabric that optically interconnects electronic processors through parallel optical channels.[1-2] We will describe its design and performance, and experimentally demonstrate its multiple switching functions.

The switch consists of a VCSEL grown on an n-GaAs substrate, above which an HBPT with an emitter-up configuration is re-grown, separated by electrical isolation layers.[3] Figure 1 shows the layout and the functional circuit diagram of a single three-terminal HBPT/VCSEL switch in an emitter-follower configuration, which can be switched by either a surface-normal optical input P_{in} or by an electrical input E_{in} applied to the base of the HBT, producing both an optical output P_{out} and an electrical voltage modulation E_{out}. A dc bias is applied to the base to set the operating current and to pre-bias the VCSEL near threshold. In addition to performing optical switching, each switch node also provides an optoelectronic interface to an electronic processor, and can receive or transmit optical data as well as to perform O$\Leftrightarrow$E data conversion. In the experimental set-up shown in Fig. 2, P_{in} produces an amplified collector current I_c and a voltage modulation E_{out}. The former (I_c) modulates the VCSEL to produce a regenerated, optically-switched (O$\Rightarrow$O) output, which is transmitted to another switch node, while the latter (E_{out}) represents *optoelectronically-switched* (O$\Rightarrow$E) data, which is sent to the associated processor. Each processor can also transmit data to another node by modulating the base voltage

E_{in} (or base current I_b) of the HBPT to produce an amplified current I_c and a modulated voltage E_{out}.[4] The former modulates a VCSEL, whose *optoelctronically-switched* (E⇒O) output is transmitted to another switch node, while the latter *electrically-switched* (E⇒E) output is routed to another processor.

The multi-functional switching characteristics of the HBPT/VCSEL switch have been demonstrated using the experimental setup shown in Fig. 2, and the results are summarized in Fig. 3. The switching functions are demonstrated using different combinations of optical and electrical input data at 200 Mb/s. Two different data patterns modulate the optical and electrical inputs to the HPT during alternate, non-overlapping time intervals. The optical input data is incident on the base-collector junction of the HPT, while the electrical data directly modulates the base voltage. The switch converts these electrical and optical input data packets into switched optical and electrical outputs, and combines them into a single packetized data stream. The first two traces in Fig.3 show the modulated collector current I_c in the presence of *only* the electrical (trace 1) or optical (trace 2) input data, demonstrating the achievement of (*E⇒E*) and (*O⇒E*) switching. Traces 3 and 4 show the modulated electrical output (I_c) and optical output (P_{out}) when optical and electrical input data are both present. Each trace contains replicas of both the optical and electrical inputs. Trace 3 demonstrates electrical (*E⇒E*) switching and optoelectronic (*O⇒E*) data conversion, while trace 4 demonstrates optical (*O⇒O*) switching and optoelectronic (*E⇒O*) data conversion. The conversion of either electrical or optical data into both optical and electrical formats has been achieved at a data rate of up to 350 Mb/s for optical (O⇒O) switching and at >500 Mb/s for optoelectronic (E⇒O) conversion.

Figure 4 shows the small-signal, (a) electrical and (b) optical modulation response of the switch to a voltage modulation applied to the base. Figure 4(a) shows the forward transmission coefficient S_{21} and the current gain h_{21}, which show a unity-gain bandwidth of >500Mhz and a corresponding time constant of τ=0.32ns. Figure 4b shows the small-signal electrical-to-optical modulation response of the switch for different values of bias current I_c, which is a product of the transconductance of the emitter-follower circuit and the resonant light-current modulation response of the VCSEL. As the bias current I_c is increased, the resonance frequency increases and the modulation bandwidth saturates at ≈4GHz. Figure 5 shows the eye diagrams for the large-signal response of the current I_c and the optical output P_o of an HBPT/VCSEL switch under 500Mb/s pseudorandom data modulation. The upper and lower traces represent the modulated light output of the VCSEL (0.35 mW) and the modulated collector current I_c, respectively. The modulated electrical pulses have symmetrical rising and falling edges, with a 10%-90% transition time (~2.2τ) of 0.6ns. The modulated optical output has a rise time of 0.6ns and a longer fall time of 0.8ns. The wide-open eye pattern suggests that modulation at a higher data rate is possible.

REFERENCES:

[1] J.Cheng, SPIE Vol. 2155, Optoelectronic Signal Processing for Phased-Array Antennas IV, 1994.
[2] J. Cheng, P. Zhou, et.al., IEEE J. of Quantum Electronics, Vol. 29, pp.741-756, 1993.
[3] Bo Lu, J. Cheng, et. al., *IEEE Photonics Technology Letters*, Vol. 6, pp. 222-226, 1994.
[4] P. Zhou, J. Cheng, et.al., *IEEE Photonics Technology Letters*, Vol. 5, pp. 1035-1038, 1993.

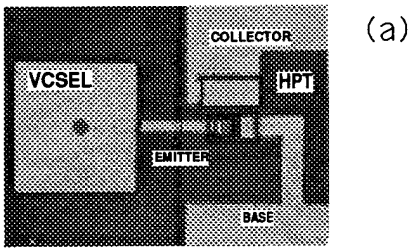

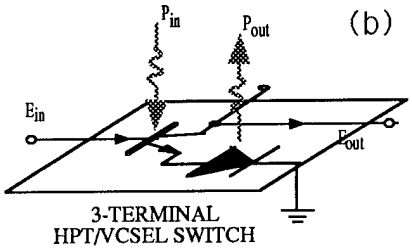

FIG. 1. (a) Layout, and (b) circuit of monolithic HPT/VCSEL switch, which has both optical and electrical inputs and outputs.

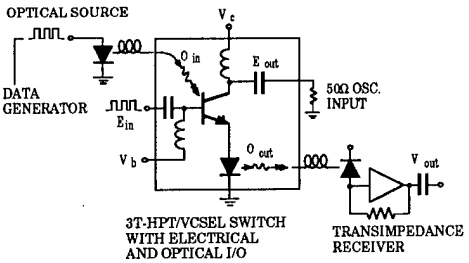

FIG. 2. Experimental set-up for the demonstration of optical and optoelectronic switching and data conversion using a monolithic HPT/VCSEL switch.

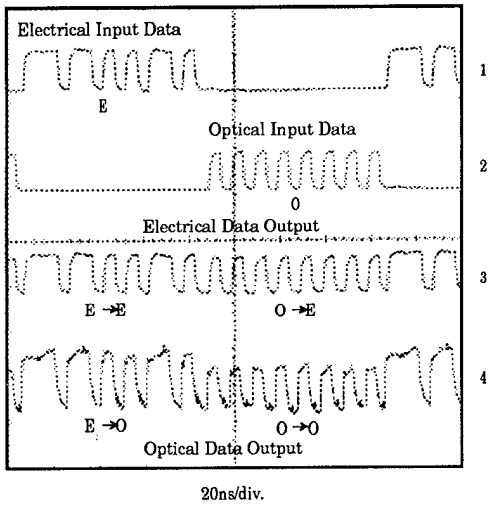

Fig. 3. Experimental demonstration of the switching and multiplexing of input electrical and optical data packets, and their conversion into a single optical or electrical output data stream at 200 Mb/s.

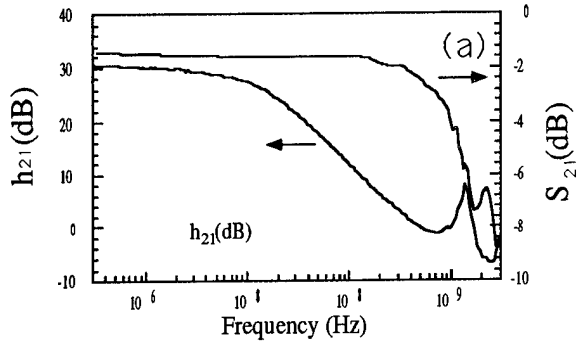

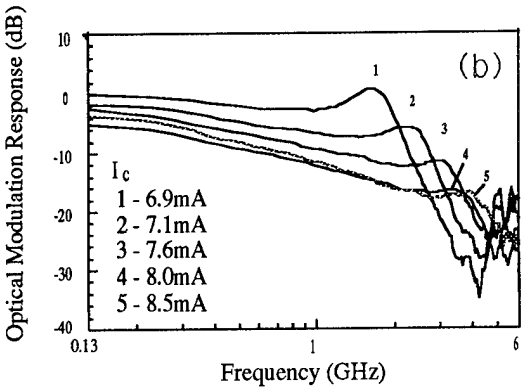

Fig. 4. (a) The small-signal electrical modulation response of the switch, as measured by the current gain h21 and the forward transconductance S21. (b) The small-signal relative optical response of the switch under electrical input modulation.

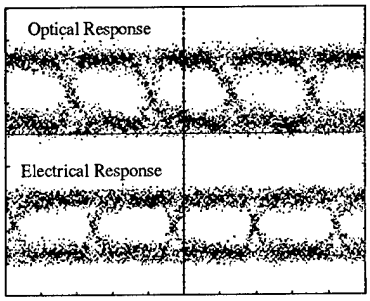

Fig. 5. Eye diagrams showing the modulated optical and electrical response of the HPT/VCSEL switch under large-signal, pseudorandom data modulation at 500 Mb/s.

High-Speed 2-D CMOS Designs of Bypass-and-Exchange Switch Arrays for Free-Space Optoelectronic MINs

Osman Kibar, Philippe J. Marchand, and Sadik C. Esener
University of California, San Diego
Department of Electrical and Computer Engineering
La Jolla, California 92093-0407

In a free-space optoelectronic multistage interconnection network, electronic bypass-and-exchange switches are required to do the local routing. It has been shown that for a MIN with N inputs and outputs, the bandwidth and the power consumption are optimized if the electronic switch planes are partitioned into $\sqrt{N}$ switches [1]. Thus, each switch has $\sqrt{N}$ inputs and $\sqrt{N}$ outputs and is defined as $\sqrt{N} \times \sqrt{N}$ switch. Two separate circuits, that use an optimized 2-D layout and are compatible with the Optical Transpose Interconnection System (OTIS) have been designed and analyzed. The first design (design A) was used as a proof of concept for the optimized 2-D layout, the second design (design B) is a bi-directional self-routing concept that uses 3 level logic.

In both cases, the building block for a fully connected switch ($\sqrt{N}$ inputs to $\sqrt{N}$ outputs) is a half-switch, which can route one of two input channels to a single output channel. This enables the half-switch to detect contention if necessary, compared to routing a single input channel to one of two output channels. Half-switches are paired to provide the equivalent functionality of a 2x2 bypass-and-exchange switch. A fully connected switch with $\sqrt{N}$ inputs and $\sqrt{N}$ outputs requires (#half-switches in a stage x #stages) = $\sqrt{N}$ x log($\sqrt{N}$) half-switches. For example, a 16x16 switch requires log(16)x16=64 half-switches. To build the fully connected switch, the half-switches are connected together following a shuffle topology, as illustrated in Figure 1. To achieve the 2-D layout, same numbered half-switches in each stage of the shuffle are grouped together, with each half-switch having the same number and length of global wires connected to it. The 2-D layout of a 16x16 switch and its equivalence to the shuffle topology is given in Figure 2 [2].

Such a switch implementation has several advantages, independent of the actual design of the half-switch. The operation is bi-directional with the direction determined by an external control signal. Thus, each triangular symbol on the 2-D layout (Figure 2) represents a modulator/detector pair. High speed performance can be achieved (i.e. up to 250Mbits/s) due to the highly pipelined structure of the switches. Performance is only limited by the propagation delay of a single half-switch. The switch is scalable both in terms of speed and global wiring complexity. As the number of inputs ($\sqrt{N}$) to the switch increases, the number of half-switches ($\sqrt{N}$ x log($\sqrt{N}$) increases even faster. However, due to its pipelined structure, the speed of the overall switch stays constant. In addition to these advantages in terms of performance, the design is modular so that various half-switch designs can be utilized to build a fully connected switch.

Design A demonstrates the full connectivity, scalability, and high speed performance of the 2-D design. This is important since the overall optoelectronic system is often limited, in terms of speed, by the electronic switches. Each half-switch has one direction (dir), one control (c), and four I/O (x0,x1,y0,y1) signals. The direction and control bits are fed externally. The direction bit determines which one of the two I/O signals are the inputs, and which one is the output (for example, dir=1 --> x0, x1 are the inputs, y0 is the output, and y1 is floating). The control bit determines which input will be routed to the output (for example, c=0 --> x0 is routed to y0, c=1 --> x1 is routed to y0, and y1 is idle in both cases). The complete truth table and the block diagram of the half-switch is provided in Figure 3. Every half-switch in the same stage gets the same control bit. In this test design, the total number of independent control bits is only four in a 16x16 switch so we can only control the output destination of one of the inputs. The other 15 inputs are mapped in a one-to-one fashion to the remaining 15 outputs. The control bit at every stage is delayed by the total propagation delay of the previous stages. Thus, for an individual half-switch, the data bit and the control bit arrive at the same time. Thus, the throughput of the half-switch and

that of the whole switch is only limited by the actual delay of a single half-switch, independent of the number of the switch size. The necessary control bits to map a given input to a given output are determined as follows: a bitwise XOR is performed between the input and the output addresses. Then, to match the 2-D layout requirements, a cyclic shift to the right is performed on the result.

For a 2.0μm CMOS technology, a half-switch was implemented with 24 transistors, occupying an area of about (170x100) μm^2. Every four half-switches occupy, including their share of the global wires, and the input/output pads, about (440x250)μm^2. The propagation delay of a single half-switch was 4ns, including a 1ns rise/fall time, and a 3ns stable period, giving the whole switch a speed of 250Mbits/s. Based on the parameters of our test chip, the total power consumption per switch-plane (i.e. $\sqrt{N}$ switches with a total of N PEs) is given as:

$$P = \sqrt{N} f \left\{ \left[8.25\sqrt{N}\left(N^{\frac{1}{4}} - 1\right)\lambda p(c=1)p(d) \right] + \sqrt{N}\log\sqrt{N}\left[\left(2.47\lambda^2 + 0.15\lambda\right)\frac{p(c)}{d} + \left(4.02\lambda^2 + 0.24\lambda\right)p(d) \right] \right\} \mu W$$

where f is the operating frequency in MHz, λ is the technology parameter in μm, p(c=1) is the probability of the control bit being 1, p(d) is the probability of the data bit switching, p(c) is the probability of the control bit switching, and d is the number of bits per data set. As an example, for N=256, $\sqrt{N}$=16, f=100MHz, λ=1 μm for 2 μm CMOS technology, and d=16, $P_{average}$ = 0.39W, and $P_{worst\ case}$ = 1.07W.

Design B is a scaled-up version of Design A, in the sense that it allows self-routing. The additional signals are defined in Figure 5. The switch works as follows: each data packet is preceded by a header, which contains the address of its output destination. Each half-switch receives an external signal (the transmission signal, t) at the right time to know that the incoming two inputs are the control bits. If both sets of data want to use the same output channel of that half-switch, one of them is dropped in a deterministic way, and the other one is routed on, just like design A (c0 and c1 are computed as shown in Figure 6a). While the transmitted packet propagates forward, a signal (contention bit, s, which corresponds to the dropped packet) starts propagating in the opposite direction, tracing back the path that the dropped packet had followed until that point, and tells the input buffer to resend the same data packet. If neither packet wants to use that output channel (i.e. both of them want to use the output channel of its partner half-switch), then the output is set to an intermediate voltage of about 2-3 V (i.e. the third logic level) during the following cycle (schematics in Figure 6b). During this cycle, the next stage computes its own control bits. If it sees 2-3V as one of the inputs, it sets its control bit to route the other input channel. The third logic level eliminates the necessity of an extra global connection between each stage, improving the speed performance and the power consumption of the switch.

Design B has the advantage of self-routing capability, where the control bits are determined from the content of the header of the data packet that needs to be transmitted. Each data packet is allowed to have its independent output destination, which naturally lends itself to contention. However, the switch is designed so that it can detect contention, and can resend a dropped data packet so that any loss of information is avoided. At this point, a 16x16 switch with design A has been fabricated in order to prove the feasibility of the 2-D layout and its high-speed performance. Within the next three months, test structures for design B (i.e. contention detection, and the three-level logic) will be fabricated, and the test results will be reported for both switch designs.

References:

[1] A. Krishnamoorthy, P. Marchand, F. Kiamilev, K. S. Urquhart, S. Esener, and S. H. Lee, "Grain-size study for a 2-D shuffle-exchange optoelectronic multistage interconnection network," *Applied Optics* **31**, 5480-5507, September 1992.

[2] A. Krishnamoorthy, P. Marchand, F. Kiamilev, and S. C. Esener, "Grain-size considerations for optoelectronic multistage interconnection networks", *Applied Optics* **31**, No:26, September 1992.

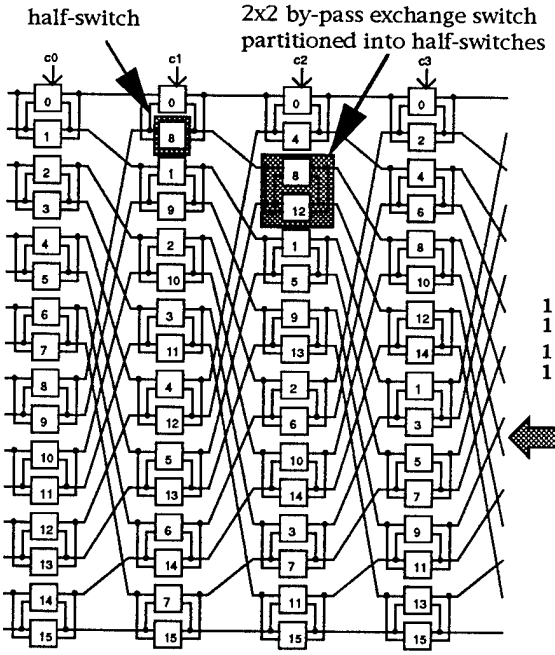

Figure 1: Block diagram of a 16x16 switch

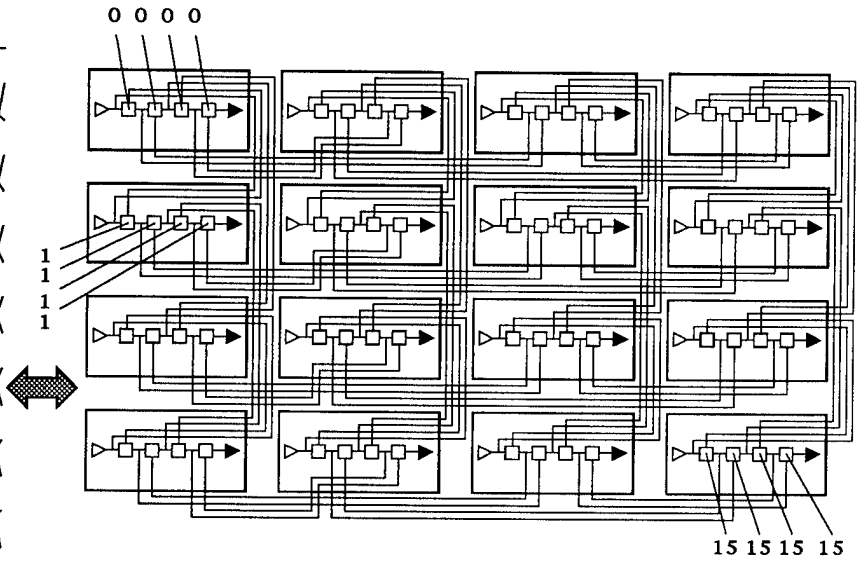

Figure 2: 2D layout of a 16x16 switch

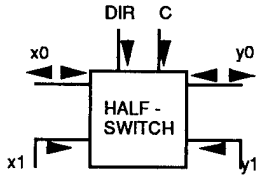

Direction	Control	Inputs	Outputs
0	0	y0&y1	x0=y0
0	1	y0&y1	x0=y1
1	0	x0&x1	y0=x0
1	1	x0&x1	y0=x1

Figure 3: Block diagram and truth table of a half-switch with design A

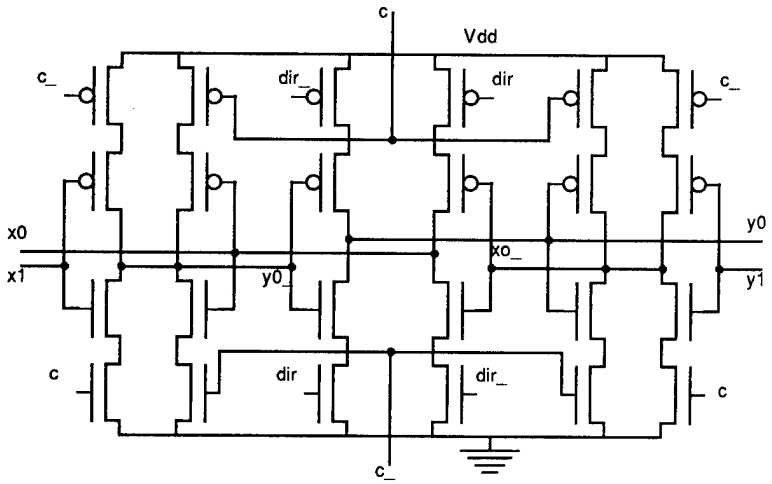

Figure 4: Schematics of a half-switch with design A

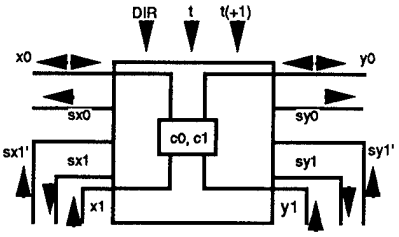

DIR : direction
t : transmission(=1 if the inputs are data bits, and =0 if they are address bits
t(+1) : t delayed by one cycle (i.e. t=0 inthe 1st cycle, t(+1)=0 in the 2nd cycle)
s : contention bit (=1 if the corresponding set of data has been dropped due to contention
c0 : corresponds to "c" of design A
c1 : =1 if c0 is a don't care (i.e. that channel is idle

Figure 5: Block diagram of a half-switch with design B and the additional signals

t=0,dir=1:

xo	x1	c0	c1
0	0	0	0
0	--	0	0
0	1	0	0
--	0	X	1
--	--	X	1
--	1	1	0
1	0	X	1
1	--	X	1
1	1	1	0

X : DON'T CARE
-- : BETWEEN 2-3 VOLTS
(i.e. the 3rd logic level)

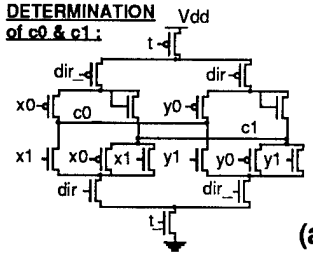

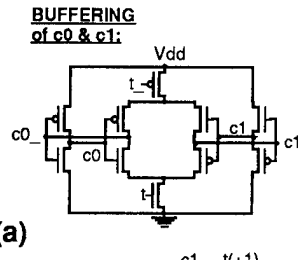

t(+1)=0, dir=1, c0=0 :

c1	x0	y0
0	0	0
0	1	1
1	X	--

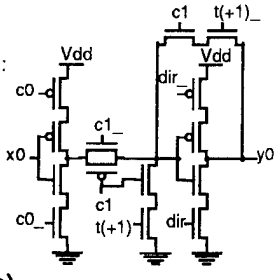

Figure 6: Schematics of a half-switch with design B. The control bit determination and its buffering (a), the addition to design A in output determination (b)

Gigabit per second switching of smart pixel receiver-transmitter pairs

G. Livescu, L.M.F. Chirovsky and T. Mullally
AT&T Bell Laboratories, Murray Hill, NJ 07974

Arza Ron
Department of Chemistry and Solid State Institute, Technion, Haifa, Israel

Smart pixels are opto-electronic circuits with optical input/output and electronic logic circuits for complex functionality [1]. Arrays of smart pixels can control two dimensional arrays of light beams in high speed, high throughput free space photonic switching systems [2]. An example are the 4x4 arrays of 2x1 embedded control routing nodes, based on GaAs/AlGaAs field-effect-transistor self-electrooptic-effect device (FET-SEED) technology [3], recently used in a five stage switching system [4]. Although this system was operated at 155Mbit/s only, the speeds of smart pixels can be made much higher. One way to achieve increased speeds is by addition of gain stages and the use of larger FETs. However, this makes the receivers and transmitters larger and more dissipative. Another way to increase the switching speed is to use short pulses as optical inputs, which, according to theory [5], considerably reduces the switching time of the receivers. Simple receivers have, indeed, been demonstrated to operate up to 1Gbit/s [6], but receiver-transmitter pairs could only operate up to 650Mbit/s [7]. The speed of the pair was limited by the performance of the transmitter used, which consisted of a FET inverter driving the common node of two modulators connected in series. One can make a faster transmitter by eliminating the load FET and one of the modulators, thus reducing the capacitance and increasing the effective charging current of the modulator. With such a transmitter, and the use of mode-locked pulses in the AROEBICS (Asynchronous Reset On Every Bit for Input Contentionless Switching) method [8], 200ps switching times were recently obtained [9,10]. This result indicated that smart pixels containing this transmitter should be capable of operating in the GHz range. In the present work we use trains of mode-locked laser pulses separated by 1ns to demonstrate the 1GHz operation of a receiver-transmitter pair.

For this first demonstration we used the simplest receiver-transmitter pair which can be operated by the AROEBICS procedure, the Pulsed OptoElectronic Toggle (POET) circuit, described in Fig.1(a). Its fabrication was described in earlier work [11]. The receiver consists of two reverse-biased GaAs/AlGaAs

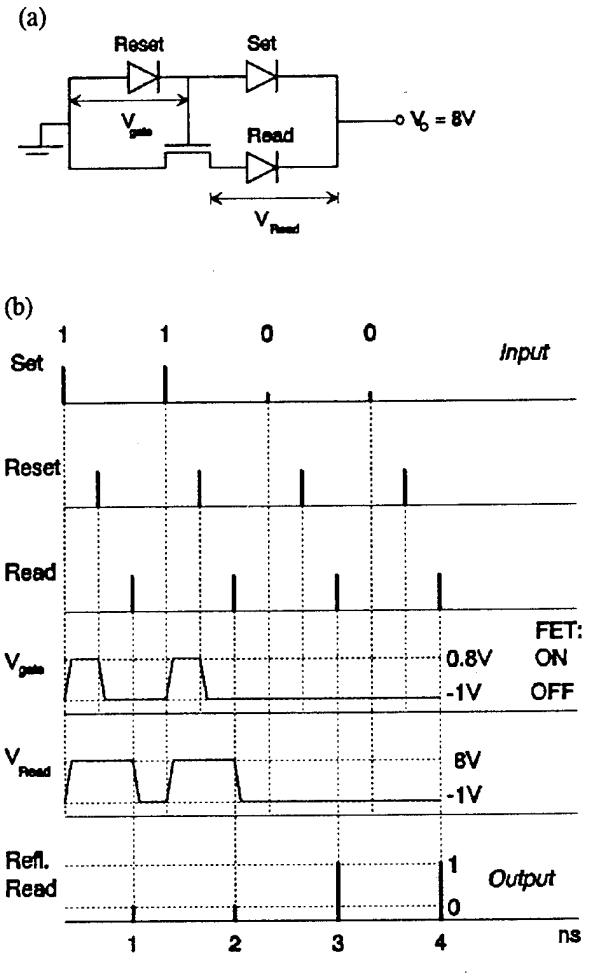

Fig.1. (a) POET circuit schematic. (b) Input and output pulse sequence.

quantum well detector diodes, Set and Reset, onto which the two input beams are incident. The transmitter consists of the Read quantum well modulator diode, reverse biased through a FET, whose gate is controlled by the receivers. The output beam is reflected off the Read diode, which is operated at a wavelength at which it acts as a "normally ON" modulator: its reflectivity is high when the voltage drop on it is zero.

The pulsed operation of the POET circuit was discussed in detail in [9,10] and is schematically described in Fig.1(b). The pulse sequence shown here illustrates the essence of the AROEBICS method, in which the input and output pulses arrive at different times. The input Set and Reset pulses control the gate voltage V_{gate}, thus the state of the FET. The Read pulse, reflected off the Read modulator, generates the output signal at the detector. A high Set or a "1" produces an increase in V_{gate}, which makes the FET conducting. As a result, the voltage drop on the output Read diode V_{read} increases, the quantum well modulator becomes absorbing and its reflectivity decreases: it is being turned "OFF". Thus a high Set or a *"1" input* produces a low Read or a *"0" output*, and vice versa. This output is "read" by the Read beam, which arrives later. In addition to being reflected off the Read diode and generating the output signal at time 1, the Read pulse also produces the photocurrent necessary to discharge the Read diode and return it to its original state. In order to also bring the FET back to its original state, ready for the next data carrying Set pulse, a constant intensity Reset pulse follows every Set pulse. As illustrated in Fig.1(b), the Reset pulse must arrive before the Read pulse, because the FET must be insulating for the Read diode to be discharged. This will not, however, affect the accuracy of the output: the Read pulse first "reads" the state, and then changes it.

This method thus allows modulation of the output with digital data encoded in the Set pulses alone, with interleaved constant amplitude Reset pulse. From our previous work on the pulsed operation of the POET circuit [9,10] we know that the switching times can be made as short as 200ps for the slowest of the transitions, the switching OFF, and shorter than that for the switching ON. This indicates that a

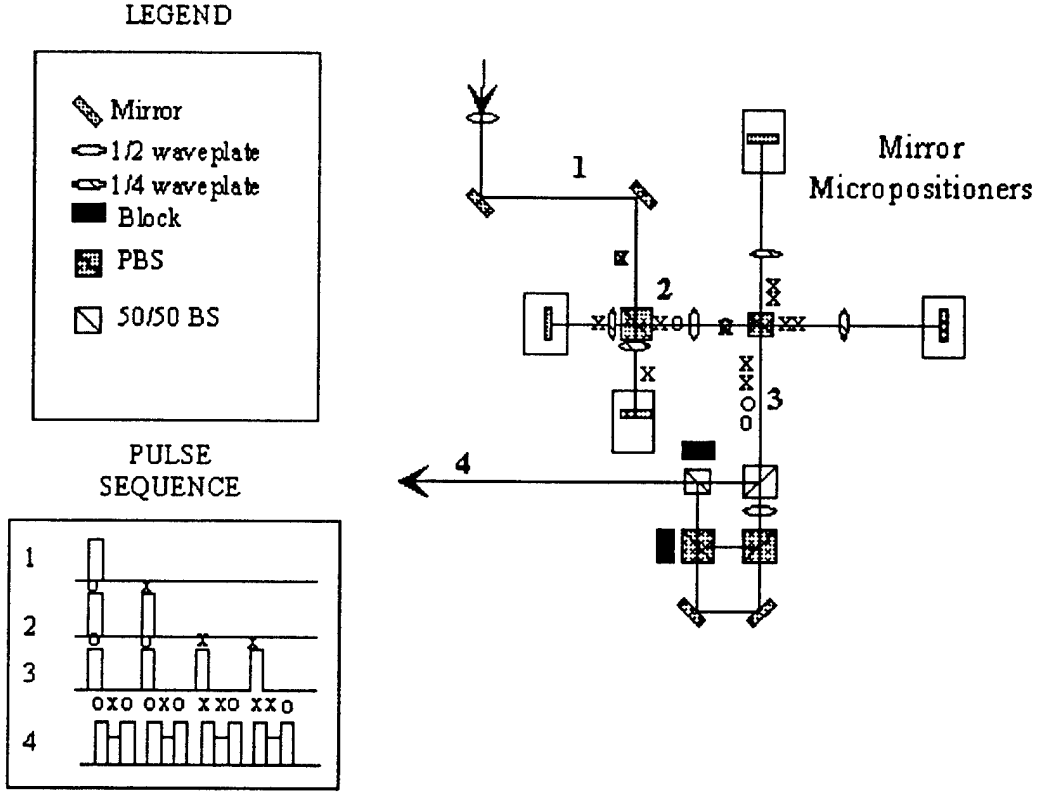

Fig.2. Split and delay scheme used to produce a train of four pulses 1ns apart (beam 3) from each pulse generated by the mode-locked Ti:sapphire laser (beam 1). Each of the four pulses is further split into three: Set, Reset and Read (beam 4).

data pattern at 1GHz can be transmitted.

In order to generate the optical inputs and outputs, we use 1.5ps pulses from a commercial mode-locked Ti:sapphire laser, whose repetition rate is 82MHz. By means of a split-and-delay technique, a train of four pulses 1ns apart is generated for every pulse emitted by the laser, simulating a 1GHz rate (Fig.2). Each of the four pulses is subsequently split into three beams: the Set, followed by the Reset 300ps later, and by the Read, 700ps later. They are then focused to 3um spots and incident on the 10um x 10um windows of their respective diodes. The reflected Read is detected with an amplified fast detector, and the detected signal is accumulated and averaged with a digital scope.

An input pattern can be created by exploiting the fact that the different pulses have different polarizations (the device is polarization independent). Note that the first two Set pulses have polarizations which are orthogonal to the last two. Therefore, by using a polarizer, one can either allow the first two Set pulses to arrive to the sample, to generate the 1100 pattern, or the last two, generating the 0011 pattern. Without a polarizer, all four pulses arrive to the sample, which corresponds to the 1111 pattern. The 0000 pattern corresponds to the absence of the Set beam. All four Reset and Read beams must be present for all the above patterns.

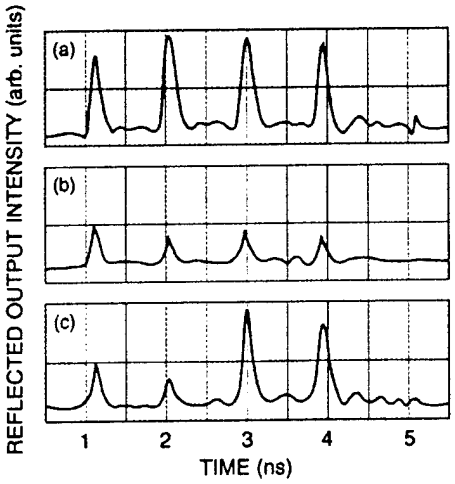

Fig. 3. Measured output patterns, for following input patterns: (a) 0000 (b) 1111 (c) 1100.

An example of the transmitted patterns is shown in Fig.3: (a) corresponds to an input pattern of 0000, (b) to 1111, and (c) to 1100. Note that the output is complementary to the input. Note also the excellent contrast ratio, which was obtained because we used Fabry-Perot modulators [9]. The operating wavelength was 862nm, chosen such as to correspond to the reflection minimum at V_0=8.3V. The pulse energies were 200fJ for the Set, and 1pJ for the Reset and Read, consistent with those reported previously [9,10]. More experiments are being carried out on various receiver transmitter-pairs, with more sophisticated receivers for lower switching energies.

We wish to thank L.A. D'Asaro, S. Hui and B. Tseng for fabrication of the smart pixels, and to R. Leibenguth, for growth of the GaAs/AlGaAs structure.

References

1 A.L. Lentine and D.A.B. Miller, IEEE J. Quantum Electron. **29**, 655 (1993).

2 H.S. Hinton, "An Introduction to Photonic Switching Fabrics" (Plenum, New York, 1993).

3 A.L. Lentine et al., IEEE Photon. Techn. Lett. **6**, 1126 (1994).

4 F.B. McCormick et al, Appl. Opt. **33**, 1601 (1994).

5 A.L. Lentine, L.M.F. Chirovsky and T.K. Woodward, IEEE J. Quantum Electron. **30**, 1167 (1994)

6 T.K. Woodward, A.L. Lentine and L.M.F. Chirovsky, Paper OS1.2, 7th Annual LEOS Meeting, Boston, MA, Oct.31-Nov.3, 1994.

7 T.K. Woodward, A.L. Lentine and L.M.F. Chirovsky, IEEE J. Quantum Electron. **30**, 2319 (1994).

8 L.M.F. Chirovsky et al., Paper M3.2, LEOS Summer Topical Meeting on Smart Pixels, Lake Tahoe, NV, July 11-13, 1994.

9 G. Livescu, G.D. Boyd, L.M.F. Chirovsky, R.A. Morgan and T. Mullally, Opt. Lett. **19**, Dec.15, 1994

10 G. D. Boyd, G. Livescu, L.M.F. Chirovsky and A.L. Lentine, Appl. Phys. Lett. **65**, Dec.12, 1994.

11 L. A. D'Asaro et al., IEEE J. Quantum Electron. **29**, 670 (1993).

Distributed Forward- and Backward-Coupling Laser
– Novel Laser Diode for Wide Wavelength Tuning –

Kenji Sato, Yoshiaki Nakano, and Kunio Tada

Department of Electronic Engineering, University of Tokyo
7-3-1 Hongo, Bunkyo-ku, Tokyo, 113, Japan
Phone: +81-3-3812-2111 ext. 6777, Facsimile: +81-3-5802-3313

I. INTRODUCTION

Wavelength tunable lasers are required in the wavelength-division-multiplexed (WDM) photonic switching networks. Over the past several years, both continuously [1] and discontinuously [2-4] tunable lasers have been intensively studied. The latter ones are more feasible when over 20 nm tuning ranges are demanded.

Recently, Amann and coworkers proposed the distributed forward coupled (DFC) laser [5] that is able to provide wide range discontinuous tuning. It is based on the codirectional mode coupling along the laser cavity in a twin-guide structure. One of its main advantages is an unambiguous and simple wavelength tuning which is achieved by only one control current.

In this paper, we propose another type of discontinuously-tunable lasers, that is, distributed forward- and backward-coupling (DFBC) laser. Here, the main mode is selected out of distributed feedback (DFB) modes rather than the Fabry-Perot modes in DFC lasers. Therefore, larger side mode suppression ratio (SMSR) as well as wide range tuning of the discontinuously-tunable lasers are expected.

II. DEVICE STRUCTURE

Figure 1 shows a schematic longitudinal cross section of the DFBC laser, which is basically a DFB laser diode incorporated with a sampled Bragg grating above the active layer and a codirectionally-coupled waveguide layer below the active layer. The whole waveguide is designed so as to hold the fundamental (odd) and second-order (even) transverse eigen modes.

When the light propagates across the border between the sections with and without the grating, the forward coupling occurs among the odd and even transverse modes in both sections. The coupling coefficient should be designed to be relatively large so that the light (the sum of the odd and even modes) may propagate zigzag with a short period between the two layers.

If the coupling period corresponding to a certain wavelength is equivalent to the sampling interval of the grating, the light is fed back most by the grating. This coupling period is very sensitive to change in the refractive index of the codirectional waveguide layer that can be induced by current injection into that layer. Small index change can give rise to a large change in the wavelength selected by the codirectional coupling and the sampled grating.

Actually, the above tunable filtering mechanism picks up one lasing mode out of a series of DFB modes produced by the grating sampling. The "channel" interval, i.e., the DFB mode spacing, is controllable through the sampling interval of the grating.

III. THEORY

We introduce envelope complex amplitudes, R's, as functions of z-coordinate along the laser cavity, which are related to the complex electrical field amplitudes, E's, as

$$E^{\pm}(x,y,z) = R_1^{\pm}(z)\varphi_1(x,y)e^{\mp j\beta_1 z} + R_2^{\pm}(z)\varphi_2(x,y)e^{\mp j\beta_2 z} \quad (1).$$

Here, the superscripts + and - indicate forward and backward waves, φ_1 and φ_2 are the transverse eigen modes of the waveguide, and the subscripts 1 and 2 denotes the odd and even modes, respectively. β_1 and β_2 are the propagation constants of the modes 1 and 2.

A 4 × 4 F-matrix, F, for the grating and nongrating section pair from $z=z_k$ to $z=z_{k+1}$ in Fig. 1 relates R's at both ends by Eq. 2, and F itself is expressed by Eq. 3:

$$\begin{pmatrix} R_1^+(z_{k+1}) \\ R_1^-(z_{k+1}) \\ R_2^+(z_{k+1}) \\ R_2^-(z_{k+1}) \end{pmatrix} = F \begin{pmatrix} R_1^+(z_k) \\ R_1^-(z_k) \\ R_2^+(z_k) \\ R_2^-(z_k) \end{pmatrix} \quad (2), \qquad F = T_{ng} F_n T_{gn} F_g \quad (3).$$

Symbols "g" and "n" denote the sections with and without grating, respectively. T_{gn} and T_{ng} are the transfer matrices at the section border, and F_g and F_n are the F-matrices for each section. They are explicitly written as

$$T_{gn} = \begin{pmatrix} a_{11} & 0 & a_{21} & 0 \\ 0 & a_{11} & 0 & a_{12} \\ a_{12} & 0 & a_{22} & 0 \\ 0 & a_{21} & 0 & a_{22} \end{pmatrix}, \qquad F_g = \begin{pmatrix} F_{1g} & \mathbf{0} \\ \mathbf{0} & F_{2g} \end{pmatrix} \quad (4),$$

where a_{ij} is the expansion coefficient from Ref. 6. F_{1g} and F_{2g} are the DFB 2 × 2 F-matrices [7] of the modes 1 and 2. T_{ng} and F_n can be expressed in similar forms.

Like the ordinary lasers [7], the resonance condition is satisfied when the absolute value of the complex round trip gain becomes 1 and its phase becomes 0. The round trip gain can be calculated by making use of the above F-matrix for the grating-nongrating pair.

IV. SIMULATION

Simulation has been carried out around 1.55 μm wavelength. Assumed thickness of each layer is shown in Fig.1. The refractive index of the active layer, n_{active}, is fixed at 3.41 whereas the refractive index of the codirectional tuning waveguide, n_{guide}, is taken as a variable parameter. It is varied from 3.380 to 3.386 in this calculation. This index variation is obtainable through carrier injection into the tuning waveguide.

The distributed feedback here is assumed to be of pure gain coupling [8] with a coupling coefficient of 20 cm^{-1} for mode 1 and 40cm^{-1} for mode 2. The length of the grating section is 12.8 μm, and that of the nongrating section is 101 μm. Therefore, the sampling interval of the grating is 113.8 μm, and its duty cycle is 11.2 %. We assume antireflection (AR)-coated devices with cavity length of 1365.6 μm (twelve periods of the grating-nongrating pair).

Figures 2 (a) and (b) show calculated amplitudes of the round trip gain versus wavelength at two different refractive index values of the tuning waveguide. The spikes in these figures correspond to sampled DFB modes. The envelope on the spikes is mainly due to the codirectional forward coupling effect. The modes with the largest round trip gain in these figures are to become lasing modes. Since the envelope moves very fast with the index change, a wide range tuning is possible.

Figure 3 illustrates simulated tuning characteristics of lasing wavelength at threshold. Although the refractive index change in the codirectional tuning waveguide is small (0.006), tuning range as large as 40 nm is achieved in the figure.

V. SUMMARY

In summary, we have described a new tunable laser diode, i.e., the distributed forward- and backward-coupling (DFBC) laser. This laser is characterized by a codirectional forward coupling between two parallel waveguides together with a backward distributed Bragg feedback due to sampled grating. It would provide a wide tuning range (over 40 nm, for example) as well as larger SMSR in principle compared with the other types of discontinuously-tunable laser diodes. Simple one current tuning scheme is another advantage of the DFBC laser. Either gain or

index coupling, or a combination of these, may be used with the DFBC laser. However, the gain coupling is preferable as it could lead to larger SMSR.

The authors would like to thank Prof. M.-C. Amann of Kassel University, Prof. R. Baets and Dr. G. Morthier of University of Gent for helpful suggestion and advice. This work was supported by the Mombusho Grant-in-Aid #06044060. The work of Y. Nakano was also supported by Murata Science Foundation.

REFERENCES

[1] M.-C. Amann et al., *IEEE Photon. Technol. Lett.*, vol. 1, pp. 253-254, 1989.
[2] V. Jayaraman et al., *IEEE Photon. Technol. Lett.*, vol. 5, pp. 489-491, 1993.
[3] R. C. Alferness et al., *Appl. Phys. Lett.*, vol. 55, pp. 2011-2013, 1989.
[4] Y. Tohmori et al., *Electron. Lett.*, vol. 29, pp. 1350-1352, 1993.
[5] M.-C. Amann et al., *Electron. Lett.*, vol. 29, pp. 793-794, 1993.
[6] H.-P. Nolting et al., *IEEE Photon. Technol. Lett.*, vol. 4, pp. 1386-1389, 1992.
[7] P. Vankwikelberge et al., *IEEE J. Quantum Electron.*, vol. 26, pp. 1728-1741, 1990.
[8] Y. Luo et al., *Appl. Phys Lett.*, vol. 56, pp. 1620-1622, 1990.

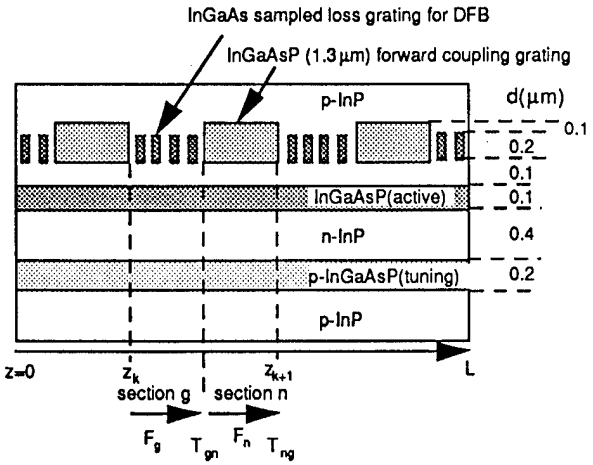

Fig.1 Schematic longitudinal cross section of the distributed forward- and backward-coupling (DFBC) laser.

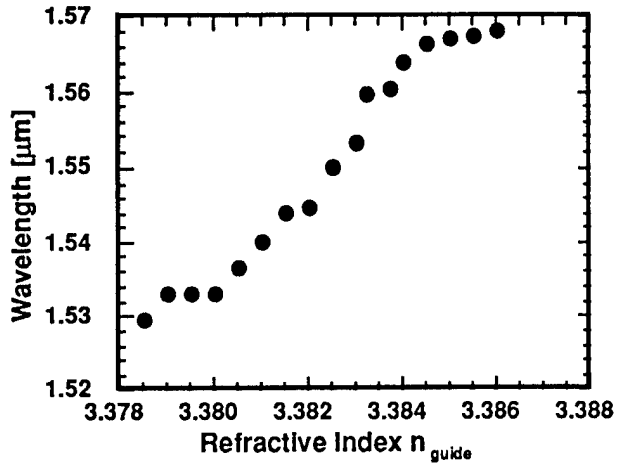

Fig.3 An example of simulated wavelength tuning characteristics of the DFBC laser showing a tuning range over 40 nm around 1.55 μm.

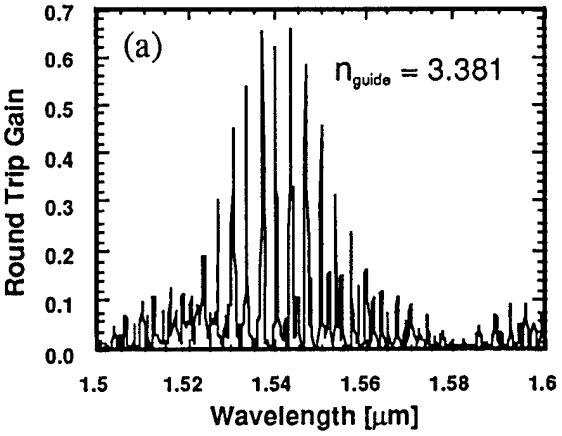

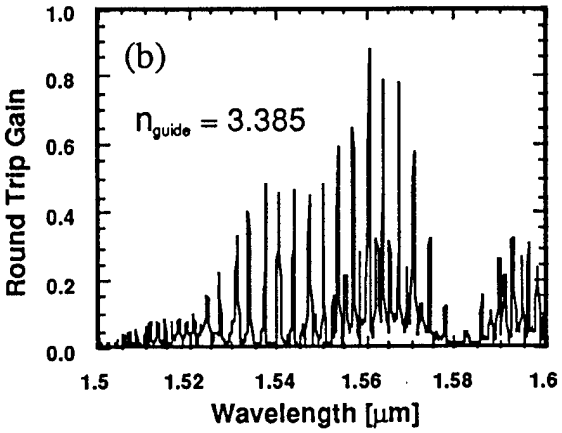

Fig.2 Dependence of round trip gain on wavelength in the DFBC laser with refractive index of the tuning layer being 3.381 (a) and 3.385 (b).

PHOTONICS IN SWITCHING
TECHNICAL PROGRAM COMMITTEE

Rod C. Alferness, *General Chair*
AT&T Bell Laboratories

Lars Thylen, *Program Chair*
Royal Institute of Technology, Sweden

Godfrey Hill, *European Chair*
British Telecom Laboratories

Kunio Tada, *Japanese Chair*
University of Tokyo, Japan

Paul Prucnal
Princeton University

Thomas J. Cloonan
AT&T Bell Laboratories

Daniel J. Blumenthal
Georgia Institute of Technology

Robert Leheny
ARPA

Jack Tomlinson
Bellcore

Rodney S. Tucker
University of Melbourne, Australia

Masahiko Fujiwara
NEC Corporation, Japan

Ken-ichi Yukimatsu
NTT Communications Switching Laboratory, Japan

Takeshi Ozeki
Sophia University, Japan

Marko Erman
Alcatel Alsthom Recherche, France

Sonny Johansson
Ellemtel Telecommunications Systems Laboratory, Sweden

H. Venghaus
Heinrich Hertz Institute, Germany